"Construction and molecular analysis of genetically modified C$_3$ plants expressing a glycolate oxidizing pathway inside the chloroplast"

Von der Fakultät für Mathematik, Informatik und Naturwissenschaften der Rheinisch-Westfälischen Technischen Hochschule Aachen zur Erlangung des akademischen Grades eines Doktors der Naturwissenschaften genehmigte Dissertation

vorgelegt von

Diplom-Biologe

Rashad Mohamed Ahmed Kebeish
aus Sharkia, Ägypten

Berichter: Universitätsprofessor Dr. F. M. Kreuzaler
Privatdozent Dr. C. Peterhänsel

Tag der mündlichen Prüfung: 10-04-2006

Diese Dissertation ist auf den Internetseiten der Hochschulbibliothek online verfügbar

Institute for Biology I (Botany and Molecular Genetics)
RHEINISCH WESTFÄLISCHE TECHNISCHE HOCHSCHULE AACHEN

PhD Thesis

"Construction and molecular analysis of genetically modified C_3 plants expressing a glycolate oxidizing pathway inside the chloroplast"

Presented by

Dipl.Biol. **Rashad Mohamed Ahmed Kebeish**
From Sharkia, Egypt

Scientific supervision
Referent: University Professor Dr. F. M. Kreuzaler
Co-referent: Privatdozent Dr. C. Peterhänsel

Aachen, April 2006

ZUSAMMENFASSUNG

Die Umsetzung von Glykolat in den Reaktionen der Photorespiration von C_3-Pflanzen verbraucht nicht nur ATP und Reduktionsäquivalente, sondern führt auch zu einem Verlust von 25% des in diesem Metabolit fixierten Kohlenstoffs. In der vorliegenden Arbeit wurde ein neuer biochemischer Reaktionsweg für die Umsetzung von Glykolat in *Arabidopsis thaliana* etabliert. Dieser neue Weg soll die CO_2-Konzentration in der Nähe von Rubisco erhöhen und dadurch die Photorespiration in C_3-Pflanzen unterdrücken. Der Reaktionsweg entstammt *E. coli* und wandelt das während der Photorespiration entstehende Glykolat in Glycerat um. Die Aktivität von drei Enzymen wird dazu benötigt: Glykolat-Dehydrogenase (GDH), Glyoxylat-Carboligase (GCL) und Tartronat-Semialdehyd-Reduktase (TSR). Die Glykolat-Dehydrogenase aus *E. coli* besteht aus mindestens drei Polypeptiden. Als Alternative wurde daher eine Glykolat-Dehydrogenase (*At*GDH) aus *A. thaliana* genutzt. Transgene *A. thaliana* Pflanzen mit den drei für diesen Reaktionsweg notwendigen Genen wurden hergestellt. Variierende Mengen der transgenen Proteine sowie RNAs wurden durch Western Blot und RT-PCR gemessen. Die enzymatische Aktivität der Proteine *in planta* konnte nachgewiesen werden.

Biochemische, physiologische und biophysikalische Analysen wurden unter normalen und photorespiratorischen Wachstumsbedingungen mit verschiedenen transgenen Linien durchgeführt, um die Bedeutung des Stoffwechselweges *in planta* zu untersuchen. Durch die Messung des Glycin/Serin-Verhältnis konnte eine deutliche Reduktion der Photorespiration in transgenen Pflanzen im Vergleich zum Wildtyp belegt werden. Ebenso deutlich war die Reduktion der Menge an CO_2, die in den Mitochondrien der Pflanzen während der Photorespiration entstand. Die Messung des freigesetzten NH_3 in einem Bioassay stellte einen zusätzlichen Beweis für die partielle Unterdrückung der Photorespiration in einigen transgenen Linien dar. Desweiteren führte die Etablierung des Glykolat-Reaktionswegs in den Chloroplasten zu einer Reduktion des CO_2-Kompensationspunkts (Γ^*). Die Assimilationsrate von CO_2 in den transgenen Linien war unter photorespiratorischen Bedingungen erhöht. Durch die Messung des Wachstums von transgenen Pflanzen, die den Glykolat-Reaktionsweg im Chloroplasten exprimieren, im Vergleich zum Wildtyp konnte eine größere Blattfläche und ein größerer Durchmesser der Rosette nachgewiesen werden. Interessanterweise wurden die meisten der beschriebenen Effekte auch in Pflanzen beobachtet, die nur eine funktionsfähige GDH überexprimierten. Allerdings waren die

Effekte in Pflanzen, die alle notwendigen Elemente des Glykolat-Reaktionswegs überexprimierten, stärker. Zudem waren die phänotypischen Effekte bei Nutzung der bakteriellen GDH im Vergleich zu dem pflanzlichen Enzym deutlich ausgeprägter. Zusammenfassend kann festgestellt werden, dass der neue Reaktionsweg in den Chloroplasten von C_3-Pflanzen nicht nur zu einer Reduktion der Photorespiration, sondern auch zu einem erhöhten Pflanzenwachstum führt.

SUMMARY

Metabolism of glycolate via the photorespiratory pathway in C_3 plants consumes not only ATP and reducing equivalents but results also in approximately 25% loss of the carbon from glycolate. In the present study, a novel biochemical pathway for the metabolism of glycolate was established in the chloroplast of *Arabidopsis thaliana* plants. The new pathway aims to increase the CO_2 concentration in the vicinity of Rubisco thereby suppressing photorespiration in C_3 plants. The pathway is derived from *E. coli* and converts the glycolate formed during photorespiration into glycerate. Three enzymatic activities are required: glycolate dehydrogenase (GDH), glyoxylate carboligase (GCL), and tartronic semialdehyde reductase (TSR). The minimal *E.coli* glycolate dehydrogenase enzyme is formed from three different polypeptides. As an alternative, a glycolate dehydrogenase (*At*GDH) derived from *A. thaliana* was used. Transgenic *A. thaliana* plants containing the necessary genes for the novel pathway were generated. Variable amounts of foreign proteins as well as RNA were detected by Western blot and RT-PCR, respectively. Enzymatic assays showed that the proteins are active in *planta*.

Biochemical, physiological and biophysical analyses were performed under ambient and enhanced photorespiratory conditions using different transgenic lines for evaluating the impact of the novel pathway in *planta*. By measuring the Gly/Ser ratio, a clear reduction in photorespiration was observed in transgenic plants expressing the novel pathway genes compared to wild type plants. A clear decrease in the amount of CO_2 released in the plant mitochondria during photorespiration was also obvious in transgenic lines. The ammonia release bioassay provides an additional evidence for the partial suppression of photorespiration in some of the transgenic lines. Furthermore, establishment of the glycolate pathway in the plant chloroplasts results in a decrease in the CO_2 compensation point (Γ_*). The CO_2 assimilation rates in transgenic plants were also enhanced under photorespiratory conditions. Finally, plant growth measurements revealed that the transgenic plants expressing the glycolate pathway in their chloroplasts have bigger leaf area as well as bigger rosette diameter compared to the control plants. Moreover, the total fresh and dry weight measurements showed that the total plant productivity was enhanced. Interestingly, most of the described effects were also observed in plants that only overexpressed a functional GDH. However, these effects were stronger in plants overexpressing all necessary elements of the

glycolate pathway. Moreover, the phenotypical effects were much stronger when the bacterial GDH was compared to the plant GDH. Taken together, it can be concluded that expression of the novel pathway in C_3 plant chloroplast does not only result in a reduction of photorespiration but it also enhances plant growth.

TABLE OF CONTENTS

1   INTRODUCTION

1.1 Photosynthesis

Photosynthesis is the fundamental chemical process in which the energy of sunlight or other light is utilized by green plants and blue-green algae to convert carbon dioxide and water into carbohydrates. In fact, most of the food we eat, the fuel we burn and the fibers we wear are resultants of the activity of green plants. Photosynthesis releases oxygen, which is the main source of atmospheric oxygen. The oxygen released from the photosynthetic process is of great importance because of its use by both plants and animals in aerobic respiration. Although oxygen is continually removed from air by the non biological processes as well as by respiration, photosynthesis is the only process that adds oxygen to the atmosphere. Photosynthesis is carried out by many different organisms, ranging from plants to bacteria. The best known form of photosynthesis is the one carried out by higher plants and algae, as well as by cyanobacteria and their relatives, which are responsible for a major part of photosynthesis in oceans. All these organisms convert CO_2 to organic material by reducing this gas to carbohydrates in a complex set of reactions. Electrons for this reduction reaction ultimately come from water, which is then converted to oxygen and protons. The photosynthetic process in plants and algae occurs in small organelles known as chloroplasts that are located inside their cells. Chloroplasts provide the energy and reduced carbon needed for plant growth and development, while the plant provides the chloroplast with CO_2, water, nitrogen, organic molecules and minerals necessary for chloroplast biogenesis. Each chloroplast is defined by an inner and an outer envelope membrane and is shaped like a convex lens that is 5-10 μm in diameter (Figure 1.1) although many different shapes and sizes can be found in plants (Staehelin, 1986). The inner envelope membrane acts as a barrier, controlling the flux of organic and charged molecules in and out of the chloroplast. Water passes freely through the envelope membranes, as do other small neutral molecules like CO_2 and O_2. Inside the chloroplast is a complicated membrane system, known as the photosynthetic membrane (or thylakoid membrane), that contains most of the proteins required for the light reactions. The proteins required for the fixation and reductions of CO_2 are located outside the photosynthetic membrane in the surrounding aqueous phase. The photosynthetic membrane is composed mainly of glycerol lipids and protein. The energy required for the photosynthetic process is provided by sunlight, which is absorbed by pigments (primarily chlorophylls and carotenoids). Chlorophylls absorb blue and red light (chl.b and chl.a, respectively) and carotenoids absorb blue-green light, but green and yellow

light are not effectively absorbed by photosynthetic pigments in plants; therefore, light of these colours is either reflected by leaves or passes through the leaves.
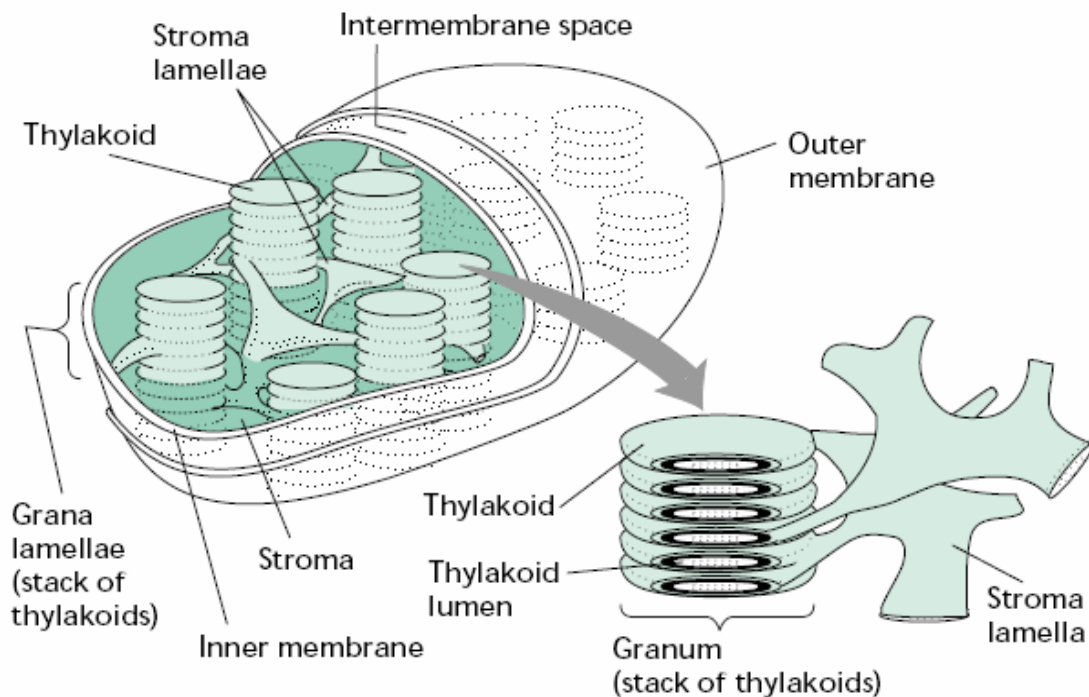
Figure 1.1: Structure of the chloroplast

The chloroplast organelle is surrounded by a double membrane. Inside the inner membrane is a complex mix of enzymes and water. This is called stroma. Embedded in the stroma is a complex network of stacked sacs. Each stack is called a granum and each of the flattened sacs which make up the granum is called a thylakoid. Each thylakoid has a series of photosystems and associated proteins that are used in the photosynthetic process. This figure was derived from Becker (1986).

In green plants, the photosynthetic process involves two basic reactions, the light and the dark reactions; the light reaction occurs in the thylakoid membrane and converts light energy to chemical energy. Chlorophyll and several other pigments such as beta-carotene are organized in clusters in the thylakoid membrane and are involved in the light reaction. Each of these differently coloured pigments can absorb a slightly different colour of light and pass its energy to the central chlorphyll molecule to start the photosynthetic process. The energy harvested via the light reaction is stored by forming ATP and NADPH molecules that is further used for the formation of sugars via the dark reaction (Lawlor, 2001). The initial CO_2 fixation reaction involves the enzyme ribulose-1,5-bisphosphate carboxylase/oxygenase (Rubisco, EC 4.1.1.39), which can react with either oxygen (leading to a process named photorespiration) or with CO_2. The probability with which Rubisco reacts with oxygen as well as with CO_2 depends on the relative concentrations of the two compounds at the site of the

reaction (Ogren, 1984a). In all organisms CO_2 is by far the preferred substrate, but as the CO_2 concentration is much lower than the oxygen concentration, photorespiration does occur at significant levels (Ogren and Jordan, 1983). For higher plants, three biochemical pathways - the C_3 pathway (Calvin cycle), the C_4 pathway (Hatch-Slack pathway) and the crassulacean acid metabolism - are involved in CO_2 assimilation.

1.1.1 C_3-photosynthesis

The vast majority of plants, including major crops such as wheat and rice, assimilate carbon dioxide via the C_3 photosynthetic pathway and thus are known as C_3 plants (Ku, 1996). Figure 1.2 represents the CO_2 assimilation pathway in C_3 plants which is known as the Calvin cycle.
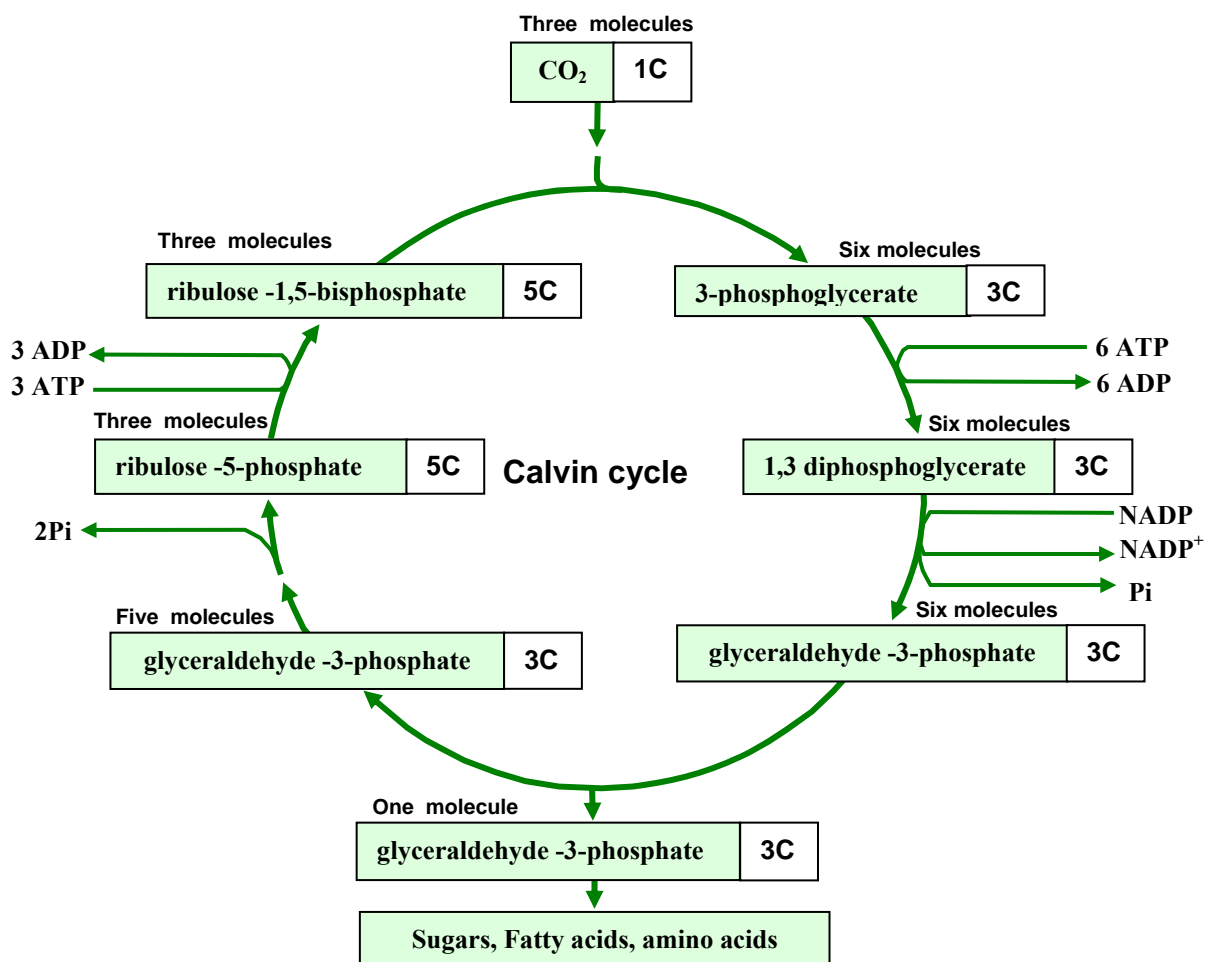
Figure 1.2: Schematic representation of the Calvin cycle.

The carboxylation reaction of Rubisco yields two molecules of 3-phosphoglycerate. This 3-phosphoglycerate is fixed and recycled to RuBP in a series of reactions that is known as the Calvin cycle. Fixation of six molecule of CO_2 requires twelve molecules of NADPH and eighteen molecules of ATP. In chloroplasts, CO_2 condenses with ribulose-1,5-bisphosphate (RuBP) to form two molecules of the C_3 compound, 3-phosphoglycerate (PGA). PGA is then reduced to triose phosphate by consuming ATP and NADPH that have been produced during the light reaction. The triose phosphate is then either utilized to regenerate ribulose-1,5-bisphosphate or to synthesize starch within chloroplasts or is transported into the cytosol for sucrose biosynthesis.

In the Calvin cycle (Calvin, 1989), a molecule of CO_2 reacts with a five-carbon compound called ribulose-1,5-bisphosphate (RuBP) producing an unstable six-carbon intermediate that immediately breaks down into two molecules of the three-carbon compound phosphoglycerate (PGA), hence the name, C_3 photosynthesis. PGA is phosphorylated by ATP, that was formed during the light reaction, to form 1,3-diphosphoglycerate. The 1,3-diphosphoglycerate is then reduced by NADPH, also produced during the light reaction, to form glyceraldehydes-3-phosphate. This triose phosphate is used either to form carbohydrates and sugars or/and to regenerate the ribulose-1,5-bisphosphate. In case of carbohydrate synthesis, the glyceraldehydes-3-phosphate molecules are converted into dihydroxyactone phosphate in the presence of triose phosphate isomerase. Phosphoglyceraldehyde-3-phosphate and dihydroxyacetone phosphate are combined by aldolase to form fructose-1,6-bisphosphate which is then converted into fructose-6-phosphate. From fructose-6-phosphate, different carbohydrates can be synthesized. On the other hand, regeneration of ribulose-1,5-bisphosphate is essential for the continuity of the photosynthetic process. The previously formed fructose-6-phosphate and glyceraldehydes-3-phosphate are used in a series of reactions to regenerate the ribulodse-1,5-bisphosphate.

1.1.2 C_4 -photosynthesis

About 7500 of the 250000 higher plant species use the C_4 photosynthetic pathway. C_4 species dominate primary productivity of warm temperate to tropical grasslands, C_4 plants often account for over 80% of the primary productivity (Sage, 2001). Relative to C_3 species, C_4 plants have an advantage in many aspects that promote ecological success in warm and low latitude habitats. They have higher maximum efficiency in terms of radiation, water and nitrogen use, and they generally have higher photosynthetic capacity. The enhancement of photosynthetic performance comes from the ability of C_4 plants to concentrate the CO_2 in the vicinity of Rubisco. The CO_2 fixation enhancement in C_4 plants is due to the co-ordination of two photosynthetic cell types, namely mesophyll cells (MC) and bundle sheath cells (BSC). These two cell types are arranged in layers concentrically around the vascular tissue, the bundle sheath cells constituting the inner layer and the mesophyll cells forming the outer layer. The MC and BSC are connected by many plasmodesmata. This arrangement of cells is known as Kranz anatomy (Hatch, 1992). C_4 plants have been divided into three subgroups based on differences in the enzymes of the decarboxylation step in BSC (Ryuzi Kanai, 1999). These are the NADP-malic enzyme (NADP-ME), NAD-malic enzyme (NAD-ME), and PEP carboxykinase (PEP-CK) types. Each C_4 type shows not only morphological differentiation in

their arrangement of bundle sheath chloroplasts and ultrastructure, but also further biochemical differences between MC and BSC, and in the method of transport of metabolites between the cells (Hatch, 1987b). Common to all C_4 plants is the initial fixation of HCO_3^- by PEP carboxylase (EC-Number 4.1.1.31) to form oxaloacetate in the MC cytoplasm. Malate and aspartate are formed from oxaloactate in MC. Malate is the main initial product in the NAD-ME type of C_4 photosynthesis whereas aspartate is the main initial product in the NAD-ME and PEP-CK types. Figure 1.3 represents the NADP-ME type. In this type of C_4 photosynthesis, the CO_2 enters the mesophyll cell and is converted to HCO_3^- by the carbonic anhydrase enzyme (CA). The HCO_3^- is converted to oxaloacetate (OAA) in the cytosol by the aid of phosphoenolpyruvate carboxylase (PEPC).
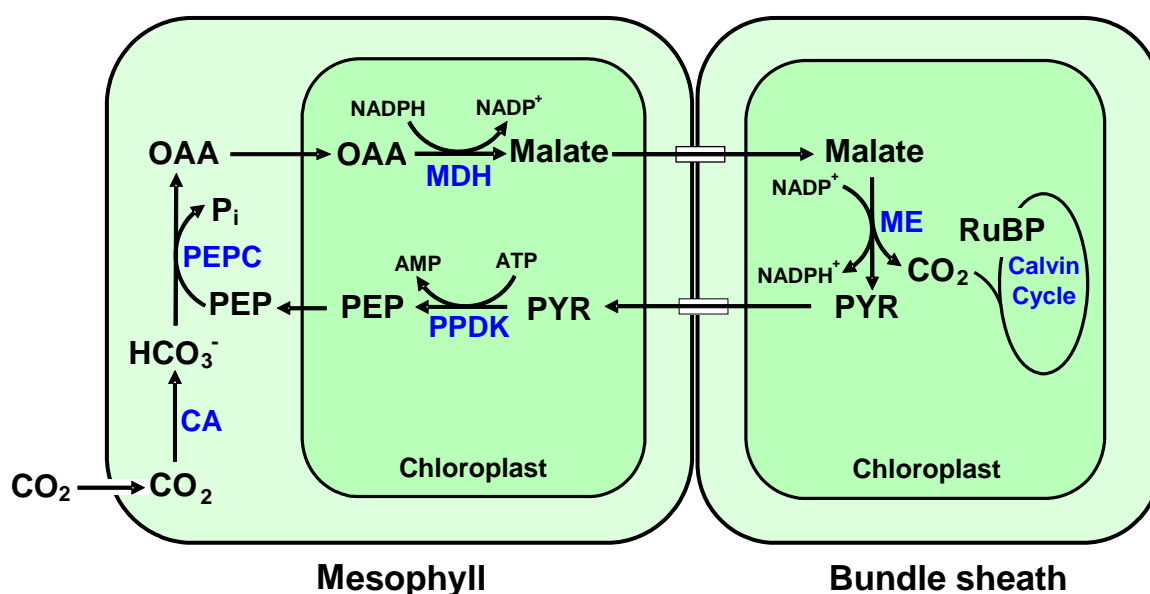
Figure 1.3: Schematic representation of the NADP-ME type of C_4 photosynthesis.
The CO_2 enters into the MC cytosol where it is converted into HCO_3^-. The HCO_3^- reacts with PEP to form oxaloacetate that diffuses into the MC chloroplast. In the MC chloroplast, the OAA is converted into malate. The malate diffuses into the chloroplast of the BSC where it is decarboxylated to form pyruvate and CO_2 is released. The pyruvate diffuses back to the MC chloroplast where it is converted into phosphoenolpyruvate and starts a new cycle of CO_2 fixation. The released CO_2 in the BSC chloroplast is used for the carbohydrate synthesis by Calvin cycle. **CA**: carbonic anhydrase, **PEPC**: phosphoenolpyruvate carboxylase, **OAA**: oxaloacetate, **MDH**: malate dehydrogenase, **ME**: malic enzyme, **PPDK**: pyruvate orthophosphate dikinase.

This OAA enters the chloroplast and reduced to malate by malate dehydrogenase (MDH). The formed malate then diffuses into a neighboring bundle sheath cell chloroplast through plasmodesmata where it is decarboxylated by malic enzyme (ME). During the decarboxylation of malate, CO_2 is released in the BSC chloroplast. The CO_2 is then fixed by Rubisco and converted to carbohydrates in the Calvin cycle. On the other hand, the pyruvate

(PYR) produced in the decarboxylation reaction diffuses back to the mesophyll cell to regenerate phosphoenolpyruvate.

1.1.3   The Crassulacean Acid Metabolism (CAM) photosynthesis

Crassulacean acid metabolism (CAM) is an important elaboration of photosynthetic carbon fixation that allows chloroplast-containing cells to fix CO_2 initially at night using phosphoenolpyruvate carboxylase (PEPC) in the cytosol (Cushman, 2001; Cushman and Bohnert, 1997) . This leads to the formation of C_4 organic acids (usually malate), which are stored in the vacuole. Subsequent daytime decarboxylation of these organic acids creates an internal CO_2 source that is reassimilated by Rubisco in the chloroplast. The refixation of this internal CO_2 generates carbohydrates via the photosynthetic carbon reduction cycle. Thus, CAM involves a temporal separation of carbon fixation modes in contrast to the spatial separation found in C_4 plants. The sequence of biochemical reactions of the CAM cycle is discussed in more detail (Ranson and Thomas, 1960). The complexity of the biochemical variations in the pathway among different CAM species, and its regulation by the environment have been studied (Osmond, 1978; Osmond, 1979). Initial nocturnal CO_2 fixation by PEPC occurs when stomata are open and transpirational water losses are low. CO_2 release during the day promotes stomatal closure and concentrates CO_2 around Rubisco, suppressing its oxygenase activity, thereby minimizing photorespiration. The net effect of this CO_2-concentrating strategy is that CAM plants exhibit a higher water use efficiency rates than C_3 and C_4 plants under comparable conditions. The CAM photosynthetic pathway is divided into two parts, the first part occurs during the night where CO_2 enters into the cells through the opened stomata. The CO_2 is converted into malate in the same way as in the C_4-photosynthetic pathway (1.1.2). The formed malate is then transported and stored in the vacuole. At the same time the phosphoenolpyruvate is regenerated during the night. The second part of the CAM photosynthetic pathway occurs during the day where the stored malate in the vacuole (during the night) is transported back to the cytosol. Malate is converted into pyruvate by NADP-ME enzyme and CO_2 is released during this reaction to be used by Rubisco for the carbohydrates biosynthesis. The formed pyruvate is then transported from the cytosol into chloroplast where it is converted to PEP by the enzyme pyruvate orthophosphate dikinase (PPDK). The PEP is further converted into 3-PGA that will be used also for the synthesis of carbohydrates.

1.2 Single-cell C4-photosynthesis

The C_4-type of photosynthesis requires the cooperation between two cell types, BSC and MC, in order to concentrate the CO_2 in the vicinity of Rubisco (Hatch, 1987b; Sage, 2004). However, there was evidence that C_4 photosynthesis can also occur within a single photosynthetic cell in terrestrial plants. Voznesenskaya *et al.* (2001) have shown that the plant *Borszczowia aralocaspica* (Chenopodiaceae) has photosynthetic features of C_4 plants, but it lacks Kranz anatomy. Also, CAM plants fix atmospheric CO_2 at night through a C_4 pathway and further process the carbon via the C_3 pathway during the day (Cushman, 2001). This will result in a temporal separation of the process rather than a spatial separation (as shown above 1.1.3). The submersed monocot *Hydrilla verticillata* is a facultative C_4 plant (Bowes, 2002; Rao *et al.*, 2002; Reiskind *et al.*, 1997; Van Ginkel *et al.*, 2001). It typically exhibits C_3 photosynthetic characteristics, but exposure to low CO_2 induces a C_4 system in which the C_4 and Calvin cycles co-exist in the same cell and the initial fixation in the light is catalyzed by phosphoenolpyruvate carboxylase (PEPC). The discovery of this single-cell C_4 photosynthetic mechanism in *Hydrilla verticillata* (Bowes, 2002) and chenopods *Borszczowia aralocaspica* (Freitag and Stichler, 2002; Voznesenskaya *et al.*, 2001) has shown that Kranz anatomy may not be essential for C_4 plant photosynthesis. The photosynthetic rates of these naturally occurring single-cell C_4 systems are low when compared with some of the common C_3 and C_4 crop plants. However, they show an increased photosynthetic rate per Rubisco catalytic sites when they are compared to their C_3 counterparts (Von Caemmerer, 2003).

1.3 Approaches for increasing C₃ plant photosynthesis

The application of advances in plant breeding, including tissue culture, DNA technology and genetic engineering, are going to be essential for increasing plant yields. These technologies will help the farmers allover the world to reduce the excessive pesticide use and to increase the nutrient values of basic foods. At the same time, it provides better varieties that are able to tolerate drought, salinity, lack of soil nutrients as well as to produce higher yields under unfavorable conditions (Conway G. and Toennissen G, 1999). Many researches are working on projects aiming to raise plant yield by increasing photosynthesis and/or reducing photorespiration. One of the challenges facing plant biotechnologists is to modify photosynthesis to achieve increases in net carbon gain. More than 95% of the terrestrial plants including many important crop species assimilate carbon through the C_3 photosynthetic pathway (Bowes, 1996). C_3 photosynthesis suffers from O_2 inhibition due to the oxygenase

activity of Rubisco (Spreitzer, 1999) and the subsequent loss of CO_2 from photorespiration (Ogren, 1984b). Under the present atmospheric conditions (21% O_2 and 0.035% CO_2), O_2 reduces the efficiency of photosynthesis by as much as 25%. This photosynthetic reduction could increase further under drought and high temperature conditions.

There was some interest in engineering Rubisco in order to increase the carboxylation over oxygenation reaction, but current chemical evidence suggests that it is unlikely that Rubisco can be engineered for increased carboxylation efficiency (Somerville, 1990; Zhu *et al.*, 2004). Several attempts to increase the specificity of Rubisco to CO_2 over O_2 by altering its active site with the techniques of site-directed mutagenesis, by inducing low oxygenase activity mutants (Somerville and Ogren, 1982), or by inserting more efficient Rubisco genes into higher plants have not been successful (Normile, 1999; Zelitch, 1989). Manipulation of Rubisco in higher plants requires a better understanding of many aspects – its catalytic mechanism, its regulation, its natural diversity, and its synthesis and assembly in plants and other organisms (Andrews and Whitney, 2003; Whitney and Andrews, 2001). Medrano *et al.* (1995) have shown that the selection of tobacco plants for survival at low CO_2 doesn't result in a decreased photorespiration or an increased efficiency of Rubisco carboxylase. The selected genotypes were able to invest more assimilate into cell production and form larger leaves increasing total leaf area per plant. These features improve light capture by the tobacco plants and increase dry matter accumulation.

The C_4 photosynthetic pathway serves as a CO_2 pump to concentrate atmospheric CO_2 at the site of Rubisco and thus represses its oxygenase activity and the associated photorespiration (Edwards and Coruzzi, 1989; Hatch, 1987b). Transfer of C_4 traits into C_3 plants to improve their photosynthetic efficiency has been an active research area in plant biology (Furbank and Taylor, 1995; Häusler *et al.*, 2002; Ku *et al.*, 1999; Ku *et al.*, 1996; Rademacher *et al.*, 2002). For example, overexpression of maize phosphoenolpyruvate carboxylase (PEPC) in rice plants resulted in a transgenic plants that exhibit reduced O_2 inhibition of photosynthesis (Agarie *et al.*, 2002; Ku *et al.*, 1999). In a similar study with *Solanum tuberosum*, overexpression of PEPC and NADP-malic enzyme resulted in a decrease in the electron requirement for CO_2 assimilation with increasing temperature. This is considered as an indication for the suppression of the oxygenase activity of Rubisco (Lipka *et al.*, 1999). Alternative approaches to improve CO_2 fixation in C_3 plants using genetic manipulations include the introduction of CO_2 concentrating mechanism from aquatic algae (Lipka *et al.*, 1999) and cyanobacterial systems. Most algae and cyanobacteria concentrate inorganic carbon by a diversity of mechanisms and possibilities (Badger, 2003; Badger and Spalding, 2000).

Recently the first transgenic plants expressing a cyanobacterial gene involved in HCO_3^- accumulation were generated by (Lieman-Hurwitz *et al.*, 2003). These transgenic plants show small increases in photosynthetic rate and growth under limiting CO_2 conditions. This leads to the conclusion that, it is possible to increase photosynthesis in C_3 plants by increasing the CO_2 concentration at the vicinity of Rubisco.

1.4 Photorespiration

Fixation of CO_2 in photosynthetic organisms is carried out by Ribulose -1,5- bisphosphate carboxylase/oxygenase (Rubisco) enzyme found in their chloroplasts. In addition to the carboxylation reaction, Rubisco can also fix O_2 (Bowes *et al.*, 1971). Rubisco favours CO_2 over O_2 by a factor of up to 100, but the concentration of O_2 in the atmosphere is much higher than that of CO_2. As a result, one molecule of O_2 is fixed by Rubisco for every three molecules of CO_2 (Sharkey, 2001). C_4 plants as well as CAM plants, overcome the problem of photorespiration by concentrating CO_2 in the vicinity of Rubisco (as described above). C_4 plants are able to concentrate CO_2 in the Rubisco containing bundle sheath cell at levels up to 3 to 20 times higher than atmospheric CO_2 (Jenkins, 1989; von Caemerer, 2003; Von Caemmerer, 1999). Because of their CO_2 concentrating mechanism, C_4 plants greatly reduce the oxygenase reaction of Rubisco (Hatch, 1987a; Hatch, 1992). The oxygenase activity of Rubisco is much more common to C_3 plants because of the absence of the CO_2 concentrating mechanism. Photorespiration inhibits photosynthesis by three mechanisms, it interferes with CO_2 fixation at Rubisco, it uses energy that could otherwise be used for photosynthetic carbon reduction and causes the release of CO_2 from previously fixed carbon (Sage, 2001; Sharkey, 1988; Sharkey, 2001). As O_2 is substituted for CO_2 at the active site of Rubisco, phosphoglycerate and phosphoglycolate result and photorespiratory pathway is used to convert the carbon diverted out of the C_3-cycle back to photosynthesis (Leegood *et al.*, 1995). The metabolism of phosphoglycolate into phosphoglycerate via the photorespiratory pathway and then further to RuBP is not only a very costly reaction, it also requires a large machinery consisting of 16 enzymes and more than 6 translocators, distributed over the chloroplast, peroxisome and mitochondrion (Douce and Neuburger, 1999).

1.4.1 The photorespiratory pathway in C_3 plants

The photorespiratory pathway proceeds in the chloroplast, the peroxisome and mitochondria. In this pathway, two molecules of phosphoglycolate are processed to form one molecule each of phosphoglycerate and CO_2, which are used for the regeneration of RuBP through the

Benson-Calvin cycle. Figure 1.4 represents the photorespiratory pathway in C_3 plants where the oxygenation reaction of Rubisco results in the formation of one molecule of phosphoglycerate and one molecule of phosphoglycolate. Phosphoglycerate enters directly into the carbohydrate biosynthesis in the Calvin cycle in the chloroplast.
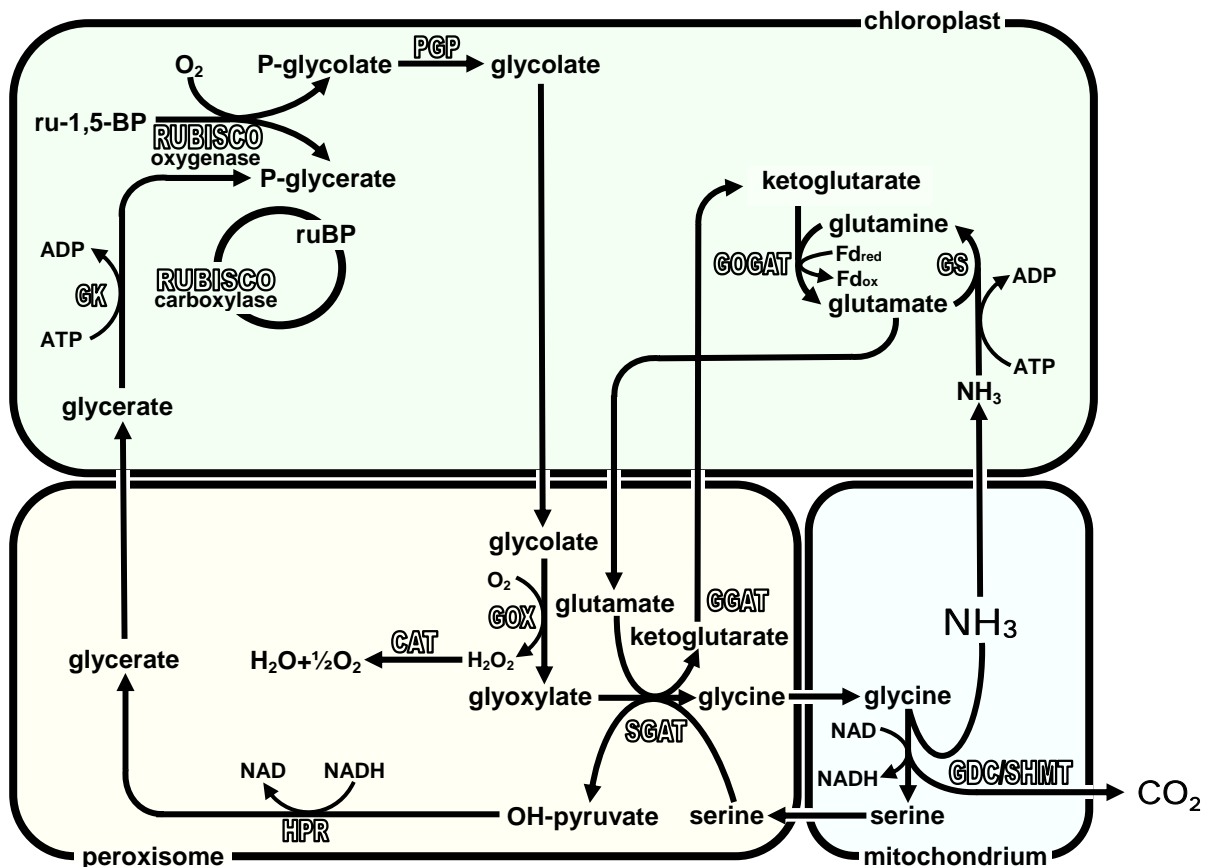
Figure 1.4: **Representation of the photorespiratory pathway in C_3 plants**

In this pathway oxygenation of RuBP by Rubisco oxygenase results in the formation of one molecule of PGA and one molecule of PG. PGA enters in the Benson Calvin cycle to form carbohydrates and also to regenerate RuBP. PG is processed to form PGA in a reaction sequence occurring in the chloroplast, peroxisomes and mitochondria. PG is converted to glycolate by PGP. Glycolate is transported from the chloroplast into the peroxisome where it is oxidized by GO enzyme to form glyoxylate. Glyoxylate is then converted to glycine by GGAT. Glycine is internally transported to the mitochondria where it is decarboxylated to form serine by GDC/SHMT. The formed serine is transported back to the mitochondria where it is converted to hydroxypyruvate by SGAT. Hydroxypyruvate is then converted to glycerate by HPR. Glycerate is then transported to the chloroplast where it is converted to PGA by GK. **Rubisco**: Ribulose-1,5-bisphosphate carboxylase/Oxygenase, **PGP**: phosphogycolate phosphatase, **GOX**: glycolate oxidase, **CAT:** Catalase; **GGAT**: glyoxylate/glutamate amino transferase, **GDC/SHMT**: glycine decarboxylase/serine hydroxymethyl transferase, **SGAT**: serine/glutamate amino transferase, **HPR**: Hydroxy-pyruvate reductase, **GK**: glycerate kinase. **GS**: glutamine synthetase, **GOGAT**: glutamate synthase.

Phosphoglycolate is dephosphorylated by phosphoglycolate phosphatase (PGP) that is located also in the chloroplast forming glycolate (Lawlor, 2001). Glycolate is transported from the

chloroplast to the peroxisome. In the peroxisome, glycolate is oxidized to form glyoxylate by the peroxisomal glycolate oxidase enzyme (GOX). Oxidation of glycolate to glyoxylate produces H_2O_2 that is directly dissociated to H_2O and ½ O_2 by catalase enzyme (CAT). Glyoxylate is then transaminated to glycine in a reaction including glutamate by the enzyme glyoxylate/glutamate amino transferase (GGAT). The resulting glycine is transported into mitochondria where it is decarboxylated to form serine. Decarboxylation of glycine is mediated by the mitochondrial glycine decarboxylase/serine hydroxymethyl transferase enzymes (GDC/SHMAT). During this decarboxylation reaction, CO_2 and ammonia are released inside the mitochondrion (Raghavendra *et al.*, 1998). The formed serine is transported back to the peroxisome, where it is converted to hydroxy-pyruvate by serine/glutamate aminotransferase enzyme (SGAT). Hydroxy-pyruvate is then reduced to glycerate by hydroxy-pyruvate reductase enzyme (HPR). Glycerate is further transported to the chloroplast where it is phosphorylated to phosphoglycerate by glycerate kinase enzyme (GK) that is located in the chloroplast. Conversion of glycine to serine in the photorespiratory pathway is probably the most important process that liberates ammonia. Ammonia liberated in the matrix of the mitochondria diffuses rapidly to the chloroplast where it is used by glutamine synthetase (GS) catalyzing the ATP-dependent conversion of glutamate to glutamine. The ferredoxin-dependent glutamate oxoglutarate aminotransferase (GOGAT) which is localized in the chloroplast catalyzes the conversion of glutamine and 2-oxoglutarate to two molecules of glutamate. One molecule of glutamate is exported to the peroxisomes as an amino donor for GGAT in exchange for 2-oxoglutarate (Ireland, 1998; Migge, 1997; Sharkey, 2001). Thus the glutamine synthetase/glutamate synthase (GS/GOGAT) pathway that refixes the ammonia consumes both ATP and reducing power. This also can be added to the energetic cost of photorespiration (Sharkey, 2001). However, it also provides the amino groups necessary for the transamination of glyoxylate in the peroxisomes.

1.4.2   Movement of molecules in the photorespiratory pathway

During the photorespiratory pathway glycolate must move from the chloroplast stroma to the peroxisome across the inner envelope membrane and glycerate must be transported in the opposite direction. Experiments with intact chloroplasts have shown that a single carrier-type transporter is responsible for the movement of both glycolate and glycerate across the chloroplast inner envelope membrane (Howitz and McCarty, 1983; Howitz and McCarty, 1991). Moreover, during the course of photorespiration, 2-oxoglutarate is massively imported

into the chloroplasts and glutamate deriving from the glutamine synthetase and glutamate synthetase cycle is exported towards the peroxisome as shown above (1.4.1).

The 2-oxoglutarate/malate translocator imports 2-oxoglutarate in an exchange for stromal malate (Flügge et al., 1996) whereas export of glutamate from the chloroplast in exchange for malate is catalyzed by the glutamate/malate translocator (Weber et al., 1995). Therefor, Malate is involved in both transport steps but probably without net malate import. Additionally, during glycine decarboxylation and deamination, one molecule of serine leaves the mitochondrion and two molecules of glycine are taken up from the peroxisome. The details of glycine and serine transport in green leaf mitochondria are not clearly observed. However, there is evidence for passive movement of glycine (Shingles and Grodzinski, 1984). Douce and Neuburger (1999) suggested that both glycine and serine might be transported through an exchange of glycine and serine and hydroxyl ions in the mitochondria. Also oxaloacetate carrier catalyzes the transfer of reducing equivalents from mitochondria to peroxisomes (Oliver et al., 1990; Raghavendra et al., 1998). The ammonia released during the conversion of glycine to serine passes through the inner membrane of mitochondria and chloroplasts. Ninneman et al., 1994 have identified a high affinity ammonia transporter on the inner membrane of the chloroplast envelope. This transporter may be involved in the transport of ammonia from the mitochondrion to the chloroplast.

1.4.3   Significance and insignificance of photorespiration for C_3 plants

The oxygenation reaction of Rubisco is seemingly a wasteful side reaction because it uses active sites that otherwise would be used for carboxylation, it consumes ribulose -1,5-bisphosphate (RuBP) and the recovery of carbon from phosphoglycolate consumes ATP and reducing equivalents in the form of $NAD/(P)H^+$ (Sage, 1999). The CO_2 release in the mitochondria during photorespiration results in 25% loss of the carbon from phosphoglycolate. Moreover, NH_3 is lost in this cycle that has to be refixed (Leegood et al., 1995). Although photorespiration is clearly deleterious to C_3 plants, it is also necessary for their protection from high light intensities. Photorespiration is effective in dissipating excess photochemical energy. Also photorespiration provides the plants with the amino acids glycine and serine that can be used for protein synthesis (Douce and Neuburger, 1999; Kozaki and Takeba, 1996; Sharkey, 2001). These two functions indicate the significance of photorespiration in C_3 plants. However, Sharkey (2001) speculated that there are other mechanisms exist in plants that can perform these two functions even better than photorespiration. In the first case, the mechanism of dissipating excess light that involves

zeaxanthin can dissipate much more energy than can photorespiration in most leaves. In the second case, the capacity for starch and sucrose synthesis exceeds the capacity for glycine and serine synthesis. As these two functions of photorespiration may be useful to the plant, the overall effect is deleterious. Often, the stimulation of photosynthesis that occurs in a high CO_2 environment results only from the suppression of photorespiration by the increased CO_2 concentration (Harley and Sharkey, 1991). This can support the speculation that suppression of photorespiration in C_3 plant could increase their photosynthetic performance under comparable conditions.

1.5 The metabolism of glycolate in *Escherichia coli*

Many bacteria have evolved biochemical pathways to metabolize glycolate, the primary product of the oxygenase activity of Rubisco. For *Escherichia coli*, this pathway has been described in great detail (Hansen and Hayashi, 1962; Kornberg and Sadler, 1961; Lord, 1972; Pellicer *et al.*, 1996). Glycolate is metabolized in *Escherichia coli* through oxidation of glycolate in a reaction catalyzed by the enzyme glycolate oxidase (GO) (EC.Number.1.1.3.1), a multiprotein complex that is capable of oxidizing glycolate in an oxygen independent manner to produce glyoxylate. So this enzyme is also known as glycolate dehydrogenase (GDH). The proteins necessary for glycolate oxidation in *E. coli* have been analyzed. It involves three protein subunits that are encoded by three different open reading frames called *glc*D, *glc*E and *glc*F, which are located in the *glc* operon of *E. coli* (Lord, 1972; Pellicer *et al.*, 1996). Glyoxylate is a branching point in the metabolic pathway since it is metabolized by two divergent condensation reactions. One reaction condenses glyoxylate with an acetyl group provided by acetyl coenzyme A and is catalyzed by malate synthase G forming malate, while the other reaction condenses two molecules of glyoxylate in a process catalyzed by glyoxylate carboligase (*GCL*) forming tartronic semialdehyde and CO_2 is released in this reaction (Chang *et al.*, 1993). Tartronic semialdehyde is further reduced to glycerate by tartronic semialdehyde reductase (*TSR*) and subsequently phosphorylated to glycerate-3-phosphate by glycerate kinase (Gotto and Kornberg, 1961). These three enzymes (glycolate dehydrogenase, glyoxylate carboligase and tartronic semialdehyde) constitute what is known as the glycerate pathway in *E. coli* (Pellicer *et al.*, 1996). A similar pathway is also discovered as a photorespiratory cycle in some green algae and cyanobacteria (Nelson and Tolbert, 1970). In this pathway, glycolate oxidation is catalyzed by a glycolate dehydrogenase that is located inside the mitochondria. The further reactions of glyoxylate metabolism seemingly

proceed in the same way as in higher plants peroxisomes (Igamberdiev and Lea, 2002; Stabenau *et al.*, 1984).

Enzymes catalyzing the oxidation of glycolate to glyoxylate have been isolated from a variety of plants and animal tissues (Frederick *et al.*, 1973; Tolbert *et al.*, 1968). It is also found in several unicellular algae (Betsche *et al.*, 1992; Suzuki *et al.*, 1991). The known glycolate oxidases of higher plants and animals differ in many aspects from bacterial and algal glycolate dehydrogenases. On the one hand, the plant and animal glycolate oxidases use O_2 as an electron acceptor, produce H_2O_2, oxidize L(+)-lactate as an alternative substrate and are cyanide insensitive. On the other hand, the algal and bacterial dehydrogenase uses an organic compound as an electron acceptor, oxidizes D(-)-lactate and is cyanide sensitive. Moreover, the algal and bacterial dehydrogenases do not produce H_2O_2. Recently, a novel glycolate dehydrogenase in the mitochondria of *Arabidopsis thaliana* (*At*GDH) was reported (Bari *et al.*, 2004). The new enzyme is dependent on organic co-factors and resembles algal glycolate dehydrogenase in its enzymatic properties. It has an open reading frame (At5g06580) with homology to the *glc*D subunit of the *Escherichia coli* glycolate oxidase and to yeast D-lactate dehydrogenase (*Sc*DLDH). *At*GDH shows all the properties of a glycolate dehydrogenase. It oxidizes D(-)-lactate over L(+)-lactate, and is cyanide sensitive. Therefore, it can be clearly discriminated from the so-far-described higher plant glycolate-oxidizing enzymes.

1.6 The aim of the present study

During photorespiration, Rubisco oxygenase activity results in the oxidation of RuBP to form phosphoglycerate and phosphoglycolate, the phosphoglycerate enters into the Benson-Calvin cycle (C_3-cycle) to form carbohydrates. On the other hand, phosphoglycolate enters in the photorespiratory cycle to regenerate phosphoglycerate after a series of reactions occurring in the chloroplast, peroxisome and mitochondria (see figure 1.4). In the progress of this pathway, CO_2 is released in mitochondria through the conversion of glycine to serine by the mitochondrial glycine decarboxylase/serine hydroxymethyl transferase enzymes GDC/SHMAT. The CO_2 release in the mitochondria during photorespiration results in approximately 25% loss of the carbon from phosphoglycolate (Leegood *et al.*, 1995).

The present study aims to introduce new methods for the partial suppression of photorespiration resulting in an improvement of CO_2 fixation and an increase in the yield in C_3 plants. The loss of CO_2 during photorespiration is due to the fact that CO_2 release and CO_2 fixation are separated in two different organelles. Thus, the proposed biochemical pathways (details of these pathways are described in the results session) are aiming to provide

genetically modified C_3 plants showing a reduced photorespiratory CO_2 release inside their chloroplasts. Parts of the novel pathway have been established in tobacco by Rafijul Bari (Institute for Biology I, RWTH-Aachen, Germany 2004). The aim of the present study was to establish the complete pathway in *Arabidopsis thaliana* and show by physiological, biochemical and biophysical analysis whether this pathway results in a reduction of photorespiration and increased photosynthetic performance or not.

The new biochemical pathways that I aim to establish inside the plant chloroplast deal with the glycolate metabolism; the first component exported from the chloroplast during photorespiration. The first pathway deals with glycolate metabolism in the same way as in *E. coli* using the GDH, TSR and GCL genes as described above (1.5). The second pathway deals also with glycolate metabolism using TSR and GCL genes from *E.coli* but glycolate dehydrogenase gene from *Arabidopsis thaliana* (*At*GDH without its mitochondrial targeting peptide) fused to a chloroplast targeting peptide (cTP-*At*GDH) (See the result session).

In the present study, all enzymes required to establish the biochemical pathways should be cloned. Transgenic *A. thaliana* plants expressing those enzymes should be generated. It was expected to prove that the enzymes involved in the establishment of the two pathways are active in the transgenic plants. Additionally, it was expected to implement physiological and biochemical analysis using the generated transgenic plants in order to prove the efficiency of the novel pathways.

2   MATERIALS AND METHODS

2.1 Materials

2.1.1   Chemicals and consumables

The chemicals used throughout the work were purchased from the following companies: Amersham Pharmacia Biotech (Freiburg), BioRad Laboratories GmbH (München), Calbiochem (Bad Soden), Carl Roth GmbH (Karlsruhe), Eurogentec (Cologne), Hartmann Analytic (Braunschweig), Invitek (Berlin, Germany), Duchefa Biochemie (Haarlem, Netherlands), Invitrogen (Leck, Netherlands), KMF Laborchemie Handels GmbH (St. Augustin), Kodak (Stuttgart), Macherey-Nagel (Düren), MBI Fermentas (St. Leon-Rot), Metabion (Planegg-Martinsried), Molecular Probes (Leiden, Netherlands), New England BioLabs (Frankfurt), Novagen (Darmstadt), Pharmacia (Freiburg), Promega (Madison, USA), QIAGEN (Hilden), Roche Applied Science (Mannheim), Röhm (Darmstadt), Sigma (Taufkirchen), Serva (Heidelberg) Sigma ARK (Taufkirchen).

The consumables were obtained from: Agilent technologies, Applied Biosystems (Darmstadt), Biometra (Göttingen), BioRad Laboratories GmbH (München), Eppendorf (Hamburg), Fuji (Düsseldorf), GGA GmbH (Moers, Germany), Gibco BRL (Eggenstein), Greiner (Solingen), Hanna Instrument (Kehl, Germany), Heraeus (Osterode), Hewlett Packard (Germany), Herolab (Wiesloch) Kodak (Stuttgart), Kontron Instruments (München), Labomedic (Bonn), Leica (Heidelberg), LI-COR$^{®}$ Biosciences (Lincoln, USA), Merck (Darmstadt), Millipore (Eschborn), MWG Biotech (München), Pharmacia (Freiburg), Raytest (Berlin, Germany), Serva (Heidelberg), Schott Glaswerke (Mainz), Sorvall (Bad Homburg), Wissenschaftliche Technische Werkstätten (Weilheim), Whatman (Maidstone, UK).

2.1.2   Enzymes and Antibodies

I) Enzymes

Table 2.1: Enzymes used throughout the work

*Afl*III	MBI Fermentas, St. Leon-Rot
Amyloglucosidase	Roche Applied Science, Mannheim
*Asc*I	New England Biolabs, Frankfurt
*Bam*HI	New England Biolabs, Frankfurt
*Bpu*1102I	MBI Fermentas, St. Leon-Rot
DNaseI	Roche Applied Science, Mannheim

*Ecl*136 II	MBI Fermentas, St. Leon-Rot
*Eco*RI	New England Biolabs, Frankfurt
*Eco*RV	MBI Fermentas, St. Leon-Rot
Fast Start High Fidelity PCR enzyme	Roche Applied Science, Mannheim
Glucose-6-phosphate dehydrogenase	Roche Applied Science, Mannheim
Hexokinase	Roche Applied Science, Mannheim
*Hind*III	MBI Fermentas, St. Leon-Rot
Invertase	Roche Applied Science, Mannheim
Klenow-DNA polymerase	MBI Fermentas, St. Leon-Rot
Lysozyme	SERVA, Heidelberg
*Mlu*I	MBI Fermentas, St. Leon-Rot
M-MLV Reverse transcriptase	Promega, Mannheim
*Nco*I	MBI Fermentas, St. Leon-Rot
*Pme*I	New England Biolabs, Frankfurt
Phosphoglucomutase (PGM)	Sigma Aldrich
Phosphoglucose isomerase(PGI)	Roche Applied Science, Mannheim
*Pvu*I	MBI Fermentas, St. Leon-Rot
*Sgr*AI	New England Biolabs, Frankfurt
T4-DNA-Ligase	New England Biolabs, Frankfurt
Taq-Aachen-DNA polymerase	Institute for Biology I, RWTH-Aachen
*Xba*I	MBI Fermentas, St. Leon-Rot
*Xho*I	MBI Fermentas, St. Leon-Rot
*Sma*I	MBI Fermentas, St. Leon-Rot
*Sal*I	MBI Fermentas, St. Leon-Rot
α-Amylase	Roche Applied Science, Mannheim

II) Antibodies

- Anti-His HRP Conjugate (Horse Radish Peroxidase) (Qiagen, Hilden).
- Anti-GlcD$_{1100}$ antibody produced from chicken (Institute of Biology I, RWTH-Aachen).
- Anti-TSR antibody produced from chicken (Institute of Biology I, RWTH-Aachen).
- Goat anti-chicken antibody (Qiagen, Hilden).

2.1.3   Instruments

- ABI-7000 (Applied biosystems, Darmstadt).

- Agarose gel electrophoresis accessories: electrophoresis chambers, gel carriers and combs (mechanical workshop of the Institute for Biology I, RWTH-Aachen), power sources (BIO-RAD, München)

- Automatic Sequencer: "4200L-2" (LI-COR, Lincoln, USA).

- Centrifuges: "RC-5B" with GS-3 and SS-34 rotors (SORVALL, Bad Hamburg), "Varifuge RF" with 5315 rotor (HERAEUS, Osterode) for Falcon tubes, "Biofuge A" and "Hermle" (HERAEUS, Osterode) for Eppendorf tubes.

- Confocal microscope: Leica TCS-SP spectral confocal microscope (Leica, Heidelberg).

- CO_2 - Analyzer: „BINOS IR-VIS/UV" (LEYBOLD).

- $^{14}CO_2$ - gassing chamber: Plexiglass chamber (200 ml) with pusher (manufactured by the mechanical workshop of the Institute for Biology I, RWTH-Aachen) (designed by Thomas Rademacher, Institute for Biology I, RWTH-Aachen).

- Cuvettes: Quartz glass cuvettes (Hellma), disposable cuvette (Sarstedt).

- Disposable reaction tubes: 1.5 and 2 ml (Eppendorf, Hamburg); 15 and 50 ml (Falcon, Eppendorf, Hamburg).

- Electroblotting apparatus: "mini-transblot" (BIO-RAD, München).

- Electropestle: motor-driving stainless steel pestle for 1.5 ml Eppendorf tubes (driven by a RZO type motor, Heidolph).

- Electroporator Micropulser^{TM} (BIO-RAD, München).

- Electrophoresis chamber: horizontal electrophoresis unit "Multiphor II" (Pharmacia, Freiburg); vertical mini gel apparatus "Mini Protein II Dual Slab Cell" (BIO-RAD, München).

- Eppendorf vaccuspeed concentrator 5301 (Eppendorf, Hamburg).

- Fuji Fluorescence scanner LAS-1000 CCC camera (Raytest, Berlin).

- Fuji Fluorescence scanner FLA-3000 (Raytest, Berlin).

- Fujifilm imaging plate for bioimaging analyzer: "BAS-MS 2040" (Japan).

- Fujifilm intelligent dark box (Raytest, Berlin).

- Fujifilm BAS Cassette 2025 (Raytest, Berlin).

- GC/MS- system: "6890 N network-GC-system" Agilent technologies.

- Hettich Centrifuge Rotina 35 (Tuttlingen, Germany).

- Hewlett Packard (*hp*) gas chromatograph chemstation 5890- series II (Germany).

- Hewlett Packard (*hp*) Mass selective detector series 5971 (Germany).

- LI-COR® photosynthetic portable measuring device Version 5 (Lincoln, USA).

- Light microscope Carl Zeiss with 2.5 x and 6.3 x (Germany).

- Microplate spectrophotometer spectra max 340 (Elisa Reader) (USA).

- Microscope: "Dialux 20 (LEITZ) with incident Fluorescence iIluminator"3-PLOEMOPAK,,.

- MSD Direct intel probe autoinjector: "Agilent technologies 7683 series,,.

- Nitrocellulose membrane: "Hybond C and Hybond ECL,, (Amersham, Freiburg).

- pH-Meter: WTW (Wiss Techn.Werkstatten, Weilheim).

- Photographic apparatus: camera "429K"; software "E.A.S.Y. store Win 32,, (Herolab, Wiesloch).

- Photometer: "Uvikon 930,, (KONTRON) with 12 temperature-controlled cuvette holders; Gene Quant RNA/DNA calculator (Pharmacia, Freiburg).

- Plant growth chamber (Snijders scientific B.V, Tilburg, Netherlands).

- Poly-Prep®- chromatography columns (BIO-RAD, München).

- Protein concentrator Amicon ultra-centrifugal filters (Millipore, USA).

- Scintillation counter: "Ls 5000TD,, (Beckmann, Fullerton, USA).

- Shaker: Innova™ 4340 incubator shaker (New Brunswick Scientific, Nürtingen).

- Sonicator Bandelin Sonopuls GM 70 (Berlin, Germany).

- Sterile filter: with the pore size of 0.22 μm (Millipore, Schwalbach).

- Thermocycler: Biometra T personal (Biometra, Göttingen), Thermocycler Primus (MWG Biotech, München), LightCycler (Roche Applied Science, Mannheim).

- Ultrathorax-MERKU: Erich polläne GmbH (Wennigsen, Germany)

- UV-chamber (Bio-Rad, München).

- UV transilluminator: wavelength 302 nm and UVT-20M (Herolab, Wiesloch).

2.1.4 Solutions, buffers and media

Most of the buffers, media and solutions were prepared as described by Sambrook and Russel, 2002 unless supplied with the kits. The pH was adjusted with 1M, 5M and 10M NaOH, 1M and 5M KOH or 37 % (v/v) HCl. Sterilization of all solutions, buffers and media was achieved by autoclaving (20 min; 120°C, 1 bar) or, for thermolabile solutions, by filtration through 0.2 μm filters. Heat-sensitive components, such as antibiotics, were prepared as stock solutions, and added to the medium/buffer after cooling to 50°C.

Buffer and media used during the present work are given in table 2.2.

Table 2.2: List of buffers and media

Name	Component	Concentration
Acrylamide/Bisacrylamide	Acrylamide	30% (w/v)
	N',N'–Methylenbisacrylamide	0.8% (w/v)
Ammonium persulfate (APS)	Ammonium persulfate	10% (w/v)
Ammonia release assay incubation medium	Potassium phosphate buffer, pH 5.8	50 mM
	Sucrose	2%
	Tween20	0.1%
	2,4-Dichlorophenoxy-acetic acid	0.1 mg/L
	Phosphinothricin	25 mg/L
Ammonia release assay Reagent I	Sodium salicylate	0.21 M
	Trisodium citrate	0.085 mol/L
	Sodium tartrate	25 g/L
	Sodium nitroprusside	0.4 mM
Ammonia release assay Reagent II	NaOH	0.75 mol/L
	Sodium dichloro isocyanurate	2.3 mM
Bradford–Solution	Coomassie Brilliant Blue G 250	100 mg/L
	Ethanol 96% (v/v)	50 ml/L
	Phosphoric acid 85% (v/v)	100 ml/L
Catalase activity assay buffer	Sodium, potassium phosphate buffer, pH 7	50 mM
	Hydrogen peroxide	30 mM

Chloroplast extraction buffer	HEPES-NaOH, pH 7.5	50 mM
	EDTA	2 mM
	MgCl$_2$	5 mM
	Triton x-100	0.1%
	Glycerol	20%
Coomassie-fixation solution	Methanol	30% (v/v)
	Acetic acid	10% (v/v)
D-Lactate Dehydrogenase assay buffer	Na-phosphate buffer, pH 7.6	30 mM
	NAD$^+$	4.8 mM
	D-Lactate	2 mM
DNA–Extraction–Buffer	Tris-HCl, pH 8.5	100 mM
	NaCl	100 mM
	EDTA, pH 8.0	10 mM
	SDS	0.2% (w/v)
dNTP–Mix	dATP	2.0 mM
	dCTP	2.0 mM
	dGTP	2.0 mM
	dTTP	2.0 mM
Fumarase activity assay buffer	Sodium-Potassium phosphate buffer, pH 7	5 mM
	Triton X-100	10%
	L-Malate	0.1 M
Gelelectrophoresis–loading Buffer	Kresolred	1 mM
	Sucrose	60% (w/v) in TAE buffer
Glucose and fructose assay buffer	Triethanolamine, pH 7.6	150 mM
	NADP	0.25 mM
	MgCl$_2$	5 mM
	ATP	2.5 mM
Grinding buffer (GB)	HEPES-KOH, pH 8	50 mM
	EDTA	10 mM
	Sorbitol	0.33 M
	BSA	0.5 g/l
	Ascorbate	5 mM
HEPES buffer I	HEPES-KOH, pH 7.5	1 mM

HEPES buffer II	HEPES-KOH, pH 7.5	1 mM
	Glycerol	10% (v/v)
Laemmli-Loading Buffer	Tris-HCl, pH 6.8	100 mM
	SDS	4% (w/v)
	DTT	100 mM
	Saccharose	10% (w/v)
	Bromophenol blue	0.04% (w/v)
Luria Bertani (LB)–Medium	Bactotryptone	1%
	Yeast extract	0.5%
	NaCl	1%
	Agar (for LB plates only)	1.5 % (w/v)
LB-Amp-Plates	Bactotryptone	1%
	Yeast extract	0.5%
	NaCl	1%
	Agar	1.5%
	Ampicillin	100 mg/L
Ligase-Buffer	Tris–HCl, pH 7.8	40 mM
	$MgCl_2$	10 mM
	DTT	10 mM
	ATP	0.5 mM
	PEG 8000	5% (w/v)
MS Medium	Murashige and Skoog Basal medium (Duchefa)	
MS + Kanamycin Medium	MS salt	2.2 g/L
	Plant agar	0.75% (w/v)
	Kanamycin	50 mg/L
MS + Kanamycin + Sulfadiazine Medium	MS salt	2.2 g/L
	Plant agar	0.75% (w/v)
	Kanamycin	50 mg/L
	Sulfadiazine	20 mg /L
MS + Sulfadiazine Medium	MS salt	2.2 g/L
	Plant agar	0.75% (w/v)
	Sulfadiazine	20 mg/L

Multiplex PCR buffer D (10x)	Tris-HCl, pH 8.3	100 mM
	KCl	500 mM
	MgCl$_2$	25 mM
PCR-Buffer (10 x)	Tris-HCl, pH 8.5	100 mM
	KCl	500 mM
	Tween 20	0.5% (v/v)
Percoll-buffer	Percoll	35%
	HEPES-KOH, pH 8.0	50 mM
	Sorbitol	0.33 M
Ponceau S-Red-solution	Ponceau S-Red	0.25% (w/v)
	Acetic acid	1% (v/v)
Protein elution buffer	Tris-HCl, pH 7.5	20 mM
	NaCl	300 mM
	Imidazol	300 mM
Protein extraction buffer	Protein resuspension buffer	
	Ascorbate	0.5% (w/v)
	DTT	5 mM
	Polyclar	2% (w/v)
Protein lysis buffer	Tris-HCl, pH 7.5	20 mM
	NaCl	300 mM
	Glycerol	10%
	DTT	5 mM
	Lysozyme	5 mg/ml
	Triton X-100	0.1%
Protein resuspension buffer	HEPES-KOH, pH 7.5	50 mM
	MgCl$_2$	5 mM
	EDTA	1 mM
Protein wash buffer I	Tris-HCl, pH 7.5	20 mM
	NaCl	300 mM
	Imidazol	5 mM
	NP-40	0.5% (v/v)

Protein wash buffer II	Tris HCl, pH 7.5	20 mM
	NaCl	300 mM
	Imidazol	30 mM
	NP-40	0.5% (v/v)
PBS buffer	Potassium-phosphate, pH 7.2	50 mM
	NaCl	150 mM
SH buffer (1x)	HEPES-KOH, pH 8.0	50 mM
	Sorbitol	0.33 M
Starch assay buffer	Na-Acetate pH 4.8	50 mM
Sucrose assay buffer	Citrate-NaOH, pH 4.6	50 mM
TAE (1 x)	Tris-Acetate, pH 8.0	40 mM
	EDTA, pH 8.0	1 mM
TBE (10 x)	Tris	0.9 M
	Boric acid	0.9 M
	EDTA	0.02 M
TBS buffer	Tris-HCl, pH 7.5	10 mM
	NaCl	150 mM
TBS-Tween buffer	Tris-HCl, pH 7.5	20 mM
	NaCl	500 mM
	Tween 20	0.05% (v/v)
	Triton X-100	0.2% (v/v)
TE (1 x)	Tris-HCl, pH 8.0	10 mM
	EDTA, pH 8.0	1 mM
TFB I	K-Acetate	30 mM
	$MnCl_2$	50 mM
	RbCl	100 mM
	$CaCl_2$	10 mM
	Glycerin	15% (v/v)
TFB II	RbCl	10 mM
	$CaCl_2$	75 mM
	MOPS	10 mM
	Glycerin	15% (v/v)
TLC-solvent-I	N-propanol / NH_3 / H_2O	6 / 3 / 1
TLC-solvent-II	N-propyl-acetate / 90% formic acid / H_2O	11 / 5 / 3

Transfer buffer (1 x)	Tris-HCl, pH 8.3	48 mM
	Glycine	39 mM
	SDS	0.037% (w/v)
	Methanol	20% (v/v)
Tris-Glycine-buffer (1 x)	Tris-HCl, pH 8.3	25 mM
	Glycine	192 mM
	SDS	0.1% (w/v)
TRIZOL	Guanidinthiocyanate	0.8 M
	Ammoniumthiocyanate	0.4 M
	Na-Acetate, pH 5.0	0.1 M
	Glycerol	5% (w/v)
	Phenol solution (H_2O)	38% (v/v)
YEB medium	Nutrient Broth or Beef Extract	5 g/L
	Yeast Extract	1 g/L
	Peptone	5 g/L
	Sucrose	5 g/L
	$MgSO_4$	2 mM
	pH	7.4
YEB-Kanamycin-Carbanecillin- Rifampicin	YEB medium	
	Kanamycin	25 mg/L
	Carbanecillin	50 mg/L
	Rifampicin	100 mg/L

2.1.4 Matrix and membranes

- Hybond^{TM}-ECL^{TM}-nitrocellulose membrane (0.45 μm) from Amersham Pharmacia biotech (Braunschweig) and Whatman no.1 paper from Whatman were used in Western blotting.

- Ni-NTA Agarose (Qiagen, Hilden).

2.1.5 *Escherichia coli* strains

- DH5α. F$^-$, Lambda$^-$, *rec*A1, *end*A1, *hsd*R17 (r$_K^-$, m$_K^+$), (*lac*ZYA-*arg*F), *sup*E44, U169, Φ80d*lac*ZΔM15, *thi*-1, *gyr*A96, *rel*A1 (Hanahan, 1983). This bacterial strain possesses a modified recombination system (*rec*A1), which results in reduced recombination probability, and lacks endonuclease (*end*A1). It was therefore used in the cloning experiments.
- ER2566: New England BioLabs (Frankfurt).

2.1.6 *Agrobacterium* strain

- GV3101 (pMP90RK): Gm^r, Km^r, Rif ^{r} (Koncz and Schell, 1986). This *Agrobacterium* strain contains a non-oncogenic Ti plasmid pMP90RK that represents one component of the binary vector system described by the above authors. This plasmid contains the *vir*-region as well as the genes for gentamycin and kanamycin resistances. After introduction of derivatives of the plasmid pS, this bacterial strain was used for the transformation of *A.thaliana* plants on the basis of kanamycin, sulfadiazine and BASTA (phosphinotricin) resistance.

2.1.7 Plant materials

- *Arabidopsis thaliana* ecotype Columbia (Col 0) plants were used for the stable expression of all genes involved in the novel biochemical pathway.

2.1.8 Synthetic oligonucleotides

The following primers (from Sigma and Metabion) were used for cloning and sequencing of the genes required for the establishment of the novel pathway.

Table 2.3 List of the primers used throughout the work

Name of the primer	Sequence
Actin2-Fw-584	GGT AAC ATT GTG CTC AGT GGT GG
Actin2-Rev-585	GGT GCA ACG ACC TTA ATC TTC AT

|	
AtGDH-FW1-1412	GGATGGAACATGTACTGGAGAACACG
AtGDH-(*Asc* I)-F -693	CG AGG CGC GCC AGG TGC GCG ATA GCT GCC TCC GCC
AtGDH-(*Xba* I)-R -694	TTG CGG ACT CTA GAG GAT CTC AGC GGT
AtGDH-TP-F-742	TAG CGG ATC CGT CAT CAT CGG CTT TGG AT
AtGDH-TP-R-753	TCG AGT CGA CGA AAC ATA CAT GAG G
AtGDH-(cDNA2)-F-912	CCA AAC GAT ATC ATG AAC CCG GGA A
AtGDH-F-158	ACG GAT CCA ATG TT AGG TCC GAA GAA GAA
AtGDH-R-159	ACC TCG AGG AAA CAT ACA TGA GGA GGA ATT
GCL-FW1-1330	CGC ACC GAC TGA AAC CTG CTT C
GCL-FW2-1335	GGA TCA ACT GTG GTC AGG CTG GTC
GCL-(cDNA2)-F-863	ACG CAC CGA CTG AAA CCT GCT
GCL-(*Mlu* I)-184	TCG AAC GCG TTA GGT GCA TGG GGA TGG CAA AAA T
GlcF-ASC-F-335	TCGAGGCGCGCCAGGTGCATGCAAACCCAATTAACTGAAG
GlcF-FW1-1332	GCC GAT AAA GCA CGT CAG GTC AGT
GlcF-FW2-1339	TCG TCA CCG CCA ACA TTG GTT GCC
GlcF-(*Nco* I)-F-563	ACG TCC ATG GGG ATG CAA ACC CAA TTA ACT G
GlcF-XBA-F-336	TCGATCTAGATTATTCCTTTTCAAGGGC
GlcF-(*Xho* I)-R-564	ACG CTC GAG TTC CTT TTC AAG GGC TTG
GlcF-(cDNA2)-F-860	TAC CTC TGT GCG TCA CTG GAT
GlcE-ASC-F-333	TCGAGGCGCGCCAGGTGCATGCTACGCGAGTGTGATTAC
GlcE-FW1-1333	TCG GAA GCT ACG GTT GTC TTG GCG
GlcE-FW2-1337	GCG GCG AAG GAT CGG TAA AAG CAG
GlcE-(*Nco* I)-F-561	ACG TCC ATG GGG ATG CTA CGC GAG TGT GAT TAC
GlcE-XBA-R-334	TCGATCTAGATCAAAGTTCCGCGTACATGCGAC
GlcE-(*Xho* I)-R-562	ACG CTC GAG AAG TTC CGC GTA CAT GCG ACC
GlcE(cDNA2)-F-861	CGT GTT TAA CCC CGG TCG CAT
GlcD-ASC-F-331	TCGAGGCGCGCCAGGTGCATGAGCATCTTGTACGAAGAG
GlcD-FW1-1334	GGC GGG CTG GAG ATG ATG GAT AAC
GlcD-FW2-1338	CGG GAA GAT CCT CGA ACT CTG CGT
GlcD(cDNA3)-F-913	TGC TGA CCC TGG GAA AAA CAT TCC
GlcD-(*Nco* I)-F-559	ACG TCC ATG GGG ATG AGC ATC TTG TAC GAA GAG
GlcD-XBA-R-332	TCGATCTAGATCAGAAACGCTCCAGTTCAGGG
GlcD-(*Xho* I)-R-560	ACG CTC GAG GAA ACG CTC CAG TTC AGG G

GlcD-F (*BamH* I)-218	TCG AGG ATC CCA TGG CTT TCG CTT CAA AAT
GlcD-R (*Sal* I)-219	TCG AGT CGA CGA AAC ATA CAT GAG GAG G
GlcD1100 F-924	ACG TCC ATG GGT GTG TTG TTG GTG ATG GCG
GO in E-coli-F-205	TCGACCATGGGCATCTTGTACGAAGAGC
GO in E-coli-R-206	TCGACTCGAGTTATTCCTTTTCAAGGGC
GT-DEF(cDNA2)-R-865	GCT CAA CAC ATG AGC GAA ACC
GT-DEF Rev-2-1340	CAC ATG AGC GAA ACC CTA TAA GAA CCC T
Oligo dT 18-245	TTT TTT TTT TTT TTT TTT
pS5`-302	GAC CCT TCC TCT ATA TAA GG
pS3`-303	CAC ACA TTA TTC TGG AGA AA
TSR-FW1-1331	CTC AAC CTG GCA CTG CAA AGT GCG
TSR-FW2-1336	AAT ATC ACC CTC GTG GGC GGT AAC
TSR (*Nco* I)-71	ACG TCC ATG GGG ATG AAA CTG GGA TTT ATT GGC TT
TSR (*Xho* I)-72	ACG CTC GAG GGC CAG TTT ATG GTT AGC ATT T
TSR(cDNA2)-F-864	TGC AGG CGC TGG AAT TAA TGG
TSR-Mlu-NEW-269	TCG AAC GCG TTA GGT GCA TGA AAC TGG GAT TTA TTG
T7-Reverse-113	GCT AGT TAT TGC TCA GCG G
T7-Universe-112	AAT TAA TAC GAC TCA TCA CTA TAG GG

2.1.9   DNA-plasmids and vectors

Cloning of *GCL*, *TSR*, *glc*D, *glc*E and *glc*F genes was done during my diploma studies (Rashad Kebeish, Institute for Biology I, RWTH-Aachen; 2002). All genes involved in the novel pathway (*GCL-TSR*, *glc*D-*glc*E and *glc*F genes) were cloned into pTRA-K-rbcS1-cTP, pTRA-Hyg-rbcS1-cTP, and pTRA-PT-rbcS1-cTP vectors respectively. In the current study, cTP-*At*GDH gene (glycolate dehydrogenase homologue from *A. thaliana*) was cloned into pSuper-PAM-Sul-rbcS1-cTP vector. Because of the difficulties in selecting transgenic *Arabidopsis thaliana* plants on hygromycin containing MS medium, *glc*D and *glc*E were recloned into pSuper-PAM-Sul-rbcS1-cTP vector. All those DNA vectors were kindly provided by Thomas Rademacher, Institute for Biology I, RWTH-Aachen). The following vectors were used throughout the work:

2.1.9.1 pTRA-K-rbcS1-cTP plasmid DNA

The Bacterial *TSR* and *GCL* genes were cloned separately and together into pTRA-K-rbcS1-cTP vector (kindly provided by Thomas Rademacher, Institute for Biology I, RWTH-Aachen). For the detailed structures of this vector, see figure 2.1.
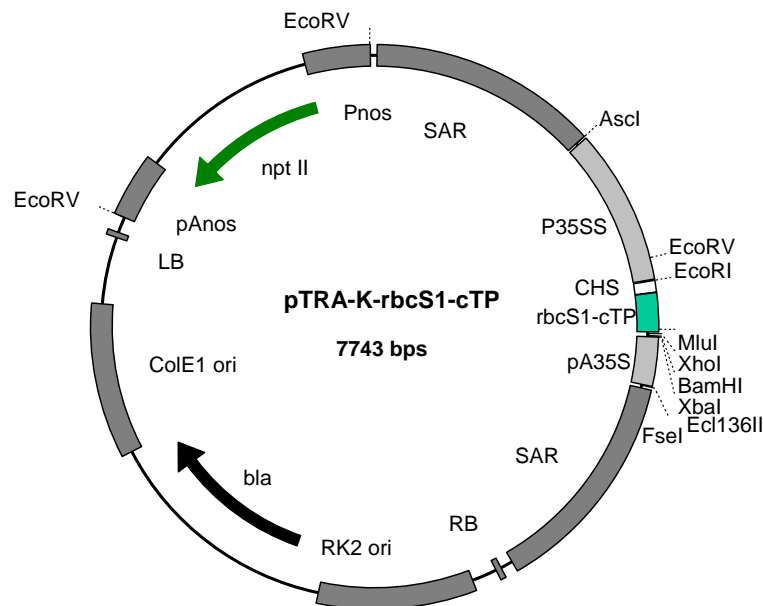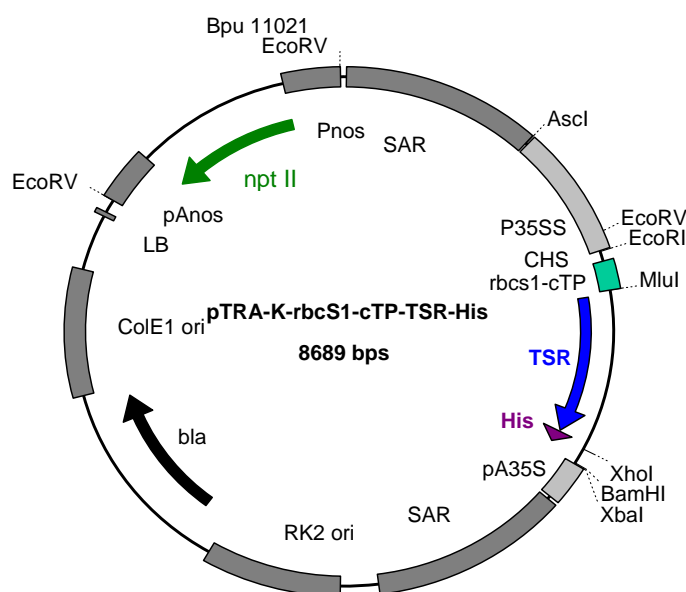

Figure 2.1: **Structure of pTRA-K-rbcS1-cTP plasmid DNA.**

p35SS/pA35S	Promotor (duplication) and Polyadenylation-/Termination sequence from CaMV
bla	ß-lactamase gene for selection in bacteria (ampicillin/carbenicillin resistance).
CHS	The coding sequence for Chalcone synthase.
ColE1 ori	Replication origin for vectors in *E. coli.*
LB and RB	Left and right border sequences of Nopalin-Ti-plasmids pTiT37.
NptII	Neomycin phosphotransferase type II that confers resistance to aminoglycoside antibiotics (i.e. kanamycin and neomycin) and was used for selection of transgenic plants in axenic culture.
PAnos	Polyadenylation promoter of Nopaline synthetase gene from *A.tumefaciens.*
Pnos	Promoter of Nopaline synthase gene from *A. tumefaciens.*
rbcS1-cTP	Transit peptide of the small subunit of Rubisco from potato. The sequence was derived from gi 21562 (gene rbcs1) and cloned by Thomas Rademacher (Institute for Biology I, RWTH-Aachen).
RK2 ori	Replication origin for vectors in *A.tumefaciens.*
SAR	Scaffold Attachment Region from the tobacco RB7 gene (gi U67919).

2.1.9.2 pTRA-K-rbcS1-cTP –TSR His plasmid DNA

The coding sequence for tartronic semialdehyde reductase from *Escherichia coli* (gi: U89279) in translational fusion to a His-tag (TSR-His) was amplified by PCR using pET-TSR plasmid DNA (kindly provided by Rafijul Bari, Institute for Biology I, RWTH-Aachen) as template. TSR-Mlu-NEW-269 and T7-Reverse-113 primers (2.1.8) were also used in the PCR system. The TSR-His insert that was obtained by restriction digestion of the TSR-His PCR product with *Mlu* I and *Bpu* 1102 I restriction enzymes was cloned into the *Mlu* I and *Ecl* 136 II sites of the pTRA-K-rbcS1-cTP vector (for plasmid structure, see figure 2.2).

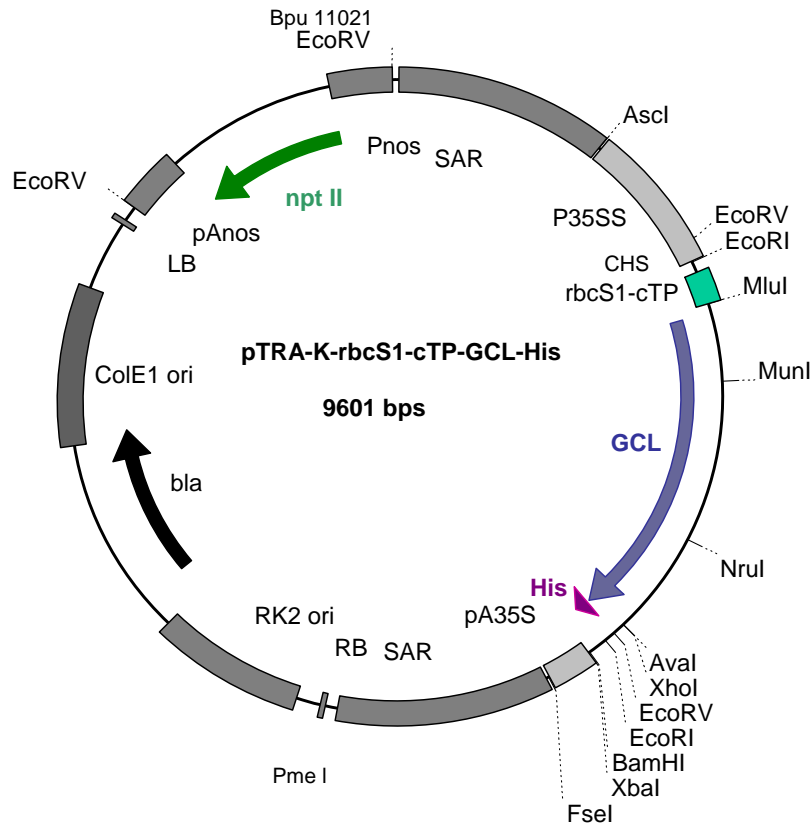**Figure 2.2: Structure of pTRA-K-rbcS1-cTP-TSR-His plasmid DNA.**

For more details, see the basal map 2.1.9.1.

TSR	The coding sequence for tartronic semialdehyde reductase.
His	The coding sequence for His-tag protein.

2.1.9.3 pTRA-K-rbcS1-cTP-GCL-His plasmid DNA

The coding sequence for glyoxylate carboligase from *Escherichia coli* (gi: 146118) in translational fusion to a His-tag (GCL-His) was amplified by PCR using pET-GCL plasmid DNA (kindly provided by Rafijul Bari, Institute for Biology I, RWTH-Aachen) as template. GCL-(*Mlu* I)-184 and T7-Reverse-113 primers (2.1.8) were also used in the PCR system for this purpose. The *GCL-His* insert that was obtained by restriction digestion of the PCR product with *Mlu* I and *Bpu* 1102 I restriction enzymes was cloned into the *Mlu* I and *Ecl* 136 II sites of the pTRA-K-rbcS1-cTP vector (for plasmid structure, see figure 2.3).

Figure 2.3: **Structure of pTRA-K-rbcS1-cTP-GCL-His plasmid DNA**.

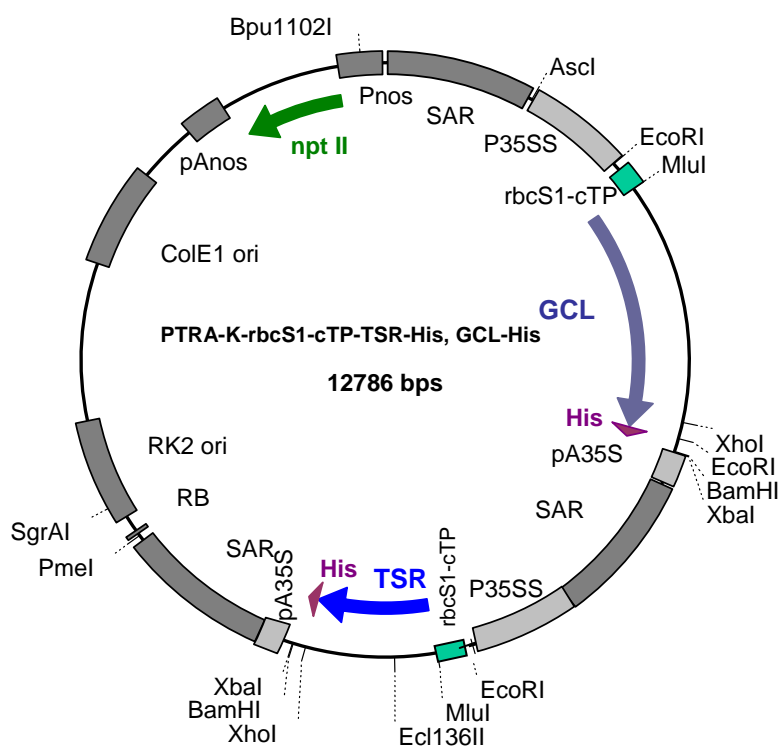For more details, see the basal map 2.1.9.1.

GCL	The coding sequence for glyoxylate carboligase.
His	The coding sequence for His-tag protein.

2.1.9.4 pTRA-K-rbcS1-cTP-TSR-His, GCL-His plasmid DNA

The pTRA-K-rbcS1-cTP-GCL-His plasmid DNA (2.1.9.3) was restricted with *Pme* I and *Bpu*1102 I in order to get GCL-His insert (5284 bps). At the same time, pTRA-K-rbcS1-cTP-TSR-His (2.1.9.2) was digested with *Asc* I, filled with klenow fragment, then restricted with *Bpu*1102 I in order to get the pTRA-K-rbcS1-cTP-TSR-His vector backbone (7502 bps). GCL-His insert was then ligated with the pTRA-K-rbcS1-cTP-TSR-His vector backbone resulting in the production of a double construct for TSR and GCL (pTRA-K-rbcS1-cTP-TSR-His,GCL-His) (for plasmid structure, see figure 2.4). Care was taken that the coding sequence of *GCL* and *TSR* is separated by a scaffold attachment region (SAR) as a transcription separator. This will reduce the possible negative impacts of the first expression cassette onto the second (Padidam and Cao, 2001).

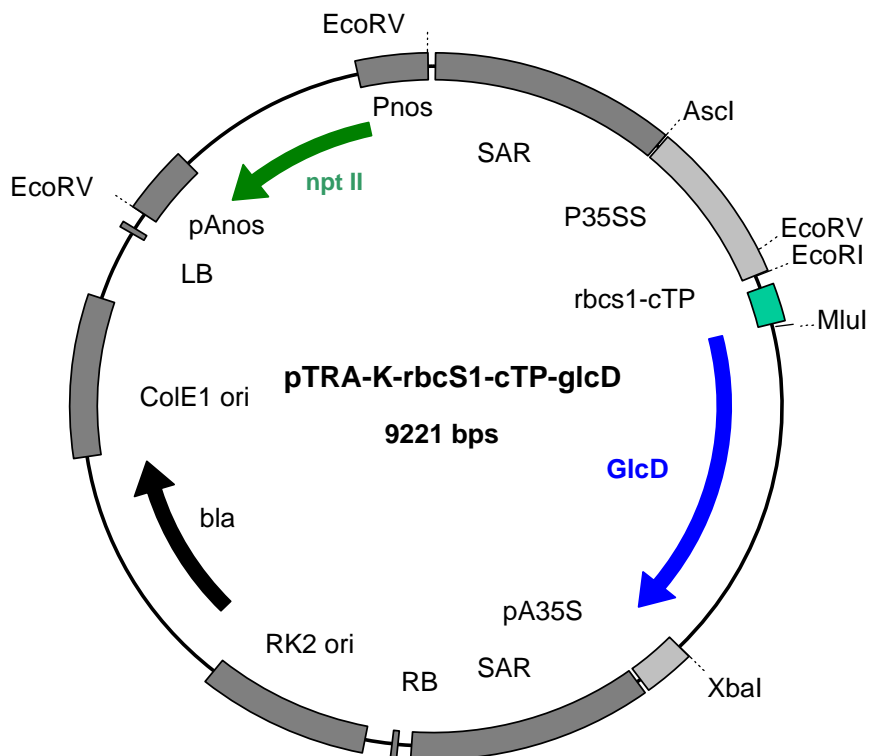**Figure 2.4: Structure of pTRA-K-rbcS1-cTP-TSR-His,GCL-His plasmid DNA.**

For more details, see the basal map 2.1.9.1.

GCL	The coding sequence for glyoxylate carboligase.
TSR	The coding sequence for tartronic semialdehyde reductase.
His	The coding sequence for His-tag protein.

2.1.9.5 pTRA-K-rbcS1-cTP-glcD plasmid DNA

The coding sequence of *glc*D subunit of the bacterial glycolate dehydrogenase was amplified by PCR using GlcD-ASC-F-331 and GlcD-XBA-R-332 primers (2.1.8). A bacterial genomic DNA was also used in the PCR system as template for this purpose. The PCR product was then restricted with *Asc* I and *Xba* I restriction enzymes. The glcD insert was then ligated with pTRA-K-rbcS1-cTP vector (2.1.9.1), which was digested with *Mlu* I and *Xba* I restriction enzymes. Thus, the coding sequence for the *glc*D subunit of glycolate dehydrogenase from *Escherichia coli* (gi/1141710/gb/L43490.1/ECOGLCC) was cloned into the *Mlu* I and *Xba* I site of the pTRA-K-rbcS1-cTP vector (for plasmid structure, see figure 2.5). This plasmid

DNA was used as an intermediate for the recloning of *glc*D into pTRA-Hyg-rbcS1-cTP vector.

Figure 2.5: Structure of pTRA-K-rbcS1-cTP-glcD plasmid DNA.

For more details, see the basal map 2.1.9.1.

GlcD   The coding sequence for the *glc*D subunit of the bacterial glycolate dehydrogenase.

2.1.9.6 pTRA-K-rbcS1-cTP-glcE plasmid DNA

The coding sequence of *glc*E subunit of the bacterial glycolate dehydrogenase was amplified by PCR using bacterial genomic DNA as template and GlcE-ASC-F-333 and GlcE-XBA-R-334 primers (2.1.8). The PCR product was then digested with *Asc* I and *Xba* I restriction enzymes. The resulted glcE insert was then ligated with pTRA-K-rbcS1-cTP vector (2.1.9.1), which was digested with *Mlu* I and *Xba* I restriction enzymes. Thus, the coding sequence of the *glc*E subunit of glycolate dehydrogenase from *Escherichia coli* (gi/1141710/gb/L43490.1/ECOGLCC) was cloned into the *Mlu* I and *Xba* I sites of the pTRA-K-rbcS1-cTP vector (for plasmid structure, see figure 2.6). This plasmid DNA was used as an intermediate for the recloning of *glc*E into pTRA-Hyg-rbcS1-cTP vector.
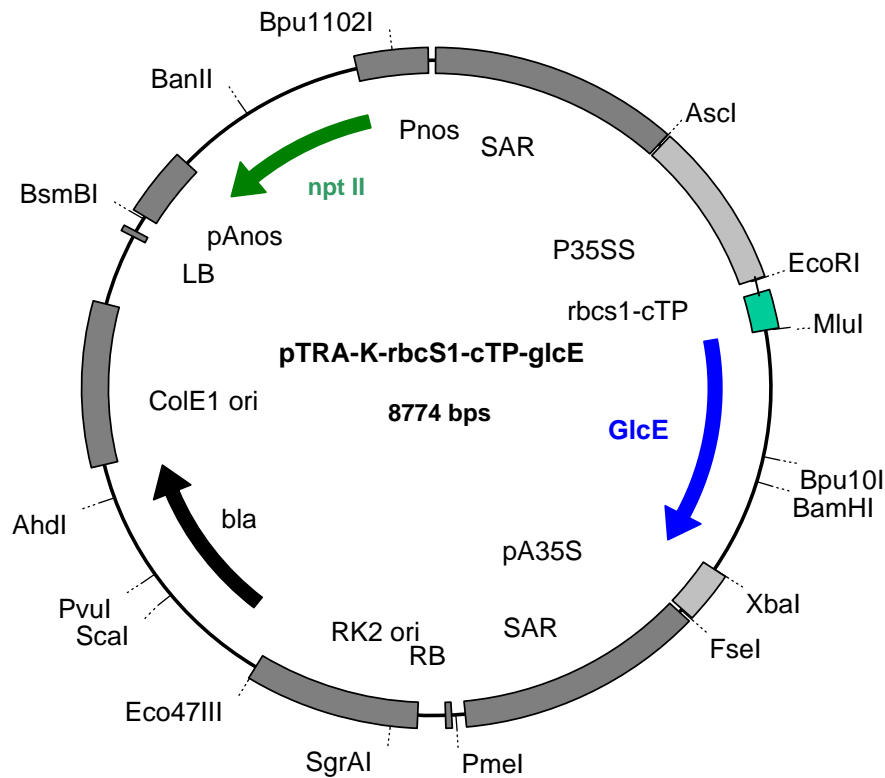
Figure 2.6: Structure of pTRA-K-rbcS1-cTP-glcE plasmid DNA.

For more details, see the basal map 2.1.9.1.

GlcE   The coding sequence for the *glc*E subunit of the bacterial glycolate dehydrogenase

2.1.9.7 pTRA-K-rbcS1-cTP-glcF plasmid DNA

The coding sequence of *glc*F subunit of the bacterial glycolate dehydrogenase was amplified by PCR using bacterial genomic DNA as template and GlcF-ASC-F-335 and GlcF-XBA-F-336 primers (2.1.8). The PCR product was digested with *Asc* I and *Xba* I restriction enzymes. The resulted glcF insert was then cloned into pTRA-K-rbcS1-cTP vector (2.1.9.1), which was digested with *Mlu* I and *Xba* I restriction enzymes. The coding sequence for the *glc*F subunit of glycolate dehydrogenase from *Escherichia coli* (gi/1141710/gb/L43490.1/ECOGLCC) was cloned into the *Mlu* I and *Xba* I site of the pTRA-K-rbcS1-cTP vector (for plasmid structure, see figure 2.7). This plasmid DNA was used as an intermediate for the recloning of *glc*F into pTRA-PT-rbcS1-cTP vector.
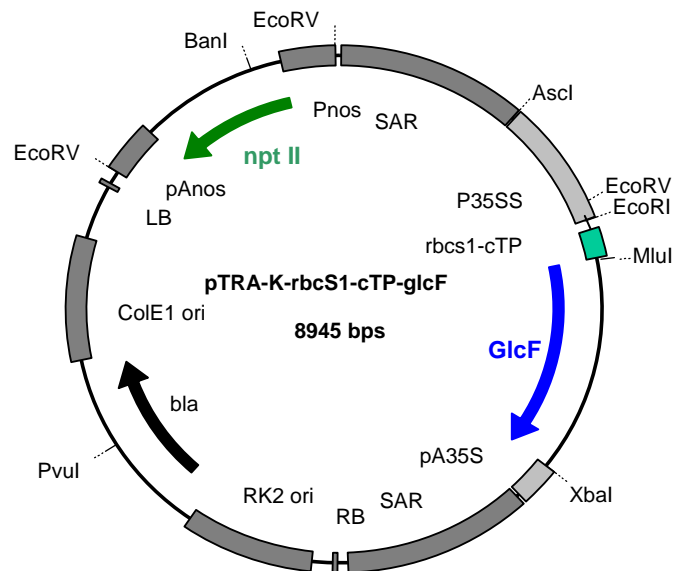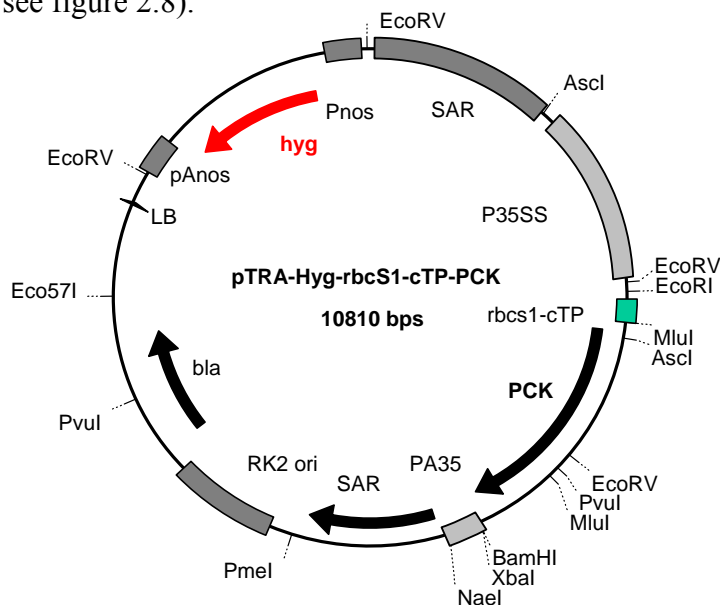
Figure 2.7: Structure of pTRA-K-rbcS1-cTP-glcF plasmid DNA.

For more details, see the basal map 2.1.9.1.

GlcF   The coding sequence for the *glc*F subunit of the bacterial glycolate dehydrogenase

2.1.9.8 pTRA-Hyg-rbcS1-cTP-PCK

This plasmid (kindly provided by Teresa Sikora; Institute for Biology I; RWTH-Aachen) was used to reclone *glc*D and *glc*E together in a double construct in order to get transgenic *A.thaliana* plants that could be selected in MS medium containing Hygromycin (for the plasmid structure, see figure 2.8).

Figure 2.8: Structure of pTRA-Hyg-rbcS1-cTP-PCK plasmid DNA.
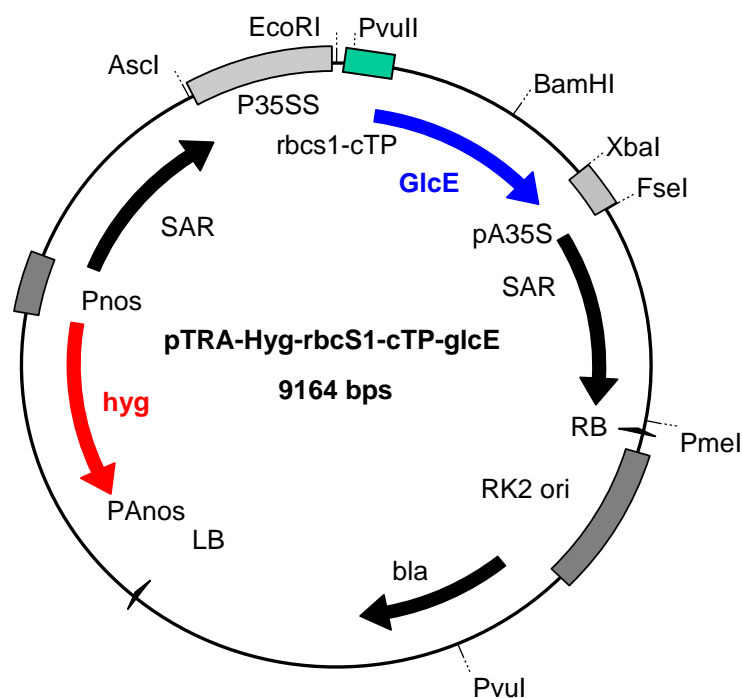
 For more details, see the basal map 2.1.9.1.

Hyg   The coding sequence, which confers resistance to hygromycin

PCK   The coding sequence of phosphoenol pyruvate carboxykinase.

2.1.9.9 pTRA-Hyg-rbcS1-cTP-glcE plasmid DNA

This plasmid was constructed by the ligation of *glc*E insert that was derived from pTRA-K-rbcS1-cTP-glcE plasmid DNA (2.1.9.6) by restriction digestion with *Asc* I and *Pme* I enzymes into pTRA-Hyg-rbcS1-cTP-PCK (2.1.9.8) that was digested with the same restriction enzymes. The coding sequence for the *glc*E subunit of glycolate dehydrogenase from *Escherichia coli* (gi/1141710/gb/L43490.1/ECOGLCC) was cloned in between the *Asc* I and *Pme* I site of pTRA-Hygr-rbcS1-cTP vector (for the plasmid structure, see figure 2.9).

Figure 2.9: **Structure of pTRA-Hygr-rbcS1-cTP-glcE plasmid DNA.**
For more details, see the basal map 2.1.9.1.

GlcE	The coding sequence for the *glc*E subunit of the glycolate dehydrogenase from *Escherichia coli*.
Hyg	The coding sequence, which confers resistance to hygromycin and used for selection of plants in axenic cultures.

2.1.9.10 pTRA-Hyg-rbcS1-cTP-glcD, glcE plasmid DNA

This plasmid was constructed by the ligation of *glc*D insert, which was derived from pTRA-K-rbcS1-cTP-glcD plasmid DNA (2.1.9.5) via restriction digestion with *Asc* I and *Sgr*A I restriction enzymes into pTRA-Hyg-rbcS1-cTP-glcE vector backbone (2.1.9.9). This vector

backbone was obtained by a double digestion with *Pme* I and *Sgr*A I restriction enzymes (for the plasmid structure, see figure 2.10).

Figure 2.10: Structure of pTRA-Hygr-rbcS1-cTP-glcD, glcE plasmid DNA.
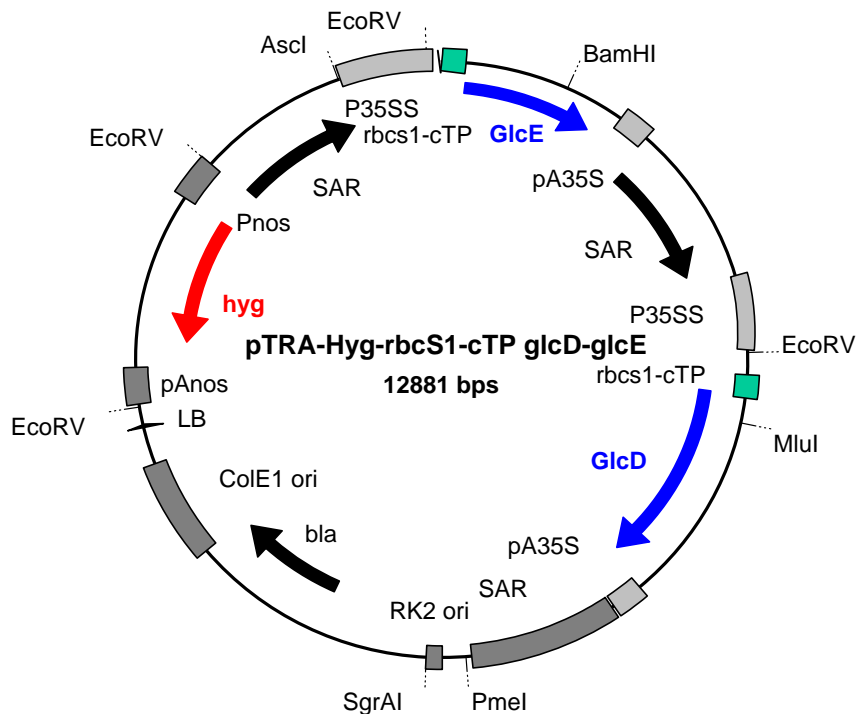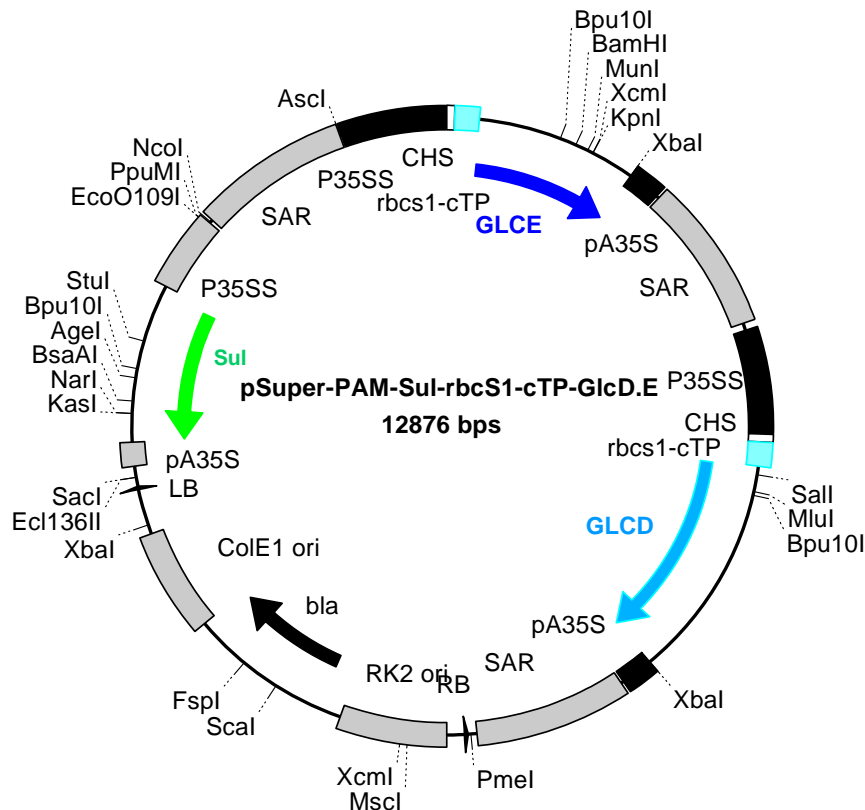For more details, see the basal map 2.1.9.1.

GlcD	The coding sequence for the *glc*D subunit of glycolate dehydrogenase from *Escherichia coli*.
GlcE	The coding sequence for the *glc*E subunit of glycolate dehydrogenase from *Escherichia coli*.
Hyg	The coding sequence that confers resistance to hygromycin and used for selection of plants in axenic cultures.

2.1.9.11 pSuper-PAM-Sul-rbcS1-cTP-GlcD.E plasmid DNA

This plasmid was constructed by the ligation of g*lc*D-g*lc*E insert into pSuper-PAM-Sul-rbcS1-cTP plant expression vector (kindly provided by Thomas Rademacher, Institute for Biology I, RWTH-Aachen). The g*lc*D-g*lc*E insert was derived from pTRA-hyg-rbcS1-cTP-GlcD.GlcE plasmid DNA (2.1.9.10) by restriction digestion with *Asc* I and *Pme* I enzymes. The pSuper-PAM-Sul-rbcS1-cTP vector was obtained by restriction digestion using the same restriction enzymes (i.e. *Asc* I and *Pme* I). Thus, the coding sequences for the *glc*D (gi/1141710/gb/L43490.1/ECOGLCC) and *glc*E (gi/1141710/gb/L43490.1/ECOGLCC) subunits of glycolate dehydrogenase from *Escherichia coli* were cloned into the *Asc* I and

Pme I sites of   pSuper-PAM-Sul-rbcS1-cTP plasmid DNA (for the plasmid structure, see figure 2.11).

Figure 2.11: Structure of pSuper-PAM-Sul-rbcS1-cTP-GlcD.E plasmid DNA.

For more details, see the basal map 2.1.9.1.

GlcD	The coding sequence for the *glc*D subunit of glycolate dehydrogenase from *Escherichia coli*.
GlcE	The coding sequence for the *glc*E subunit of glycolate dehydrogenase from *Escherichia coli*.
Sul	The coding sequence, which confers resistance to sulfadiazine.

2.1.9.12 pTRA-PT-rbcS1-cTP-gfp

This plasmid (kindly provided by Teresa Sikora; Institute of Biology I, RWTH-Aachen) was used to reclone the coding sequence of *glc*F subunit of the bacterial glycolate dehydrogenase into a construct, which is BASTA (phosphinothricin) resistant. This will help in production of transgenic *A.thaliana* plants that could be selected in medium containing BASTA (phosphinotricin) (for the plasmid structure, see figure 2.12).

Figure 2.12: **Structure of pTRA-PT-rbcS1-cTP-gfp plasmid DNA.**

For more details, see the basal map 2.1.9.1.

PAT	The coding sequence that confers resistance to BASTA (phosphinothricin) and was used for selection of transgenic plants in axenic culture and in soil.
gfp	The coding sequence for green fluorescence protein.

2.1.9.13 pTRA-PT-rbcS1-cTP-glcF plasmid DNA

This plasmid was constructed by the ligation of *glc*F insert which encodes the (F) subunit of the bacterial glycolate dehydrogenase into pTRA-PT-rbcS1-cTP plant expression vector. Firstly, glcF insert was derived from pTRA-K-rbcS1-cTP-glcF plasmid (2.1.9.7) by restriction digestion with *Eco*R I and *Xba* I restriction enzymes. Secondly, pTRA-PT-rbcS1-cTP vector was obtained by restriction digestion of pTRA-PT-rbcS1-cTP-gfp plasmid DNA (2.1.9.12) with the same restriction enzymes. Finally, the glcF insert was ligated with the pTRA-PT-rbcS1-cTP vector resulting in the production of pTRA-PT-rbcS1-cTP-glcF (for the plasmid structure, see figure 2.13).

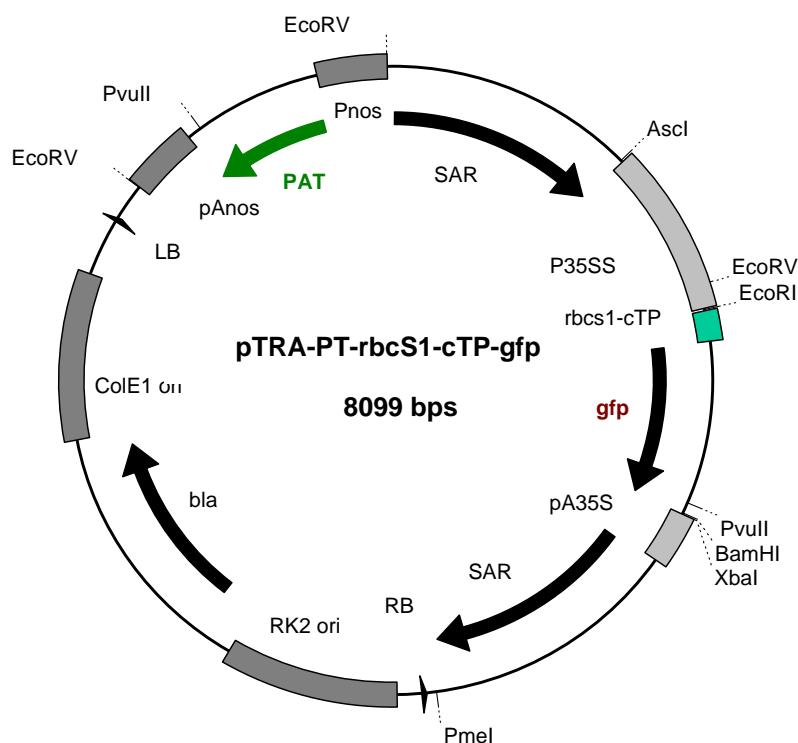**Figure 2.13: Structure of pTRA-PT-rbcS1-cTP-glcF plasmid DNA.**
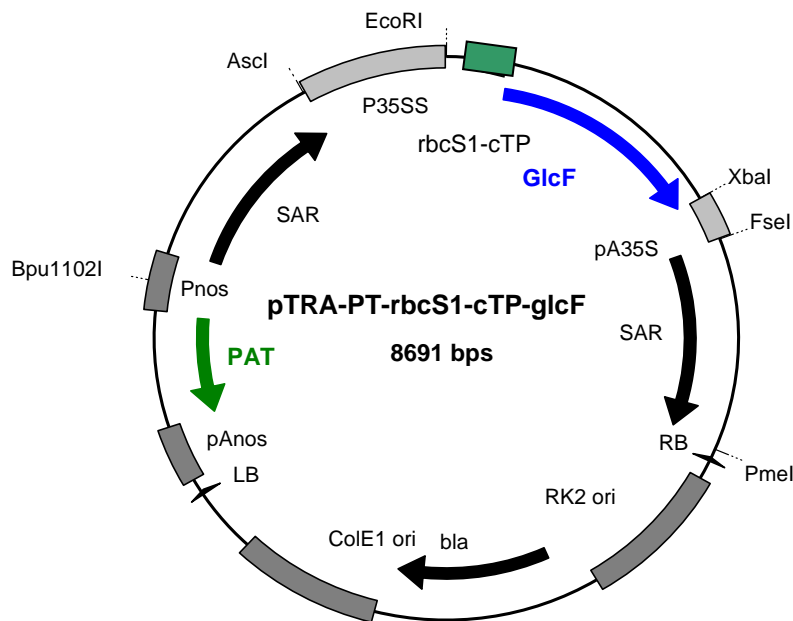
For more details, see the basal map 2.1.9.1.

GlcF   The coding sequence of the *glc*F subunit of the bacterial glycolate dehydrtogenase

PAT   The coding sequence that confers resistance to BASTA (phosphinothricin).

2.1.9.14 pTRA-GB-SB-RFP plasmid DNA

This plasmid was used to obtain the dsRED insert by restriction digestion with *Nco* I and *Xba* I restriction enzymes. This plasmid DNA was kindly provided by Thomas Rademacher (Institute for Biology I, RWTH-Aachen) (for the plasmid structure, see figure 2.14).
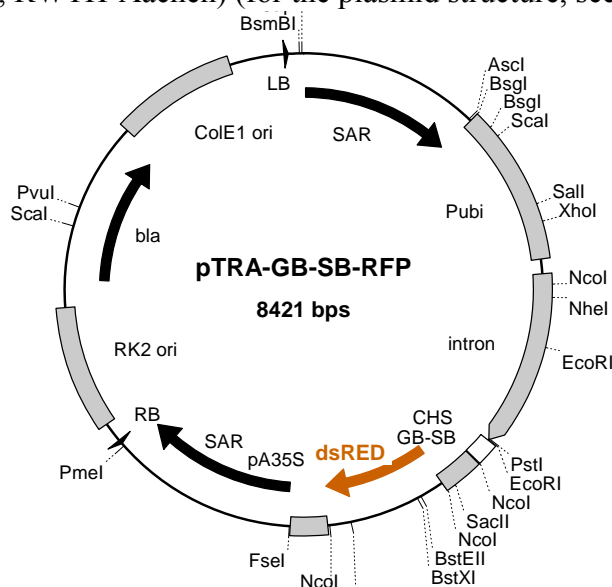
Figure 2.14: Structure of pTRA-GB-SB-RFP plasmid DNA.

For more details, see the basal map 2.1.9.1.
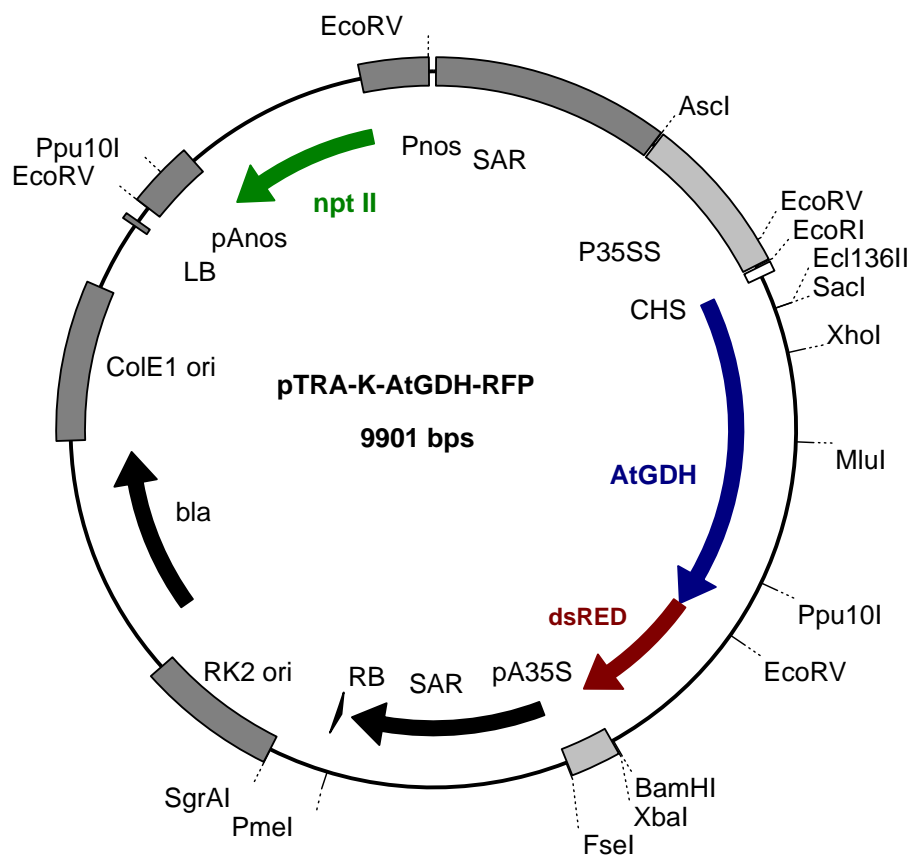
dsRED   The coding sequence for red fluorescence protein.

2.1.9.15 PTRA-K-AtGDH-RFP plasmid DNA

pTRA-GB-SB-RFP plasmid DNA (2.1.9.14) (kindly provided by Thomas Rademacher, Institute for Biology I, RWTH-Aachen) was restricted with *Nco* I, filled with Klenow fragment, and then restricted with *Xba* I enzyme. This restriction step was performed in order to get the dsRED insert. The pTRA-K-AtGDH vector (kindly provided by Rafijul Bari, Institute for Biology I, RWTH-Aachen) was digested with *Sma* I and *Xba* I restriction enzymes in order to obtain the pTRA-K-AtGDH vector. Both dsRED insert and pTRA-K-AtGDH vector backbone were ligated together. This final ligation step resulted in the production of pTRA-K-AtGDH-RFP plasmid DNA (for the plasmid structure, see figure 2.15). This plasmid DNA was used for determination of the actual localization of the complete *At*GDH protein in *Arabidopsis thaliana* plant cells.

Figure 2.15: Structure of pTRA-K-rbcS1-cTP-AtGDH.His plasmid DNA.

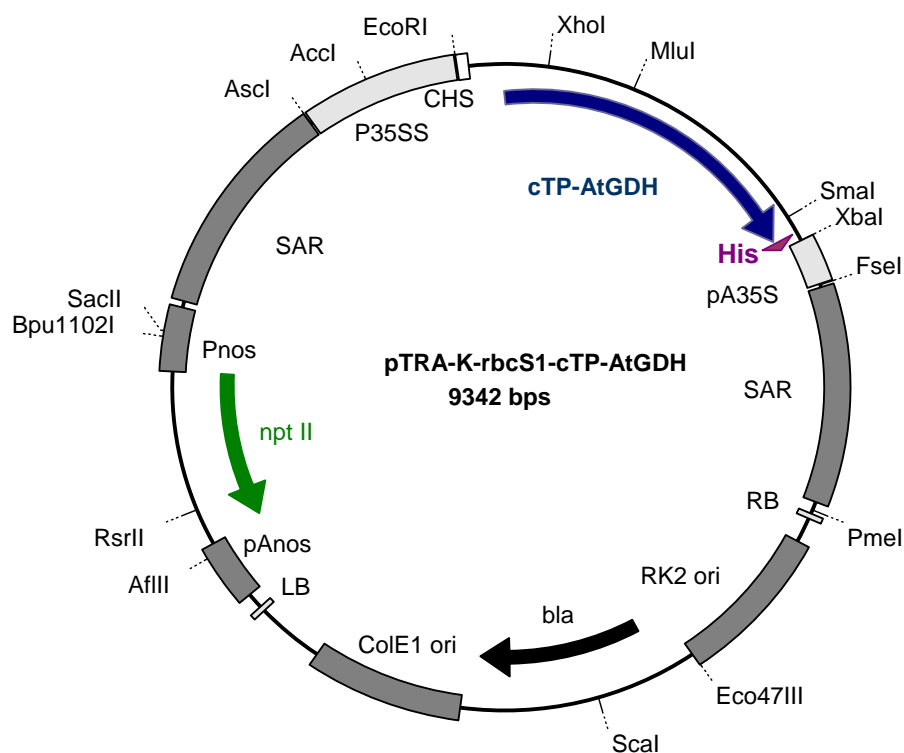For more details about the plasmid structure, see the basal map 2.1.9.1.

AtGDH	The coding sequence for *A. thaliana* glycolate dehydrogenase (At5g06580).
dsRED	The coding sequence for the red fluorescence protein.

2.1.9.16 pTRA-K-rbcS1-cTP-AtGDH plasmid DNA

This plasmid was constructed by the ligation of *At*GDH w/o mTP (without the endogenous **m**itochondrial **T**argeting **P**eptide) insert in translational fusion to a His-tag into pTRA-K-rbcS1-cTP vector. Firstly, *At*GDH w/o mTP gene was amplified by PCR using AtGDH-(*Asc* I)-F -693 and AtGDH-(*Xba* I)-R -694 primers (2.1.8) and pET-AtGDH plasmid DNA (kindly provided by Rafijul Bari, Institute of Biology I, RWTH-Aachen) as template. The PCR product was then digested with *Asc* I and *Xba* I restriction enzymes.secondly, AtGDH w/o mTP insert was cloned into pTRA-K-rbcS1-cTP vector (2.1.9.1.), which was digested with *Mlu* I and *Xba* I restriction enzymes. The coding sequence for the *At*GDH from *A. thalianai* (At5g06580) without the mitochondrial targeting peptide was cloned in between the *Mlu* I and *Xba* I site of pTRA-K-rbcS1-cTP vector (for the plasmid structure, see figure 2.16). This plasmid DNA was used as an intermediate for recloning of cTP-*At*GDH into pSuper-PAM-Sul-rbcS1-cTP plant expression vector that confers resistance to sulfadiazine.

Figure 2.16: Structure of pTRA-K-rbcS1-cTP-AtGDH.His plasmid DNA.
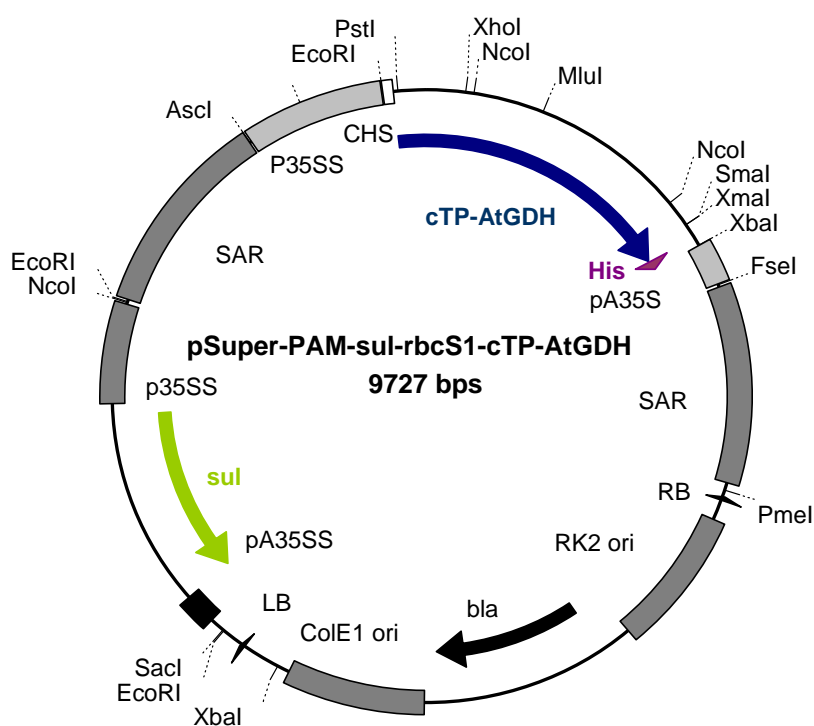
For more details, see the basal map 2.1.9.1

cTP-AtGDH   The coding sequence for *A. thaliana* glycolate dehydrogenase fused to chloroplast targeting peptide.

His   The coding sequence for the His-tag protein.

2.1.9.17 pSuper-PAM-Sul-rbcS1-cTP-AtGDH plasmid DNA

This plasmid was constructed by the ligation of cTP-*At*GDH in translational fusion to a His-tag into pSuper-PAM-Sul-rbcS1-cTP vector backbone. The cTP-*At*GDH insert was derived from pTRA-K-rbcS1-cTP-AtGDH plasmid DNA (2.1.9.16) by restriction digestion with *Asc* I and *Pme* I enzymes. The pSuper-PAM-Sul-rbcS1-cTP vector backbone was also derived by restriction of pSuper-PAM-Sul-rbcS1-cTP plasmid DNA with *Asc* I and *Pme* I restriction enzymes. Thus, the coding sequence for *At*GDH w/o mTP from *A. thalianai* (At5g06580) fused to a chloroplast targeting peptide (cTP) and tagged with a His-tag protein was cloned into the *Asc* I and *Pme* I site of pSuper-PAM-Sul-rbcS1-cTP vector (for the plasmid structure, see figure 2.17).

Figure 2.17: **Structure of pSuper-PAM-Sul-rbcS1-cTP-AtGDH plasmid DNA.**
For more details, see the basal map 2.1.9.1.

cTP-AtGDH	The coding sequence for *A. thaliana* glycolate dehydrogenase w/o mTP fused to a chloroplast targeting peptide.
Sul	The coding sequence, which confers resistance to sulfadiazine.
His	The coding sequence for His-tag protein.

2.1.9.18 pET-TSR-His plasmid DNA

This plasmid DNA was kindly provided by Rafijul Bari; Institute for Biology I, RWTH-Aachen. It was used as a template for the amplification of TSR-His gene by PCR in order to be cloned into pTRA-K-rbcS1-cTP plant expression vector. This plasmid DNA was also used for the expression of TSR protein in ER2566 bacteria. The TSR protein was used further as a control in the enzymatic assays. TSR protein was also used as an antigen for the production of anti-TSR antibodies from chicken (2.2.3.16). For the plasmid structure, see figure 2.18A.

2.1.9.19 pET-GCL-His plasmid DNA

This plasmid DNA was kindly provided by Rafijul Bari; Institute of Biology I, RWTH-Aachen. It was used as a template for the amplification of GCL-His gene by PCR in order to be cloned into pTRA-K-rbcS1-cTP plant expression vector (see figure 2.18B). It is also used for the expression of GCL protein that was further used as a control in the enzymatic assays.
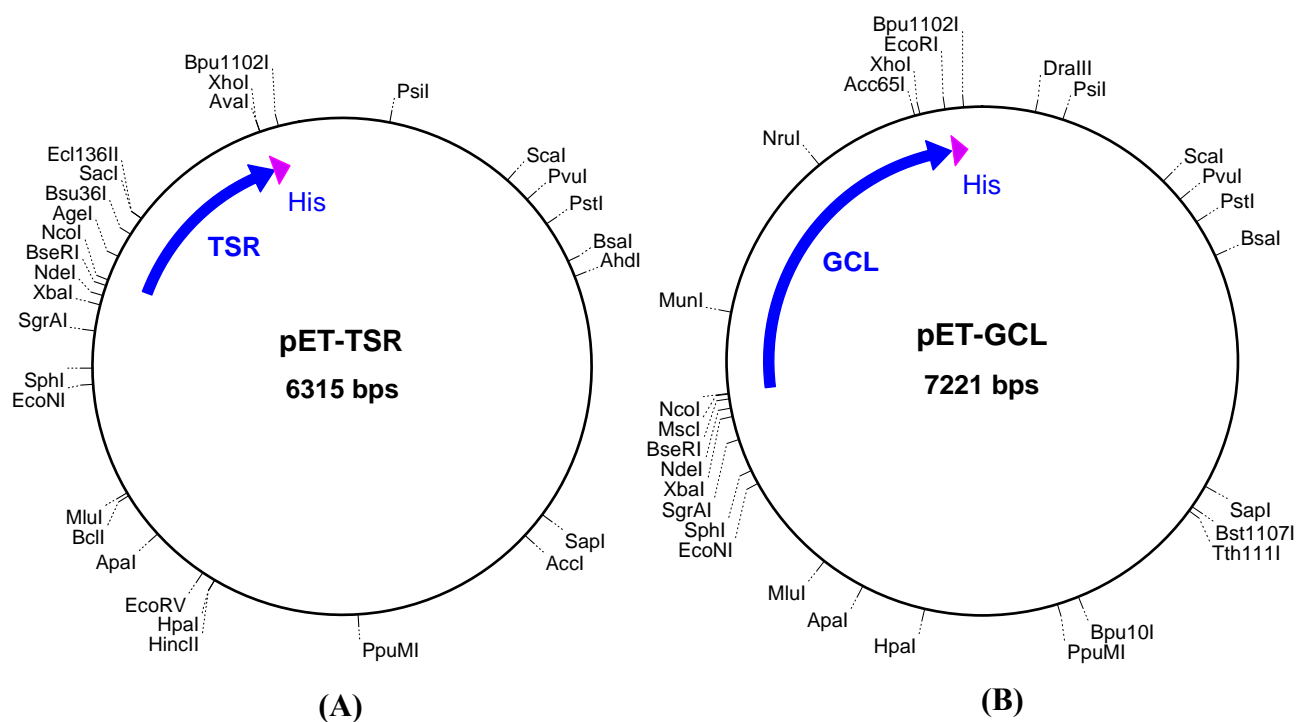
Figure 2.18: Structure of pET-TSR plasmid DNA (A) and pET-GCL plasmid DNA (B).

GCL	The coding sequence for glyoxylate carboligase enzyme.
TSR	The coding sequence for tartronic semialdehyde reductase enzyme.
His	The coding sequence for His-tag protein.

2.1.9.20 pET-GO plasmid DNA

This plasmid was used for the expression of the bacterial glycolate dehydrogenase protein in ER2566 bacteria. The enzyme was used in the glycolate dehydrogenase enzymatic assays (GDH-assay) as a control. This plasmid DNA was kindly provided by Rafijul Bari (Institute for Biology I, RWTH-Aachen). The coding sequences of all glycolate dehydrogenase genes (*glc*D, *glc*E and *glc*F) were amplified by PCR from *E. coli* genomic DNA using GO in E-coli-F-205 and GO in E-coli-R-206 primers (2.1.8). The PCR product was then restricted with *Nco* I and *Xho* I. The GO insert was cloned into pET22b (+) vector that was restricted with the same enzymes (i.e. *Nco* I and *Xho* I restriction enzymes), for the plasmid structure, see figure 2.19.
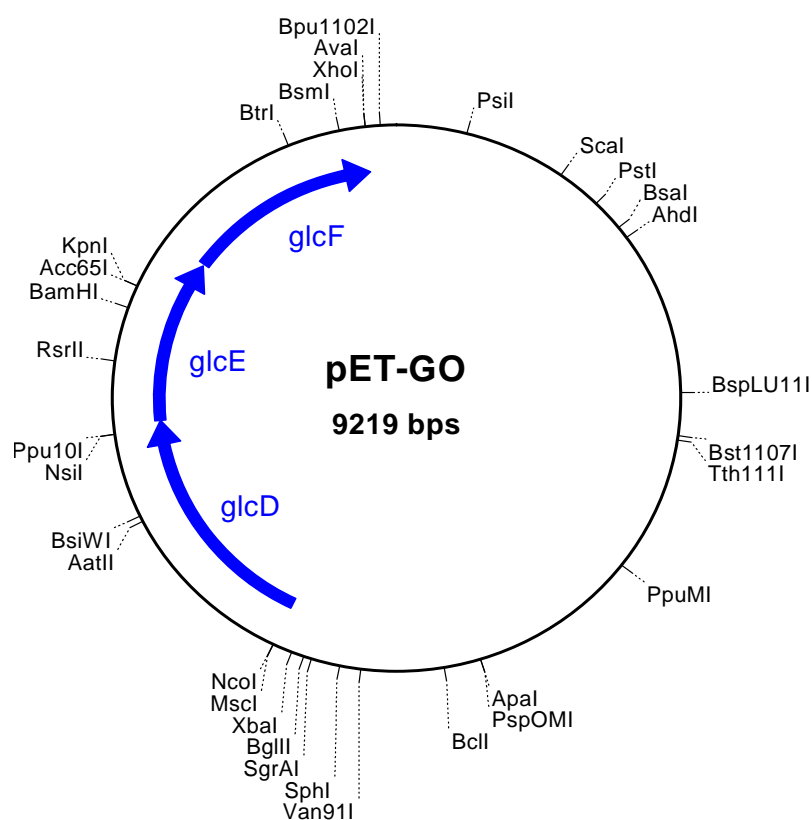
Figure 2.19: Structure of pET-GO plasmid DNA.

GlcD	The coding sequence for the *glc*D subunit of glycolate dehydrogenase from *Escherichia coli* (gi/1141710/gb/L43490.1/ECOGLCC).
GlcE	The coding sequence for the *glc*E subunit of glycolate dehydrogenase from *Escherichia coli* (gi/1141710/gb/L43490.1/ECOGLCC).
GlcF	The coding sequence for the *glc*F subunit of the glycolate dehydrogenase enzyme from *Escherichia coli* (gi/1141710/gb/L43490.1/ECOGLCC).

2.1.9.21 pET-AtGDH w/o mTP plasmid DNA

This plasmid was constructed by the ligation of *At*GDH w/o mTP (without the **m**itochondrial **T**argeting **P**eptide) insert into into pET22b (+) vector. The coding sequence of *At*GDH w/o mTP was amplified by PCR using AtGDH-TP-F-742 and AtGDH-TP-R-753 primers (2.1.8) and pTRA-K-W-AtGDH plasmid DNA (kindly provided by Rafijul Bari, Institute for Biology I, RWTH-Aachen) as template. The PCR product was then restricted with *Nco* I and *Xho* I restriction enzymes. The AtGDH w/o mTP insert was then cloned into pET22b(+) vector that was restricted with the same enzymes (i.e. *Nco* I and *Xho* I restriction enzymes). This plasmid DNA was used for the expression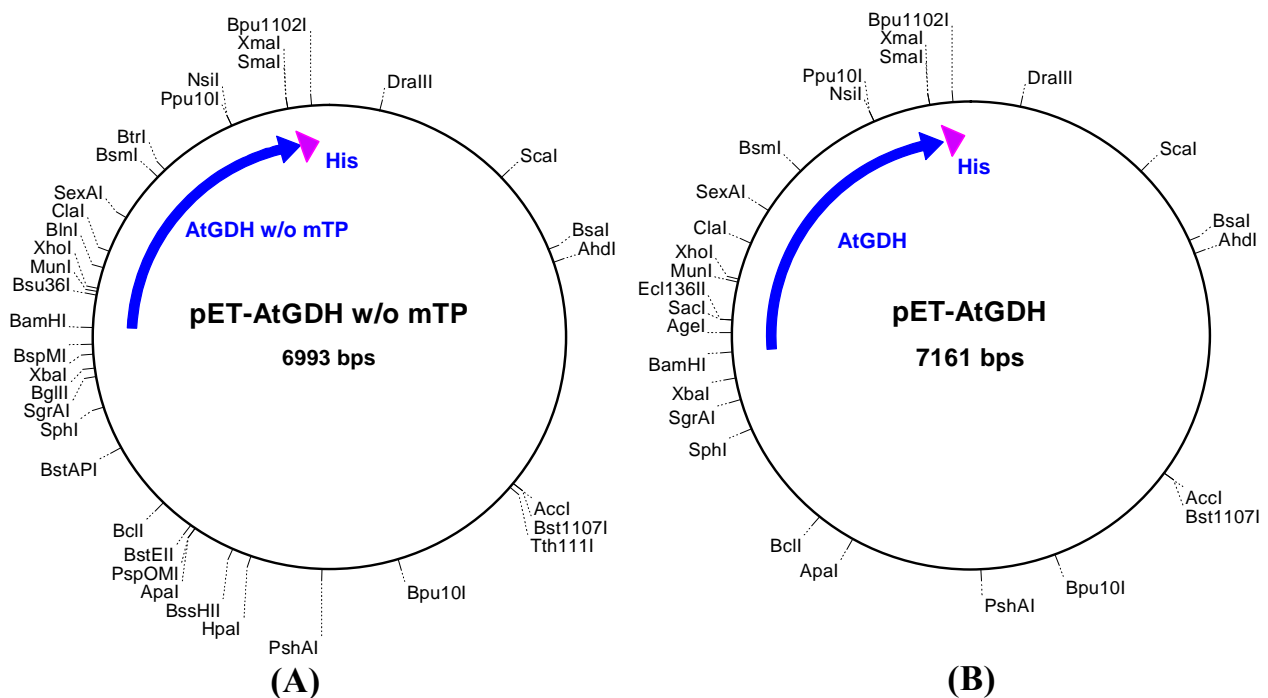 of *A. thaliana* glycolate dehydrogenase (*At*GDH w/o mTP) in ER2566 bacteria. The expressed protein was then used for testing the function *At*GDH w/o mTP protein as a glycolate dehydrogenase *in vitro*. For the pET-AtGDH w/o mTP plasmid structure, see figure 2.20A).

Figure 2.20: Structure of pET-AtGDH w/o mTP (A) and pET-AtGDH (B) plasmid DNA.

|	
AtGDH w/o mTP	The coding sequence for *A. thaliana* glycolate dehydrogenase without its endogenous mitochondrial targeting peptide sequence.
AtGDH	The coding sequence for *A. thaliana* glycolate dehydrogenase with its endogenous mitochondrial targeting peptide sequence (At5g06580).
His	The coding sequence for His-tag protein.

2.1.9.22 pET-AtGDH plasmid DNA

The coding sequence for the complete *At*GDH gene (At5g06580) was amplified by PCR using a cDNA synthesised from *A. thalian* RNA as template and AtGDH-F-158 and AtGDH-R-159 primers (2.1.8). The PCR product was restricted with *Bam*H I and *sal* I enzymes. Then the resulting *At*GDH insert was ligated into the *Bam*H I and *Xho* I sites of the pET22b(+) (Novagen, Darmstadt, Germany). This plasmid DNA was used for expressing *At*GDH protein in ER2566 bacteria. The *At*GDH protein was further used in the enzymatic assays as a glycolate dehydrogenase active control. (See figure 2.20B).

2.1.9.23 pET-GlcD (1100) plasmid DNA

This plasmid was constructed as follows: the coding sequence of the first 1100 bps of *glc*D subunit of the bacterial glycolate dehydrogenase was amplified by PCR using GlcD1100 F-924 and GlcD-(*Xho* I)-R-560 primers (2.1.8) and pTRA-K-rbcS1-cTP-GlcD plasmid DNA (2.1.9.5) as template. The PCR product was then restricted with *Nco* I and *Xho* I restriction enzymes. The *glc*D1100 insert was then cloned into pET22b(+) vector that was restricted with the same enzymes (i.e. *Nco* I and *Xho* I restriction enzymes). This plasmid DNA was used for the expression of 1100 bps fragment of the *glc*D subunit in ER2566 bacteria (see figure 2.21). The expressed protein was used as an antigen for the production of anti- g*lc*D antibodies from chicken (2.2.3.16).
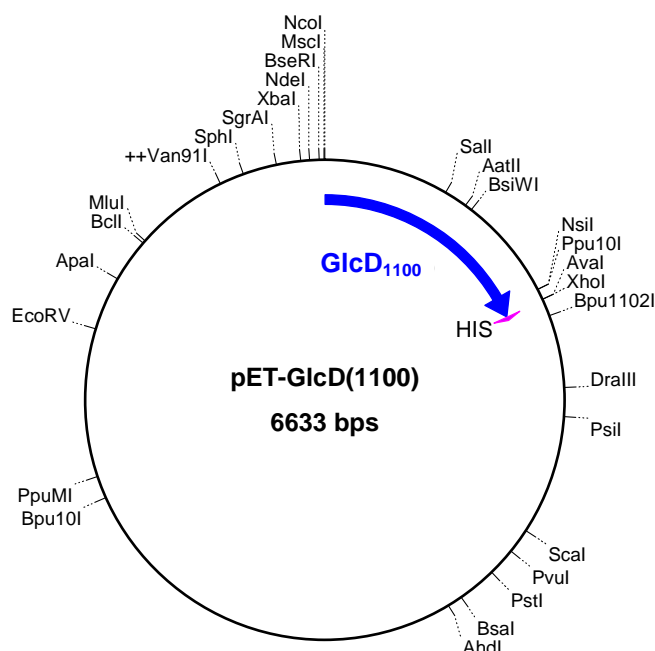
Figure 2.21: The structure of pET-GlcD$_{1100}$ plasmid DNA

GlcD$_{1100}$	The coding sequence of the first 1100 bps of the *glc*D subunit of the *E. coli* glycolate dehydrogenase operon.
His	The coding sequence for His-tag protein.

2.2 Methods

2.2.1   Molecular methods

2.2.1.1 Isolation of plasmid DNA

Plasmid DNA maxi and mini kits (Qiagen and Invitek) were used to isolate plasmid DNA from transformed DH5α bacteria (competent *E. coli* strain) that were transformed with different constructs according to the instructions provided with these kits. For verification of quality and quantity, 2-5 µl of the total DNA eluate were visualized on a 1% (w/v) agarose gel containing ethidium bromide.

2.2.1.2 Isolation of plant genomic DNA

50-100 mg of leaf materials were harvested, frozen into liquid nitrogen and homogenized with pestle. 500 µl of DNA extraction buffer (Table 2.2) were added to the homogenized leaf materials. 1 vol of phenol/CHCl$_3$ (1/1) was added and mixed gently for 10 minutes on a shaker followed by centrifugation at 15000 x g for 10 minutes. The upper phase was transferred to a new tube and 0.1 vol of 3 M Na-acetate (pH 5.2) and 2 vol of ethanol (96%) were added and mixed well. Genomic DNA was precipitated by incubation for 30 minutes at 20°C followed by centrifugation (15000 x g/4°C/20 min). The resulting pellet was washed with 700 µl of 70% ethanol, dried and resuspended in 100-200 µl of sterile H$_2$O.

2.2.1.3 Agarose gel electrophoresis

All the gel electrophoresis was performed according to (Sambrook and Russel, 2002).

2.2.1.4 Isolation of DNA fragments from agarose gel

To isolate DNA fragments (70 bp - 10 kb) from agarose gels, the QIAquick Gel Extraction Kit (Qiagen) was employed according to the manufacturer's instruction.

2.2.1.5 Polymerase chain reaction (PCR)

Polymerase chain reaction (PCR) is a method for enzymatic amplification and modification of a target DNA sequence flanked by two known sequences (Saiki *et al.*, 1988). Two synthetic oligonucleotides complementary to the (+)- and (−)-strands, respectively, of this sequence were used as primers. After heat denaturation of the target double-stranded DNA, these primers hybridize to their opposite strands. New (−)- and (+)-strands fragments are then synthesized across the region between these primers by the catalysis of a thermostable *Taq* DNA polymerase. The newly created DNA strands are themselves templates for the PCR primers. Repeating the cycles of denaturation, primer annealing, and extension results in an exponential accumulation of the target DNA fragment. The reaction conditions (e.g. template concentration, annealing temperature and extension duration) were optimized for individual experiments on the basis of standard conditions.

2.2.1.6 Multiplex PCR

In this type of PCR, it is possible to amplify more than one DNA fragment using more than one primer pairs in the same PCR reaction mixture. In this study, the multiplex PCR was used for checking the transgenic *A.thaliana* plants on the DNA level. Two multiplex PCR systems were used, GTA system and GT-DEF system, in order to check GTA and GT-DEF transgenic *A. thaliana* plants, respectively. In GTA system, GCL-FW1 (1330), TSR-FW2 (1336), AtGDH-FW1 (1412), and GT-DEF- Rev (865) primers (Table 2.3) were used whereas the GCL-FW1 (1330), TSR-FW1 (1331), GlcF-FW1 (1332), GlcE-FW1 (1333), GlcD-FW1 (1334), and GT-DEF- Rev (865) primers (table 2.3) were used in the GT-DEF system. In both systems, the following components were used:

Template	50-150 ng genomic DNA or 1-10 ng plasmid DNA
dNTPS mix	0.5 µl of 10 mM stock concentration
Each forward primer	0.5 µl of 10 pmol stock concentration
Reverse primer	1.5 µl of 10 pmol stock concentration for GTA system and 2.5 µl for GT-DEF system
10 x multiplex PCR buffer D (2.1.4)	2.5 µl
FastStart High Fidelity PCR enzyme	0.25 µl (2.5 units)

DMSO	1 µl of 100% stock (4% final concentration)
H_2O	Up to 25µl

The thermocycler program was as follows:

95 ˚C	2 mins	
95 ˚C	20 sec	
60 ˚C	20 sec	35 X
72 ˚C	1 min	
72 ˚C	5 mins	
4 ˚C	forever	

2.2.1.7 Restriction enzyme digestion

Restriction and ligation reactions were performed as described in (Sambrook and Russel, 2002).

2.2.1.8 DNA sequencing

Sequencing reactions were kindly performed by Jost Muth and colleagues at the Institute of Molecular Biotechnology, RWTH Aachen. 20 pmol of the used primers were added to 1.2-1.5 µg of plasmid DNA and sequencing reactions were performed using the di-desoxy chain termination method with labeled nucleotides and a cycle sequencing protocol (Sanger *et al.*, 1977).

2.2.1.9 Isolation of total RNA from plant leaves

For the extraction of total RNA from transgenic *A.thaliana* leaves, frozen leaves were ground in liquid nitrogen to a fine powder with a mortar and/or pestle. Total RNA was extracted using 1 ml of Trizol (Table 2.2) per 150 mg leaf material, mixed for 5 min, and incubated 5 min at room temperature. 0.1 vol of Bromchlorpropan was added to induce the separation of organic and aqueous phases. The suspension was then mixed for 1 min and incubated at room temperature for 10 min. The sample was centrifuged for 10 min (20000 x g/ 4°C). The upper water phase was carefully transferred to a new reaction tube, and then 1 vol isopropanol was added. The sample was mixed and incubated at room temperature for 10 min then it was centrifuged for 10 min (20000 x g/4°C). The supernatant was decanted and the RNA pellet was washed with 70% (v/v) ethanol followed by spin down (20000 x g/4°C/10 min). The

sample was left some time at room temperature to dry then was resuspended in 30 µl bidest H_2O and visualized on 1% agarose gel with ethidium bromide.

2.2.1.10 First strand cDNA synthesis from RNA.

The isolated total RNA samples from transgenic *A.thaliana* plants were digested with DNase enzyme to remove the genomic DNA. 1 unit of the DNase enzyme was added to 5 µl of the isolated RNA and then the reaction mixture was incubated at 37°C for 10-15 min. The DNase activity in the reaction mixture was stopped by incubating the sample at 65°C for 15 min. 1 µl from the sample was then visualized on 1% (w/v) agarose gel containing ethidium bromide to check whether the genomic DNA was digested or not and to be sure that the RNA was not affected. After that the cDNA was synthesized as follows: 2 µl from the isolated RNA sample (about 100-800 ng) were mixed to 10 µl bidest H_2O and 1 µl Oligo-dT 18 primer (10 pmol/µl). The reaction mixture was incubated 5 min at 65°C, cooled and 2 µl dNTPs, 4 µl MMLV-RT buffer (5 x reverse transcriptase buffer) and 1.5 units of reverse transcriptase enzyme (MMLV-RT) were added. Then the reaction mixture was incubated for 40 min at 37°C. After that the enzyme activity was stopped by incubation at 65°C for 15 min. For negative samples, the enzyme reverse transcriptase was not added, i.e. in the negative samples, no cDNA should be synthesized but conditions are otherwise identical. The synthesized cDNA was used as a template for Real Time RT-PCR amplification.

2.2.1.11 Real Time RT-PCR

The quantitative or Real Time RT-PCR is used not only for the amplification of specific fragments of DNA but also for the quantitative analysis of the resulting products in each cycle throughout the amplification reaction. In this type of PCR, SYBR Green I is used to give the fluorescence signals that indicate the formation of double stranded DNA and as a result the amount of double stranded PCR product can be measured each cycle by this fluorescence. If fluorescence is plotted against cycle number, the accumulation of PCR products can be visualized on a sigmoidal curve. The melting temperature curves, which are formed as a result of plotting the first deviation of the fluorescence against temperature help in the identification of the products in addition to other functions (Meuer *et al.*, 2001). The ABI-7000 (Applied Biosystems) was used for amplification of about 300 bps from the first strand cDNA that was synthesized from the isolated RNA from the transgenic plants. By this, it is possible to check the expression of the transgenes at the RNA level. The instructions in the qPCR[TM] Core Kit for SYBR[®] Green I (Eurogentec) were followed using reading frame specific forward and

reverse primers. The resulting products from the Real Time PCR were visualized on 2% (w/v) agarose gel containing ethidium bromide.

2.2.1.12 Analysis of transcript abundance

RNA was isolated from transgenic plants (2.2.1.9) and first strand cDNA synthesis was performed as described above (2.2.1.10). Quantitative PCR reactions were performed on an ABI PRISM® 7700 Sequence Detection System (Applied Biosystems, Weiterstadt, Germany) following the manufacturer's instructions. Amplifications were performed in the presence of SYBR Green as the fluorescent dye using 2% of a reverse transcription reaction as a template. Reaction kits were derived from Eurogentec (Cologne, Germany) and oligonucleotides were purchased from Metabion. For the detection of GCL, TSR, *glc*D, *glc*E, *glc*F and cTP-*At*GDH transcripts, forward primers were GCL-(cDNA2)-F-863, TSR-(cDNA2)-F-864, GlcD-(cDNA3)-F-913, GlcE-(cDNA2)-F-861, GlcF-(cDNA2)-F-860 and *At*GDH-(cDNA2)-F-912 respectively (Table 2.3). The reverse primer for all these transcripts was GT-DEF- (cDNA2)-R-865 (Table 2.3). The final primer concentration in the reaction mixture for all of these transcripts was 500 nM. For detection of the Actin2 transcripts, primers were Actin2 Fw and Actin2 Rev (Table 2.3) with a final primer concentration of 900 nM in the reaction mixture. The $MgCl_2$ concentration was always 2.25 mM and the dNTP concentration 200 µM. Amplification conditions were 10 min of initial denaturation at 95°C, followed by 40 cycles of each 15 sec denaturation at 95°C and 1 min combined annealing and extension at 60°C.

2.2.1.13 Subcellular localization of *At*GDH

Plant expression vector containing the coding sequence for *At*GDH w/o mTP in translational fusion to Dsred (2.1.9.15) was transformed into *A. tumefaciens* GV3101 by electroporation (2.2.2.2). The recombinant *A. tumefaciens* were selected in YEB medium containing appropriate antibiotics (rifampicin 100 µg/ml, kanamycin 25 µg/ml, and carbenicillin 50 µg/ml). The construct was transferred to *Arabidopsis thaliana* by floral dip transformation (Clough and Bent, 1998a) and regeneration of kanamycin-resistant transgenic plants was carried out according to standard protocols (2.2.6). For Dsred localization and mitochondrial staining, leaves were collected from 4 weeks old plants and cut in small pieces. Protoplasts were isolated by incubating the leaf pieces in protoplast isolation buffer (0.5 M D-mannitol, 5 mM MES pH 5.8, 10 mM $CaCl_2$, 3% (v/v) Rohalase 7069 (Röhm), Rohament PL 2% (v/v) (Röhm) and 0.12% (w/v) Mazeroenzyme R-10 (Serva) at 30°C for 2h. Supernatant containing protoplasts was collected carefully followed by staining with MitoTracker Green (Molecular

Probes) as described by the supplier. Images of the protoplasts were taken with a Leica TCS-SP spectral confocal microscope (Leica). Images were acquired with a 1.2 N.A. 63 x oil immersion PLAN-APO objective. The entire sample was excited with the 488 nm and 568 nm laser line. The confocal sections were collected using a 515-535 nm emission setting for MitoTracker Green, 570-610 nm emission setting for Dsred and 660-720 nm emission setting for chlorophyll fluorescence.

2.2.2   Microbiological methods

2.2.2.1 Culture of bacteria

I) *Escherichia coli*

E. coli was cultured in LB medium on a roller or shaker at 37°C.

II) *Agrobacterium tumefaciens*

A. tumefaciens was cultured in YEB medium at 28°C.

2.2.2.2 Transformation of bacteria

I) *Preparation of competent E. coli (DH5α) cells for heat shock transformation*

A single colony from a LB plate containing competent bacterial colonies was inoculated into 5 ml LB medium and incubated overnight at 37°C with continuous shaking (200 x g/min). 200 ml LB medium were inoculated with 1 ml of the overnight culture. The cells were left to grow at the same conditions until the OD_{600} reached 0.5 - 0.6. Cells were spun down for 10 min (4791 x g/4°C), then washed twice with 50 ml and 25 ml ice-cold TFBI (Table 2.2), respectively. The cells were then incubated on ice for 10 min and spun down by centrifugation for 10 min (4791 x g/ 4°C). The pellet was resuspended afterwards in 4 ml TFBII (Table 2.2) and 100 µl-aliquotes of the suspension were dispensed into prechilled Eppendorf tubes, frozen immediately in liquid nitrogen and stored at -80°C.

II) *Transformation of competent E. coli (DH5α) by heat-shock*

As soon as the competent cells were thawn, plasmid DNA (up to 100 ng) or 1-3 µl from the ligation products were mixed gently with the competent cells and then incubated on ice for 30 min. The cells were incubated at 42°C for 90 seconds and placed directly on ice for 2 min. 1 ml of LB medium was added immediately to the tubes containing the heat shocked bacteria. The transformed cells were incubated at 37°C for 45 min with continuous shaking (200 x g). 100 µl of the transformed cells were plated onto LB-agar plates supplemented with ampicillin and incubated at 37°C overnight.

III) *Preparation of competent Agrobacterium cells for electroporation.*

A single colony of *Agrobacterium tumefaciens* grown on YEB-agar plates containing 100 μg/ml rifampicin (rif) and 25 μg/ml kanamycin (kan) (YEB-rif-kan) was inoculated in 5 ml of YEB-rif-kan medium in a 100 ml Erlenmeyer flask and incubated at 28°C for two days with shaking (200 x g). 1 ml of the culture was transferred into 400 ml of YEB-rif-kan medium and the culture was incubated at 28°C for 15-20 h with shaking (200 x g) until the OD_{600} reached 1-1.5. The cells were chilled on ice for 15 min and spun down by centrifugation (4791 x g/4°C/5 min). The culture medium was decanted and the cells were washed three times with 100 ml, 50 ml and 25 ml HEPES buffer I (Table 2.2), respectively, and one time with 10 ml HEPES buffer II (Table 2.2). The cells were centrifuged (4791 x g/4°C/5 min) and resuspended in 500 μl of sterile HEPES buffer II (Table 2.2). 45 μl aliquots of the suspension were dispensed into prechilled eppendorf tubes, frozen immediately in liquid nitrogen and stored at -80°C.

IV) *Transformation of Agrobacterium by electroporation*

0.2-1.0 μg of plasmid DNA in dest. H_2O was added to a thawn aliquot of *Agrobacterium* electrocompetent cells and incubated on ice for 3 min. The cell/DNA mixture was transferred into a prechilled electroporation cuvette (0.2 cm) and assembled into a safety chamber. After application of the pulse (25 μF/2.5 kV/200 Ω), the cells were diluted in 1 ml of YEB medium in a 2 ml eppendorf tube and incubated at 28°C with shaking (200 x g) for 2 h. Finally, 1-10 μl of the cells were plated on YEB-agar medium containing 100 μg/ml rifampicin (rif), 25 μg/ml kanamycin (kan) and 50 μg/ml carbenicillin (carb) (YEB-rif-kan-carb plates) and incubated at 28°C for 2-3 days.

2.2.3   Biochemical methods

2.2.3.1 Recombinant protein expression in bacteria

The respective constructs were transformed into the bacterial strain ER2566 (2.1.5). For protein expression, a 2 L culture of LB-medium was grown up to an OD_{600} of 0.4. The expression of the proteins was induced by adding 1 mM IPTG and culture growth was continued for 2 h at 37°C. The cells were washed once in 10 mM potassium phosphate (pH 8.0) and were resuspended in the same buffer to give a 15-20% (v/v) cell suspension. After the cells were lysed by sonication on ice (40% duty cycle, 2 x 1 min, Sonicator Bandelin Sonopuls GM 70, Berlin), the cell extract was centrifuged for 30 min at 30000 x g. The

presence of specific protein in the supernatant was tested by Western blot using an Anti-His-HRP conjugate antibodiy (Qiagen) following the protocol provided by the supplier.

2.2.3.2 Extraction of proteins from bacterial cells

Proteins were extracted from bacterial cells either by ultrasonication or by lysozyme method.

I) *Ultrasonication method*

Single colonies of bacterial cells were inoculated into 5 ml LB medium with appropriate antibiotics and were grown overnight at 37°C. The overnight grown bacterial cultures were diluted 100 x and were grown until it reaches the logarithmic growth phase. 50 ml of bacterial culture from the logarithmic growth phase was centrifuged (4791 x g/4°C/10 min) to collect cells. The resulting pellet was washed twice with 20 ml of extraction buffer, resuspended in 1 ml of extraction buffer, and transferred to 2 ml eppendorf tubes for ultrasonication. Ultrasonic cell disintegration was performed on ice by 40% duty cycle, 2 x 1 min (Sonicator Bandelin Sonopuls GM 70, Berlin) with a 30 sec interval. The cell debris was pelleted by centrifugation (15000 x g/4°C/20 min). The supernatant was transferred to fresh tubes on ice and used for determinations of protein concentrations and enzymatic activities.

II) *Lysozyme method*

The bacterial cultures were grown in the same way as described for protein extraction by ultrasonication until OD_{600} reaches at the logarithmic growth phase. The cells were collected by centrifugation (4791 x g/4°C/10 min). The resulting pellet was washed twice with resuspension buffer (table 2.2) and resuspended in resuspension buffer containing 5 mg/ml lysozyme, 5 mM DTT and an appropriate amount of DNase. The cells were then incubated either at room temperature or on ice depending on further experiments. The cells debris was pelleted by centrifugation (30000 x g/4°C/20 min) and the supernatant was transferred to fresh tubes on ice and used for further analysis.

2.2.3.3 Extraction of proteins from plant leaves

For the extraction of proteins from plant leaves, the frozen leaves were ground in liquid nitrogen to a fine powder with a mortar or pestles. 700 µl of protein extraction buffer (Table 2.2) was added to the ground leaf materials followed by centrifugation (30000 x g/15 min/4°C). The supernatant was taken in a 1.5 ml eppendorf tube and the centrifugation step (30000 x g/15 min/4°C) was repeated. The pellet was discarded and the supernatant was transferred into a new 1.5 ml eppendorf tube. The concentration of protein in the supernatent

was measured using Bradford solution and the isolated protein was stored at an appropriate temperature.

2.2.3.4 Determination of protein concentrations in leaf extracts

Proteins were determined according to the method described by (Bradford, 1976). 2 μl of leaf protein extract was mixed with 1 ml of Bradford reagent (Table 2.2). After 15 min incubation at RT, the basic extinction at 595 nm was measured against a reagent blank prepared from 2 μl of the corresponding extraction buffer and 1 ml of Bradford reagent. Bovine serum albumin pH 7.0 (Serva) was used as a standard in a range between 1 and 10 μg.

2.2.3.5 Purification of proteins by Ni-NTA column

A single colony of *E. coli* strain ER2566 harboring recombinant plasmid DNA was inoculated in 5 ml of LB medium containing 100 μg/ml ampicillin and incubated overnight at 37°C. 1 ml of the overnight culture was transferred into 1000 ml LB + Amp medium and cultured at 37°C to OD_{600nm} of 0.4-0.6. The culture was induced for 1-3 h at the same temperature by addition of IPTG to a final concentration of 1 mM. Cells were harvested by centrifugation (4791 x g/4°C/10 min) and resuspended in 5 ml of cold protein lysis buffer. The cells were then disrupted by ultrasonication or lysozyme (2.2.3.2). The His-tagged protein of interest was affinity purified by IMAC. A 0.5 cm (diameter) x 20 cm (length) column (Bio-Rad) was packed with 150 μl of prosep chelating matrix (Ni-NTA agarose). The cleared supernatant was then applied to the column. Non-specifically bound proteins were removed by washing with 10 column vol of protein-wash-buffer I and protein-wash-buffer II (2.1.4). Ni-NTA bound His-tagged proteins were eluted using 3 x 100 μl of protein elution buffer.

2.2.3.6 Extraction of protein from SDS-PAGE

To elute and purify specific protein fragments (10-150 kDs) from SDS-PAGE, the ProteoPLUS^{TM} Kit (Q-BIOgene-France) was used according to the manufacturer's instruction.

2.2.3.7 Isolation of chloroplast from *A. thaliana* plant leaves

5-10 g of leaves from 4 weeks old *Arabidopsis* plants were ground in 80 ml of ice-cold grinding buffer (GB) in an ultrathorax (1 x 10 sec; 75% power) followed by filtration through four layers of miracloth. The chloroplasts were pelleted by centrifugation at 10000 x g for 1 min in a SS34 rotor (Sorvall). The resulting pellet was resuspended in 1 ml 1 x SH buffer. 1

ml of 35% percoll-buffer was overlayed with 0.5 ml of resuspended chloroplast solution in a 2 ml eppendorf tube followed by centrifugation for 3 minutes at 500 x g at 4°C. The supernatant was carefully taken off and the pellet was washed with 1 x SH and centrifuged at 4500 x g for 1 min at 4°C. The washing step was repeated once more. The chloroplast protein was extracted by resuspending the chloroplast pellet in 500-800 μl of chloroplast extraction buffer (Table 2.2) then incubating the extracts on ice for 10 min. The extract was spun down at 30000 x g for 15 min at 4°C. The extracted chloroplast protein either stored at − 80°C or used immediately for enzymatic assays. Catalase and fumarase assays were performed using chloroplast extracts in order to check the prsesnce of peroxisomal and/or mitochondrial contaminations within the extracted chloroplast proteins.

2.2.3.8 Extraction of soluble and insoluble metabolites from *A. thaliana* leaves

The soluble and insoluble metabolites were extracted from leaf discs of *A. thaliana* according to (Stitt *et al.*, 1989). 2 leaf discs (each 1.5 cm^2) per plant were used for this purpose. The plant leaf discs were harvested in 2 ml eppendorf tubes and immersed immediately in liquid nitrogen. 1 ml of 80% (v/v) hot ethanol was added to the leaf discs. Samples were incubated 15 min at 90°C in a heating block. The leaf discs were then transferred into a new 2 ml eppendorf tube containing 1 ml hot 80% (v/v) ethanol and incubated as before. The extracted leaf discs were then transferred into a new 2 ml eppendorf tube and were kept for starch extraction. Ethanol was evaporated either by incubation in a heating block at 90°C or dried in a vaccuspeed. The pellet was then resuspended in 500 μl bidest. H$_2$O and was then spun down. Supernatent was collected and used for the determination of soluble sugars as glucose and fructose. For extraction of starch, 250 μl of 2 M KOH was added to the extracted leaf discs (as described above). The leaf discs were then homogenized and 250 μl of 2 M KOH was added. The samples were then incubated at 95°C for 45 min. The samples were centrifuged and 400 μl from the supernatant were transferred into a new 2 ml eppendorf tube. 900 μl of 1 M acetic acid were then added in order to have a pH of 4.8. Samples were then either stored at -20°C or used directly for measuring the starch content. The glucose, fructose, starch and sucrose contents were estimated enzymatically as described by (Stitt *et al.*, 1989). The enzymatic assay tests were performed in 96 well microtiter plates and the OD$_{340}$ change was measured via microplate spectrophotometer (spectra max 340 ELISA Reader, USA) (2.1.3).

I) *Determination of glucose and fructose content*

Glucose and fructose were extracted as described above (2.2.3.8) and were estimated enzymatically as follows: 20 µl from the previously extracted soluble metabolites were transferred into a microtiter plate well containing 180 µl of the glucose/fructose assay buffer (2.1.4) and the basic extention (λ=340) was measured at 30˚C (blank; E_0). Then 2 µl of HK/G6PDH (0.7 units hexokinase/glucose-6-phosphate dehydrogenase) (Table 2.1) were added. The microtiter plate was then incubated for 15 min at 37˚C and the basic extinction (λ=340) (E_1) was recorded. 2.5 µl of PGI (1.75 units; phosphogluco-isomerase) (Table 2.1) were added to the tested samples. The plate was further incubated for 15 min at 37˚C and the basic extinction (λ=340) (E_2) was recorded.

II) *Determination of starch content*

 For determination of starch contents, 100 µl from the starch extract (insoluble metabolites) were mixed with 400 µl of Na-acetate; pH 4.8 (Table 2.2). Then 1 unit of amyloglucosidase and 2 units of α-amylase (Table 2.1) were added to the assay mixture. Samples were then incubated 15 h at 50°C. During this incubation starch was converted into glucose equivalents. Samples were then spun down and 20 µl of the supernatants were used for measuring glucose-equivalents as described above (2.2.3.8-I).

III) *Determination of sucrose content*

For estimation of sucrose contents, 100 µl from the soluble metabolite extract (2.2.3.8) were mixed with 100 µl of 100 mM citrate-NaOH buffer (Table 2.2). 2 µl of invertase (2 units) were added and the samples were then incubated at 37˚C for 1 h. 20 µl from this mixture were used for the determination of glucose-equivalents as described above (2.2.3.8-I). The amounts of glucose, fructose, sucrose, and starch were estimated from the following equation:

$$c\,(mol\,/\,A) = \frac{\Delta E_{340} \cdot V_K \cdot V_E}{V_P \cdot A \cdot \varepsilon \cdot d}$$

- ΔE_{340} = $E_{end} - E_{blank.}$
- V_K (L): Volume of the reaction mix (here, 0.0002 L)
- V_E (L): Volume of the metabolite extracts (here, 0.0005 L)
- V_P (L): Volume of metabolite sample in the reaction mix (here, 0.0002 L)
- A (m^2): the total area of leaf discs used (here, 0.0003 m^2)
- ε (L x mol^{-1} x cm^{-1}): molar extinction coefficient

- NADP$^+$/NADPH: 6310 L x mol^{-1} x cm^{-1}
- NAD$^+$/NADH: 6220 L x mol^{-1} x cm^{-1}

- d (Cocciolone *et al.*): the microtiter plate well length (here, 0.6 cm)

2.2.3.9 SDS-Polyacrylamide Gel electrophoresis

Discontinuous SDS-polyacrylamide gels (for the stacking gel: 5 % (w/v) acrylamide/bisacrylamide 29:1, 0.125 M Tris/HCl, pH 6.8; for the separating gel: 10 % (w/v) acrylamide/bisacrylamide 29:1, 0.375 M Tris/HCl, pH 8.8) were used for the separation of protein samples under denaturing conditions according to (Laemmeli, 1970). The BIO-RAD MINI PROTEIN II apparatus was used for all gel electrophoresis. After preparation, each protein sample was mixed with 5 x SDS-PAGE-samples buffer (Table 2.2), boiled at 95°C for 5 min, chilled on ice and spun down for 5 seconds. Then the boiled sample was loaded into submerged wells. 1 x SDS-PAGE electrophoresis buffer (Table 2.2) was used for the electrophoresis that was performed for 120 min at 120 V/cm. Separated proteins were visualized by gel staining with Coomassie brilliant blue (2.2.3.10) or transferred onto a nitrocellulose membrane for Western blot analysis (2.2.3.11) (Ausubel *et al.*, 1994).

2.2.3.10 Coomassie brillant blue staining

Protein precipitation and non-specific protein staining with coomassie blue (Wilson, 1993) was used to visualize protein bands. The separating gel was placed carefully in coomassie dye solution (2.1.4) and stained for 30 min at room temperature while shaking gently. Non-specific background staining was removed using coomassie-destaining solution overnight at room temperature.

2.2.3.11 Western blot

Electrophoretically separated proteins were transferred from a SDS-PAGE gel to a Hybond^{TM}-ECL^{TM}-nitrocellulose membrane (0.45 μm). A piece of nitrocellulose membrane was cut according to the gel dimensions and soaked in transfer buffer (Table 2.2) for few minutes. The opened gel holder was positioned in a way that the gray panel (cathode) lays flat on the bottom. Then a pre-soaked fiber pad was put on the gray panel of the cassette. Two pieces of transfer buffer saturated Whatman filter paper were placed on top of the fiber pad and overlaid with 5ml transfer buffer. The equilibrated gel was carefully transferred on top of the filter papers. The gel surface was covered with transfer buffer and the pre-wetted nitrocellulose membrane was put on the top of the gel. The surface of the membrane was

submersed with buffer, the sandwich completed by placing two pieces of saturated Whatman filter papers on the top of the membrane and a saturated fiber pad was put on the top of the filter papers. A glass pipette was rolled over the top of the membrane to remove all air bubbles from the area between the gel and the membrane. The cassette setup was closed and the gel holder was transferred to the buffer tank so that the gray panel of the holder faced the black cathode electrode panel. The tank was filled with transfer buffer and placed in an icebox. Protein transfer was performed at 250 mA for 1 h. Upon completion of the protein transfer, the remaining free binding sites on the membrane were washed two times 10 min each with TBS buffer (Table 2.2) at room temperature then incubated 1h or over night in blocking buffer (Table 2.2) at 4°C. The blocked membrane was washed 4 times 10 min each at room temperature with TBS-Tween/Triton buffer (Table 2.2) and two times for 10 min each with TBS buffer then incubated in Anti-His HRP conjugate solution (Qiagen) containing 1/2000-1/1000 dilution of antibody in blocking buffer (Qiagen) at room temperature for 1h. Then the membrane was washed 4 times for 10 min, each time with TBS-Tween/Triton buffer (Table 2.2) at room temperature and 2 times 10 min each with TBS buffer (Table 2.2) at room temperature. Lumi-Light Western blotting substrate (lumi-light stable peroxide solution : lumi-light luminol/enhancer solution = 1:1 from Roche Diagnostics GmbH, Mannheim, Germany) was added and incubated in dark for 5 min then luminescence was recorded on a LAS3000 CCD camera (Raytest) according to the manufacturer's recommendations.

2.2.3.12 Feeding of *A. thaliana* leaf discs with $^{14}CO_2$

The primary fixative products of photosynthesis were characterized by feeding the *Arabidopsis thaliana* leaves with $^{14}CO_2$. The feeding procedures were done as described in the PhD thesis of Thomas Rademacher, institute of biology I, RWTH-Aachen 2002. A $^{14}CO_2$ - gassing chamber (2.1.3) was used for this purpose (figure 2.22). 2 plant leaf discs (1.5 cm^2) were harvested after 4 hs of illumination. The leaf discs were placed on a wetted whatman paper in a petridish and were allowed to be illuminated for 30 min at 100 µmol m^{-2}s^{-1} PFd. 100 µl H_2SO_4 (20%) were mixed with 50 µl $NaH^{14}CO_3$ (12.5 µCi) in a syringe. Once the two components mixed, the $^{14}CO_2$ released into the $^{14}CO_2$-gassing chamber. The released $^{14}CO_2$ was allowed to be mixed with the air inside the feeding chamber via a magnetic stir for one minute. After the illumination period, the plant leaf discs were exposed to the $^{14}CO_2$ for 10 seconds. The labelled leaf discs were placed immediately in a 2 ml eppendorf tube containing hot 80% (v/v) ethanol (95°C) in order to stop the metabolic activities in the leaf discs as well

as to extract their metabolites. The leaf discs were transferred into a new eppendorf tube containing 1 ml hot 80% (v/v) ethanol. This step was repeated twice.
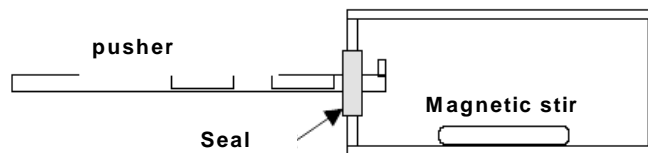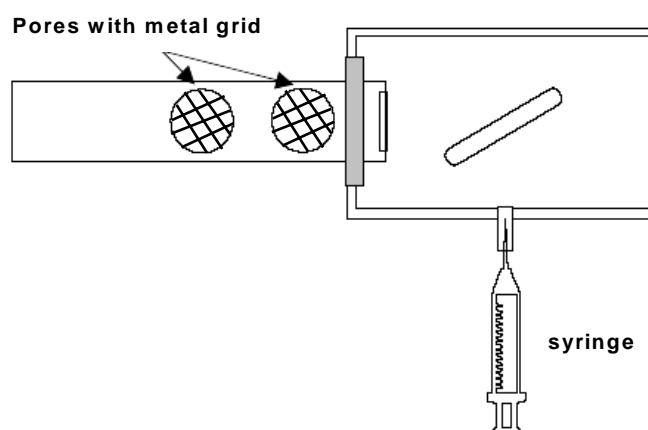
Figure 2.22: Sketch of the $^{14}CO_2$ - gassing chamber.

The whole extract was collected in one eppendorf tube and the ethanol was completely evaporated. The pellet was then resuspended in 20 µl of 40% (v/v) ethanol. The resuspended pellet was spun down and 10 µl of the radioactive extract was characterized on a 2 dimensional thin layer chromatography (2D-TLC). The amount of radioactivity in the extracts was estimated by mixing 10 µl of the extract with 5 ml of the scintillation cocktail (Rotiscent 22 x, ROTH) that was counted after that in the scintillation counter (2.1.3) where the dpm (detection per minute) was determined. The radioactivity in the non-soluble fraction of the extracted leaf discs were counted by mixing the extracted leaf discs with 5 ml of the scintillation cocktail. The ^{14}C- labelled products were characterized on two dimension thin layer chromatography (see 2.2.3.13).

2.2.3.13 Feeding of ^{14}C-glycolate to chloroplast extracts of *A. thaliana*

The ^{14}C-glycolate was fed to chloroplast extracts isolated from *A.thaliana* plants and characterized using two dimension thin layer chromatography following a protocol provided by Martin Parry (Rothamsted Experimental Station, Harpenden; UK). The chloroplast

proteins were isolated from *A.thaliana* plant leaves as described before (2.2.3.7). 20 µl of ^{14}C-glycolate (2 µ*C*i) were used for each single feeding experiment. Feeding of chloroplast extracts isolated from wild type plants with ^{14}C-glycolate was performed in 100 mM potassium phosphate buffer; pH 8 using 25 µg chloroplast proteins. Feeding of chloroplast extracts isolated from transgenic *A. thaliana* plants expressing bacterial or *A. thaliana* glycolate dehydrogenase gene with ^{14}C-glycolate was performed in glycolate dehydrogenase enzymatic assay buffer (2.2.3.17). Feeding of chloroplast extractes isolated from transgenic *A. thaliana* plants expressing GCL and TSR genes with ^{14}C-glycolate was performed in glyoxylate carboligase enzymatic assay buffer (2.2.3.17). Feeding of chloroplast extractes isolated from transgenic *A. thaliana* plants expressing GTA or GT-DEF pathway with ^{14}C-glycolate was performed in two stepwise reactions. The ^{14}C-glycolate was added to glycolate dehydrogenase enzymatic assay buffer, incubated for 20 min at room temperature then same volume of glyoxylate carboligase assay buffer was added. Samples were further incubated for 20 min and the reaction was stopped by adding same volume of hot 98% (v/v) ethanol. In all feeding experiments, ethanol was evaporated and 5-10 µl from the labelled samples were characterized on two dimension thin layer chromatography as follow: Samples were applied to a spot 2.5 cm from the left edge of the glass plate and 2.5 cm from the bottom edge. After applying the samples onto the silica-gel plates (one sample per plate), the plates were placed in a glass tank containing TLC-solvent-I (2.1.4) that was sufficient to cover the bottom half cm of the thin layer plates. Once the solvent developed till 0.5 cm away from the top of plate, the plates were taken out of the chromotank and dried for 1 h. The plates were placed once more in the same solvent and solvent development was repeated. The plates were allowed to dry for 3 h. The plates were then turned 90° so that the starting point lies at the bottom right hand corner and were placed into a glass tank containing TLC-solvent-II (2.1.4). The second solvent was allowed to develop twice as described before. The plates were then dried and subjected to a Fujifilm imaging plate (2.1.3). The TLC plates with the imaging plates were incubated 2 days in dark in a fujifilm BAS Cassette (2.1.3). The radioactive products on the TLC plates were visualised via Fuji Fluorescence scanner FLA-3000 (Raytest, Berlin) and identified based on a standard map.

2.2.3.14 Measurement of total glyoxylate content in *A. thaliana* plants

The total glyoxylate content of *A. thaliana* plants was estimated spectrophotometrically by measuring the basic extinction at 324 nm (Lord, 1972). 100 mg frozen leaf material were ground in liquid nitrogen to a fine powder with a mortar or pestles. 270 µl of 1 M HClO$_4$ were

added and the pestles were washed with the same volume of 0.1 M $HClO_4$. Samples were centrifuged (30000 x g/4 min). 470 µl from the supernatent were transferred into a new eppendorf tube containing 25 µl of 5 M K_2CO_3. The eppendorf tubes were kept opened for 5 min in order to evaporate all the evolved gas (CO_2). Samples were then centrifuged (30000 x g/4 min). 50 µl from the supernatent were transferred into a new eppendorf tube containing 450 µl dest. H_2O (10 x dilution). 50 µl of 12 M HCl were added to the diluted samples that were then incubated for 5 min at room temperature. 100 µl of 0.1 M phenylhydrazine·HCl were added and the samples were further incubated for 10 min at room temperature. The basic extinction at λ_{324nm} was measured compared to a set of potassium glyoxylate standards.

2.2.3.15 Measurement of chlorophyll content of *A. thaliana* plants

The chlorophyll content was measured as described by Nybom (1955); Rau and Senger (1965) as follows: 100 mg of fresh plant leaves were harvested in a 2 ml eppendorf tube and immediately frozen in liquid nitrogen. The leaf samples were ground and 1 ml of 80% acetone were added. Samples were vortexed vigorously then spun down (30000 x g/10 min). The basic extinction at 663, 645, and 440 nm corresponding to Chl A, Chl B, and Carotenoids respectively were measured. The amounts of Chl A, Chl B, and Carotenoids were estimated from the following equations:

$$\text{Chl. A+B} = 20.2 \cdot E_{645} + 8.02 \cdot E_{663}.$$
$$\text{Chl. A} = 9.78 \cdot E_{663} - 0.99 \cdot E_{645}.$$
$$\text{Chl. B} = 21.4 \cdot E_{645} - 4.65 \cdot E_{663}$$
$$\text{Carotenoids} = 4.69 \cdot E_{440} - 0.268 (\text{Chl. A} - \text{Chl. B}).$$

E_{440}: The basic extinction of Carotenoids at 440 nm.

E_{645}: The basic extinction of Chl. B at 645 nm.

E_{663}: The basic extinction of Chl. A at 663 nm.

2.2.3.16 Production of antibodies from chicken

I) *Production of anti-TSR antibodies*

The pET-TSR plasmid DNA (2.1.9.18) was transformed into competent ER2566 bacteria (2.2.2.2). The TSR gene was expressed (2.2.3.1) and total bacterial proteins were isolated from bacteria (2.2.3.2). The TSR protein was purified by Ni-NTA affinity column as described before (2.2.3.5). 200 µg of the purified TSR protein were used for the immunization of chicken within 8 weeks. 50 µg of the TSR protein were mixed with 120 µl adjuvans and

completed to 500 µl end volume with PBS buffer (2.1.3). This mixture was then injected into the muscle of the chicken chest. This immunization process was repeated 3 times each 2 weeks interval. After 2 weeks from the last immunization process, the chicken eggs were collected and anti-TSR antibody was isolated from egg yolk (2.2.3.16-III).

II) *Production of anti-glcD$_{1100}$ antibodies*

The first 1100 bps from the glcD coding sequence were cloned into pET22b(+) bacterial expression vector (see 2.1.9.23). The *glc*D1100 protein was expressed in ER2566 bacteria (2.2.3.1). The total bacterial proteins were isolated simply by boiling the bacterial pellet in lammilli loading buffer (Table 2.2). The isolated protein was subjected to 10% SDS-PAGE and the *glc*D$_{1100}$ (35 kDa) protein band was extracted from the SDS-PAGE fragment as described before (2.2.3.6). The chicken was then immunized by using the purified *glc*D$_{1100}$ protein as an antigen in the same way described above (2.2.3.16-I).

III) *Isolation of total antibodies from egg Yolk*

In order to isolate the total antibodies from egg yolk, egg yolk was separated carefully from egg white. Egg yolk was then transferred into a glass measuring cylinder in order to determine its volume. Four yolk volumes of PBS buffer were added to the egg yolk and the mixture was stirred for 10 min. 3.5% (w/v) PEG-6000 was added to the previous mixture with continous stirring. Samples were placed on ice then centrifuged (12000 g /20 min/ 4°C). The supernatant was filtered through 4 layers of miracloth then 8.5% (w/v) PEG-6000 was added in order to precipitate the antibodies. Samples were then centrifuged (12000 g /20 min/ 4°C). Supernatant was discarded and the pellet was resuspended in 2.5 yolk volumes ice-cold PBS buffer. 12% (w/v) PEG-6000 was added to the sample, stirring and centrifugation steps were repeated. Pellet was resuspended in 0.25 yolk volume ice-cold PBS buffer. In order to remove the PEG-6000, 0.25 yolk volume of 50% ethanol was added and the sample was immediately centrifuged (15000 g /25 min/ 4°C). The supernatant was discarded and the pellet (containing the antibodies) was resuspended in 0.25 yolk volume PBS buffer. The concentration of the isolated antibodies was measured as described before (2.2.3.4). 50% (v/v) glycerol was added to the isolated antibodies and the antibodies were then stored at -80°C.

2.2.3.17 Enzymatic assays

I) *Glyoxylate carboligase (GCL)/Tartronic semialdehyde (TSR) coupled assay.*

The GCL/TSR coupled assay was performeded according to Gotto and Kornberg (1961). The activity of both enzymes was assayed spectrophotometrically by measuring the rate of NADH oxidation when these enzymes were incubated with glyoxylate, in the presence of the required cofactor Mg^{2+} ions and thiamine pyrophosphate. The complete system contained in 1 ml: 100 mM potassium phosphate, pH 7.5; 5 mM $MgCl_2$; 0.5 mM thiamine pyrophosphate; 0.2 mM NADH; 30 µg of chloroplast extract isolated from transgenic *A. thaliana* plants expressing *GCL* and *TSR* genes. OD_{340nm} was recorded for 1-2 min after that the reaction was started by addition of 6 mM sodium glyoxylate.

II) *Glycolate dehydrogenase (GDH) assay*

Glycolate dehydrogenase activity was assayed according to Lord (1972). Bacterial cell extract containing 100 µg of protein or 30 µg of chloroplast extract from transgenic plants were added to 100 µmoles of potassium phosphate (pH 8.0), 0.2 µmole of DCIP, 0.1 ml of 1% (w/v) PMS, and 10 µmoles of potassium glycolate. At fixed time intervals, individual assays were terminated by the addition of 0.1 ml of 12 M HCl. After standing for 10 min, 0.5 ml of 0.1 M phenylhydrazine·HCl was added. The mixture was allowed to stand for a further 10 min, and then the basic extinction due to the formation of glyoxylate phenylhydrazone was measured at λ_{324nm}.

III) *Lactate dehydrogenase (LDH) assay*

Lactate dehydrogenase activity was assayed according to Gutheil (1998). Cell extract containing 50 µg of protein was added to a 1 cm cuvette containing 4.8 mM NAD^+ and 1.0 mM D-lactate, in 0.1 mM Tris·HCl, pH 8.5, in a final volume of 1 ml and the activity was determined from the progress curve at λ_{340nm}. As an inhibitor, 1 mM KCN was added to the reaction mixture before addition of the protein extract.

IV) *Catalase and Fumarase activity assays*

These two assays were performed in order to check the degree of purity of the isolated chloroplast from *A. thaliana* plants (2.2.3.7). Catalase activity assay is an indicator for the presence of peroxisomes whereas fumarase assay is an indicator for the mitochondria.

A) Catalase assay.

Catalase assay was performed as described by Aebi (1984). The catalase activity deals with the H_2O_2 formed in the peroxisomes during the oxidative convesion of glycolate to glyoxylate by the peroxisomal enzyme glycolate oxidase. Firstly the chloroplast extract was added to a quartz cuvette containing 2 ml of the sodium-potassium phosphate buffer (table 2.4) then 1 ml of H_2O_2 was added. The OD_{240nm} change per min was estimated. The catalase activity was calculated according to Lambert-Beer law as follows:

$$v_p = \frac{\Delta A \cdot 1000}{\varepsilon_{mol} \cdot c \cdot d} \left[\frac{\text{mol}}{\text{Min. µg protein}} \right]$$

v_p : The activity in mol $min^{-1}µg^{-1}$

ΔA : The OD_{240} change per min.

ε_{mol}: The molar extinction coefficient of H_2O_2 (3940 L mol^{-1} cm^{-1}).

C : protein concentration in µg ml^{-1}

D : The length of the cuvette (1 cm).

Table 2.4: Catalase assay mixture

Components	Concentration
Na;K-Phosphate buffer, pH 7.0	50 mM
H_2O_2	30 mM

B) Fumarase assay

Fumarase assay was performed as described by Hatch (1978). The fumarase activity deals with the conversion of L-malate to fumarate in the mitochondria. Firstly the chloroplast extract was added to a quartz cuvette containing 900 µl of the sodium-potassium phosphate buffer (table 2.5) then 100 µl of L-malate was added. The OD_{240nm} change per min was estimated. The fumarase activity was calculated according to Lambert-Beer law as follow:

$$v_p = \frac{\Delta A \cdot 1000}{\varepsilon_{mol} \cdot c \cdot d} \left[\frac{\text{mol}}{\text{Min. µg protein}} \right]$$

v_p : The activity in mol $min^{-1}µg^{-1}$.

ΔA : The $OD_{240\ nm}$ change per min.

ε_{mol}: The molar extinction coefficient of fumarate (2440 L mol^{-1} cm^{-1}).

C : protein concentration in µg ml^{-1}.

D : The length of the cuvette (1 cm).

Table 2.5: Fumarase assay mixture

Components	Concentration
Na;K-Phosphate buffer, pH 7.0	5 mM
Triton X-100	10%
L-Malate	100 mM

2.2.3.18 Ammonia release assay

The ammonia release assay was performed as described by Gaunt *et al.* (1998). 4 leaf discs from *A. thaliana* plants (5 mg each) were harvested and placed in 4 wells of a microtiter plate containing 200 µl each of incubation medium (Table 2.2). As a blank, 4 wells containing only incubation medium were used. The tested samples were incubated under 100 Microeinstein light intensity for 6 h at 26°C. 20 µl from each well were transferred into a new microtiter plate containing 100 µl of reagent-I (Table 2.2). Samples were mixed and 100 µl of reagent-II (2.1.4) were added. Samples were then incubated at 37°C in dark for 15 min. The samples were then incubated at room temperature for further 15 min. The presence of ammonium ions in the tested samples resulted in an emerald green to dark blue colour which was quantified by measuring the basic extinction at 655 nm in Microplate spectrophotometer (spectra max 340 ELISA Reader, USA) (2.1.3) compared to a set of ammonium standards.

2.2.4 Gas Chromatography – Mass Spectroscopy (GC-MS)

The gas chromatography mass spectrometry is a coupled procedure for the regulation of gases and volatile substances. First a temporal separation of the compounds is reached by the gas chromatography. The mass spectrometer serves then for the detection of the components and permits additionally their identification on the basis of their mass spectrum.

2.2.4.1 Gas chromatography

Separation of substances in gas chromatography takes place on the basis of their molecular characteristics such as mass and polarity. Once the specimen injected into the injector port of the GC-MS instrument, it vaporizes immediately and then carried by a carrier gas through a capillary column to the detector port of the machine. The carrier gas is usually an inert gas (as Helium). The column is a metal tube, often packed with a sand-like material (modified polysiloxan) to promote maximum separation. As the sample moves through the column, the different molecular characteristics determine how each substance in the sample interacts with the column surface. The column allows the various substances to partition themselves. The

time elapsed between injection and elution is called the retention time. The retention time can help to differentiate between some compounds. The separated substancs move to the end of the column into the detector port of the GC machine. Each component produces a specific spectral peak that is recorded electronically (see figure 2.23).
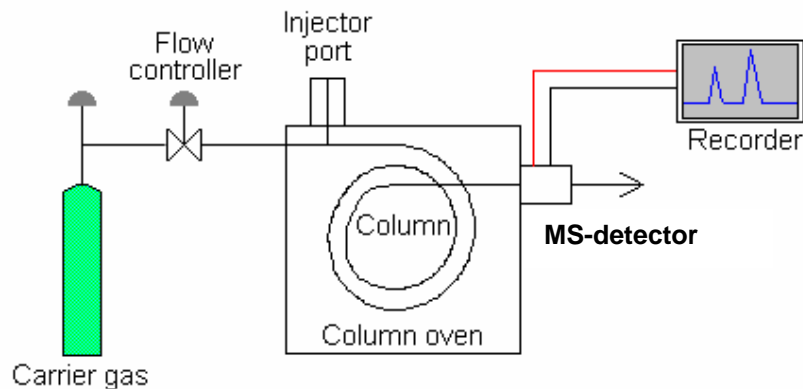
Figure 2.23: Diagramatic representation of the GC-MS system.

The GC-MS machine is working with a standerd temperature program throughout the separating process as follows:

Injector: 250°C

Detector: 280°C

Starting temperature: 70°C, 5 min

Heating level: 5°C/min

Ending temperature: 300°C, 1 min

2.2.4.2 Mass Spectrometry (MS)

The used mass spectrometer is involved in the GC-MS unit (2.1.3) as a detector. This mass spectrometer formed of an ionization source, a molecule accelerator, and a detector. Once the sample left the GC-column, it enters the ionization chamber where a beam of electrons is accelerated with a high voltage. The sample molecules are shattered into well-defined fragments upon collision with the high voltage electrons. Each fragment is charged and travels to the accelerator as an individual particle. In the acceleration chamber the charged particle's velocity increases due to the influence of an accelerating voltage. The charged particles travel in a curved path towards the detector. When an individual charged particle collides with the detector surface, several electrons (also charged particles) emit from the detector surface. These electrons accelerate towards a second surface, generating more electrons, which bombard another surface. Each electron carries a charge. Eventually, multiple collisions with multiple surfaces generate thousands of electrons which emit from the

last surface. The result is an amplification of the original charge through a cascade of electrons arriving at the collector. At this point the instrument measures the charge and records the fragment mass as the mass is proportional to the detected charge. The MS unit produces the output by drawing an array of peaks, the "mass spectrum"(m/t). Each peak represents a value for a fragment mass. Peak's height increases with the number of fragments detected with one particular mass. In the current study, two different modes of the MS-scanning were used; Scan-mode and Single-Ion-Monitoring mode (SIM-mode). In the Scan-mode, the mass spectra (m/t) for all substances present in the tested sample are quantified. This type of scanning is used for qualification and quantification of all the sample components. This will result in an increase in the background as well as in the quantification results. For this, all the quantification experiments for glycine, serine and ribitol was done in SIM-mode. The mass spectra (m/t) for these components were identified by scanning a standard sample containing glycine, serine and ribitol in the Scan-mode of the GC-MS machine. Then the other quantification experiments were performed in the SIM-mode scanning. The main mass spectra for glycine were 147, 174, and 248, for serine were 116, 204, and 218, and for ribitol were 205, 217, and 319.

2.2.4.3 Preparation, derivatisation and injection of samples

In the current study, the amounts of the amino acids glycine and serine in the leaves of *A. thaliana* were quantified. The samples were prepared according to Roessner *et al.* (2000) where 100 mg of leaves from *A. thaliana* plants were harvested and frozen immediately in liquid nitrogen. The frozen leaves were ground in liquid nitrogen to a fine powder with a mortar. 300 µl pre-cold methanol was added. This methanol solution contains 16 µg Ribitol per 1 ml methanol as an internal standard of 25 ng end concentration to be injected into the GC-MS machine. Samples were vortexed and incubated for 15 min at 70°C. 200 µl chloroform was added and then the samples were vortexed vigorously. Then 400 µl dest. H_2O was added and the samples were vortexed vigorously. The samples were then centrifuged (30000 x g) for 10 min. 200 µl from the aquous phase were taken and allowed to dry in the vaccuspeed (2.1.3). After the samples were completely dried, 20 µl pyridine was added. In order to completely dissolving the dried pellets, the samples were incubated 1 h at 37°C. Because the volatility of amino acids is normally small and the separation of substance in GC-MS occurred only in its gaseous phase, it was necessary to derivatize the samples before injecting it into the GC-MS system (see figure 2.24). For derivatizing the samples, 35 µl of the N-Methyl-N-(trimethylsilyl) trifluoroacetamide (MSTFA) was added. Derivatization

makes the substances more volatile. Samples were then incubated for 3 h at 70°C. At the same time, using of pyridine for dissolving the samples after drying is important. Pyridine acts as proton acceptor (Supelco, 1997); thus the reaction balance is directed toward the derivatization reaction.

Serine-N,N,O,O-TMS   **Glycine-N,N,O-TMS**
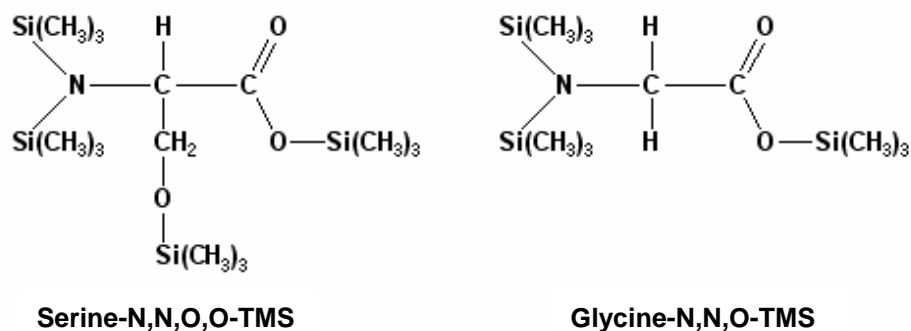
Figure 2.24: The complete trimethylsilylation of glycine and serine.

The figure is showing the full-derivatisation state of the amino acid glycine and serine.
Glycine-N,N,O-TMS = Glycine-N,N,-bis-(trimethylsilyl)-trimethylsilylester; **Serine-N,N,O,O-TMS** = serine-N,N,O-tris-(trimethylsilyl)-trimethylsilylester.

Finally, samples were spun down and 1 µl was injected into the GC-MS machine (2.1.3) using automatic sample injector (2.1.3). In order to determine the mass spectra of the substance of interest (glycine, serine or ribitol), a standard sample containing all the three substances was injected into the GC-MS machine and the scan-mode was used. The scan mode programm was as follow:

01-10 min	Solvent delay for maintaining the filament lifespan.
10-30 min	Main scanning.
30-52 min	MS-detector off.

In the quantification of the amino acids"glycine and serine,,, the SIM-mode was used. The SIM-mode program was as follow:

01-10 min	Solvent delay for maintaining the filament lifespan.
10-16.5 min	Glycine scanning; m/t = 147, 174, and 248.
16.5-20 min	Serine scanning; m/t = 116, 204, and 218.
20-30 min	Ribitol scanning; m/t= 205, 217, and 319.
30-52 min	MS-detector off.

2.2.4.4 Data interpretation

The quantification analysis was done using the „HP chemstation"software as well as the agilent technologies software (2.1.3) provided with the GC-MS system. The maximum spectra, peak area and retention time were quantified via the auto-integration function of involved in this software. The real amounts of the single substances were calculated based on a series of standards (glycine and serine) and corrected by ribitol concentration in each experiment.

2.2.5   Gas-exchange and chlorophyll fluorescence measurements

All gas-exchange and fluorescence measurements were carried out using the LI-COR[®] photosynthesis portable measuring device"Version 5„ (Lincoln, NE) (2.1.3). A leaf chamber fluorometer (LCF) together with an infrared gas analyzer (IRGA) was provided with the measuring device. The measurements were performed according to Lipka *et al.*, 1999 and Pinelli and Loreto, 2003. The gas exchange characteristics of *Arabidopsis* leaves were measured using the previously described device at a leaf temperature of 20-25 °C. The air humidity was kept at 30-50%. The rates of CO_2 assimilation (*A*) and transpiration (*E*) as well as the intercellular CO_2 concentrations (C_i) were calculated automatically by the software provided in the measuring device. Modulated chl.*a* fluorescence emission from the upper surface of the leaf was measured with a pulse amplitude modulation fluorometer that is included in the LCF unit of the measuring device. The quantum efficiency of electron flux through photosystem II (ΦPSII) was estimated according to Genty *et al.* (1989); Maxwell and Johnson (2000) from the ratio of (F'm - Fs)/ F'm (F'm is the maximum fluorescence and Fs is the steady state fluorescence). The rate of photosynthetic electron transport (ETR) was calculated from determinations of ΦPSII as follows: ETR = ΦPSII·I·F/2; where I equals the incident PFD (photon flux density) on leaf level and F the average light absorption factor of the leaf (F = 0.84). The electron requirement for CO_2 assimilation (e/A) was assessed from the quotient of photosynthetic electron transport and the apparent rate of CO_2 assimilation. The CO_2 compensation point (Γ*); „The CO_2 concentration at which no gas–exchange between the leaf and air was detected, i.e. between 30 and 50 ppm" was measured by measuring a series of A C_i-curves at different light intensities (here I used 20, 40, 80, 100, 150, 200, 300 and 600 µmol photon m^{-2} s^{-1}). The A/C_i-curve was etimated by measuring the assimilation rates (A) at different CO_2 concentrations (*C*a) (here I used 40, 60, 80, 100, 150, 200, 250, 300, 350 and 400 ppm). The post illumination burst (PIB) was measured according to Atkin *et al.* (1998) where the plants were dark adapted overnight then plant leaf was

placed in the measuring device under a photorespiratory conditions (i.e. 1000 µmol photon m$^-$^{2} s^{-1} , 100 ppm CO_2). The plant leaf was left to be adapted to the measuring environment for 10 min. The plant leaf was allowed to achieve a steady-state rate of photosynthesis then it was suddenly darkened. As aresult, a momentary rapid outburst of CO_2 was recorded before the leaf achieved a steady-state dark respiration (R_n). The difference between this CO_2 burst and Rn equals PIB. The assimilation rates were recorded continuously through out the measurements using a timed lamp automatic program as shown in table 2.6.

Table 2.6: The PIB measuring protocol

Time	PAR	Ca	Measuring intervals
180 sec	1000 µmol m^{-2} s^{-1}	100 ppm	2 sec
600 sec	0 µmol m^{-2} s^{-1}	100 ppm	2 sec
180 sec	1000 µmol m^{-2} s^{-1}	100 ppm	2 sec

PAR: Photosynthetic Active Radiation; **Ca**: The external CO_2 concentration in the measuring chamber.

2.2.6   Generation and characterization of transgenic plants

2.2.6.1 Transformation of *Arabidopsis* plants through *Agrobacterium*-mediated floral dip transformation.

I) *Preparation of Agrobacterium*

A single colony of *Agrobacterium tumefaciens* carrying the recombinant plasmid was inoculated into 5 ml YEB medium (with 100 µg/ml rifampicin, 25 µg/ml kanamycin, 50 µg/ml carbenicillin) (Table 2.2) to prepare the pre-culture. The culture was incubated at 28°C for 2 days with shaking at 150 x g. This pre-culture was then inoculated into 200 ml YEB medium (100 µg/ml rifampicin, 25 µg/ml kanamycin, 50 µg/ml carbenicillin) and incubated for further 2 days at 28°C with shaking at 200 x g. Cells were spun down at 4791 x g at 4°C for 20 min. The pellet was resuspended in 5% sucrose till OD_{600} reaches 0.8. Then 0.04% silwet L-77 (400 µl/1000 ml) was added to the resuspended cells and the cells were used directly for floral dip transformation of *Arabidopsis thaliana*.

II) *Transformation of Arabidopsis plants (floral dip transformation)*

Transformation was performed as described by Clough and Bent (1998) as follows:

Arabidopsis wild type seeds were allowed to grow for three weeks under short day conditions (8 h light, 16 h dark at 20°C). The growing plants were transferred to long day conditions (16

h light and 8 h dark at 23-25°C) to enhance flower production. The first bolts were clipped to encourage the proliferation of many secondary inflorescences. The *Agrobacterium tumefaciens* containing the desired constructs were prepared as described before. The above ground parts of the *Arabidopsis* plants were dipped in the *Agrobacterium* solution three times for 3 to 10 min each. The dipped plants were placed under a dome or cover for 16 to 24 hours in order to maintain high humidity. The plants were then transferred to normal growth conditions (16 h light and 8 h dark at 23-25°C). The loosed bolts were tied with wax paper and after seed maturation, watering the plants was stopped and the dry seeds were harvested and were then selected on MS medium containing the appropriate antibiotics.

2.2.6.2 Selection of the transgenic plants

The harvested seeds were sterilized by submerging in 70% (v/v) ethanol for 15 min then washed three times with 98% (v/v) ethanol, and then the seeds were left to dry on a sterile whatman paper. The transgenic seeds were selected on the basis of the involved selectable markers in MS-medium containing the appropriate amounts of antibiotics (i.e. 50 µg/ml Kan; for kanamycin-resistant plants and 20 µg/ml sul; for sulfadiazine-resistant plants). Plants that confer resistance to phosphinotricin were selected according to Brukhin *et al.* (2000) and Hadi *et al.* (2002). Seeds were cultivated in soil and irrigated with water containing BASTA (1 ml BASTA/L H_2O. The selected plants were allowed to grow in short day conditions (light intensity, 80-100 Microeinsteins) for 10-15 days. Then the survived plants were allowed to grow for 10-20 days in the same conditions and were after that transferred to long day conditions to enhance flowering and seed production.

2.2.6.3 Growing of transgenic plants in a low CO_2 environment

A low CO_2 plant growth unit (figure 2.25) was used for this purpose. This unit was designed by me and other colleagues (Christoph Peterhänsel and Ruben Rosenkranz) in the Institute for Biology I, RWTH-Aachen and it was constructed and assembled by the mechanical workshop of the Institute for Biology I, RWTH Aachen. In this unit, ambient air (350-400 ppm CO_2) was allowed to be pumped through a series of glass bottles containing Soda Lime (ROTH GmbH, Karlsruhe, Germany). The soda lime absorbed all the CO_2 from the pumped air i.e. the output of this process is a CO_2-free air. The CO_2 free air was then mixed with ambient air supply in a ratio of 4/1 respectively (i.e. 20 L/h CO_2-free air were mixed with 5 L/h normal air in order to get a final CO_2 concentration of 100 ppm). The flow of CO_2-free air and normal air was controlled via rotameters (ROTH GmbH, Karlsruhe, Germany). The 100 ppm containing

air was then pumped into a plant growth chamber (2.1.3). The temperature and light intensity inside the chamber was controlled (here temperature was 23°C and light intensity was 80-100 Microeinsteins). The plant growth chamber was adjusted with a short day growing conditions (i.e. 8 h light, 16 h dark). The CO_2 concentration in the pumped air into the plant growth chamber was measured by CO_2-Analyzer: „BINOS IR-VIS/UV"(LEYBOLD) (2.1.3). In order to keep a suitable humidity for plant growth inside the chamber, the 100 ppm CO2 containing air was allowed to pass through water before entering the plant growth chamber. The air inside the plant growth chamber was replaced every one hour in order to keep a constant CO_2 concentration of 100 ppm around the growing plants.
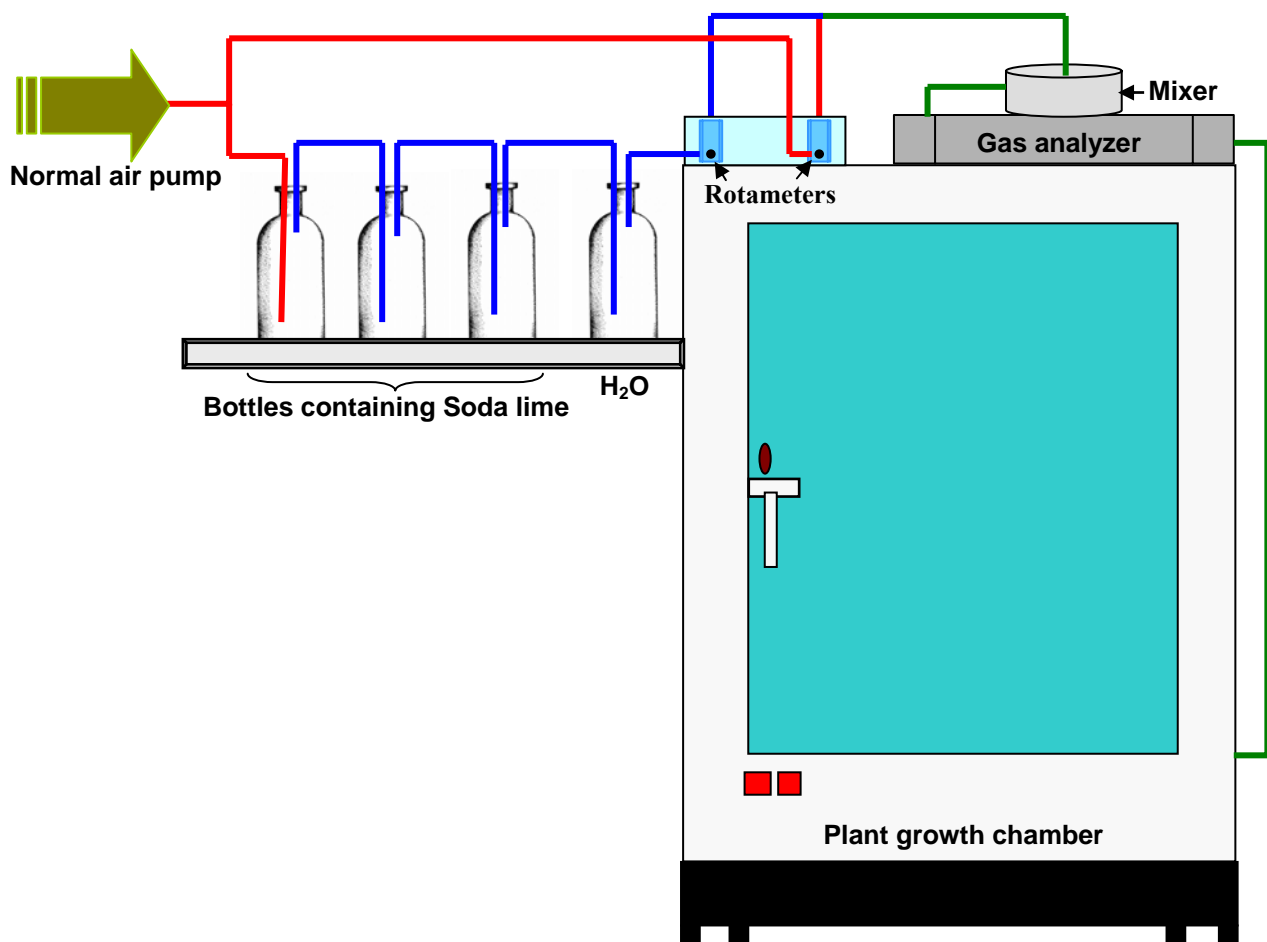
Figure 2.25: Sketch illustrating the Low CO_2 Plant growth unit

Red lines: represent normal air flow; **Blue lines**: represent CO_2-free air flow; **Green lines**: represent 100 ppm CO_2 containing air flow.
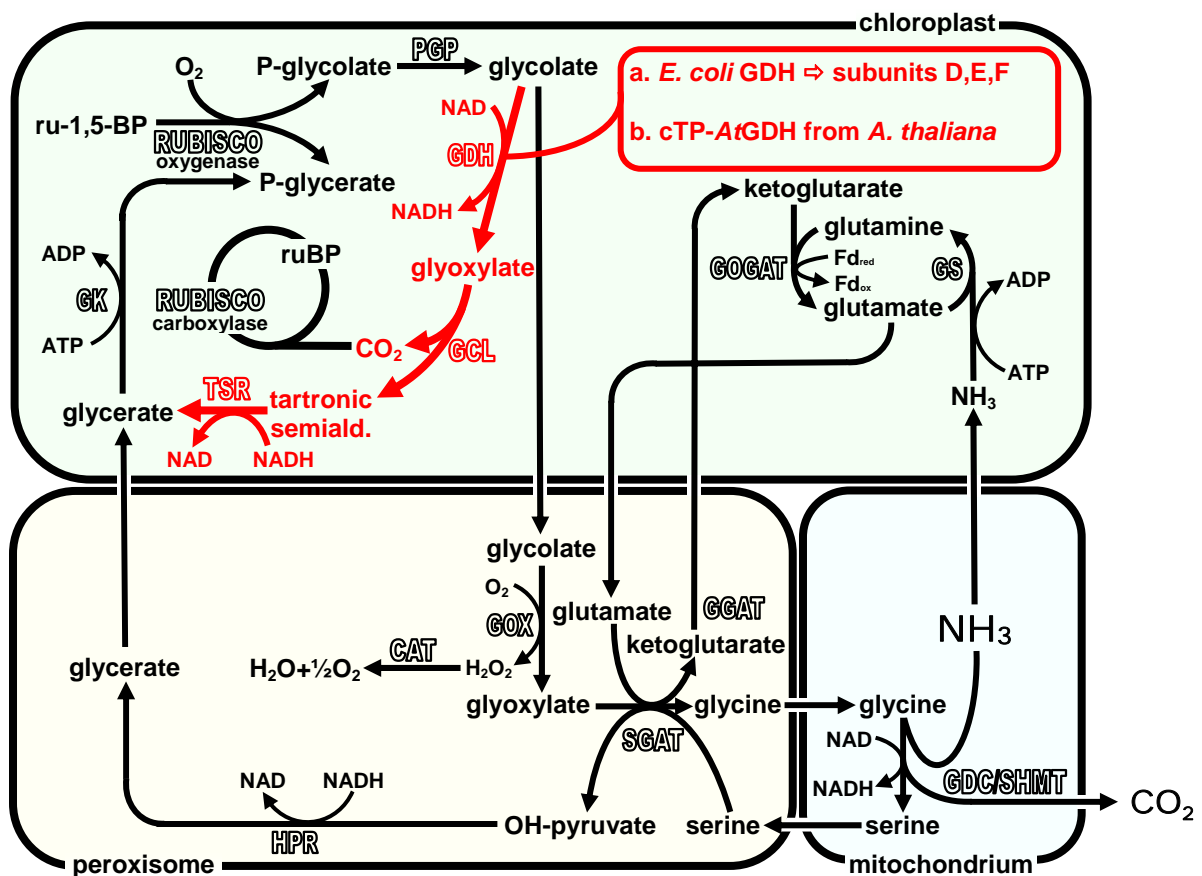
3   RESULTS

3.1 A novel biochemical pathway aiming to increase CO_2 concentration in the chloroplast of C_3 plants

Rubisco catalyses both the carboxylation and the oxygenation of ribulose-1,5-bisphosphate (RuBP). Carboxylation accounts for net CO_2 fixation whereas oxygenation leads to the loss of CO_2 in photorespiration. The recycling of glycolate-2-phosphate into glycerate-3-phosphate via the photorespiratory pathway and then further to ribulose-1,5-bisphosphate is not only a very costly reaction, but also requires a large machinery involving 16 enzymes and more than 6 translocators, distributed over the chloroplast, the peroxisome and mitochondria in close contact to each other (Leegood *et al.*, 1995). The CO_2 release in the mitochondria during photorespiration results in 25% loss of the carbon from phosphoglycolate. Moreover, NH_3 is lost in this cycle that has to be refixed. The loss of CO_2 during photorespiration is due to the fact that CO_2 release and CO_2 fixation are separated in two different organelles.

This PhD study was aiming to construct genetically modified *Arabidopsis thaliana* plants (as a C_3 plant) showing photorespiratory CO_2 release inside the chloroplast in order to increase the CO_2 concentration in the vicinity of Rubisco. This will subsequently suppress photorespiration resulting in an improvement of CO_2 fixation. For this, a biochemical pathway from *E. coli* converting glycolate to glycerate was installed inside the plant chloroplasts. The enzymes involved in the novel pathway comprise Tartronic Semialdehyde Reductase (TSR), Glyoxylate Carboligase (GCL) and NAD/(P) dependent, oxygen-independent Glycolate Dehydrogenase (GDH) derived from *E. coli*. In addition to the *E. coli* glycolate dehydrogenase (*Ec*GDH), an alternative gene from *Arabidopsis thaliana* called cTP-*At*GDH was used. *At*GDH metabolizes glycolate in the same way as the bacterial GDH and it is localized in the mitochondria of *A. thaliana* plant cells (Bari *et al.*, 2004). Therefore, the endogenous mitochondrial targeting sequence of *At*GDH was replaced by a chloroplast transit peptide (cTP). *Ec*GDH is made up from three protein subunits that are encoded by three different open reading frames called *glc*D, *glc*E and *glc*F in the glycolate dehydrogenase operon. In contrast, cTP-*At*GDH is a single open reading frame.

Figure 3.1 shows the proposed pathway on the background of the photorespiratory pathway. In this pathway, phosphoglycolate produced from the oxygenase reaction of Rubisco is dephosphorylated to glycolate by phosphoglycolate phosphatase (PGP) which is present in the chloroplast. The glycolate is then oxidized by NAD/(P) dependent glycolate dehydrogenase

(*Ec*GDH or *At*GDH) to form glyoxylate. Two molecules of glyoxylate are condensed in a reaction catalyzed by glyoxylate carboligase (*GCL*), which simultaneously decarboxylates the condensation product to tartronic semialdehyde. In this reaction, CO_2 is released because of the decarboxylation reaction. Tartronic semialdehyde is reduced to glycerate by the enzyme tartronic semialdehyde reductase (*TSR*). Glycerate is subsequently phosphorylated to glycerate-3-phosphate in a reaction catalyzed by glycerate kinase (*GK*) which is present in the chloroplast of C_3 plants. In the final step, glycerate-3-phosphate enters into the Calvin cycle, where it is used in the biosynthesis of carbohydrates and in the regeneration of RuBP.

Figure 3.1: Representation of the photorespiratory pathway (black) in C_3 plants and the proposed pathway (red) for the conversion of glycolate to glycerate.

The oxygenase reaction of Rubisco results in the formation of P-glycerate and P-glycolate. P-glycolate is dephosphorylated by PGP forming glycolate that is oxidized by GDH to form glyoxylate. Two molecules of glyoxylate are condensed by GCL forming tartronic semialdehyde and CO_2 is released in the chloroplast. Tartronic semialdehyde is then reduced by TSR forming glycerate. Glycerate is phosphorylated by GK to form P-glycerate that is used directly for carbohydrate biosynthesis through the Benson Calvin cycle. **PGP** = phosphoglycolate phosphatase; **GDH** = glycolate dehydrogenase; **cTP-AtGDH** = *A. thaliana* glycolate dehydrogenase fused to a chloroplast targeting peptide (cTP); **GCL** = glyoxylate carboxyligase; **TSR** = tartronic semialdehyde reductase; **GK** = glycerate kinase, the photorespiratory enzymes are described in chapter 1.4.

The assembly of the novel pathway in transgenic plants will be explained in chapter 3.2 and chapter 3.3. The influence of the novel pathway on the suppression of photorespiration, photosynthetic characteristics and growth performance of transgenic plants will be explained in chapter 3.4, 3.5 and 3.6, respectively.

3.2 Establishment of *E. coli GCL*, *TSR* and *GDH* activity in *A. thaliana* chloroplasts

The proposed biochemical pathway consists of three enzymatic functions. Therefore, it was decided that *TSR* and *GCL* genes should be transferred first to the nuclear genome of *A. thaliana* wild type plants followed by the transformation of a gene encoding a glycolate dehydrogenase activity, because the latter step seemed to be the most problematic due to the complex structure of *Ec*GDH enzyme. To achieve this purpose, all the necessary genes for the establishment of the novel biochemical pathway were cloned into different plant expression vectors as N-terminus fusion to a chloroplast targeting peptide (cTP), since the expressed proteins should be targeted to the plant chloroplast. The expression of the foreign genes in all the used vectors is under the control of a derivative of the constitutive CaMV 35S promoter.

### 3.2.1   Generation of *GCL, TSR* and *GCL-TSR* transgenic *A. thaliana* plants

The *TSR* and *GCL* genes in translational fusion to a His-tag (*TSR-His*, *GCL-His*) were cloned separately and together into the plant expression vector pTRA-K-rbcS1-cTP (2.1.9.1). The cloning of the single and double constructs was done during my diploma study (Rashad Kebeish, Institute for Biology I, RWTH-Aachen, Germany, 2002). The details of the cloning of the single and double constructs are also described in the materials and methods chapter (2.1.9). Stable transformation of *Arabidopsis thaliana* plants ecotype Columbia (Col-0) with constructs carrying both genes together and separately was carried out by *Agrobacterium* mediated floral dip transformation (Clough and Bent, 1998b). The details of the transformation process are described in the materials and methods chapter (2.2.6.1). Transformation of wild type *A. thaliana* plants with a single construct containing either *TSR* or *GCL* gene helps to study the effects that could appear in the transgenic plants due to the expression of a single gene inside the plant chloroplast.

3.2.1.1 *TSR* and *GCL* expression in planta

The expression of *GCL* and *TSR* genes in *planta* was tested either on the protein level by Western blot analysis from crude leaf protein extracts or on the RNA level using RT-PCR.

I) *Analysis of TSR and GCL Expression on protein level*

The expression of *GCL* in transgenic plants was measured on the protein level by western blot using an antibody specific for the His-tag whereas the expression of *TSR* protein was analyzed using an anti-TSR antibody, which was produced from chicken (2.2.3.16 above) because the His tag could not be detected from plant extracts for unknown reasons. Figure 3.2A shows the results of the western blot analysis for the proteins isolated from 9 transgenic *A. thaliana* plants containing *GCL* and *TSR* genes (simply named GT plants).
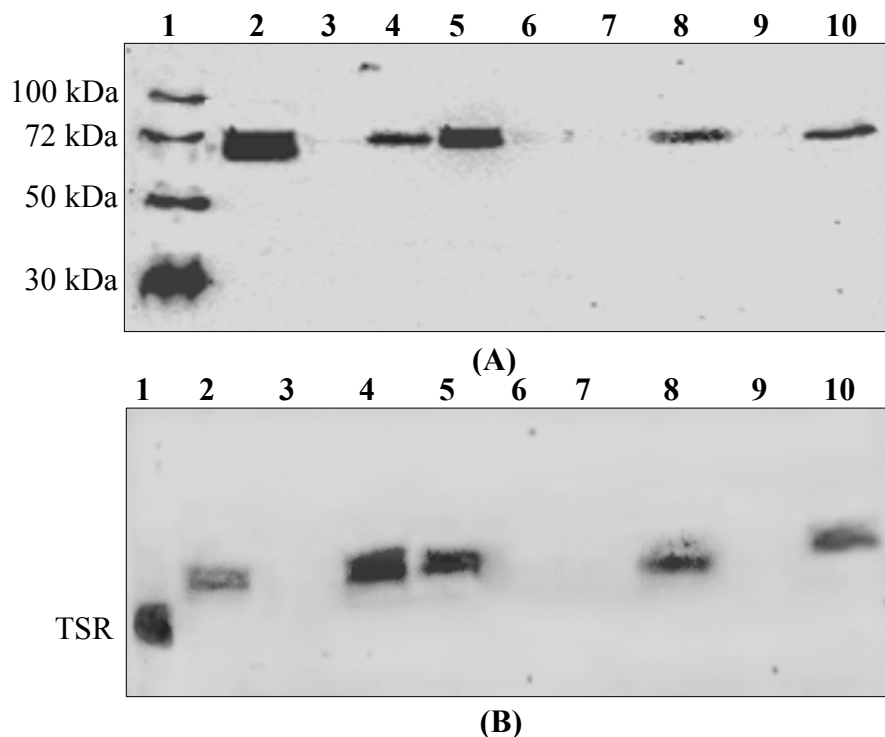
Figure 3.2: *GCL* and *TSR* genes expression in plants.

Shown are two different chemiluminescent Western photographs of the proteins isolated from different transformed *Arabidopsis* plants with pTRA-K-rbcS1-cTP-TSR-His,GCL-His construct (simply named GT plants). 15 µg of leaf protein extracts were separated on a 10% SDS-PAGE gel and transferred to a nitrocellulose membrane. His-tagged proteins were detected using an anti-His antibody covalently linked to horseradish peroxidase**.** TSR proteins were detected using an anti-TSR antibody that was detected with a secondary antibody (Goat anti-chicken antibody). Luminescence was recorded on a LAS3000 CCD camera. In figure 3.2A, Lane 1 = His protein marker. In figure 3.2B, Lane 1 = TSR protein that was purified from bacteria. In figure 3.2A and 3.2B, Lane 2-lane 9 = transgenic plants GT 1-GT 9, respectively.

A 6x His protein marker was used as a control for determining the molecular weight of the proteins (lane 1 in figure 3.2A). A single band was visible in some samples as in lane 2, lane 4, lane 5, lane 8 and lane 10. The single band corresponds in size to the *GCL* protein fused to the His-tag (65 kDa). The samples from some plants show no expression for *GCL* (for example, lane 3, 6, 7 and lane 9 in figure 3.2A). However, in none of the tested plants any expression of the *TSR* (approximately 30 kDa) could be detected although the TSR protein is also fused to a His-tag. Approximately 25 *GCL-TSR*-transgenic lines (containing the *GCL-TSR* double construct) and 19 *TSR*-transgenic lines (containing *TSR* single construct) were analyzed by western blot using anti-His antibody (data not shown). Surprisingly, many of the plants containing *TSR* and *GCL* genes have shown varying expression levels of *GCL* whereas none of them showed expression of *TSR*.

It was suggested that the TSR protein may be pelleted with the cell debris during the centrifugation step of the protein extraction. Thus, the detection of *TSR* protein from transgenic plant extracts required a special protein extraction technique. It was finally detected with a specific antibody prepared from immunized hen eggs. Figure 3.2B shows the result of the western blot analysis for the total proteins isolated from leaves of *A. thaliana* plants transgenic for GT using anti-*TSR* antibody. In lane 1, *TSR* protein was purified from bacteria and used as a positive control. The tested plants that showed expression for *GCL* (GT1, GT3, GT4, GT7 and GT9 plants) also showed expression for *TSR* (lane 2, 4, 5, 8 and 10 in figure 3.2B). No phenotypic effects in *Arabidopsis thaliana* plants transgenic for GT were detected (3.6.2). Transgenic plants GT1 and GT4 were used to generate homozygous lines expressing *GCL* and *TSR* genes.

II) *Analysis of TSR and GCL expression on the RNA level*

In later generations after selfing of positive GT lines (GT1 and GT4), the accumulation of *GCL* and *TSR* transcripts in their leaf tissues was measured by Real-Time RT-PCR (2.2.1.11). The amount of *TSR* and *GCL* signal in the different RNA preparations was standardized for the abundance of the Actin2 transcripts (Igarashi *et al.*, 2003). The analysis of the transcript abundance of *TSR* and *GCL* genes in *planta* is described in the materials and methods chapter (2.2.1.12). Figure 3.3 shows the accumulation of *TSR* (grey bars) and *GCL* (black bars) transcripts. The tested transgenic plants are the T2 generation derived from GT1 and GT4 transgenic lines (3.2.1.1). 4 lines from the GT1 offspring were tested. Three of them show more or less similar expression levels for *GCL* and *TSR* (GT1-1, GT1-3, and GT1-4 in figure 3.3). GT1-2 shows no expression for both genes.
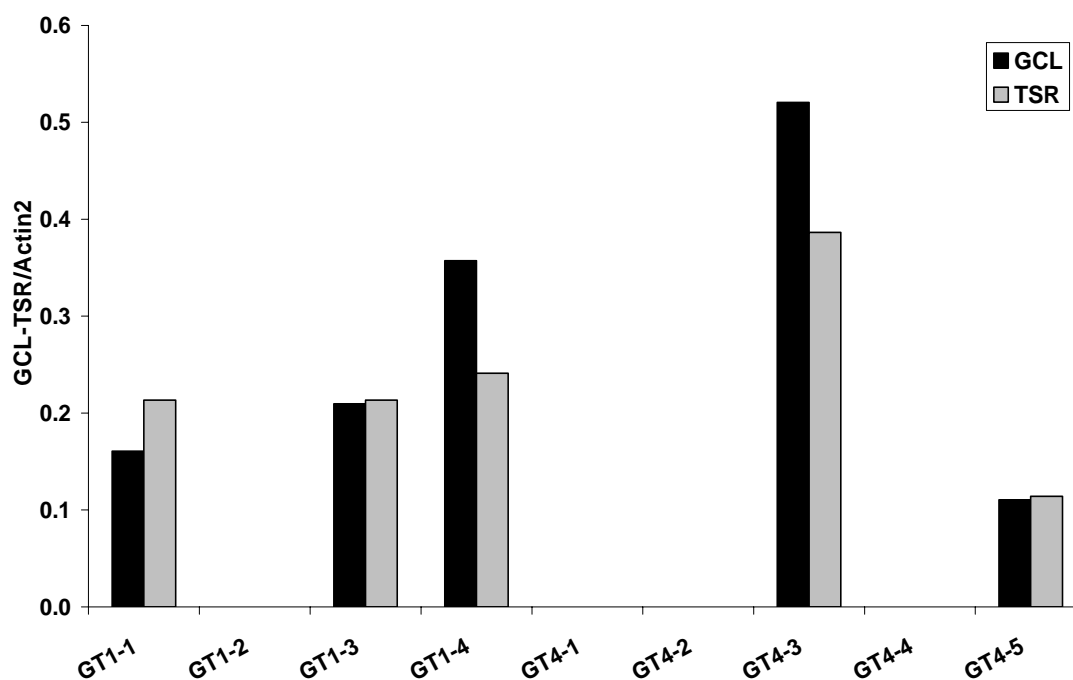
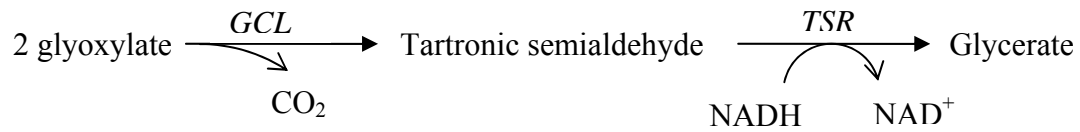**Figure 3.3: Accumulation of *TSR* and G*CL* transcripts in plants transgenic for GT.**

The amount of *GCL* and *TSR* mRNA was measured by Real-Time RT-PCR and calculated in arbitrary units by comparison to a standard dilution series of GT plasmid DNA. Each value is the relative accumulation of the respective RNA compared to the Actin2 levels measured in the preparation.

5 lines from the T2 generation of GT4 plants were also tested. Two of them show varying expression levels for *GCL* and *TSR* genes (GT4-3 and GT4-5 in figure 3.3) whereas the other three don't show any signals in the RT-PCR analysis for the expression of *TSR* and *GCL* genes (GT4-1, GT4-2, and GT4-4 in figure 3.3). Although there are little differences in the expression levels between the tested plants, no phenotypic differences were detected. Because of the higher expression levels of GT1-4 and GT4-3 lines, it was decided to pass these two lines into the T3 and T4 generations in order to generate GT homozygous lines. 25 lines from the T3 generation were analyzed based on the survival of their seeds in the selection medium as well as their expression levels for *TSR* and *GCL* genes. One homozygous line was characterized named GT1-4-5.

3.2.1.2 *GCL* and *TSR* proteins from the chloroplasts of GT-transgenic plants are active *in vitro.*

Chloroplast extracts isolated from GT transgenic plants were assayed for the conversion of glyoxylate to glycerate. The enzymatic activity of glyoxylate carboligase and tartronic semialdehyde reductase was measured spectrophotometrically as described in the materials and methods (2.2.3.17) *in vitro*. The assay was performed in a coupled reaction where

glyoxylate carboligase condenses two molecules of glyoxylate into one molecule of tartronic semialdehyde. Tartronic semialdehyde is further reduced to glycerate by tartronic semialdehyde reductase. The overall reaction is as follows:

$$2 \text{ glyoxylate} \xrightarrow[\text{CO}_2]{\text{GCL}} \text{Tartronic semialdehyde} \xrightarrow[\text{NADH} \quad \text{NAD}^+]{\text{TSR}} \text{Glycerate}$$

The assay with chloroplast extracts from plants transgenic for GT shows a higher oxidation of NADH compared to the chloroplast extract from wild type (see figure 3.4). In the presence of glyoxylate (black bars in figure 3.4), The GT-chloroplast extract shows an approximately 7-fold activity over the wild type extract in this assay whereas in the absence of substrate (grey bars in figure 3.4), both extracts (either from GT-transgenic or wild type plants) show more or less the same activity. Based on this result, it can be concluded that both enzymes are therefore seemingly active inside the plant chloroplasts.
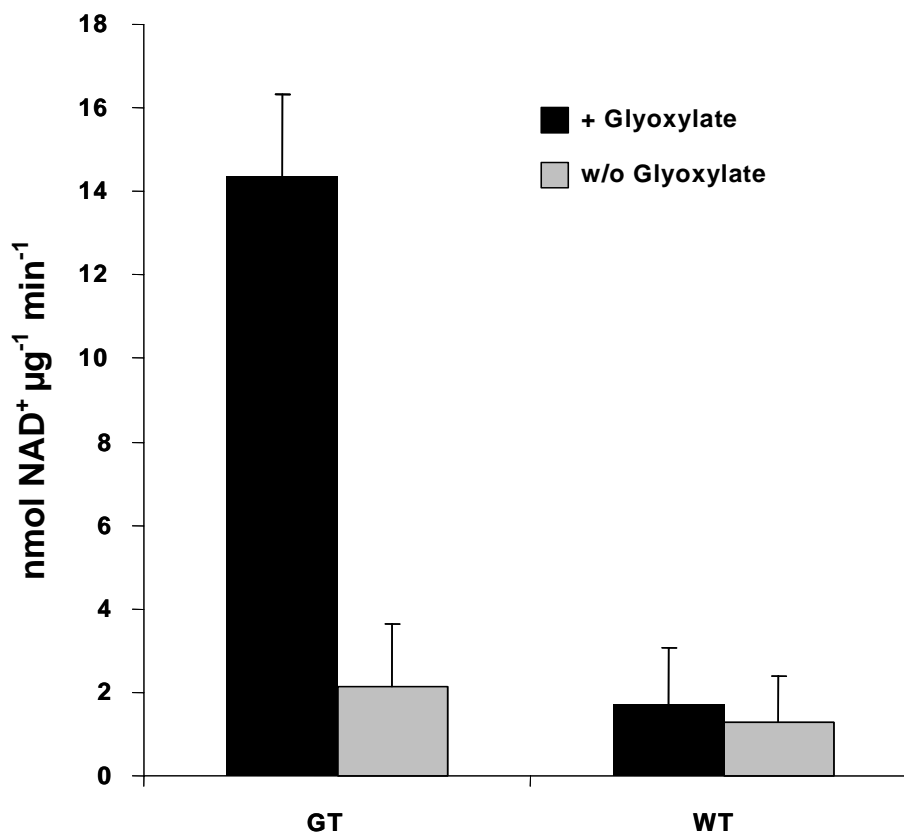
Figure 3.4: Measurement of *GCL*/*TSR* activity in GT plants.

Chloroplast extracts isolated from 6 weeks old wild type plants and GT transgenic plants expressing *GCL* and *TSR* genes were tested for glyoxylate carboligase and tartronic semialdehyde reductase activity in the presence (black bars) or absence (grey bars) of glyoxylate. Each data point shows the amount of NADH oxidized per minute and is based on at least three independent experiments. Vertical bars show standard deviations. WT = chloroplast extracts isolated from wild type *A. thaliana* plants; GT = chloroplast extracts isolated from plants transgenic for *GCL* and *TS*R.

3.2.2   Generation of transgenic *A. thaliana* plants expressing *glc*D, *glc*E and *glc*F genes in their chloroplasts

The minimal *E. coli* glycolate dehydrogenase enzyme is formed from three different polypeptides that are encoded by three different open reading frames named *glc*D, *glc*E and *glc*F (Lord, 1972; Pellicer *et al.*, 1996). To build up a bacterial glycolate dehydrogenase activity inside the chloroplast of *A. thaliana* plants, a simple strategy was used: Firstly, the coding sequence for *glc*F subunit of the *Ec*GDH operon was cloned into a plant expression vector (pTRA-PT-rbcS1-cTP) that confers resistance to phosphinotricin (BASTA). This single construct was transferred to the nuclear genome of wild type *A. thaliana* plants. Transgenic plants expressing *glc*F (simply named F plants) were characterized and homozygous lines were generated. Secondly, the *glc*D and *glc*E genes were cloned together into a single plant expression vector (pSuper-PAM-Sul-rbcS1-cTP) that confers resistance to sulfadiazine antibiotics. Finally, the homozygous lines expressing *glc*F were retransformed with the double construct containing *glc*D and *glc*E (pSuper-PAM-Sul-rbcS1-cTP-GlcD,GlcE). This final step results in the production of transgenic plants that express all necessary *E. coli* GDH genes (i.e *glc*D, *glc*E and *glc*F genes) simply named DEF plants. At the same time, the pSuper-PAM-Sul-rbcS1-cTP-GlcD,GlcE double construct was transformed into wild type *A. thaliana* plants in order to check the phenotypic effects that could appear in the transgenic lines expressing both genes.

3.2.2.1 Generation of homozygous *A. thaliana* plants transgenic for *glc*F.

The *glc*F gene was firstly cloned into pTRA-K-rbcS1-cTP plant expression vector (2.1.9.1) resulting in the pTRA-K-rbcS1-cTP-GlcF construct. This construct was then used as an intermediate for recloning of the *glc*F gene into the pTRA-PT-rbcS1-cTP-gfp plant expression vector (2.1.9.12). This resulted in the production of pTRA-PT-rbcS1-cTP-GlcF construct (2.1.9.13). Stable transformation of *Arabidopsis thaliana* plants ecotype Columbia (Col-0) with pTRA-PT-rbcS1-cTP-GlcF was carried out by *Agrobacterium* mediated floral dip transformation (2.2.6.1). The transgenic seeds were selected directly in soil using BASTA herbicides (2.2.6.2). 20 plants from the T1 generation were analyzed on the RNA level by RT-PCR. 8 plants showed varying expression levels for the *glc*F gene whereas the other 12 plants showed no expression (data not shown). No phenotypic differences in the different *glc*F expressing plants were detected. The best *glc*F expressing plant (simply named F8) was used to generate homozygous plants transgenic for F after growing its seeds for further three generations (T2, T3 and T4) based on its resistance to BASTA treatment. In each generation,

the selection and RT-PCR analysis (2.2.6.2 and 2.2.1.12, respectively) were performed. Eight homozygous lines expressing *glc*F were generated. Five lines out of these eight, simply named F8-2-1, F8-2-2, F8-4-2, F8-8-1 and F8-8-2 were chosen, based on their expression levels for the *glc*F gene, to be retransformed with pSuper-PAM-Sul-rbcS1-cTP-GlcD,GlcE double construct to generate transgenic *A. thaliana* plants expressing the complete *Ec*GDH.

3.2.2.2 Generation of DE and DEF-transgenic *A.thaliana* plants

In order to clone *glc*D and *glc*E genes into the pSuper-PAM-Sul-rbcS1-cTP plant expression vector that confers resistance to sulfadiazine (2.1.9.11), the genes were firstly cloned separately into the pTRA-K-rbcS1-cTP plant expression vector (2.1.9.1) then they were recloned together in a double construct into the pTRA-Hyg-rbcS1-cTP (2.1.9.8) plant expression vector. The pTRA-Hyg-rbcS1-cTP-glcD,GlcE (2.1.9.10) plasmid DNA was used as an intermediate for the recloning of *glc*D and *glc*E genes into pSuper-PAM-Sul-rbcS1-cTP plant expression vector. The cloning procedures are described in more details in the materials and methods chapter (2.1.9). Five of the homozygous *A. thaliana* plants transgenic for *glc*F (3.2.2.1) were retransformed with the pSuper-PAM-rbcS1-cTP-GlcD,GlcE double construct via *Agrobacterium* mediated floral dip transformation. At the same time, wild type *A. thaliana* plants were transformed with the same construct (pSuper-PAM-rbcS1-cTP-GlcD,GlcE) in order to generate transgenic plants expressing *glc*D and *glc*E genes. The transgenic plants containing *glc*D and *glc*E genes were selected on MS medium supplemented with sulfadiazine. For more details, see materials and methods (2.2.6.2).

3.2.2.3 Expression of *glc*D, *glc*E and *glc*F in DE and DEF- transgenic *A. thaliana* plants

During the cloning of *glc*D, *glc*E, and *glc*F genes, no His-tag was added to these polypeptides. The aim was to target each subunit independently to the chloroplast where those were expected to assemble the active glycolate dehydrogenase enzyme. The expression of *glc*D, *glc*E and *glc*F genes (simply named DEF genes) was analyzed mainly by RT-PCR on the RNA level. Moreover, the expression of *glc*D gene in the DE and DEF transgenic plants was also analyzed by Western blot using an anti-GlcD$_{1100}$ antibody produced from chicken (2.2.3.16).

I) *Analysis of glcD, glcE and glcF expression in DEF-transgenic A.thaliana plants on the RNA level*

16 DEF transgenic plants were analyzed on the RNA level by RT-PCR (2.2.1.11).The analysis of transcript abundance of the DEF genes in DEF plants is described in the materials and methods chapter (2.2.1.12). Figure 3.5 shows the accumulation of *glc*D (black bars), *glc*E (grey bars) and *glc*F (white bars) transcripts in the T1 generation of DEF transgenic plants.
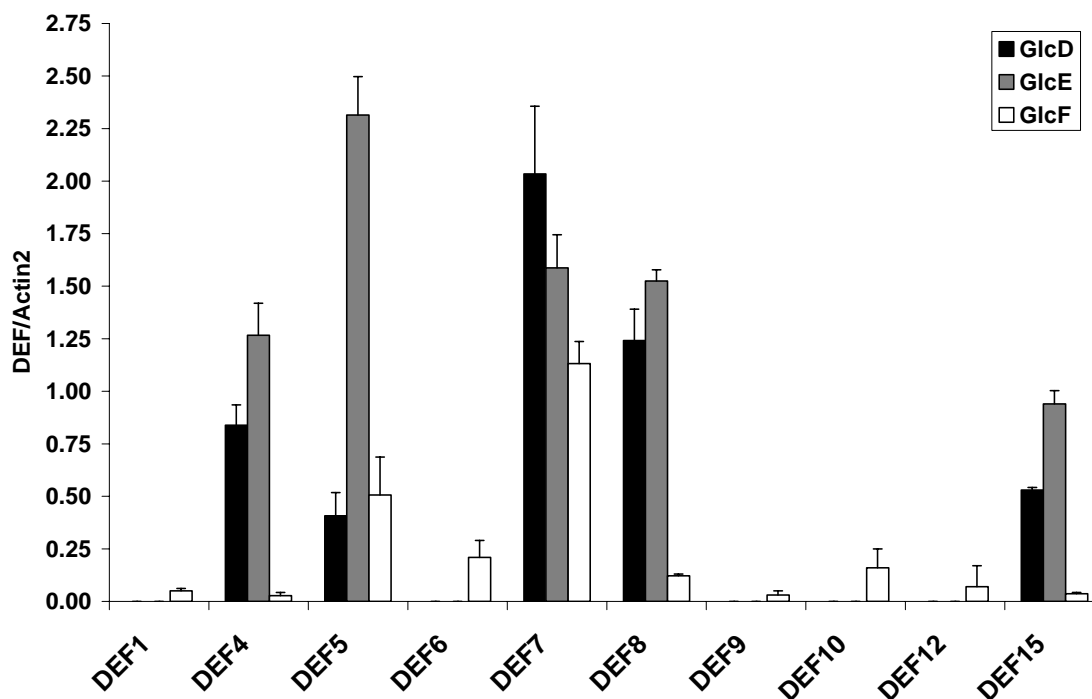

Figure 3.5: Accumulation of DEF transcripts in DEF transgenic plants.

The amount of *glc*D, *glc*E and *glc*F mRNA was measured by Real-Time RT-PCR and calculated in arbitrary units by comparison to a standard dilution series of DEF plasmids DNA mixture. Each value is the relative accumulation of the respective RNA compared to the Actin2 levels measured in the preparations. Each data point is based on at least three independent RNA preparations. Vertical bars show standard deviations. Black bars = *glc*D; Grey bars = *glc*E; White bars = *glc*F.

In five of the tested plants, all the three transgenes were expressed. However, only lines 5 and 7 showed comparable expression levels for all the three transgenes. For most lines, the *glc*F expression was clearly lower compared to the expression of *glc*D and *glc*E. This was unexpected, because the expression of *glc*F was followed through several generations before retransformation of these plants with the DE double construct. Some of the transgenic lines did no show any expression for *glc*D and *glc*E, for example DEF1, DEF6, DEF9, DEF10, and DEF12 in figure 3.5. DEF5 and DEF7 lines were chosen to be crossed to the offspring of the GT1-4-5 homozygous GT-transgenic plant in order to complete the installation of the novel biochemical pathway in *A. thaliana* plants.

II) *Analysis of glcD expression in DE and DEF transgenic A. thaliana plants on the protein level*

In addition to the RT-PCR analysis of DEF expression, *glc*D gene expression was also analyzed on the protein level. An anti-GlcD$_{1100}$ antibody was generated from chicken (2.2.3.16) for this purpose. Figure 3.6 shows the result of the Western blot analysis of the total proteins isolated from leaves of *A. thaliana* plants transgenic for DE and DEF.
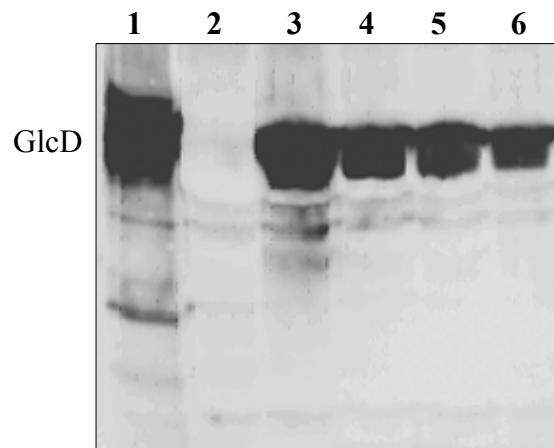

Figure 3.6: G*lc*D expression in plants transgenic for DE and DEF

Shown is a chemiluminescent western photograph of the proteins isolated from 6-7 weeks old *A. thaliana* plants transgenic for DE and DEF. 15 µg of leaf protein extracts were separated on a 10% SDS-PAGE gel and transferred to a nitrocellulose membrane. *Glc*D protein was detected using an anti-glcD$_{1100}$ antibody that was detected with a secondary antibody (Goat anti-chicken). Luminescence was recorded on a LAS3000 CCD camera. Lane 1 = *glc*D protein isolated from bacteria and was used as a positive control. Lane 2 = wild type leaf protein extract that was used as a negative control. Lane 3 = DE10 plant; Lane 4-6 = DEF5-1, DEF5-2 and DEF5-3 respectively.

In lane 1, *glc*D protein isolated from bacteria was used as a positive control. In lane 2, a wild type total protein extract was used as a negative control. One DE-transgenic plant was tested in this western analysis to ensure the expression of *glc*D gene in DE-double transgenic plants (lane 3 in figure 3.6). Three DEF-transgenic plants from the T2 generation of DEF5 plants were tested to check the expression of *glc*D in DEF-transgenic plants (lane 4-6). A single band was visible in some samples as in lane 3, lane 4, lane 5 and lane 6. The single band corresponds in size to the *glc*D protein (45 kDa). Wild type extract shows no interaction with the used antibodies (lane 2 in figure 3.6). Based on this result, it can be concluded that plants transgenic for DE and DEF are expressing *glc*D protein.

3.2.2.4 *glc*D, *glc*E, and *glc*F protein subunits of *E. coli* GDH are rightly assembled in DEF plant chloroplasts.

The *E. coli* glycolate dehydrogenase uses an organic compound as an electron acceptor, oxidises D(-)-lactate preferentially over L(+)-lactate as an alternative substrate and is cyanide sensitive (Nelson and Tolbert, 1970; Pellicer *et al.*, 1996). In contrasts, higher plant peroxisomal glycolate oxidase uses oxygen as an electron acceptor, oxidises L(+)-lactate preferentially over D(-)-lactate and is cyanide insensitive. In order to find out whether the *glc*D, *glc*E and *glc*F protein subunits are correctly assembled the active *E. coli* GDH enzyme in the chloroplast of DEF plants, glycolate dehydrogenase and D-lactate dehydrogenase assays (D-LDH) were performed *in vitro* using chloroplast protein extracts in the presence and absence of KCN. Chloroplasts were isolated from 6 weeks old DEF5 and DEF7 transgenic plants. The chloroplast proteins were extracted as described in chapter (2.2.3.7). In order to exclude a contamination with mitochondrial or peroxisomal proteins, fumarase and catalase enzymatic assays were performed respectively (2.2.3.17). Figure 3.7 represents the results from the GDH assay with WT, DEF5 and DEF7 chloroplast protein extracts.
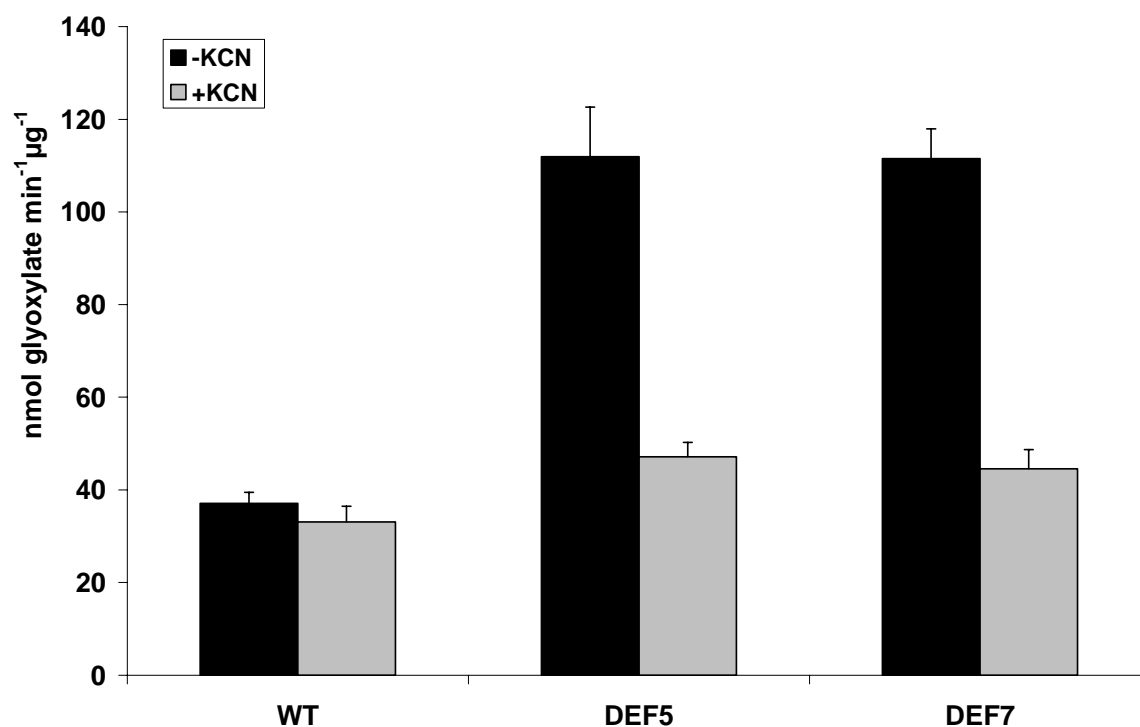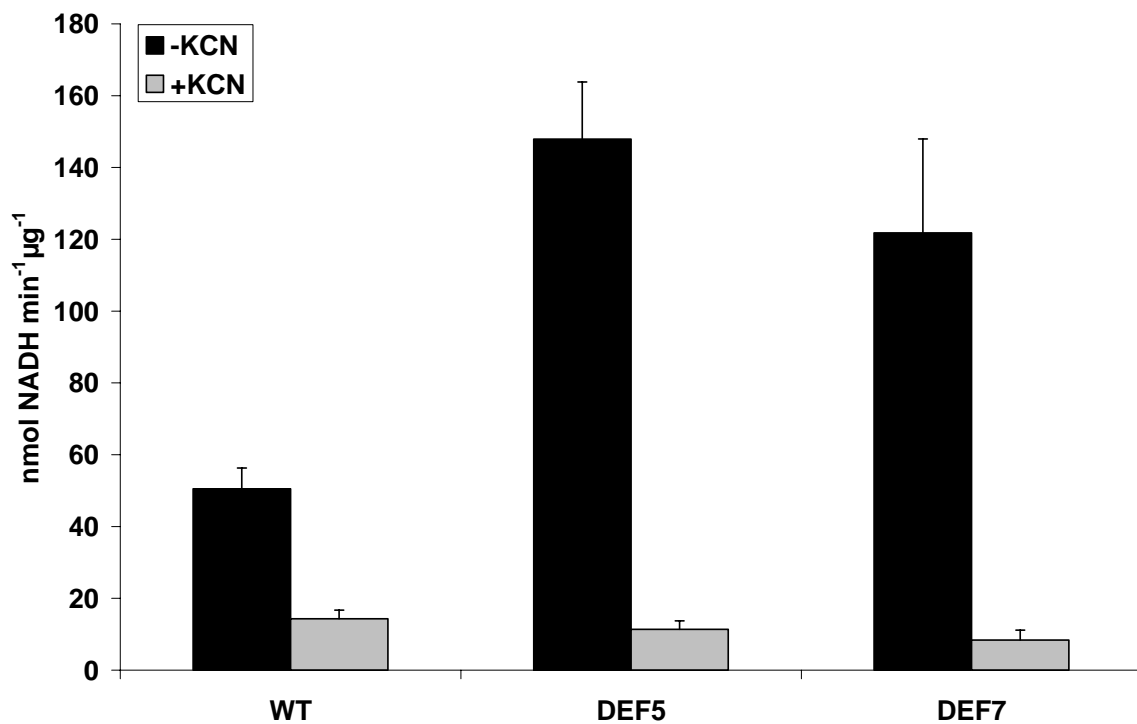

Figure 3.7: GDH assay from chloroplast extracts.

Chloroplast protein extracts isolated from 6 weeks old WT as well as DEF5 and DEF7 plants were tested for glycolate dehydrogenase activity. Each data point shows the amount of glyoxylate formed per minute and is based on at least three independent experiments. Vertical bars show standard deviations. Black bars = -KCN; grey bars = +KCN; WT, DEF5 and DEF7 = chloroplast extracts isolated from wild type, DEF5 and DEF 7 plants, respectively.

DEF5 and DEF7 chloroplast extracts show an approximately 2-fold higher activity than chloroplast extracts from WT plants in the absence of KCN. This activity is reduced to same background levels in the presence of KCN when it is compared to WT extracts. This background is due to a little peroxisomal contamination during the isolation and extraction of chloroplast proteins from the tested plant leaves (i.e. presence of the peroxisomal glycolate oxidase). The difference in the activity levels in DEF5 and DEF7 chloroplast extracts is due to the presence of DEF proteins in the tested samples. From this, it can be concluded that the DEF proteins are active *in vitro*.

In order to ensure that the DEF proteins are active *in vitro*, a D-LDH assay was additionally performed using the same DEF5, DEF7 and WT chloroplast extracts that were used for the glycolate dehydrogenase assay. Figure 3.8 shows the results from the D-LDH assay.

Figure 3.8: D-LDH assay from chloroplast extracts.

Chloroplast protein extracts isolated from WT as well as DEF5 and DEF7 plants were tested for D-LDH activity. Each data point shows the amount of NADH produced per minute and is based on at least three independent experiments. Vertical bars show standard deviations. Black bars = -KCN; grey bars = +KCN; WT, DEF5 and DEF7 = chloroplast extracts isolated from wild type, DEF5 and DEF7 plants, respectively.

DEF5 and DEF7 chloroplast extracts show an approximately 3-fold higher activity compared to chloroplast extracts from WT plants. This activity is inhibited in both WT and DEF chloroplast extracts in the presence of KCN. The activity observed in the chloroplast extract from WT plants may be due to the presence of other enzymes that use NAD^+ and are cyanide

sensitive.The results from both assays show that the extracts from transgenic lines show enhanced glycolate dehydrogenase activity that is strongly inhibited by cyanide. Based on these results, it is concluded that the *Ec*GDH subunits correctly assemble inside the plant chloroplast.

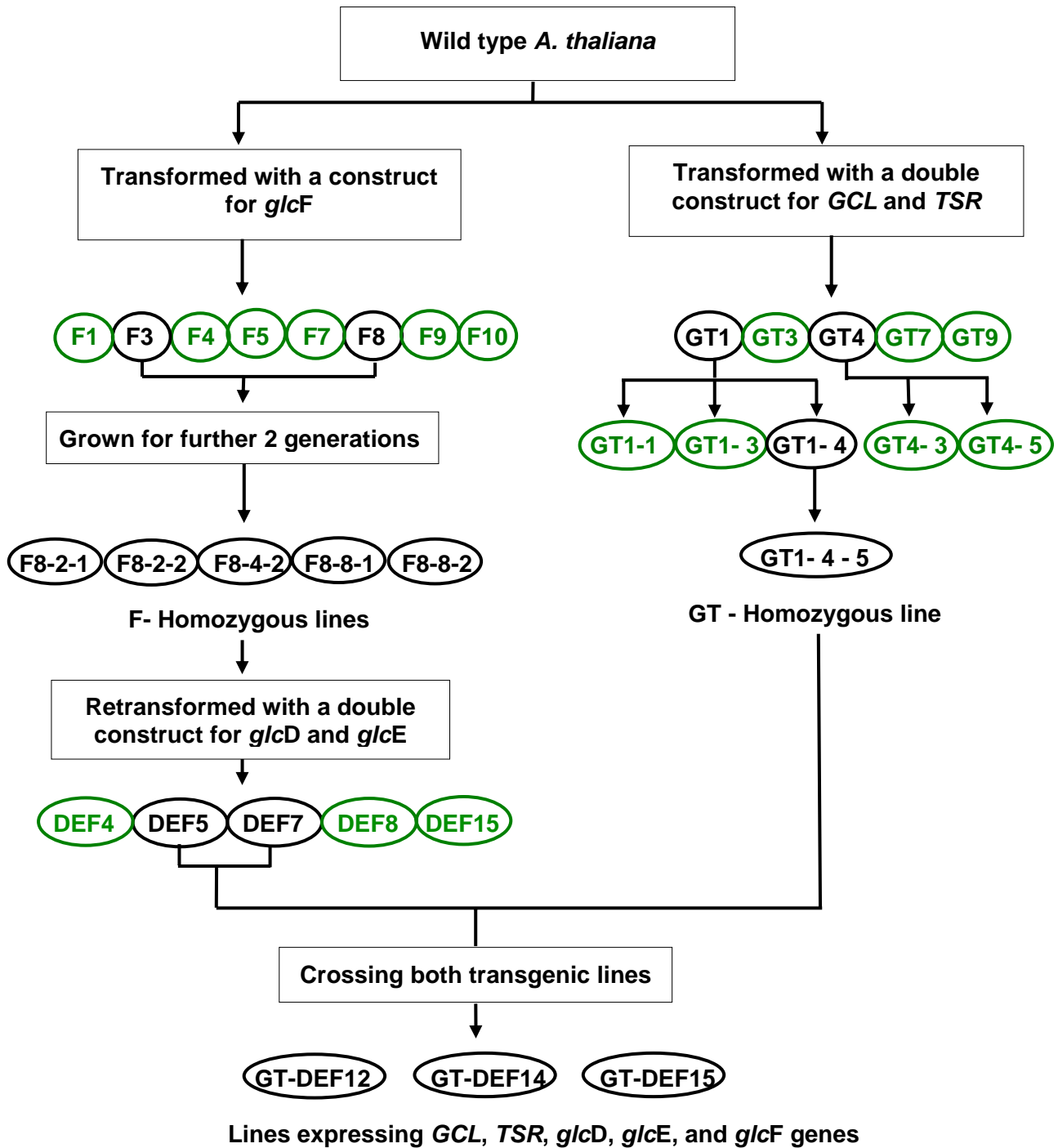### 3.2.3   Survey of the generation of GT-DEF transgenic plants

This chapter will summarize the approach for the generation of transgenic lines overexpressing the complete glycolate pathway as shown in figure 3.9.

A double construct for *GCL* and *TSR* genes that confers resistance to kanamycin (2.1.9.4) was transferred into the nuclear genome of WT *A. thaliana* plants by *Agrobacterium* mediated floral dip transformation. A homozygous transgenic line expressing the bacterial *GCL* and *TSR* genes (GT1-4-5 in figure 3.9) was generated as described in chapter (3.2.1).

A single construct for *glc*F conferring resistance to phosphinotricin (2.1.9.13) was also transferred to the nuclear genome of other WT *A.thaliana*. Homozygous lines were generated (F8-2-1, F8-2-2, F8-4-2, F8-8-1 and F8-8-2 in figure 3.9) as described in chapter 3.2.2.1. The homozygous plants transgenic for F were retransformed with a double construct for expression of *glc*D and *glc*E subunits of *Ec*GDH (3.2.2.2). The DE-construct confers resistance to sulfadiazine (2.1.9.11). This last transformation step results in the generation of transgenic plants expressing all *Ec*GDH protein subunits (DEF4, DEF5, DEF7, DEF8 and DEF15 in figure 3.9).

The offspring of DEF5 and DEF7 (T2 generation of DEF5 and DEF7) was then crossed reciprocally to the descendants of GT1-4-5 in order to generate transgenic plants expressing all the necessary genes for the establishment of the novel pathway (GT-DEF12, 14 and 15 plants in figure 3.9).

Physiological, biochemical and biophysical analysis were implemented using the T2 generation of GT-DEF plants for evaluating the impact of the novel biochemical pathway in *planta*.

Figure 3.9: Sketch represents the generation of GT-DEF transgenic plants.

Shown is a simplified diagram representing how the GT-DEF transgenic plants were generated. GT = plants expressing GCL and TSR genes; F = plants expressing glcF gene; DEF = plants expressing *glc*D, *glc*E and *glc*F genes; GT-DEF = plants expressing all genes necessary for the novel pathway (i.e. *GCL, TSR* and DEF genes). Green colour = plants expressing the genes but they were not involved in the generation of GT-DEF plants; black colour = plants that were used for the generation of GT-DEF plants.

3.2.3.1 Analysis of GT-DEF transgenic plants on the DNA and RNA levels

Crossing between GT-homozygous plants and DEF plants results in the production of GT-DEF transgenic plants (3.2.3). The seeds produced from the crossing step were cultivated directly in soil without any selection pressure. The resulting plants were analyzed for the presence of the five foreign genes (*GCL*, *TSR*, *glc*D, *glc*E and *glc*F) in their genome by PCR. A multiplex PCR system was optimized in order to test many transgenic plants in a short time period with less effort (2.2.1.6). Figure 3.10 shows the results of the GT-DEF multiplex PCR results. A mixture of GT-DEF plasmids DNA was used as a positive contol (Lane 2 in figure 3.10).
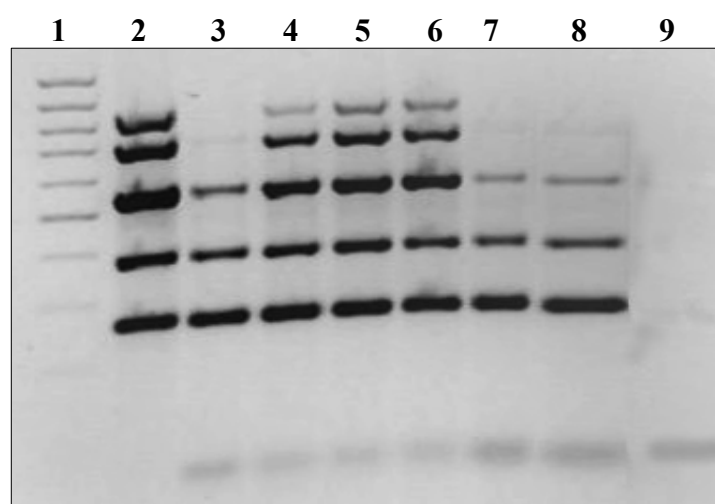
Figure 3.10: GT-DEF multiplex PCR result.

Shown is the ethidium bromide mediated fluorescence of GT-DEF multiplex PCR products after UV excitation. The multiplex PCR products were subjected to a 2% (w/v) agarose gel in 1 x TAE buffer for 120 min at 70 V.Five different bands of the expected size range corresponding to *GCL* (259 bps), *TSR* (384 bps), *glc*F (550 bps), *glc*E (720 bps) and *glc*D (847 bps) are obtained. Lane 1 = 100 bps DNA marker; Lane 2 = GT-DEF plasmid DNA mixture used as a positive control; Lane 3-8 = GT-DEF 8, 12, 14, 15, 18 and 24 plants respectively; Lane 9: negative control.

Some plants show positive signals for all genes for example lane 4, 5 and 6 in figure 3.10 whereas only signals for *GCL*, *TSR* and *glc*F genes were also detected in the tested plants as Lane 3, 7 and 8 in figure 3.10. Total 26 plants were analyzed by multiplex PCR; three of them contain all the GT-DEF genes in their genome (named GT-DEF12, 14 and 15 plants) whereas the other tested plants show signals for DEF, GT and GT-F genes. These GT-DEF plants were further checked on the RNA level for the expression of all GT-DEF genes by RT-PCR (data not shown). All the three GT-DEF plants show varying expression levels for each single gene. The expression levels of *glc*F, *GCL* and *TSR* genes are less compared to *glc*D and *glc*E

counterparts. However, the expression levels of those genes are clearly detectable and far above background. From these results, it is concluded that the tested plants are expressing the novel pathway genes in their chloroplasts.

3.3 Establishment of *GCL*, *TSR* and cTP-*At*GDH activity in *A. thaliana* chloroplasts

In another approach, *At*GDH gene from *A. thaliana* together with the bacterial *GCL* and *TSR* was used for the establishment of the novel pathway in the chloroplast of *A. thaliana* plants.

3.3.1   Subcellular localization and enzymatic characteristics of *At*GDH

Bari *et al.* (2004) have shown that the coding sequence of the first 77 amino acids of *At*GDH in translational fusion to red fluorescent protein (dsRED) targets proteins to the mitochondria. In this chapter, the subcellular localization of the whole *At*GDH protein in *A. thaliana* plant cells is shown. Moreover, the function of *At*GDH w/o mTP as a glycolate dehydrogenase was also tested.

3.3.1.1 Subcellular localization of *At*GDH in *A. thaliana* plants

To ensure that the whole *At*GDH coding sequence is also targeted to the mitochondria but not to the chloroplast, wild type *A. thaliana* plants were transformed with pTRA-K-AtGDH-RFP construct containing the whole coding sequence of *At*GDH in translational fusion to red fluorescent protein (dsRED) (Jach *et al.*, 2001). Details of cloning and subcellular localization of *At*GDH are described in the materials and methods chapter (2.1.9.15 and 2.2.1.13, respectively).

Microscopic analysis of transgenic lines revealed an accumulation of the red fluorescence in particles of approximately 1 μm in size resembling mitochondria (data not shown). For further analysis, protoplasts were prepared from leaves of 4 weeks old transgenic plant leaves and mitochondria were specifically stained with the MitoTracker Green dye. The confocal laser images in figure 3.11 show the chlorophyll fluorescence of chloroplasts in blue, the stained mitochondria in green and the dsRED-mediated fluorescence of the fusion protein in red. Care was taken that the green fluorescence of the MitoTracker Green dye was not visible in the red channel detecting the fluorescence of the dsRED protein and *vice versa*. The mitochondrial stain shown in figure 3.11B, almost perfectly co-localizes with the dsRED fluorescence shown in figure 3.11A, indicating that the complete *At*GDH protein is targeted to

mitochondria *in vivo*. Therefore, the function of *At*GDH w/o mTP as a glycolate dehydrogenase was tested (3.3.1.2).

A	B
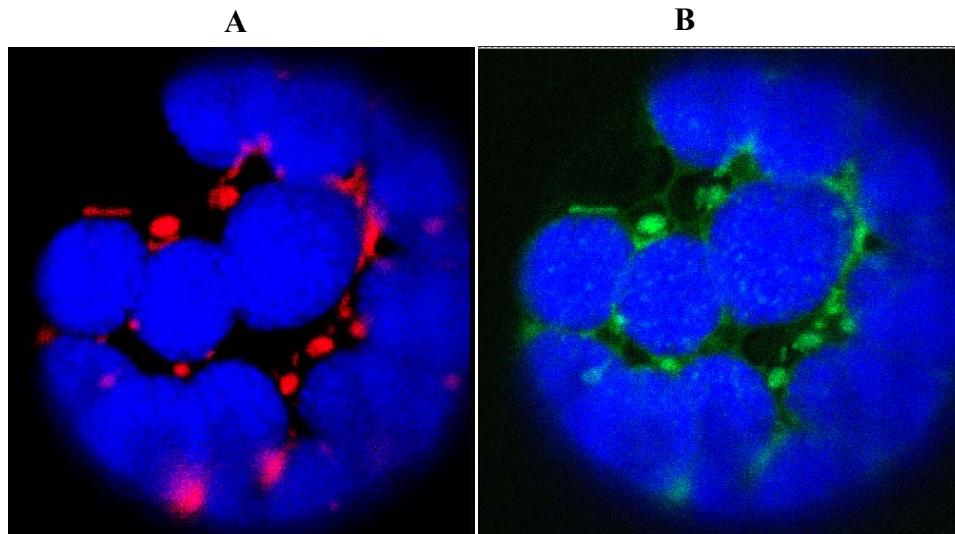
Figure 3.11: Subcellular localization of *At*GDH

The picture shows epifluorescence photographs of protoplasts from *Arabidopsis* plants that were transformed with a construct expressing *At*GDH in translational fusion to red fluorescent protein (dsRED). Excitation wave lenghts were 488 nm and 568 nm and emission filters were 515-535 nm (MitoTracker Green, shown in green), 570-610 nm (dsRED, shown in red) and 660-720 nm (chlorophyll fluorescence, shown in blue). Magnification is 630 x. In figure 3.11, A = overlay of chlorophyll fluorescence and dsRED-mediated fluorescence and B = overlay of chlorophyll fluorescence and MitoTracker Green-mediated fluorescence.

3.3.1.2 *At*GDH w/o mTP shows the same enzymatic activities of the complete *At*GDH

Activity assays were only performed for the complete *At*GDH protein including the mitochondrial targeting peptide (Bari *et al.*, 2004). In order to use this *At*GDH as an alternative for *Ec*GDH, the coding sequence for mTP should be replaced with a chloroplast targeting peptide. Therefore, the coding sequence of *At*GDH w/o mTP was cloned in translational fusion to six histidine residues into the pET22b(+) bacterial expression vector (2.1.9.21). The *At*GDH w/o mTP was expressed in ER2566 bacteria (2.2.3.1). The GDH and D-LDH enzymatic assays (2.2.3.17) were performed using crude extracts isolated from overexpressing bacteria. Figure 3.12 shows the GDH (A) and D-LDH (B) assays for the *At*GDH w/o mTP (Background on these assays is described in 3.2.2.4). Crude extracts from bacteria transformed with empty pET22b(+) bacterial expression vector were used as a negative control in both assays. Crude extracts isolated from bacteria expressing the *Ec*GDH proteins (i.e. transformed with pET-GO construct (2.1.9.20)) and other bacteria expressing the complete *At*GDH (i.e transformed with pET-AtGDH construct (2.1.9.22)) were used as positive controls. Both constructs were kindly provided by Rafijul Bari (Institute for Biology

I, RWTH-Aachen). The extracts containing *Ec*GDH, *At*GDH and *At*GDH w/o mTP show appreciable formation of glyoxylate from glycolate as specifically determined by the formation of glyoxylate phenylhydrazone in a coupled reaction.

(A)

(B)
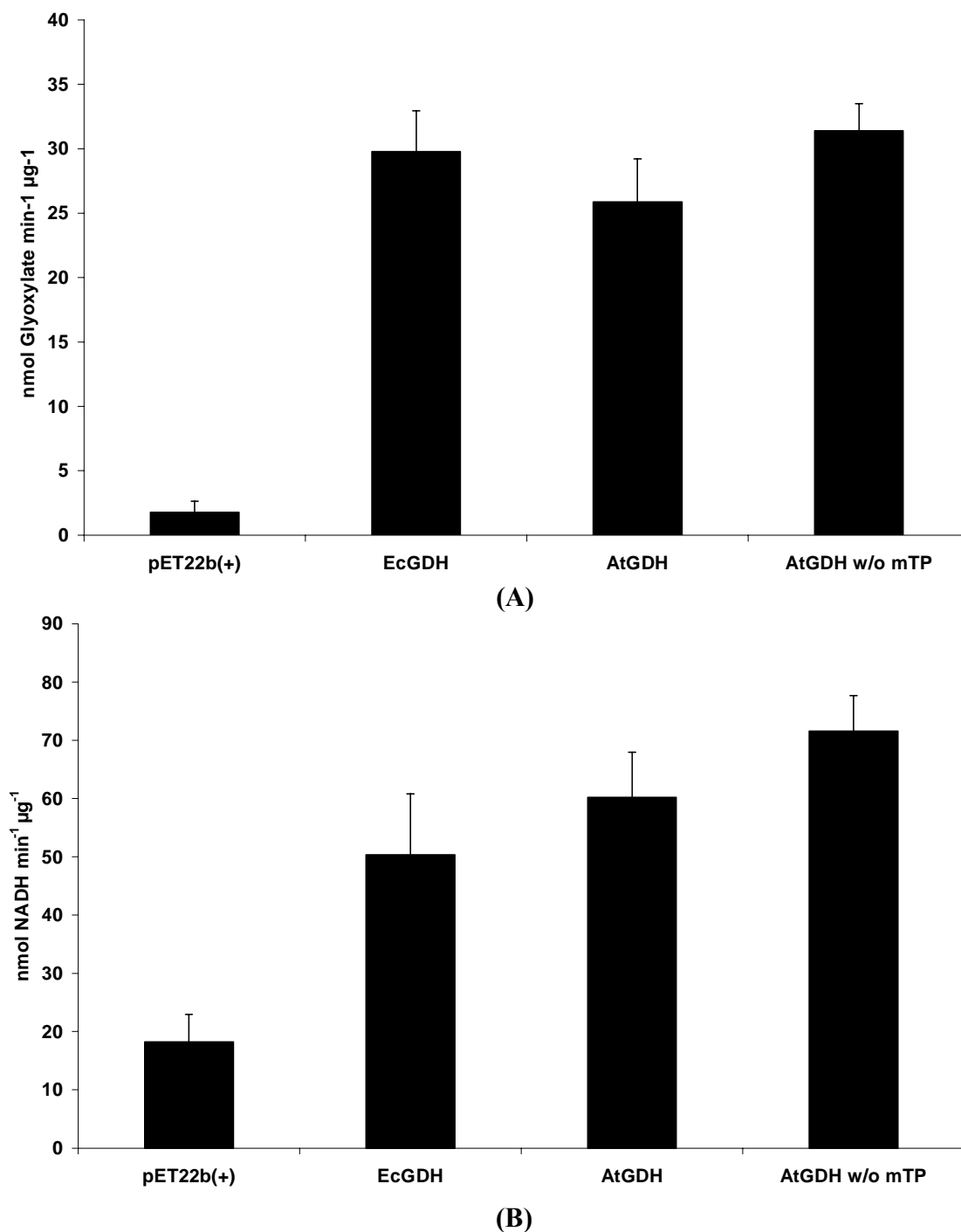
Figure 3.12: GDH and D-LDH assays for *At*GDH w/o mTP.

Shown are the GDH (A) and D-LDH (B) assays that were performed using different bacterial crude extracts. Each data point shows the amounts of glyoxylate (A) or NADH (B) formed per minute and is based on at least three independent experiments. Vertical bars show standard deviations. pET22b(+) = crude extracts from bacteria transformed with empty pET22b(+) bacterial expression vector as negative control in both assays; *Ec*GDH; *At*GDH; *At*GDH w/o mTP = Crude extracts isolated from different bacteria transformed with pET-GO, pET-AtGDH, and pET-AtGDH w/o mTP, respectively.

These levels are reduced to background if pET22b(+) crude extract (isolated from bacteria after induction of expression) is used (figure 3.12A). Similar results were obtained in the D-LDH assay (figure 3.12B). Based on these results, it can be concluded that *At*GDH w/o mTP has the same enzymatic characteristics as the complete *At*GDH. Therefore, the endogenous mitochondrial targeting sequence of *At*GDH was replaced by a chloroplast transit peptide (cTP) and was then used as an alternative to the complicated *Ec*GDH in the novel pathway.

3.3.2   Generation of transgenic *A. thaliana* plants expressing *GCL, TSR* and cTP-*At*GDH in their chloroplasts

In order to generate transgenic *A. thaliana* plants expressing *GCL, TSR* and cTP-*At*GDH in the chloroplast, homozygous GT plants (see chapter 3.2.1) were retransformed with a construct for cTP-*At*GDH (2.1.9.17). This retransformation step results in the production of transgenic plants expressing *GCL, TSR* and cTP-*At*GDH genes named GTA plants. At the same time, wild type *A. thaliana* plants were transformed with the same construct in order to generate plants expressing cTP-*At*GDH.

3.3.2.1 Cloning of *At*GDH w/o mTP into pSuper-PAM-Sul-rbcS1-cTP plant expression vector

Because GT-homozygous plants are resistant to kanamycin, it was necessary to clone the *At*GDH w/o mTP gene into a plant expression vector that has another selectable marker. Firstly, the coding sequence for *At*GDH w/o mTP gene in translational fusion to a His tag was cloned into the pTRA-K-rbcS1-cTP plant expression vector (2.1.9.1). Secondly, the resulting pTRA-K-rbcS1-cTP-*At*GDH (2.1.9.16) from the first step was used as an intermediate for the recloning of the cTP-*At*GDH insert (*At*GDH w/o mTP fused to a chloroplast targeting peptide) into another plant expression vector that confers resistance to sulfadiazine resulting in the production of pSuper-PAM-Sul-rbcS1-cTP-*At*GDH (2.1.9.17). By this cloning strategy, the transgenic plants that contain *GCL, TSR* and cTP-*At*GDH could be selected on MS medium supplemented with kanamycin and sulfadiazine antibiotics.

3.3.2.2 Stable transformation of *A. thaliana* plants with cTP-*At*GDH, *GCL* and *TSR* genes

Wild type *A. thaliana* plants were transformed with pSuper-PAM-Sul-rbcS1-cTP-AtGDH construct by *Agrobacterium* mediated floral dip transformation. Transgenic plants expressing

cTP-*At*GDH were generated. The descendants of GT1-4-5 homozygous plant (see chapter 3.2.1) were retransformed with the same construct (pSuper-PAM-Sul-rbcS1-cTP-AtGDH). This last transformation step results in the production of transgenic *A. thaliana* plants expressing all genes needed for the establishment of the novel pathway (i.e. *GCL*, *TSR* and cTP-*At*GDH).

3.3.2.3 Expression of *GCL*, *TSR* and cTP-*At*GDH in *planta*

The expression of *GCL*, *TSR* and cTP-*At*GDH in *planta* was mainly tested on the RNA level using Real Time RT-PCR. Total 15 plants transgenic for cTP-*At*GDH (simply named A-plants) were analyzed. Eight plants showed varying expression levels for cTP-*At*GDH whereas the rest of the tested plants did not show any expression for the cTP-*At*GDH (data not shown). No phenotypic effects were detected in the expressing plants.

Ten GTA-transgenic plants were tested for the expression of *GCL*, *TSR* and cTP-*At*GDH on the RNA level. Seven plants show varying expression levels for all genes and three plants showed only expression for GT-genes (i.e. *GCL* and *TSR*) but not for cTP-*At*GDH (data not shown). The T2 generation of GTA5 plants that showed comparable expression levels for all the three genes was used for further analyis of GTA transgenic plants.

Figure 3.13 shows the accumulation of cTP-*At*GDH (black bars), *GCL* (grey bars) and *TSR* (white bars) transcripts in the T2 generation of GTA5 transgenic plants. Most of the tested plants show varying expression levels for all the three genes as GTA5-3, GTA5-4, GTA5-5, GTA5-7, GTA5-8, GTA5-9 and GTA5-10 in figure 3.13 whereas some of the tested plants show only expression for *GCL* and *TSR* as GTA5-14 in figure 3.13. Based on these results, the transgenic GTA plants express all the necessary genes for the novel pathway in their chloroplasts.
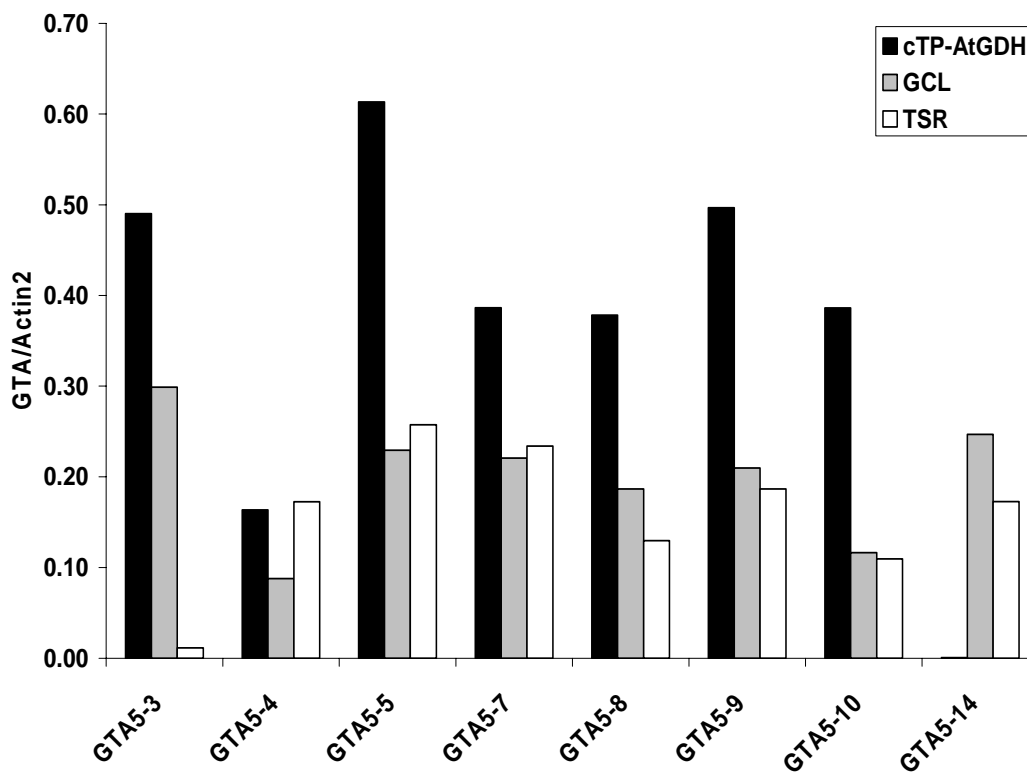
Figure 3.13: Accumulation of GTA transcripts in the T2 generation of GTA5 transgenic plant.

The amount of cTP-*At*GDH, *GCL* and *TSR* mRNA was measured by Real-Time RT-PCR and calculated in arbitrary units by comparison to a standard dilution series of a GTA plasmids DNA mixture. Each value is the relative accumulation of the respective RNA compared to the Actin2 levels measured in the preparation. Black bars = cTP-*At*GDH; Grey bars = *GCL*; White bars = *TSR*.

3.3.2.4 Analysis of GTA transgenic plants on the DNA level

For testing the GTA transgenic plants on the DNA level, a multiplex PCR system was optimized for this purpose (2.2.1.6). Figure 3.14 shows the results of the multiplex PCR using genomic DNA isolated from the T2 generation of GTA5 transgenic plants. A mixture of GTA plasmids DNA (pTRA-K-rbcS1-cTP-TSR.His, GCL.His and pSuper-PAM-Sul-rbcS1-cTP-AtGDH) was used as positive contol (lane 2 in figure 3.13). Some plants show positive signals for all the genes of interest (*GCL*, *TSR* and cTP-*At*GDH) for example lane 3, 5, 6, 7, 8 and 9 in figure 3.14 whereas others show only signals for *GCL* and *TSR* genes (lane 4 in figure 3.14). The GTA and GT-DEF multiplex PCR systems help in identifying the real transgenic plants in a short time with less effort before analyzing the expression of the single genes by Real Time RT-PCR on the RNA level for further analysis.
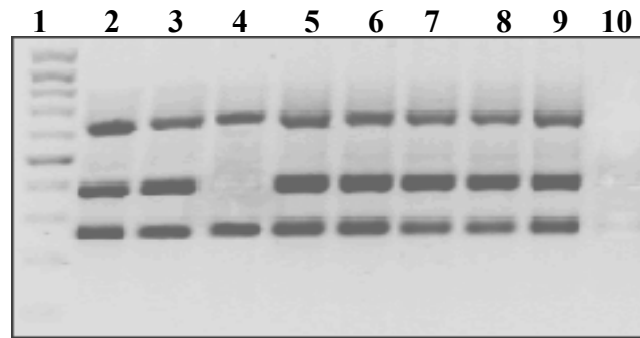
Figure 3.14: GTA multiplex PCR

Shown is the ethidium bromide mediated fluorescence of GTA multiplex PCR products after UV excitation. The multiplex PCR products were subjected to a 2% (w/v) agarose gel in 1 x TAE buffer for 120 min at 70 V. Three different bands of the expected size range corresponding to GCL (259 bps), TSR (640 bps) and cTP-*At*GDH (380 bps) are obtained. Lane 1 = 100 bps DNA marker; Lane 2 = GTA plasmid DNA mixture used as positive control; Lane 3-9 = GTA5-1, GTA5-2, GTA5-3, GTA 5-4, GTA5-5, GTA5-7 and GTA5-8 plants, respectively; Lane 10: negative control.

3.3.2.5 *At*GDH protein isolated from the chloroplast of plants transgenic for A is active *in vitro*

Glycolate dehydrogenase (GDH) and D-lactate dehydrogenase assays (D-LDH) were performed *in vitro* in the presence and absence of KCN using chloroplast extracts isolated from plants transgenic for A. Chloroplasts were isolated (2.2.3.7) from 6 weeks old T2 generation descendants of plant 14 transgenic for A in addition to wild type plants. Plant 14 transgenic for A showed the highest expression level for cTP-*At*GDH compared to other plants transgenic for A. Figure 3.15 represents the results from the GDH assay using chloroplast protein extracts isolated from WT and plants transgenic for A. Chloroplast extracts isolated from plants transgenic for A show an approximately 3-fold higher activity than chloroplast extracts from WT plants in the absence of KCN (black bars in figure 3.15). This activity is reduced to similar background levels in the presence of KCN (grey bars in figure 3.15) when it is compared with WT extracts. This background may be due to little peroxisomal and mitochondrial contamination during the isolation and extraction of chloroplast proteins from the tested plant leaves (i.e. presence of the peroxisomal glycolate oxidase and mitochondrial *At*GDH). Additionally, this background may be related to the presence of free glyoxylate in the chloroplast extracts. The difference in the activity levels in chloroplast extracts isolated from plants transgenic for A is due to the presence of cTP-*At*GDH protein in the tested samples. This leads to the conclusion that overexpressed cTP-*At*GDH protein in the chloroplast is active *in vitro*.
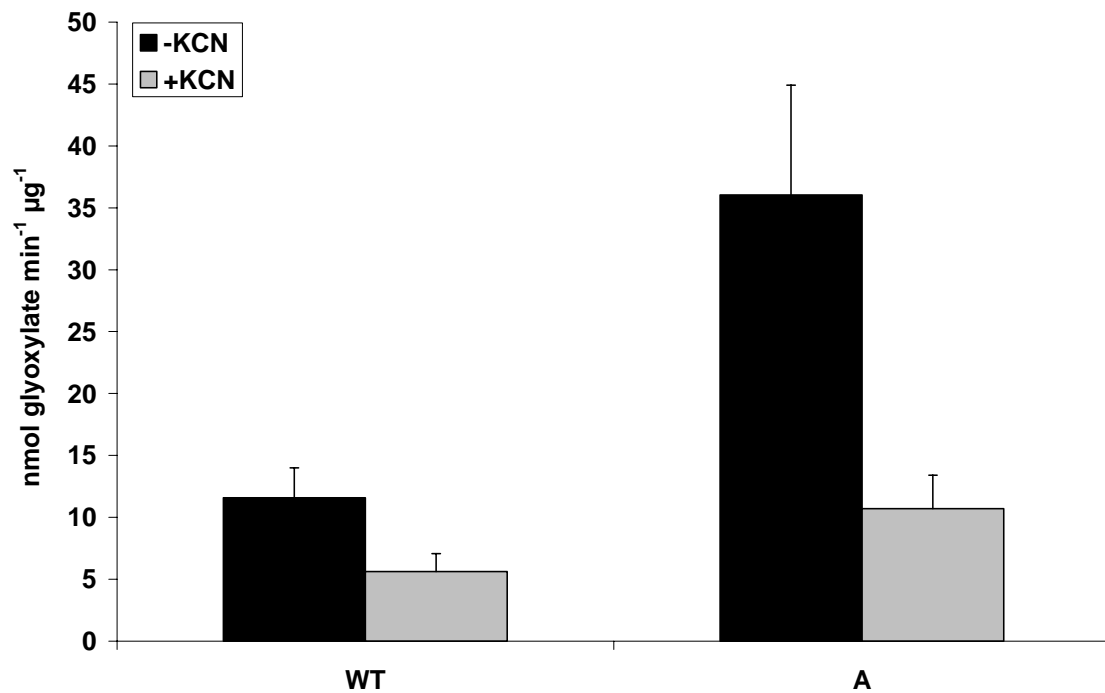
Figure 3.15: GDH assay from WT and A-chloroplast extracts

Chloroplast protein extracts isolated from 6 weeks old WT plants as well as from plants transgenic for A were tested for glycolate dehydrogenase activity. Each data point shows the amount of glyoxylate formed per minute and is based on at least three independent experiments. Vertical bars show standard deviations. Black bars = -KCN; grey bars = +KCN; WT and A = chloroplast extracts isolated from wild type and plants transgenic for A, respectively.

At the same time, a D-LDH assay was performed using the same chloroplast extracts, isolated from wild type plants and plants transgenic for A, that were used for the glycolate dehydrogenase assay (see figure 3.16). Chloroplast protein extracts isolated from plants transgenic for A show an approximately 3-fold higher activity than chloroplast extracts from WT plants in the absence of KCN (black bars in figure 3.16). This activity is inhibited in both chloroplast extracts in the presence of KCN (grey bars in figure 3.16). The activity observed in the chloroplast extract from WT plants is perhaps due to a little contamination with mitochondria during the chloroplast isolation step (i.e. presence of the mitochondrial AtGDH). Presence of other enzymes that are sensitive to cyanide and use NAD^+ as cofactor may also be a reason for the appearance of such background.
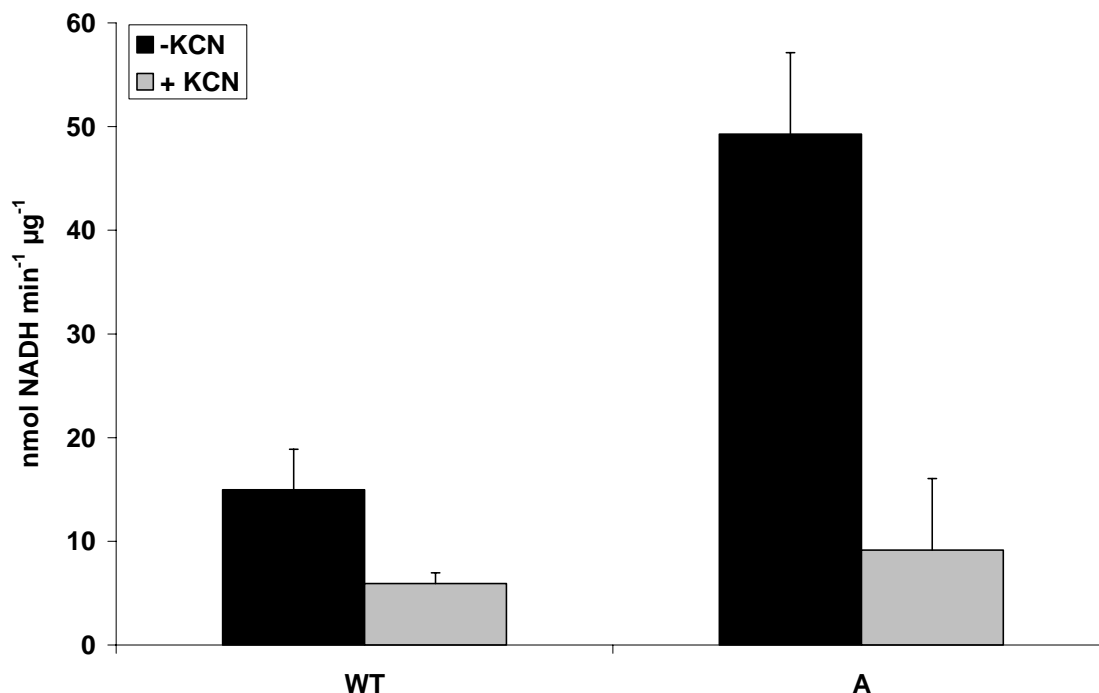
Figure 3.16: D-LDH assay from WT and A-chloroplast extracts.

Chloroplast protein extracts isolated from 6 weeks old WT plants and plants transgenic for A were tested for D-LDH activity. Each data point shows the amount of NADH produced per minute and is based on at least three independent experiments. Vertical bars show standard deviations. Black bars = -KCN; grey bars = +KCN; WT and A = chloroplast extracts isolated from wild type and plants transgenic for A, respectively.

The results from both assays revealed that the chloroplast extracts from plants transgenic for A showed a glycolate dehydrogenase activity that is inhibited by cyanide. It can be concluded that the cTP-*At*GDH protein is therefore active *in vivo*.

Taken together, the alternative approach using a plant glycolate dehydrogenase show similar effects compared to the other approach using *Ec*GDH. Therefor, all further analyses were performed using transgenic plants expressing both pathways (i.e. GTA and GT-DEF plants).

3.4 Biochemical analysis of DEF, GT-DEF, A, GTA and GT transgenic plants

3.4.1 Measurement of glycine/serine ratio as a marker for the rate of photorespiration

In order to check the efficiency of the novel pathway in transgenic plants expressing the complete novel pathway genes, the ratio of the amino acid glycine to serine was measured. Measuring Gly/Ser ratios in C_3 plants   is considered as a marker for the rate of

photorespiration (Novitskaya *et al.*, 2002). GT, A, GTA, DEF and GT-DEF transgenic *A. thaliana* plants in addition to wild type plants were grown under ambient (350 ppm) and low (100 ppm) CO_2 conditions (2.2.6.3) in order to measure the Gly/Ser ratio under normal and enhanced photorespiratory rates, respectively.
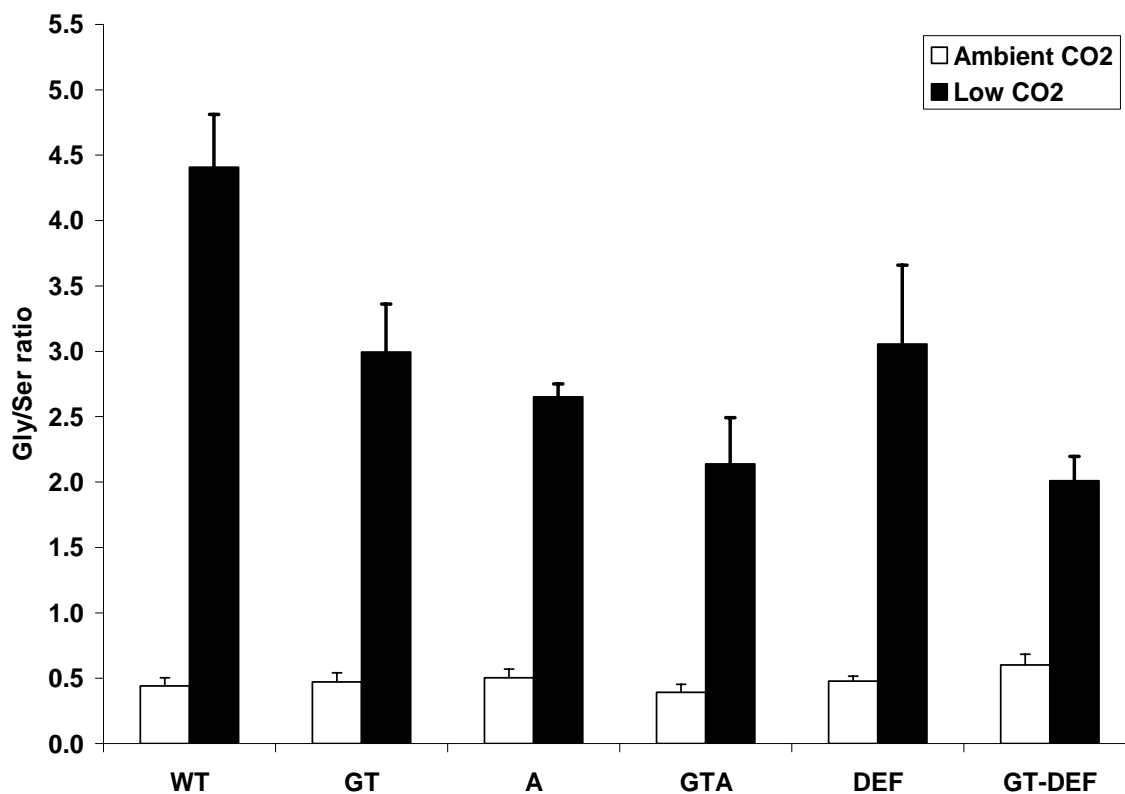
Figure 3.17: Glycine/Serine ratios measured from transgenic plants.

Shown are the different Gly/Ser ratios measured under ambient (350 ppm CO_2) and low CO_2 (100 ppm) conditions from different transgenic *A. thaliana* plants. Each data point shows the average of Gly/Ser ratios measured from at least 4 sister plants. Vertical bars show standard deviations. Black bars = Gly/Ser ratios measured from 8 weeks old plants that were grown for 4 h under low CO_2 conditions; White bars = Gly/Ser ratios measured from 8 weeks old plants that were grown under ambient conditions. WT = wild type; GT = plants expressing *GCL* and *TSR*; A = plants expressing cTP-*At*GDH; GTA = plants expressing *GCL*, *TSR* and cTP-*At*GDH; DEF = plants expressing *Ec*GDH; GT-DEF = plants expressing *GCL*, *TSR* and *Ec*GDH.

The amounts of glycine and serine from leaf samples harvested from the tested plants were quantified using Gas Chromatography/Mass Spectroscopy (GC/MS) (2.2.4). Figure 3.17 shows the results of the measured Gly/Ser ratios. All transgenic plants (GT, A, GTA, DEF and GT-DEF) show more or less similar levels of Gly/Ser ratio compared to wild type plants when all the tested plants are grown under ambient conditions (white bars in figure 3.17). By growing the same plants in low CO_2 environment (i.e. enhanced photorespiration) for 4 h, the Gly/Ser ratios increase in both wild types and transgenic plants (black bars in figure 3.17). Transgenic plants expressing only *GDH* in their chloroplasts (A and DEF in figure 3.17) have lower Gly/Ser ratios compared to WT plants. This decrease in Gly/Ser ratio is enhanced by

the expression of all the necessary genes for the novel pathway (GTA and GT-DEF in figure 3.17). Interestingly, overexpression of *GCL* and *TSR* in the chloroplast of *A. thaliana* plants results also in a lower Gly/Ser ratio compared to WT plants in low CO_2 environment (GT in figure 3.17). These results lead to the conclusion that the expression of the novel pathway genes in *A. thaliana* chloroplasts results in a partial suppression of photorespiration independent of whether the pathway has been assembled partially or completely.

3.4.2   Measurement of the ammonia release during photorespiration

Ammonia is released in the photorespiratory pathway during the conversion of glycine to serine in the mitochondria. The released ammonia is refixed by the GS-GOGAT cycle (1.4.1). Lacuesta *et al.* (1989); Tachibana *et al.* (1986); Wild and Ziegler (1989) have shown that the herbicide phosphinotricin is a glutamate analogue that irreversibly inhibits glutamine synthetase activity and as a result ammonia accumulates inside the plant leaf tissues. A multiwell ammonium-evolution bioassay was introduced by De Block *et al.* (1995) which allowed a quantitative assessment of the ammonia accumulated in the plant leaf tissues. The assay works on the basis that leaf tissues incubated in medium supplemented with phosphinotricin are not able to assimilate ammonium. The ammonia accumulating in the leaf tissues diffuses into the surrounding medium where a colourimetric reaction indicates ammonium concentration. Under phosphinotricin treatment, higher ammonia accumulation means higher photorespiratory rates and *vice versa*.

Based on these facts, it was decided to measure the amounts of ammonia released from transgenic plant leaf tissues as another marker for the rate of photorespiration (see 2.2.3.18). The results of the measurements are shown in figure 3.18. Plants transgenic for A show less ammonia release compared to wild type plants (A in figure 3.18). The amount of ammonia released from GTA plant leaf tissues is even lower than the amount of ammonia accumulated in plants transgenic for A (GTA in figure 3.18). These results can also be added to the positive impacts of the novel biochemical pathway on the suppression of photorespiration. It can be concluded that the expression of *GCL*, *TSR* and cTP-*At*GDH in the chloroplasts of *A. thaliana* plants results in a partial suppression of photorespiration and this is also true for transgenic plants expressing only cTP-*At*GDH. Such measurements could not be performed with plants transgenic for DEF because these plants are resistant to phosphinotricin.
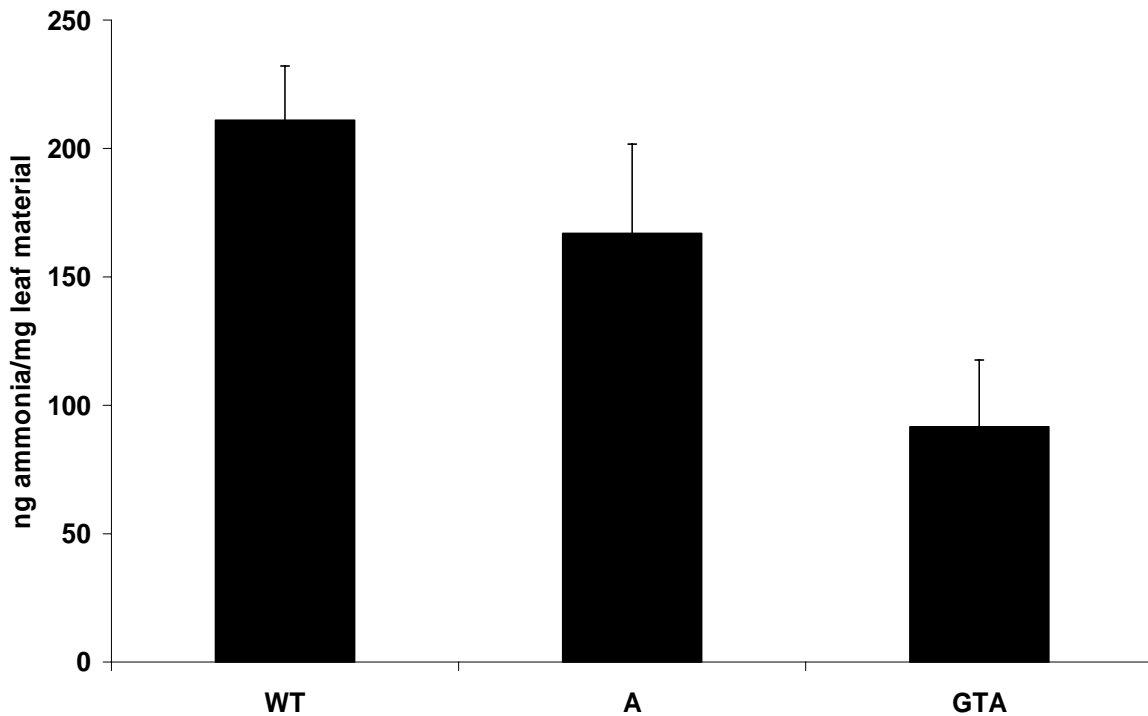
Figure 3.18: Ammonia release from transgenic plants.

Shown is the ammonium-evolution bioassay that was performed using leaf tissues harvested from 8 weeks old WT, GTA and plants transgenic for A that were grown under ambient conditions. The amount of ammonia released was measured from plant leaf discs (5 mg each) incubated in medium supplemented with phosphinotricin. Each data point shows the amount of NH_3 released and is based on at least three independent experiments. Vertical bars show standard deviations. WT = wild type; A = plants expressing cTP-*At*GDH; GTA = plants expressing *GCL*, *TSR* and cTP-*At*GDH.

3.4.3   Total glyoxylate content of transgenic plants

Glycolate oxidation in plant peroxisomes during photorespiration results in the formation of glyoxylate. Glyoxylate is further metabolized to form phosphoglycerate as an end product of the photorespiratory pathway (1.4.1). Since glyoxylate could be used by glyoxylate carboligase (*GCL*) in the novel biochemical pathway (3.1), it was decided to measure the total glyoxylate content from different transgenic lines in addition to wild types grown under normal and enhanced photorespiratory conditions (350 ppm and 100 ppm CO_2, respectively). Figure 3.19 shows the total glyoxylate content measured from the indicated genotypes (2.2.3.14). Under ambient conditions, transgenic plants for A, GTA, DEF and GT-DEF show similar levels of glyoxylate content compared to WT plants (white bars in figure 3.19). On contrast, GT plants show a clear reduction in glyoxylate content under the same growing conditions. By growing all plants for 4 h under low CO_2 conditions (black bars in figure 3.19), GTA and GT-DEF plants show no clear response to low CO_2 growing conditions whereas DEF plants show a little increase in their gloyxylate content compared to WT plants.

Moreover, plants transgenic for A show a clear increase in their glyoxylate content compared to their WT counterparts. Although the amount of glyoxylate increases in GT plants under low CO_2 conditions, they still show a clear reduction in their glyoxylate content compared to all the tested plants.
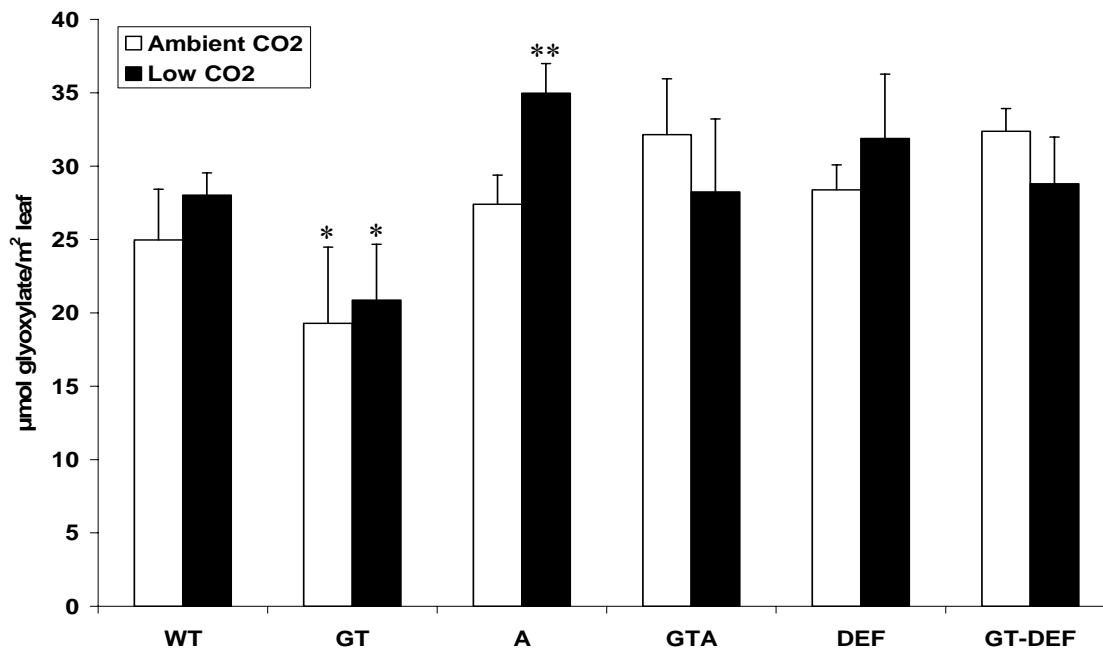
**Figure 3.19: Total glyoxylate content measured from transgenic plants.**

Shown are the total glyoxylate contents measured from leaf tissues harvested from 8 weeks old WT, GT, A, GTA, DEF and GT-DEF plants. Each data point shows the average of glyoxylate content measured from at least 4 sister plants. Vertical bars show standard deviations. Black bars = amounts of glyoxylate measured from plants that were grown for 4 h under low CO_2 conditions; White bars = amounts of glyoxylate measured from plants that were grown under ambient conditions. WT = wild type; GT = plants expressing *GCL* and *TSR*; A = plants expressing cTP-*At*GDH; GTA = plants expressing *GCL, TSR* and cTP-*At*GDH. DEF = plants expressing *Ec*GDH; GT-DEF = plants expressing *GCL, TSR* and *Ec*GDH; * and ** denote deviations from the wild types with P<0.1 and P<0.05, respectively.

The reduction in glyoxylate content in GT plants can be due to the consumption of glyoxylate by glyoxylate carboligase (*GCL*) in their chloroplasts. The increased levels of glyoxylate content in plants transgenic for A and DEF under low CO_2 conditions can be due to the production of glyoxylate in their chloroplasts from glycolate oxidation, since both genotypes express glycolate dehydrogenase in their chloroplasts (i.e. cTP-*At*GDH or *Ec*GDH). GTA and GT-DEF transgenic plants did not only consume glyoxylate by glyoxylate carboligase (*GCL*) but those plants produce also glyoxylate through the oxidation of glycolate by glycolate dehydrogenase (cTP-*At*GDH or *Ec*GDH, respectively) in their chloroplasts. Thus, glyoxylate content of both genotypes could not be changed. These results lead to the conclusion that the novel pathway enzymes are active in *planta*.

3.4.4 Measurements of glucose, fructose, sucrose, and starch contents of transgenic plants

Since glucose, fructose, sucrose and starch are end products of plant photosynthesis, it was decided to measure these metabolites from different transgenic plants. Figure 3.20 shows the different soluble and insoluble metabolites measured from WT and different transgenic plant leaf tissues.
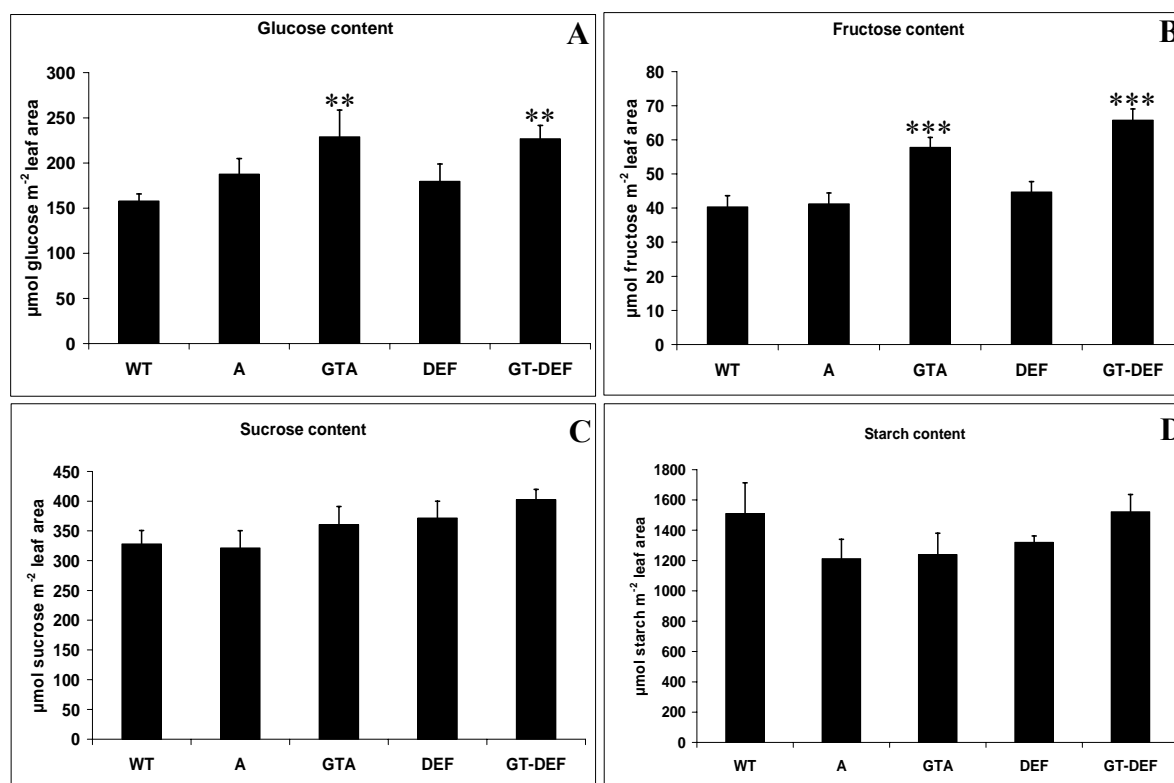
Figure 3.20: Soluble and insoluble metabolites measured from transgenic plants

Shown are the different soluble (glucose, fructose and sucrose) and insoluble (starch) metabolites measured from 8 weeks old different transgenic *A. thaliana* plants. Each data point shows the average of metabolites measured from 4 sister plants and is based on at least three independent experiments. Vertical bars show standard deviations. A = Glucose content; B = Fructose content; C = Sucrose content and D = Starch content. WT = wild type; A = plants expressing cTP-*At*GDH; GTA = plants expressing *GCL, TSR* and cTP-*At*GDH. DEF = plants expressing *Ec*GDH; GT-DEF = plants expressing *GCL, TSR* and *Ec*GDH; *, **, and *** denote deviations from the wild types with $P<0.1$, $P<0.05$ and $P<0.001$, respectively.

The total soluble (glucose, fructose and sucrose) and insoluble (starch) metabolites were extracted from plant leaf tissues and quantified enzymatically as described (2.2.3.8). Transgenic plants for A and DEF show more or less similar levels of soluble and insoluble metabolites compared to WT plants (figure 3.20A, B, C and D). GTA and GT-DEF show higher levels of glucose and fructose (figure 3.20A and B) and more or less similar levels of sucrose and starch (figure 3.20 C and D) compared to the other tested plants. Higher levels of

glucose and fructose in GTA and GT-DEF plants can be added to the positive significance of the novel pathway in the transgenic plants. It can be concluded that the expression of the novel pathway genes inside plant chloroplasts has no negative impacts on the basic metabolic pathways of the tested plants.

3.4.5 Analysis of the primary photosynthetic fixation products

The primary photosynthetic fixation products in transgenic *A. thaliana* plants were characterized by feeding plant leaf discs with $^{14}CO_2$ for 10 seconds (2.2.3.12). Figure 3.24 shows the results of $^{14}CO_2$ feeding to WT, GT, A, DEF, GTA and GT-DEF plants. The ^{14}C-labelled soluble metabolites were extracted from the plant leaf discs. The amount of radioactivity of the soluble (extracts) and insoluble (leaf materials) fractions was measured from each plant. The amount of radioactivity in the insoluble fraction was more than 2-fold higher than that in the soluble fraction. Same amounts of the radioactive soluble fraction were subjected to 2D-TLC in order to estimate the abundance of various photosynthetic products formed in the plant leaves.

All the tested plants show similar products on the autoradiogram and also similar spot intensities with the exception of slight differences in the concentrations of some products for example glucose-6-phosphate and fructose-1,6-bisphosphate (spot 14 and 17 respectively, in figure 3.21). DEF and GT-DEF plants produce more amounts of the two sugars compared to the other tested plants. It was expected to identify one of the products of the novel pathway - as glyoxylate or tartronic semialdehyde- but it seems that either these two compounds are unstable or that they are consumed quickly *in vivo* or that the running conditions on the TLC were not suitable. This result provides new evidence that expression of the novel pathway genes in the chloroplast of the transgenic plants did not interfere with the basic plant metabolism.
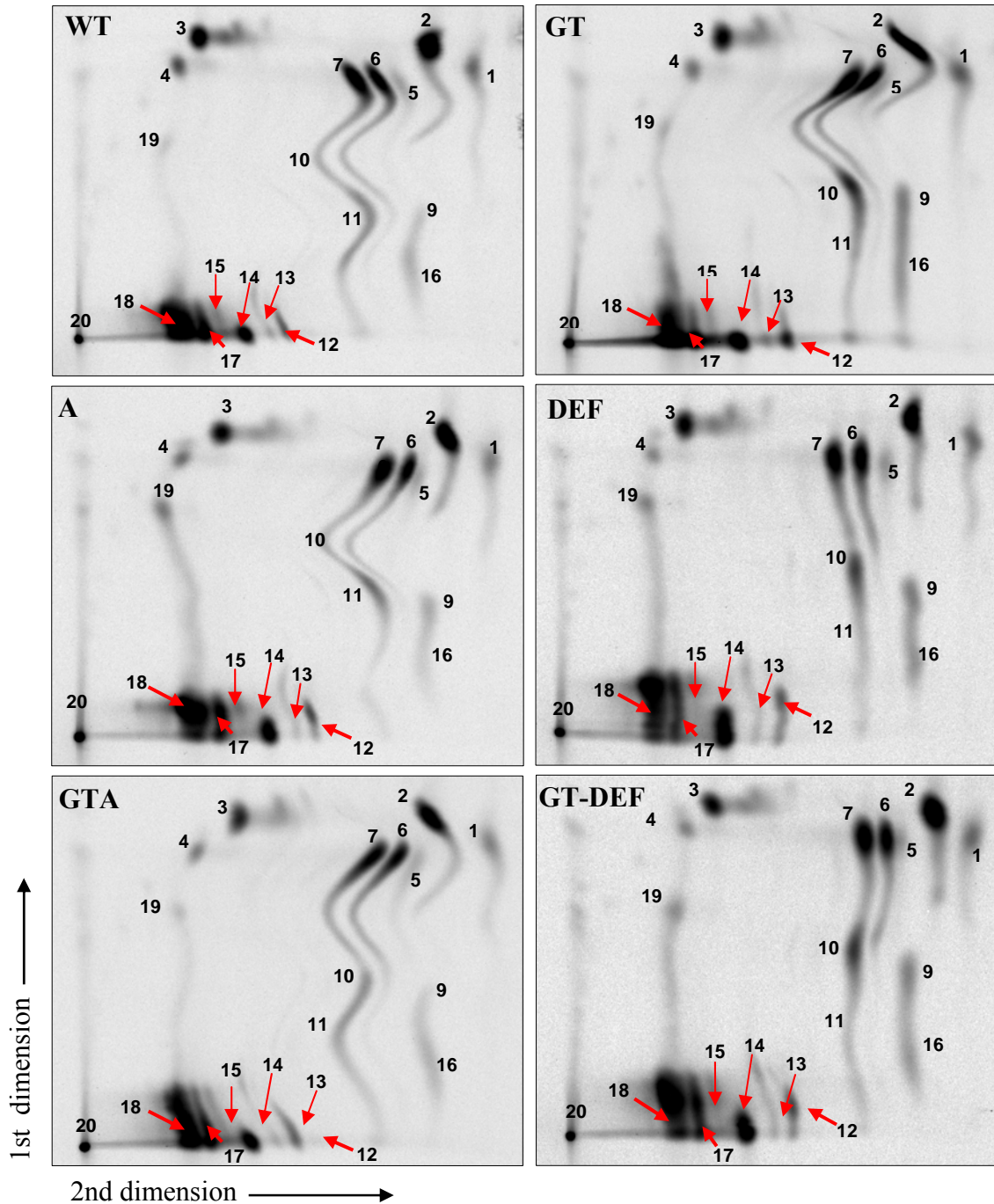
Figure 3.21: Autoradiogram of the primary photosynthetic fixation soluble products from transgenic plants.

Shown are 6 different autoradiograms from two dimension TLC analysis of the soluble metabolites extracted from 8 weeks old different plant leaf discs subjected to short time labeling (10 secs) with $^{14}CO_2$. The different spots on the autoradiogram were identified based on a standard map. WT = wild type; GT = plants expressing *GCL* and *TSR*; A = plants expressing cTP-*At*GDH; GTA = plants expressing *GCL, TSR* and cTP-*At*GDH; DEF = plants expressing *Ec*GDH; GT-DEF = plants expressing *GCL, TSR* and *Ec*GDH. In each autoradiogram: 1 = Glycolate, 2 = Glycerate, 3 = Sucrose, 4 = Sedoheptulose, 5 = Malate, 6 = Glutamate, 7 = Aspartate, 9 = Succinate, 10 = Citrate, 11 = phosphoenolpyruvate, 12 = Ph-glycolate, 13 = Ph-glycerate, 14 = Glucose-6-phosphate, 15 = Fructose-6-phosphate, 16 = Fumarate, 17 = Fructose-1,6-bisphosphate, 18 = ribulose-1,5-bisphosphate, 19 = U-diphosphate glucose and 20 = starting point.

3.4.6 Measurements of chlorophyll contents from leaves of transgenic plants

As an additional photosynthetic parameter, the different photosynthetic pigments (Chl.a, Chl.b and carotenoids) were measured from the different transgenic plant leaf tissues under ambient (350 ppm CO_2) and low CO_2 (100 ppm CO_2) growth conditions (2.2.3.15). WT, GT, A, GTA, DEF and GT-DEF plants show similar levels of Chl.a, Chl.b and carotenoids under ambient conditions (data not shown). By growing the same lines for 15 days under low CO_2 environment, the amounts of Chl.a (black bars in figure 3.22), Chl.b (grey bars in figure 3.22) and carotenoides (white bars in figure 3.22) are decreased to similar levels as in WT, GT, A and GTA plants in figure 3.22. However, DEF and GT-DEF transgenic plants that were allowed to grow for 15 days under low CO_2 condition show a little decrease in their pigment contents (figure 3.22) compared to the other tested plants. This might be due to their accelerated growth rates and their morphological characteristics (3.6.1 and 3.6.2 below). It was obvious that DEF and GT-DEF plants have faster growth rates compared to wild type plants starting from the seedling phase. Thus, the expression of the novel pathway genes in plant chloroplasts has no deleterious effects on their photosynthetic pigments.
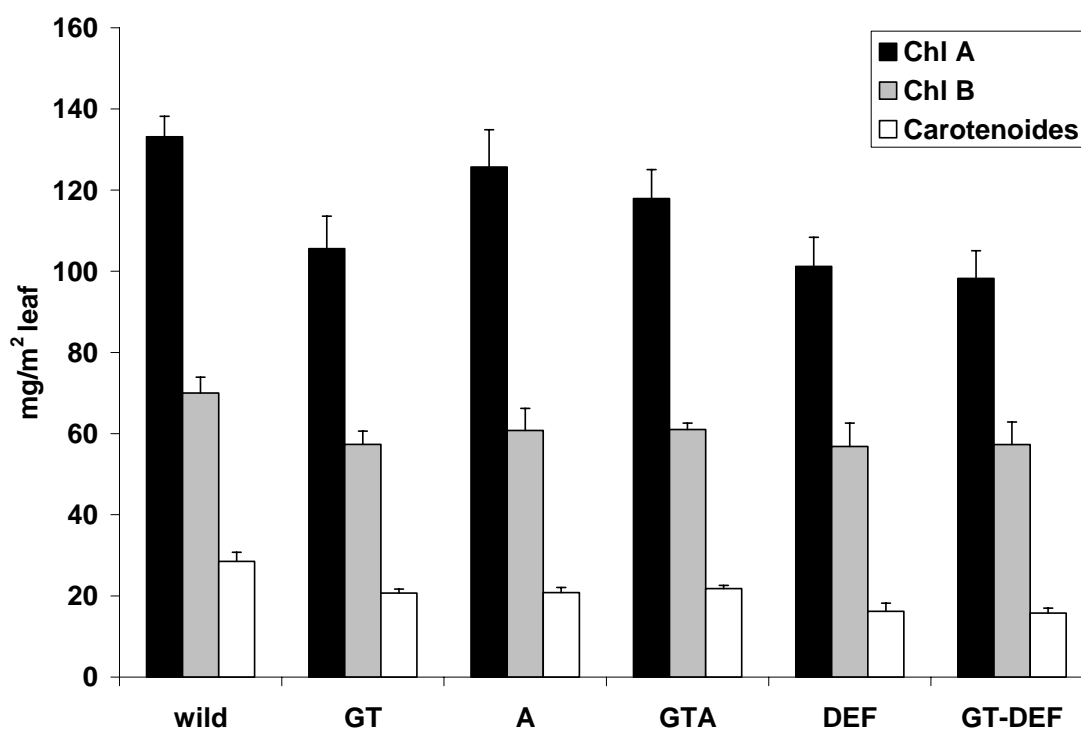
Figure 3.22: Total chlorophyll contents measured from transgenic plants.

Shown are the different amounts of plant leaf photosynthetic pigments measured from 8 weeks old different transgenic *A. thaliana* plants in addition to wild types after their growth for 15 days under low CO_2 conditions. Each data point shows the average of Chl.A (black bars), Chl.B (grey bars) and Carotenoids (white bars) from 4 sister plants and is based on at least three independent measurements. Vertical bars show standard deviations. WT = wild type; A = plants expressing cTP-*At*GDH; GTA = plants expressing *GCL*, *TSR* and cTP-*At*GDH. DEF = plants expressing *Ec*GDH; GT-DEF = plants expressing *GCL*, *TSR* and *Ec*GDH.

3.5 Photosynthetic performance of transgenic plants

Beside a possible impact of the novel pathway on the plant metabolism, overexpression of the novel pathway genes in transgenic plants should also change their photosynthetic performance. Therefore, postillumination burst (PIB), apparent CO_2 compensation point (Γ), internal CO_2 compensation point (Γ_*) and Chl.*a* fluorescence were measured.

3.5.1   Postillumination burst (PIB) as a marker for the rate of photorespiration

If a C_3 plant is exposed suddenly to darkness after a period of illumination (where the plant achieves steady-state rates of photosynthesis), a momentary rapid outburst of CO_2 occurrs before the plant achieves a steady-state dark respiration (R_n). This outburst represents the amounts of CO_2 released in the plant mitochondria during photorespiration (Atkin *et al.*, 1998; Bulley and Tregunna, 1971). Based on these observations, it was decided to determine the postillumination burst (PIB) from transgenic as well as wild type plants as a measure for the photorespiratory flow in these plants. PIB was measured via a fast-response CO_2 exchange system (LI-COR$^{®}$ photosynthesis portable measuring device) (2.2.5). The postillumination burst was calculated as shown in figure 3.23A. PIB equals the difference between the maximum CO_2 release after 20-120 seconds from switching off the light and the amout of CO_2 release during steady-state dark respiration (R_n).

Figure 3.23B shows the different postillumination bursts measured from WT, A, GTA, DEF and GT-DEF plants. Plants transgenic for A and DEF plants show a decrease in the amounts of CO_2 release during photorespiration as indicated by their PIB values compared to their WT counterparts. This decrease in the PIB is enhanced by expression of all the novel pathway genes in the plant chloroplasts (GTA and GT-DEF in figure 3.25B). These results show that the expression of the novel pathway genes in *A. thaliana* plant chloroplasts leads to a clear reduction in the photorespiratory CO_2 release in the mitochondria up to 20%. This can also be added to the positive significance of the novel pathway concerning the suppression of photorespiration.
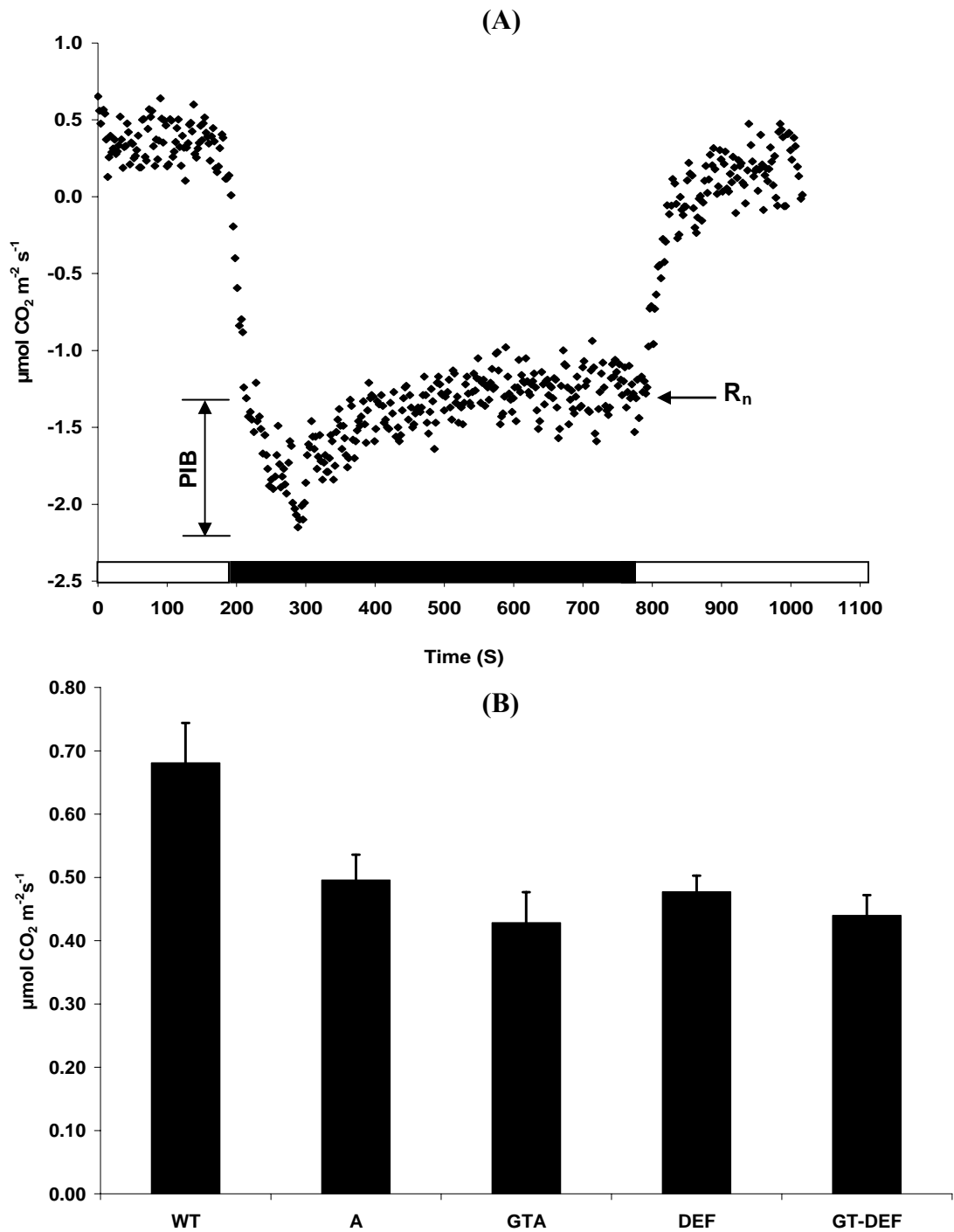
Figure 3.23: Postillumination burst from transgenic plants

Shown are a time course of net CO_2 exchange from a wild type *A. thaliana* plant leaf under 1000 μmol photons m^{-2} s^{-1} and 100 ppm CO_2 (A) and the different postillumination bursts measured from WT and different transgenic plants (B). In figure 3.23A: PIB = Postillumination burst and R_n = plant dark respiration; white bars = light on and black bars = light off. In figure 3.23B: Each value represents the PIB and is based on at least three independent measurements of five independent plants for each line. Vertical bars show standard error. WT = wild type; A = plants expressing cTP-*At*GDH; GTA = plants expressing *GCL, TSR* and cTP-*At*GDH; DEF = plants expressing *Ec*GDH; GT-DEF = plants expressing *GCL, TSR* and *Ec*GDH.

3.5.2   Determination of the apparent CO_2 compensation point (Γ)

At the apparent CO_2 compensation point, the amount of CO_2 fixation by a plant equals the amount of CO_2 released from the plant by photorespiration and respiration. The apparent Γ was measured from WT plants as well as from plants transgenic for A, GTA, DEF and GT-DEF by measuring their photosynthetic rates at different leaf internal CO_2 concentrations (the so called A/Ci- curve) as described in the materials and methods chapter (2.2.5). Figure 3.24 shows the different A/Ci curves that were measured from the indicated genotypes. Γ was calculated as the crossing point between the measured A/Ci-curve and the X-axis.
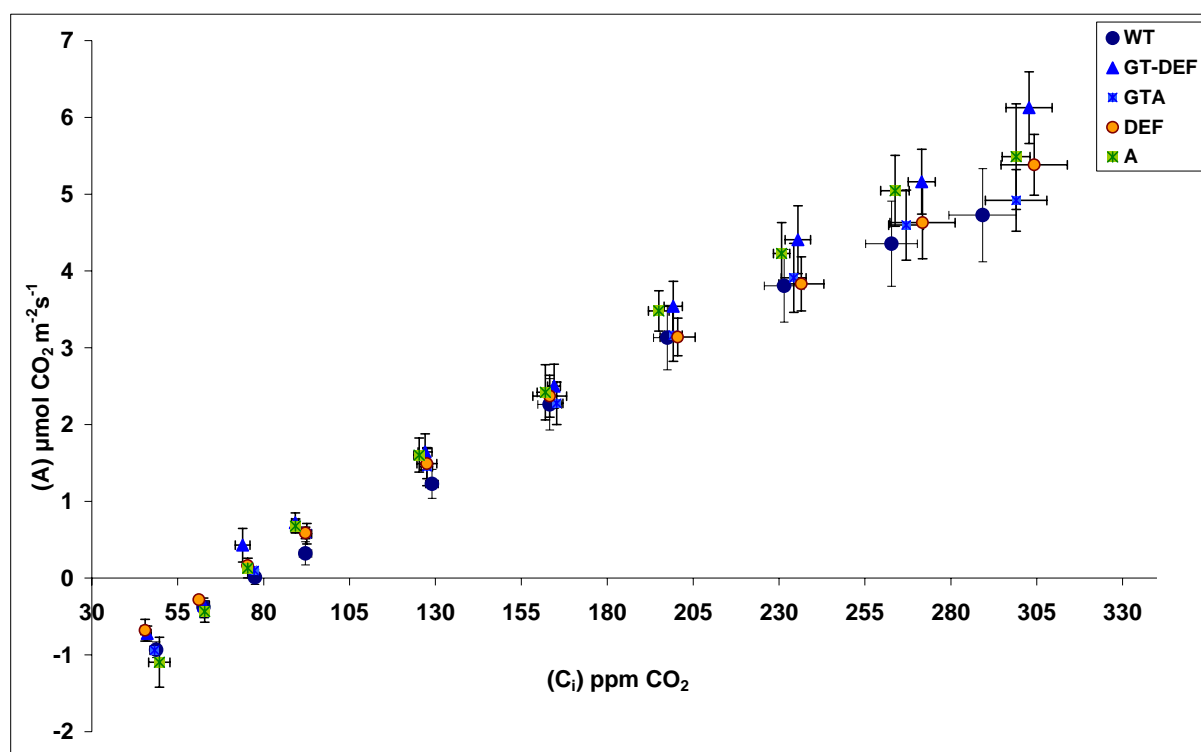
Figure 3.24: A/Ci-curve from WT and transgenic plants

Shown are different A/Ci-curves measured from 9-10 weeks old WT, A, GTA, DEF and GT-DEF plants under illumination of 1000 µmol photons m^{-2} s^{-1} and different external CO_2 concentrations (Ca) (400, 350, 300, 250, 200, 150, 100, 80, 60 and 40 ppm CO_2).Each value represents the assimilation rate and is based on at least 4 independent measurements from 4 sister plants for each line. Vertical and horizontal bars show standard error. (A)= Assimilation rate; (Ci) = internal CO_2 concentration in leaf intercellular spaces; WT = wild type; A = plants expressing cTP-*At*GDH; GTA = plants expressing *GCL*, *TSR* and cTP-*At*GDH; DEF = plants expressing *Ec*GDH; GT-DEF = plants expressing *GCL*, *TSR* and *Ec*GDH.

The apparent CO_2 compensation points for all the tested plants are listed in table 3.1. WT plants show the highest values of apparent CO_2 compensation point compared to the other tested plants. Plants transgenic for A and GTA plants have more or less similar values of Γ.

DEF and GT-DEF plants have the lowest levels of Γ compared to the other tested plants (see table 3.1). Based on this result, it can be concluded that the tested transgenic plants have higher rates of photosynthesis compared to their WT counterparts.

Plant	Apparent CO_2 compensation point (Γ)
WT	77.70 ± 2.45 ppm CO_2
A	73.06 ± 2.34 ppm CO_2
GTA	74.46 ± 3.36 ppm CO_2
DEF	68.50 ± 3.95 ppm CO_2
GT-DEF	66.80 ± 4.88 ppm CO_2

Table 3.1: The apparent CO_2 compensation points of WT and different transgenic plants

Shown are the apparent CO_2 compensation points measured from 9-10 weeks old wild type and different transgenic plants. WT = wild type; A = plants expressing cTP-*At*GDH; GTA = plants expressing *GCL*, *TSR* and cTP-*At*GDH; DEF = plants expressing *Ec*GDH; GT-DEF = plants expressing *GCL*, *TSR* and *Ec*GDH.

3.5.3   Determination of the CO_2 compensation point (Γ_*) of the transgenic plants

Because the apparent CO_2 compensation point represents not only the plant photorespiration but also the plant respiration, it was decided to measure the internal CO_2 compensation point (Γ_*). Γ_* refers to the internal CO_2 concentration (Ci) at which the rate of CO_2 assimilation equals the rate of photorespiration (Atkin *et al.*, 1998; Laisk, 1977; Laisk *et al.*, 1984). Thus, Γ_* gives not only a clear indication of the amounts of CO_2 releases in plant mitocondria during the photorespiratory pathway but also the amount of the CO_2 concentration in the vicinity of Rubisco at a given Ci. Γ_* was calculated by performing different A/Ci-curves at different light intensities for each individual plant (2.2.5). Figure 3.25 shows 4 different A/Ci-curves measured from plant transgenic for A under varying irradiances (here, 150, 80, 40 and 20 μmol photons $m^{-2}s^{-1}$) together with their trend lines in order to measure the internal CO_2 compensation point (Γ_*). For all irradiences, the CO_2 fixation decreases with the decrease in Ci values. The apparent CO_2 compensation point decreases with higher light intensities, because net photosynthesis increases. Nevertheless, all curves meet in a single point in the negative range of CO_2 assimilation. According to Laisk, (1977), the Ci value at this point represents Γ_*.
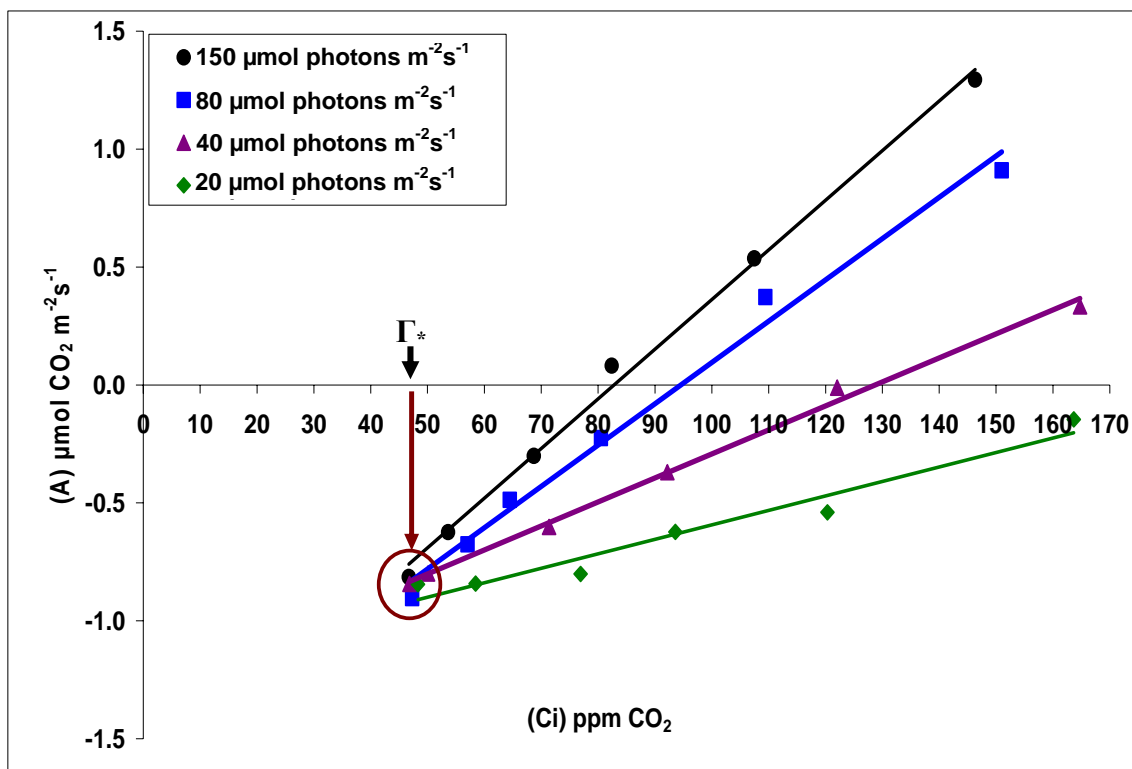
Figure 3.25: Measurement of Γ_* from plants transgenic for A.

Shown are different A/Ci-curves measured from 9-10 weeks old plants transgenic for A under illumination of 150, 80, 40 and 20 μmol photons m^{-2} s^{-1} and different Ca concentrations (200, 150, 100, 80, 60 and 30 ppm CO_2). (A)= Assimilation rate; (Ci) = internal CO_2 concentration in leaf intercellular spaces; Γ_* = the internal CO_2 compensation point.

The relative values of Γ_* for each individual plant were calculated mathematically based on the trend lines of A/Ci-curves measured from each individual plant. Because in each single measurement the crossing points between the individual trend lines are usually varying, the average of all crossing points was determined. The CO_2 compensation point measured from wild type plants is in the expected and theoretically predicted range (WT in figure 3.26, Γ_* = 50.4 ppm CO_2). Plastidial glycolate oxidation in plants transgenic for A and DEF plants is sufficient to reduce their Γ_* (A and DEF in figure 3.26, Γ_* = 46.50 and 46.35, respectively). Establishment of the complete pathway in the plant chloroplasts enhances the decrease in Γ_* (GTA and GT-DEF in figure 3.26, Γ_* = 45.40 and 43.92, respectively). The reduction in the CO_2 compensation point of the transgenic plants provides a new evidence for the physiological significance of the novel biochemical pathway in C_3 plants. Hence, the expression of the novel pathway genes inside the plant chloroplast results in a reduction of photorespiratory flow and in turn an increase in CO_2 concentration in the vicinity of Rubisco.
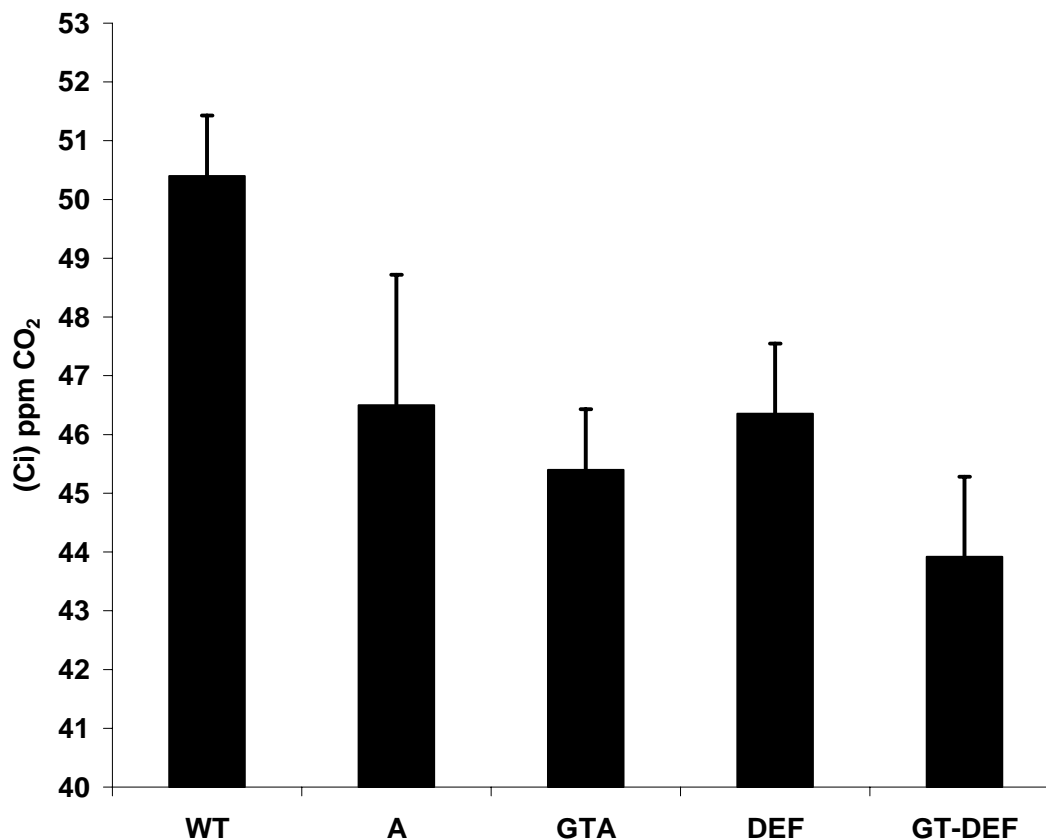
**Figure 3.26: CO_2 compensation points (Γ_*) measured from transgenic plants.**

Shown are the CO_2 compensation points (Γ_*) measured from 9-10 weeks old wild type and different transgenic plants. Each data point represents the CO_2 compensation point (Γ_*) and is based on at least 4 independent measurements from 4 sister plants from each line. Vertical bars show standard error. (Ci) = internal CO_2 concentration in leaf intercellular spaces; WT = wild type; A = plants expressing cTP-*At*GDH; GTA = plants expressing *GCL*, *TSR* and cTP-*At*GDH. DEF = plants expressing *Ec*GDH; GT-DEF = plants expressing *GCL*, *TSR* and *Ec*GDH.

3.5.4   Determination of the electron requirements for CO_2 assimilation (e/A) in *planta*

In order to study the potential physiological effects of the novel pathway, in addition to the previous gas exchange measurements, it was decided to measure the chl.*a* fluorescence parameters. The chlorophyll fluorescence measurements help in determining the electron requirements for CO_2 assimilation (e/A) as described in the materials and methods chapter (2.2.5). The e/A is correlated with the carboxylation/oxygenation ratio of Rubisco. The e/A decreases when the rate of Rubisco oxygenation is decreased relative to carboxylation and reaches minimum values in the absence of photorespiration (Lipka *et al.*, 1999). The e/A is therefore a helpful tool for measuring the rate of Rubisco carboxylation in plants. Figure 3.27 shows the e/A values measured from WT and different transgenic plants at different CO_2 concentrations.
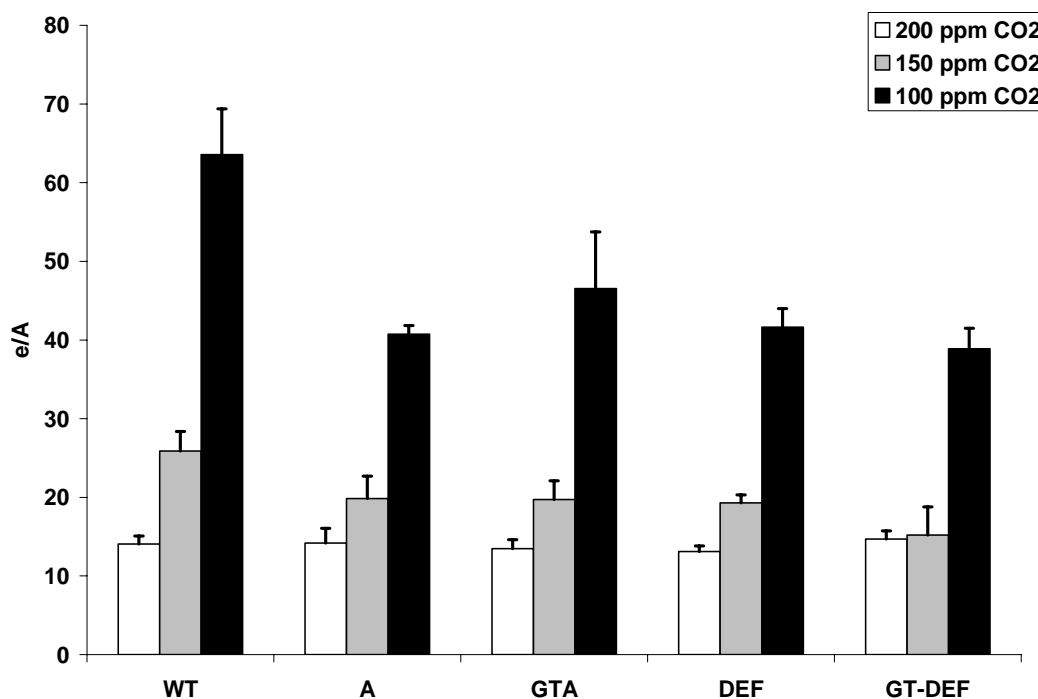
Figure 3.27: The e/A ratio in transgenic plants

Shown are the e/A values measured from 8-10 weeks old WT and different transgenic plants. Each data point represents the electron requirements for CO_2 assimilation (e/A) and is based on at least 4 independent measurements of 4 sister plants from each line. Vertical bars show standard error. White bars, grey bars and black bars = e/A at 200, 150 and 100 ppm CO_2, respectively; (e/A) = the electron requirements for CO_2 assimilation; WT = wild type; A = plants expressing cTP-*At*GDH; GTA = plants expressing *GCL*, *TSR* and cTP-*At*GDH; DEF = plants expressing *Ec*GDH; GT-DEF = plants expressing *GCL*, *TSR* and *Ec*GDH.

At 200 ppm external CO_2 (i.e. Ca = 200 ppm CO_2), the e/A values are similar in all the tested plants (white bars in figure 3.27). All the transgenic plants show a decrease in the e/A values compared to wild types when all plants are allowed to grow at Ca of 150 ppm CO_2 (grey bars in figure 3.27) as well as at Ca of 100 ppm CO_2 (black bars in figure 3.27). GT-DEF plants have the lowest e/A values compared to the other tested plants at 150 and 100 ppm CO_2. By combining this result with the results concerning the photosynthetic performance of the transgenic plants (3.5.2 and 3.5.3), it becomes clear that overexpression of the novel pathway genes in the chloroplast of *A. thaliana* plants enhances the plant photosynthesis. This results in the conclusion that overexpression of a glycolate dehydrogenase (*Ec*GDH or cTP-*At*GDH) inside the plant chloroplast leads not only to a decrease in the rate of photorespiration but also to an increase in the photosynthetic performance. Indeed, this decrease in the rate of photorespiration as well as the increase in the photosynthetic performance is enhanced by the expression of all the novel pathway genes in the plant chloroplasts (GTA and GT-DEF).

3.6 What is the influence of the novel pathway on plant growth?

In this chapter, the phenotypic effects together with leaf area of the different transgenic plants will be shown. Moreover, measurements of the total fresh and dry weight of transgenic plants under ambient and low CO_2 conditions will also be presented.

3.6.1 Phenotypic effects of DE, F, and DEF overexpressing lines

No phenotypic effects were observed either in plants transgenic for F or in plants transgenic for DE compared to their wild type counterparts. Surprisingly, DEF transgenic plants have different phenotypes. Figure 3.28A shows the different phenotypes of DEF5 and DEF7 (plant A and B in figure 3.28A) compared to wild type plants (plant C and D in the same figure). DEF transgenic plants are bigger in size compared to WT plants. Moreover, the rosette diameter in DEF plants is also bigger. The leaf shape of WT, F and DE plants are seemingly similar whereas DEF transgenic plant leaves are looking different (DEF4, DEF5 and DEF7 in figure 3.28B). DEF plants have seemingly flat leaf blades and a slightly elongated leaf petiole. The conclusion based on these results is that the presence of DEF genes together in one plant results in the appearance of these phenotypes. Nevertheless, the expression levels of each single gene in DEF plants is varying (3.2.2.3-I).

(A)   (B)
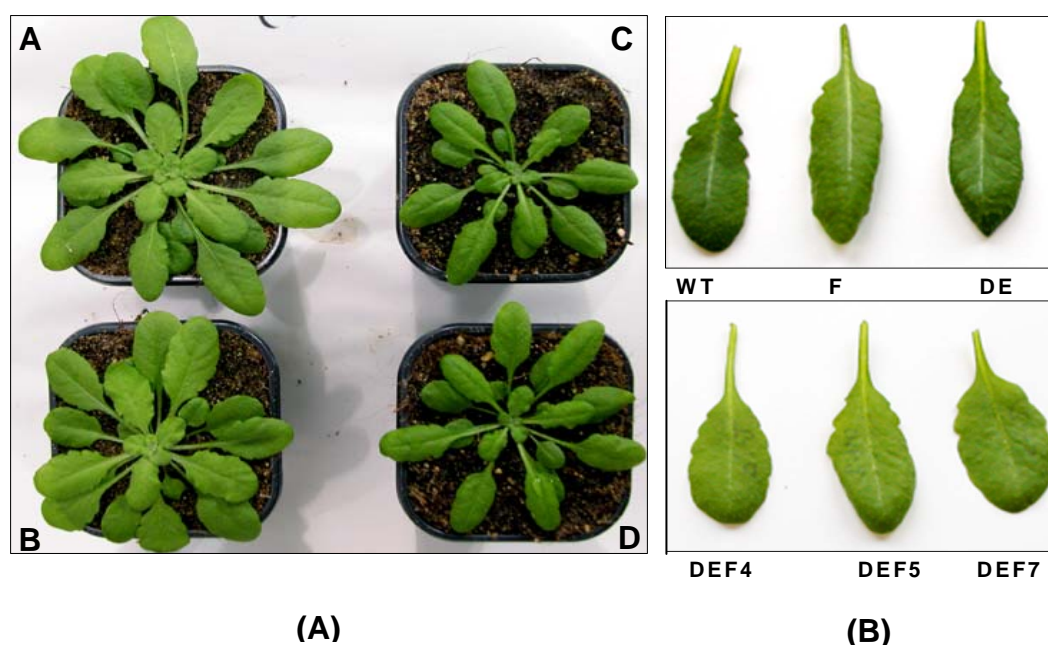
Figure 3.28: Phenotypic effects of DE, F, and DEF transgenic plants.

Shown are 6 weeks old transgenic plants expressing the complete *E. coli* GDH genes (A) and typical leaves of WT, F, DE and DEF plants. In figure 3.29A: A = DEF5; B = DEF7; C and D = WT.

3.6.2   Phenotypes of GT, A, GTA, and GT-DEF transgenic plants

The GT-DEF transgenic plants (picture D in figure 3.29) have phenotypes similar to DEF-plants (picture C in figure 3.29) with the exception that GT-DEF plants are even bigger in size. The growth rates of DEF and GT-DEF plants are faster than wild types as well as the other transgenic plants. A tendency towards the same effect can also be observed in GTA plants (picture F in figure 3.29). GT and A plants (picture B and E, respectively in figure 3.29) as well as DE and F plants (not shown) have similar phenotypes to wild type plants (picture A in figure 3.29). Expression of DE or F genes separately in the chloroplast of *A. thaliana* plants induces no phenotypic effects between the different expressing plants. The expression of *Ec*GDH in the chloroplast of *A. thaliana* plants (DEF and GT-DEF plants) results in the appearance of the previously described phenotypes whereas these phenotypic effects are absent in plants transgenic for A (picture E in figure 3.29). Expression of *GCL* and *TSR* together or separately in *A. thaliana* chloroplast doesn't induce any phenotypic effects. Interestingly, expression of all necessary genes for the novel biochemical pathway does not only show any harmfull effects in the expressing plants but also enhances plant growth.


Figure 3.29: Phenotypic effects of GT, A, GTA, and GT-DEF transgenic plants

Shown are the phenotypes of 7-8 weeks old GT, DEF, GT-DEF, A and GTA transgenic plants compared to wild type plants. A = WT plants; B = GT-plants; C = DEF-plants; D = GT-DEF-plants; E = Plants transgenic for A and F = GTA-plants.

3.6.3   Effect of the novel pathway on the plant leaf area and the rosette diameter

I) *Measurement of the plant leaf area*

As some of the genotypes investigated show a faster growth compared to wild type, this effect was quantified by determining the leaf area of plants 7 weeks after sowing. In order to evaluate the influence of the novel pathway on the growth of the transgenic plants, the plant leaf area was measured from all transgenic lines parallel with wild type plants. Figure 3.30 shows the relative plant leaf area measured from the indicated genotypes.
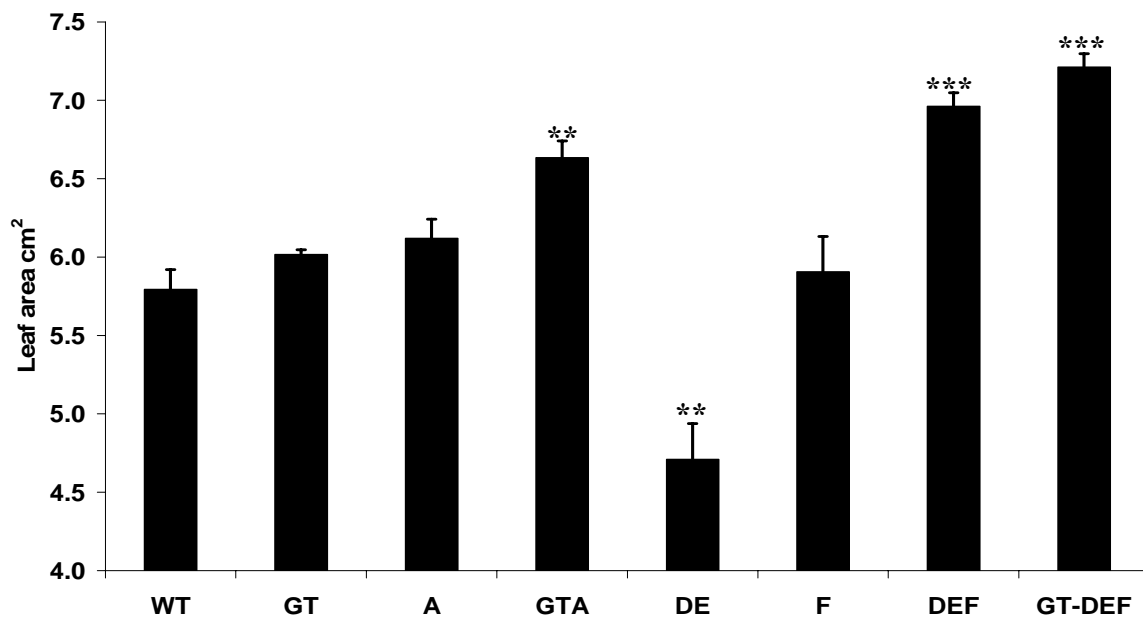
Figure 3.30: Plant leaf area measurements.

Shown are the relative values of plant leaf area measured from 7 weeks old WT and all the generated transgenic lines growing under short day conditions (8 h light, 16 h dark) in cm^2. Firstly, the tested plants were grown for 3 weeks under short day growth conditions on MS medium supplemented with the suitable antibiotics for each genotype. Plants transgenic for F and wild type plants were also grown for 3 weeks on MS medium without any selection pressure. Secondly, all genotypes were then transferred into soil and allowed to grow for further 4 weeks under short day growth conditions. Finally, the plant leaf area was determined from each genotype. Each value represents the average of leaf area measured from at least 5 sister plants for each line. WT = wild type *A. thaliana* plants; A = plants expressing cTP-*At*GDH; GT = plants expressing *GCL* and *TSR*; GTA = transgenic plants expressing *GCL, TSR* and cTP-*At*GDH; DE = plants expressing the *glc*D and *glc*E subunits of *Ec*GDH; F = transgenic *A. thaliana* plants expressing the *glc*F subunit of *Ec*GDH; DEF = plants expressing the complete *Ec*GDH and GT-DEF = plants expressing *GCL, TSR* and the complete *Ec*GDH; ** and *** denote deviations from the wild types with P<0.05 and P<0.001, respectively.

Leaf area measurements reveal that plants transgenic for A, F and GT have similar values of leaf area compared to WT plants. Plants transgenic for DE develop a smaller leaf area compared to all the tested plants (DE in figure 3.30). In contrast to DE plants, GTA, DEF and GT-DEF plants show a clear increase in their leaf area compared to wild type plants (see figure 3.30). Expression of the complete *Ec*GDH in *A. thaliana* chloroplasts results in an increase in the plant leaf area whereas expression of *glc*F or *glc*D and *glc*E separately inside

the plant chloroplast did not induce any increase in plant leaf area. At the same time, expression of cTP-*At*GDH alone inside the plant chloroplast did not show any influence on the plant leaf area whereas expression of cTP-*At*GDH together with *GCL* and *TSR* inside the plant chloroplast results in an increase in the plant leaf area (GTA in figure 3.30). Interestingly, expression of *Ec*GDH together with *GCL* and *TSR* inside the plant chloroplasts results in further or more drastic increase in plant leaf area compared to the other transgenic plants since GT-DEF plants show the highest values of plant leaf area. This can also be added to the positive impacts of the GT-DEF and GTA pathways in the transgenic plants.

II) *Measurement of the rosette diameter*

The rosette diameter was measured from 8 weeks old transgenic plants growing under ambient conditions as shown in figure 3.31. Plants transgenic for A, GT, GTA, DE and F show similar values of rosette diameter compared to wild type plants.

On the other hand, DEF and GT-DEF plants have an increased rosette diameter compared to the other tested plants. This increase in the rosette diameter in both genotypes was expected because both lines have bigger leaf area as well as longer leaf petioles compared to the other tested genotypes (3.6).
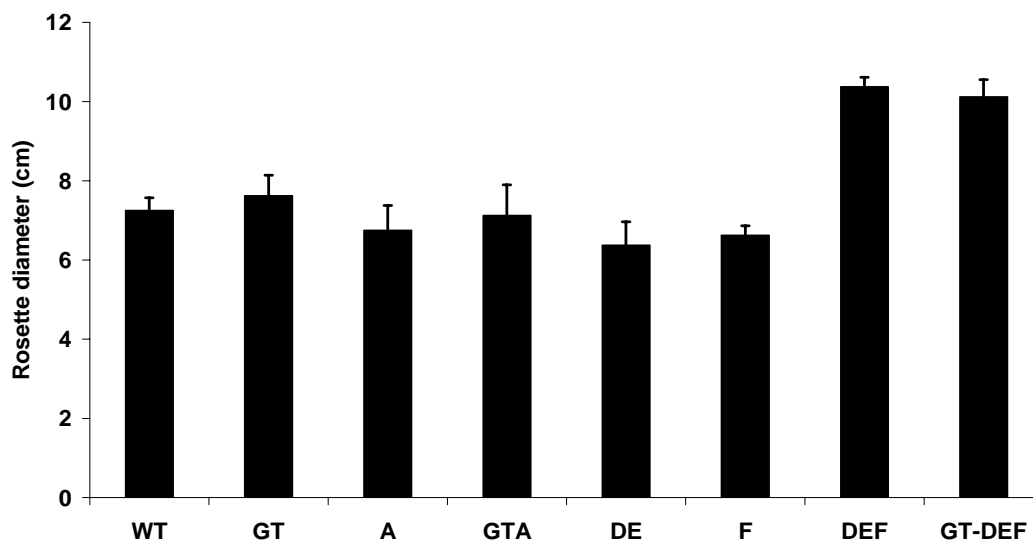
**Figure 3.31: Rosette diameters of the transgenic plants.**

Shown are the relative rosette diameters measured from 8 weeks old *A. thaliana* plants growing under ambient conditions. Each data point represents the average of the plant rosette diameter measured from at least 4 sister plants for each line. WT = wild type *A. thaliana* plants; A = plants expressing cTP-*At*GDH; GT = plants expressing *GCL* and *TSR*; GTA = plants expressing *GCL*, *TSR* and cTP-*At*GDH; DE = plants expressing *glc*D and *glc*E subunits of *Ec*GDH; F = plants expressing *glc*F subunit of *Ec*GDH; DEF = plants expressing the complete *Ec*GDH and GT-DEF = plants expressing *GCL*, *TSR* and the complete *Ec*GDH.

3.6.4   Measurement of the total fresh and dry weight of the transgenic plants

In another approach, the total fresh and dry weight of the different transgenic plants was measured. Plants were allowed to grow for 6 weeks from the seedling stage under ambient conditions. Some of the plants were harvested at this time point (6 weeks old) and the total fresh and dry weight was determined. Additional plants were allowed to grow for another two weeks (8 weeks old) under the same conditions and the measurement was repeated. The aim was to calculate the increase in fresh and dry weight from the indicated genotypes during the two weeks growth period as shown in figure 3.32. Plants transgenic for GT, A, DE and F show similar changes in their fresh weight compared to wild type plants (figure 3.32A). GTA, DEF and GT-DEF plants show a clear increase in their fresh weight compared to wild type plants (figure 3.32A).

Similar results were obtained by measuring the total dry weight of the tested plants. The clearest increase in the total dry weight can be observed for GTA, DEF and GT-DEF plants. Plants transgenic for A show a little increase in their dry weight compared to wild type plants (figure 3.32B). The same experiment was performed with plants growing for 2 weeks at a reduced atmospheric CO_2 concentration of 150 ppm. However, the growth conditions (light intensity and air humidity) in the low CO_2 growing chamber (2.2.6.3) are not the same compared to the ambient growing conditions. So, it was not possible to compare the total fresh and dry weight of the tested plants under both growing conditions. Under low CO_2 growing conditions, only GT-DEF transgenic plants show a clear increase in their fresh and dry weight compared to the other tested plants (data not shown). The increase in fresh and dry weight of plants transgenic for A, GTA, DEF and GT-DEF under ambient conditions provide evidence for a positive influence of the novel pathway on plant prodctivity. Moreover, the increase in fresh and dry weight of GT-DEF plants under low CO_2 growing conditions provides a clear evidence for the efficiency of the novel pathway for the plant growth under photorespiratory conditions. This result reflects also the positive significance of the novel pathway in reducing the flow through photorespiration in the expressing plants.

(A)

(B)
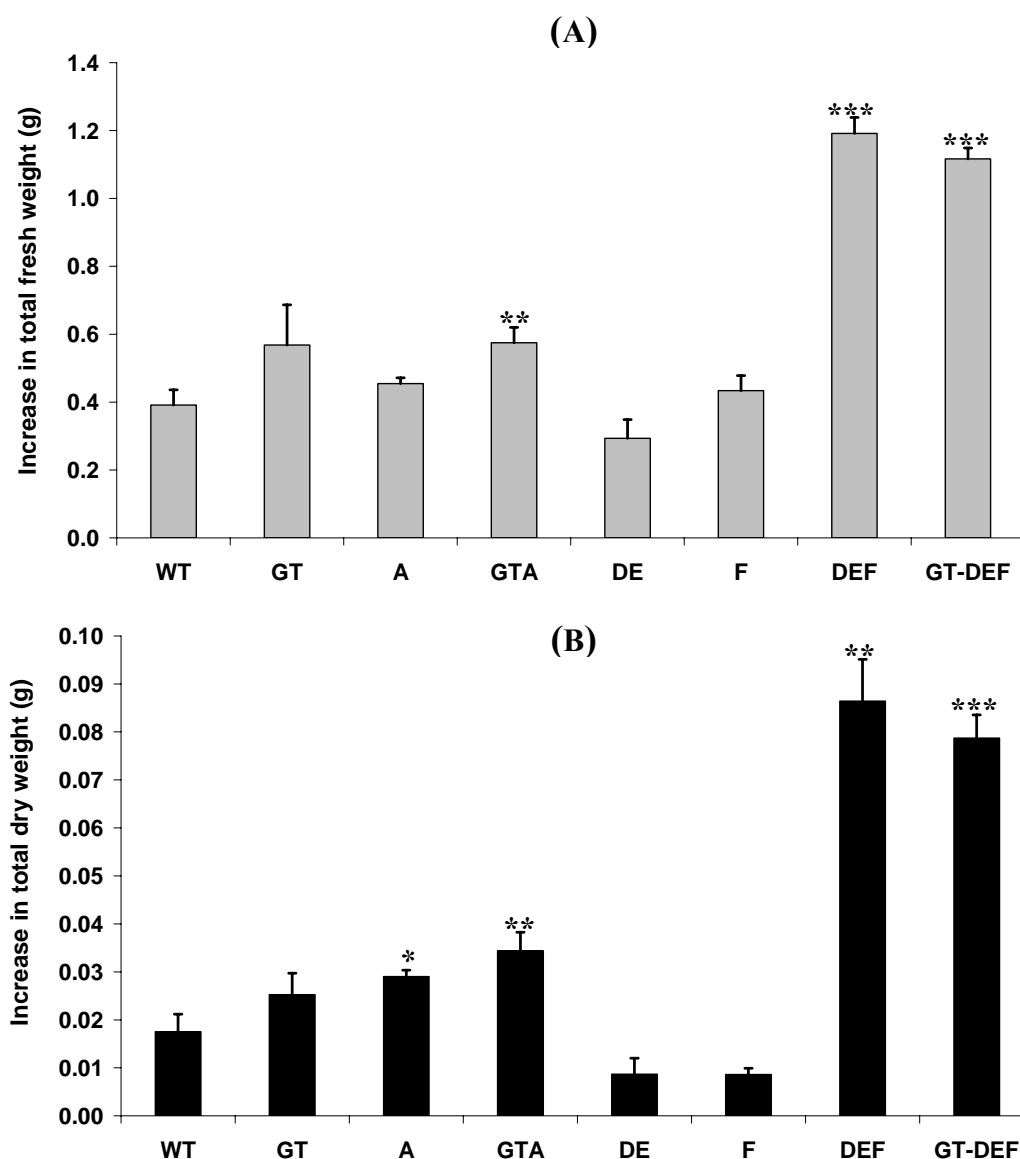
Figure 3.32: The total fresh and dry weight of transgenic plants.

Shown are the relative changes in the total fresh (A) and dry weight (B) measured from 5 and 7 weeks old WT and different transgenic plants growing under short day conditions (8 h light, 16 h dark) in g. Firstly, the tested plants were allowed to grow for 3 weeks under short day growth conditions on MS medium supplemented with the suitable antibiotics for each genotype. Plants transgenic for F and wild type plants were also allowed to grow for 3 weeks on MS medium without any selection pressure. Secondly, all genotypes were then transferred into soil and allowed to grow for further 2 weeks under short day growth conditions. At this time point, the fresh and dry weight was determined from all genotypes. Some other plants (including all genotypes) were allowed to grow for 2 more weeks under the same growth conditions. The total fresh and dry weight measurements were then repeated. Each value represents the average of changes in plant fresh and dry weight measured from at least 4 sister plants for each line. WT = wild type *A. thaliana* plants; A = plants expressing cTP-*At*GDH; GT = plants expressing *GCL* and *TSR*; GTA = plants expressing *GCL, TSR* and cTP-*At*GDH; DE = plants expressing *glc*D and *glc*E subunits of *Ec*GDH; F = plants expressing *glc*F subunit of *Ec*GDH; DEF = plants expressing the complete *Ec*GDH and GT-DEF = plants expressing *GCL, TSR* and the complete *Ec*GDH; *, **, and *** denote deviations from the wild types with P<0.1, P<0.05 and P<0.001, respectively.

Based on all the presented results, the expression of the novel pathway enzymes in the plant chloroplast shows positive impacts on the plant growth. GT-DEF and GTA plants showed a

clear reduction in their photorespiratory flow. This effect was obvious from the biochemical analysis that was performed using both genotypes (3.4.1, 3.5.1 and 3.4.2). GT-DEF and GTA plants showed also an increase in their photosynthetic rates under photorespiratory conditions (3.5). Both genotypes have lower CO_2 compensation point compared to wild type plants. Moreover, both genotypes have a better growth performance compared to wild type plants. This effect was observed from the measurements of the total fresh and dry weight and also from the measurements of plant leaf area (3.6.4 and 3.6.3, respectively). Concerning all these results, transfer of the novel pathway into C_3 plants will ultimately lead to a decrease in their photorespiratory rates and inturn an increase in the total plant productivity under unfavourable growth conditions.

4 DISCUSSION

4.1 The Rubisco problem and photorespiration

The enzyme that is responsible for fixing CO_2 in photosynthesis, Rubisco; EC 4.1.1.39, is a bifunctional enzyme. In addition to its carboxylation function, it can also fix O_2 (Bowes *et al.*, 1971). CO_2 and O_2 are mutually competitive at the same large subunit active site of Rubisco. Rubisco favours CO_2 over O_2 by a factor of up to 100, but the concentration of O_2 in the atmosphere is much higher than that of CO_2. As a result one molecule of O_2 is fixed by Rubisco for every three molecules of CO_2 (Sharkey, 2001). When Rubisco fixes CO_2, two molecules of phosphoglycerate are produced that are directly used for the biosynthesis of carbohydrates as well as for the regeneration of ribulose-1,5-bisphosphate in a reaction sequence requiring ATP and NADPH (Calvin, 1989). When O_2 is substituted for CO_2, one phosphoglycerate and one phosphoglycolate are produced. Plants metabolize phosphoglycolate to phosphoglycerate in a side reaction sequence that occurs in the chloroplast, the peroxisomes and mitochondria (1.4), with the release of CO_2 and ammonia in the mitochondria (Andrews and Lorimer, 1987; Leegood *et al.*, 1995). The photorespiratory pathway in C_3 plants requires a large machinery consisting of 16 enzymes and more than 6 translocators (Douce and Neuburger, 1999). CO_2 release during the photorespiratory pathway results in the loss of one-quarter of the carbon from phosphoglycolate (Leegood *et al.*, 1995). In this way photorespiration lowers the photosynthetic efficiency particularly in C_3 plants, which include the major crops like wheat and rice.

Rates of photorespiration in isolated bundle sheath strands of C_4 plants under ambient atmospheric conditions have been estimated at 3 to 7% of the rate of CO_2 fixation (Farineau *et al.*, 1984). However, Maroco *et al.* (1998) demonstrated that in C_4-cycle limited mutants, atmospheric levels of O_2 (20 kPa) caused increased inhibition of photosynthesis as a result of higher levels of photorespiration. Thus, photorespiration in C_4 plants is considered insignificant because of the suppression of the oxygenase reaction of Rubisco by concentrating CO_2 in the bundle sheath cells (Edwards *et al.*, 2001). C_4 plants developed a mechanism to avoid the oxygenation reaction of Rubisco. They have employed enzymes already present in their C_3-ancestor, but changed the degree of expression as well as the localization on a sub-cellular and cell-type specific level (Hatch, 1987a). This mechanism occurs by the aid of cooperation between two cell types in the leaves of C_4-plants, bundle sheath cells and mesophyll cells (1.1.2).

Moreover**,** CAM plants fix atmospheric CO_2 at night through a C_4 pathway and further process the carbon via the C_3 pathway during the day (1.1.3). This will result in a temporal separation of the process rather than a spatial separation (Cushman, 2001). Beside these mechanisms, some aquatic plants (as *Hydrilla verticillata*) have developed C_4-like mechanisms acting within one cell. In this mechanism, CO_2 released and refixed in chloroplast in the same way like C_4 plants. This unicellular C_4-like pathway results in a partial suppression of photorespiration with reduced sensitivity to oxygen (Bowes, 2002; Rao *et al.*, 2002; Reiskind *et al.*, 1997; Van Ginkel *et al.*, 2001).

Many researches are working on projects aiming to raise C_3 plant yield by increasing photosynthesis and/or reducing photorespiration. These approaches are described in the introduction chapter (1.3). Although photorespiration seems to be deleterious, photorespiration helps C_3 plants in two ways. Firstly, photorespiration provides C_3 plants with the amino acids glycine and serine that are used for protein synthesis (Sharkey, 2001). Secondly, photorespiration protects C_3 plants from high irradiances (Kozaki and Takeba, 1996). However, other mechanisms exist in C_3 plants that can perform the required functions better than photorespiration. In the first case, the capacity for starch and sucrose synthesis exceeds the capacity for glycine and serine synthesis. In the second case, dissipating excess light by a mechanism involving zeaxanthin can dissipate much more energy than can photorespiration in most leaves (Sharkey, 2001). While these two functions of photorespiration may be useful to the plant, the overall effect of photorespiration is deleterious. In two studies with *Arabidopsis* (Beckmann *et al.*, 1997) and barley (Wingler *et al.*, 1997) mutants deficient in photorespiration, the growth of both photorespiratory mutants is not affected under high CO_2 concentration (where no or little photorespiration and enhanced photosynthesis is observed). By growing both mutants under lower CO_2 concentration (high photorespiratory rates), the plant growth was retarded or the plants died. So photorespiration helps C_3 plants to survive under conditions where the oxygenase activity of Rubisco is high. The previous results supported the argument that partial suppression of photorespiration in C_3 plants might not be harmful for C_3 plant growth.

4.2   A novel pathway in the chloroplast of *Arabidopsis thaliana*

In this study, a novel pathway aiming to increase the CO_2 concentration in the vicinity of Rubisco and to suppress the CO_2 loss resulting from photorespiration in C_3 plants has been established. The novel pathway is dealing with the metabolism of glycolate produced in the chloroplast during photorespiration. The novel pathway will compete with the existing

photorespiratory pathway and will reduce photorespiratory CO_2 loss by modifying the metabolic pathways of the products resulting from Rubsico oxygenase activity. In this chapter, the origin of the novel pathway as well as the enzymes involved in glycolate oxidation will be discussed. Moreover, the benefits from the establishment of the novel pathway in C_3 plants will be also discussed.

Important knowledge has been gained about the genes and enzymes that are involved in the metabolism of glycolate in *E. coli* (1.5) (Hansen and Hayashi, 1962; Kornberg and Sadler, 1961; Lord, 1972; Pellicer *et al.*, 1996). In this cycle, glycolate is oxidized by glycolate dehydrogenase (GDH) to form glyoxylate. Two molecules of glyoxylate are then ligated by the aid of glyoxylate carboxyligase (*GCL*) to form tartronic semialdehyde. During this reaction, CO_2 is released. The formed tartronic semialdehyde is then reduced by the action of tartronic semialdehyde reductase (*TSR*) to form glycerate. Under high oxygen concentration, glycolate is also synthesized and metabolized in algae. The metabolism of glycolate in algae occurs more or less in the same way like in higher plants. However, there are differences concerning the localization and mode of action of the enzymes involved in this metabolic pathway. Three groups of algae may be distinguished concerning their glycolate metabolism. The first group possesses microbodies containing all the characteristic enzymes present in the plant leaf peroxisomes (Stabenau and Säftel, 1981; Stabenau *et al.*, 1984; Winkler *et al.*, 1982). The second group also contains microbodies similar to leaf peroxisomes, except that the glycolate oxidizing enzyme is a dehydrogenase rather than an oxidase (Collins and Merrett, 1975; Nelson and Tolbert, 1970). However, the enzymes of glycolate pathway in this group can also be located in the mitochondria (Collins and Merrett, 1975; Yokota *et al.*, 1985a; Yokota and Kitaoka, 1979a). In the third group, mitochondria are the only organelles containing enzymes of the glycolate pathway (Stabenau and Beevers, 1974). It was decided to install the glycolate pathway genes of *E. coli* in the C_3 plant cells although the *Ec*GDH is a complex enzyme that needs cloning of three different genes of the glycolate dehydrogenase subunits (*glc*D, *glc*E and *glc*F). In addition to the bacterial and algal glycolate dehydrogenases, there are three other enzymes that act as a glycolate dehydrogenase. The first enzyme is the plant glycolate oxidase (GO; EC 1.1.3.15) that converts glycolate to glyoxylate and located in the peroxisome. The plant glycolate oxidase is an oxygen dependent enzyme and produces H_2O_2, which is rapidly hydrolized by a catalase present in the peroxisome of the plant (Tolbert, 1997). Such a catalase is not reported yet in the chloroplast of the plant. So the introduction of higher plant glycolate oxidase into the chloroplast of *A. thaliana* plant would produce H_2O_2 that can have a very damaging effect. Therefore using this enzyme as an

alternative to the complicated EcGDH was excluded from the present work. The second enzyme is the human glyoxylate reductase (HGR; EC 1.1.1.26/79) that was cloned from human liver cDNA (Davis and Goodman, 1992; Fry and Richardson, 1979; Giafi and Rumsby, 1998; Young $et\ al.$, 1973). $In\ vitro$, HGR readily catalyzed the reduction of glyoxylate to glycolate but not the reverse reaction (data kindly provided by Rafijul Bari, Institute for Biology I, RWTH-Aachen, Germany). The equilibrium of this reaction is still unclear. Therefore it was decided that this enzyme is not suitable for the present work. Recently, a novel glycolate dehydrogenase in the mitochondria of $Arabidopsis\ thaliana$ (AtGDH; At5g06580) was reported (Bari $et\ al.$, 2004). The new enzyme is dependent on organic co-factors and resembles algal glycolate dehydrogenases in its enzymatic properties. However, AtGDH was not characterized at the beginning of the practical work on the novel pathway in this study. Therefore, AtGDH was used in a later step as an alternative to the complicated EcGDH in the novel pathway. For this purpose, the mitochondrial targeting peptide (mTP) of AtGDH was replaced by a chloroplast targeting peptide (cTP).

Metabolizing glycolate in the chloroplast via the novel pathway will concentrate CO_2 in the vicinity of Rubisco. Thus, the novel pathway will suppress the photorespiratory pathway in C_3 plants. C_3 plants will benefit from the novel pathway in two ways. Firstly, the flow through photorespiration will be decreased to very low levels and thus the energy loss during photorespiratory pathway is avoided. Secondly, the alternative pathway will increase the CO_2 concentration inside the chloroplast resulting in higher rates of photosynthesis and in turn higher biomass production. Drastic increases in the performance of several crop species have been observed already when the external CO_2 concentration is doubled under greenhouse conditions (Arp $et\ al.$, 1998; Kimball, 1983). However, this approach is not applicable to the huge areas used for agricultural production. On the other hand, the novel pathway increases the concentration of CO_2 inside the chloroplast thus it will be applicable for agricultural production.

4.3 Could the novel pathway act as a CO_2 concentrating mechanism in C_3 plants?

The mechanism by which the proposed pathway suppresses the photorespiration has been described (3.1). However, it is still a general question whether any CO_2 concentrating mechanism would work in C_3 plants. Badger and Spalding (2000) and Leegood (2002) have discussed the main characteristics of C_4 photosynthesis that are essential for their CO_2

concentrating mechanism. Whether the novel pathway would be compatible with these prerequisites or not is discussed in this chapter.

C_4 photosynthesis requires an active CO_2 capture system. This role is taken by PEP carboxylase that is highly expressed specifically in mesophyll cells (Stockhaus *et al.*, 1997). The novel pathway does not require such a system because it uses the CO_2 capturing system existing in C_3 plants (Rubisco carboxylase reaction). All reaction steps up to the formation of glycolate are identical to the photosynthesis/photorespiration as described for C_3 plants. The novel pathway will only modify the metabolic pathways of the products resulting from the Rubsico oxygenase activity.

C_4 photosynthesis requires extra energy to perform. The novel pathway will only work under photorespiratory conditions and not constitutively because its activity depends on the amount of glycolate available. However, the novel pathway will produce extra energy. One molecule of NADH is produced during the conversion of glycolate to glyoxylate. Two molecules of glyoxylate are required to produce one molecule of tartronic semialdehyde. Thus, two molecules of NADH will be produced. On the other hand, one molecule of NADH is used by tartronic semialdehyde reductase. So one molecule extra NADH will be produced. It has been argued that over-reduction of the chloroplast under high light might cause deleterious effects, where NADPH production is high. Photorespiration might act as a valve for reducing equivalents. On the other hand, there is an efficient shuttle for reducing equivalents between the cell compartments as the oxaloacetate/malate shuttle (Giersch, 1982; Pastore *et al.*, 2003). Transgenic *A. thaliana* plants expressing the novel pathway genes (GTA and GT-DEF) did not show any deleterious effects on the plant growth. Thus, the extra reducing equivalents produced in the chloroplast have no negative impacts on the viability of the plant chloroplasts.

C_4 photosynthesis requires an intermediate pool of captured CO_2 such as malate and aspartate, which act as transient stores of fixed CO_2 (Hatch *et al.*, 1971). In contrast, the novel pathway releases CO_2 in the vicinity of Rubisco in the chloroplast (see 3.1). Thus, CO_2 can be refixed without being transported as an organic compound.

In the C_4 pathway, a mechanism is required to release CO_2 from the intermediate pool. This role is taken by specific enzymes decarboxylating C_4 acids in the bundle-sheath cells (Leegood, 2002). The CO_2 is released by the novel pathway in the plant chloroplast through

the *GCL* activity since two molecules of glyoxylate are ligated forming tartronic semialdehyde with the release of CO_2. This effect was also obvious in GTA and GT-DEF plants where those two genotypes have lower CO_2 compensation points compared to wild type plants (3.5.3). Additionally, the assimilation rates in those plants are higher compared to wild type plants (3.5.2). This can be due to the release of CO_2 in the chloroplast by the novel pathway.

The C_4 pathway needs co-operation between two different cell types (mesophyll cells and bundle sheath cells) in which it concentrates CO_2 around Rubisco (Hatch *et al.*, 1971; Hatch, 1987a; Hatch, 1992). In most of the C_4 plants the photosynthetic cells within the leaf are organized in two concentric cylinders known as Kranz anatomy (1.1.2). The novel pathway provides a mechanism by which CO_2 is released in the chloroplast without any need for such spatial separation.

C_4 plants developed systems to reduce the leakage of CO_2 from the site of CO_2 elevation (Leegood, 2002). The thick wall of bundle sheath cells is a major barrier to the diffusion of solutes and gases. The C_4 stucture provides a long liquid diffusion pathway from the bundle sheath organelles to the intercellular spaces surrounding the mesophyll cells in some C_4 species. The diffusion of CO_2 in C_3 plants is determined by leaf anatomy, liquid path lengths and membrane properties (Evans and Von Caemmerer, 1996). C_3 leaves have large intercellular airspaces and chloroplasts are closely oriented to the cell wall, thus greatly increasing internal CO_2 diffusion. Von Caemmerer and Furbank (2003) compared the CO_2 diffusion in C_3 plants and C_4 plants utilizing a mathematical model and analyzed the possibility of introducing single cell C_4 photosynthesis into C_3 plants. They concluded that, a single-cell C_4 system with the current C_3 diffusion characteristics is clearly not efficient as a CO_2 concentrating mechanism with its high leakiness and energy requirements. However, under strong photorespiratory conditions when the stomata are closed, presence of a CO_2 concentrating mechanism could be helpful to the plants (Von Caemmerer and Furbank, 2003). All their calculations valid for the transfer of a C_4-like pathway to C_3 plants are also applicable for the pathway proposed in this study. The only difference: No extra-energy is required-instead it produces energy. Therefore, it will be as effective in lower canopy as higher canopy in CO_2 limiting condition. This makes the novel pathway more applicable to the field conditions.

The affinity of Rubisco for CO_2 in C_4 plants is lower compared to the Rubisco of C_3 plants (The Km of Rubisco in C_4 plants ranges between 28-60 μM, in C_3 plants it ranges between 13-26 μM). An increased catalytic turnover of Rubisco is always associated with a reduced affinity for CO_2 when comparing different species (Badger and Spalding, 2000; Von Caemmerer, 2003). In C_3 pathways, the catalytic turnover of Rubisco is lower than in C_4 pathways. However, overexpression of the Calvin cycle enzyme sedoheptulose-1,7-bisphosphatase in tobacco plants results in an increase in their photosynthetic rates. Higher levels of sucrose and starch accumulated during the photoperiod, and an increase in leaf area and biomass of up to 30% was also evident. Lefebvre *et al.* (2005) and Miyagawa *et al.* (2001) suggest that this increase in photosynthesis could be attributed to an increase in ribulose-1,5-bisphosphate regenerative capacity. The proposed pathway will not only increase the CO_2 concentration in the vicinity of Rubisco but it will also produce glycerate inside the chloroplast. The increased CO_2 concentration will enhance the Rubisco carboxylase activity and glycerate will be involved in the regeneration of ribulose-1,5-bisphosphate. Thus, the novel pathway will not negatively affect the ribulose-1,5-bisphosphate regenerative capacity. Transgenic *A. thaliana* plants expressing the novel pathway genes showed higher rates of CO_2 assimilation compared to wild type plants (3.5). Moreover, GTA and GT-DEF plants showed also an increase in their biomass compared to wild type plants (3.6.4). Therefore, the regenerative capacity is seemingly not the only limiting pathway for net Rubisco function *in vivo*.

Additionaly, C_3 plants also lack many transporters that are present in C_4 plants. Thus, it is necessary to introduce specific transporters in order to engineer an efficient C_4 like pathway in C_3 plants (Leegood, 2002). All the enzymes required for the proposed pathway are present in one single organelle, the chloroplast. Thus, the proposed pathway does not require any transporters since there are no metabolic movements across membranes or in between the cells. I conclude that the proposed pathway fulfills the criteria described by (Badger and Spalding, 2000; Leegood, 2002) for an efficient system to ameliorate the CO_2 concentration in C_3 plants and in turn their photosynthetic performance.

4.4 Establishment of the novel pathway in *A. thaliana* plants

Installation of a glycolate oxidizing activity in the chloroplast can be brought about by nuclear transformation of plants or plant cells with the coding sequence of *TSR*, *GCL* and *Ec*GDH or cTP-*At*GDH. In this chapter, the establishment of the novel pathway in *A. thaliana* plants with special reference to the structure of the used plant expression vectors will be discussed. The

transgene expression, enzymatic assays and the phenotypic effects of the differently expressing plants will be also mentioned.

The genes encoding the respective proteins of this pathway were cloned into different plant expression vectors that contain a chloroplast targeting sequence (cTP). The expression of all foreign genes in the used plant expression vectors is under the control of a derivative of the constitutive CaMV 35S promoter. The used plant expression vectors contain a single 5` untranslated region (CHS) upstream to the cTP sequence and a polyadenylation-/termination sequence from CaMV (pA35S) downstream of the foreign genes as a 3`-UTR. This would ultimately help in stabilizing the protein expression in the transgenic plants (Bock and Hagemann, 2000; Staub and Maliga, 1995; Staub and Maliga, 1994) (see 2.1.9). The aim was to have a high level of transgene expression under different growth conditions. However, the expression levels of *GCL*, *TSR* and *glc*F genes in homozygous lines were low compared to their heterozygous counterparts. This was expected due to gene silencing, co-suppression effects and integration sites of the transgenes on the chromosomes (Day *et al.*, 2000; Plasterk and Ketting, 2000). The integration site should not cause the differences observed for heterozygous and homozygous lines, but rather the huge variations between different lines. Plant transgenes can be silenced at either the transcriptional or post-transcriptional level (Dougherty and Parks, 1995; Fagard and Vaucheret, 2000). Transcriptional silencing involves promoter methylation and structural changes in chromatin (Ye and Signer, 1996). Thus, using the same promoter for controlling the transgene expression in the present study could be a reason for the lower expression levels of the transgenes. Post-transcriptional silencing results in a strong reduction of mRNA accumulation in the cytoplasm without significant changes in the rate of transcriptional initiation in the nucleus. It can affect the expression of transgenes and homologous host genes, a phenomenon referred to as co-suppression (Elmayan *et al.*, 1998). Additionally, post-transcriptional silencing can also affect the expression of transgenes sharing no sequence homology with host genes (Elmayan *et al.*, 1998; Mourrain *et al.*, 2000). The lower expression levels of *GCL*, *TSR* and *glc*F in homozygous lines could be related to transcriptional and/or post-transcriptional silencing (i.e. promoter methylation and/or co-suppression, respectively). Whether the lower transgene expression is due to promoter methylation or co-suppression is still unclear for us. However, this effect could be impeded by using weaker promoters and/or appropriate modification of codon usage. This should result in a reduced variability of transgene expression in populations of transformants (Schubert *et al.*, 2004). Elmayan *et al.* (1998) have characterized *Arabidopsis* mutants that are able to impede specifically transgene-induced post-transcriptional gene silencing. These mutants could be

used as alternatives to wild type *A. thaliana* plants in order to exclude the possibility of post-transcriptional transgene silencing. Because of the lower expression levels of *GCL*, *TSR* and *glc*F, a huge number of transgenic lines were screened to obtain comparable expression levels of all transgenes that were used for further analysis (3.4, 3.5 and 3.6).

In order to generate transgenic *A. thaliana* plants expressing all the necessary genes for the novel pathway, *TSR* and *GCL* translationally fused to a His-tag were cloned in a double construct into pTRA-K-rbcS1-cTP plant expression vector that confers resistance to kanamycin. *Glc*D and *glc*E genes that encode the D and E protein subunits of *Ec*GDH were cloned together into the plant expression vector pSuper-PAM-Sul-rbcS1-cTP that confers sulfadiazine resistance. Padidam and Cao (2001) demonstrated that when two genes are cloned head to tail (⸱⸱⸱⸱▸ ⟶), the expression of the downstream gene is reduced by 80% compared to the upstream gene. When two genes are cloned together tail to tail (⸱⸱⸱⸱▸ ◀⸻) the expression of the upstream gene is reduced by 53% through the expression of the downstream gene. If the orientation of the genes are head to head (◀⸱⸱⸱⸱ ⟶), no interference of expression is observed. The authors suggest that the transcriptional interference of the genes is a result of RNA polymerase read through and/or antisense RNA production. However, Paddidam and Cao also demonstrated that the transcriptional interference can be eliminated by inserting a transcription blocker (TB) sequence or a sequence from λ phage (Padidam and Cao, 2001). Therefore cloning of two genes (*TSR* and *GCL* or *glc*D and *glc*E) in double constructs was performed on the basis that the coding sequence of both genes is separated by a scaffold attachment region (SAR) as a separator. This will reduce the possible negative impacts of the first expression cassette onto the second (Padidam and Cao, 2001). The *glc*F gene that encodes the F subunit of *Ec*GDH was cloned into pTRA-PT-rbcS1-cTP that confers BASTA (phosphinothricin) resistance. Finally, *At*GDH w/o mTP was cloned into the pSuper-PAM-rbcS1-cTP plant expression vector. In this way, plants transgenic for GT-DEF can be selected on medium supplemented with kanamycin, sulfadiazine and phosphinotricin. On the other hand, plants transgenic for GTA can be selected on medium supplemented with kanamycin and sulfadiazine. GT-DEF and GTA plants were generated by successive nuclear transformation of wild type *A. thaliana* plants with the respective constructs. During each round of transformation, plants were selected on MS medium supplemented with the suitable antibiotics based on the selectable markers they contain. Moreover, the transgene expression was also tested in each generation. In another strategy that was used by one colleague at the same institute (Rafijul Bari, Institute for Biology I, RWTH-Aachen), transfer of GT-DEF

genes into tobacco plants was performed by direct chloroplast transformation. Unfortunately, this transformation process was not successful. Direct transformation of the chloroplast offers several advantages over nuclear transformation (Bock, 2001). In plastid transformation, high levels of transgene expression occur, foreign transgenes are normally highly stable, several transgenes can be introduced as a single operon, and position effects or epigenetic inhibition are mostly absent. In contrast, nuclear transformation often suffers from low levels of transgene expression. However, plastid transformation is not routinely available as a technique for *Arabidopsis* and I wanted to use the advantages of this plant like the ease of transformation and the short generation times (Hays, 2002; Meinke *et al.*, 1998). Therefore, it was decided to generate GT-DEF and GTA transgenic *A. thaliana* plants by successive nuclear transformation.

Wild type *Arabidopsis* plants were transformed with the *TSR* and *GCL* genes in a double construct (pTRA-K-rbcS1-cTP-TSR-His,GCL-His). The expression of both genes was checked on the protein level and on the RNA level. Both genes showed higher levels of expression and there were no detectable phenotypic changes within the different GT expressing plants (3.6). In contrast, transgenic tobacco plants that were transformed with the same construct (pTRA-K-rbcS1-cTP-TSR-His,GCL-His) (PhD thesis, Rafijul Bari, Institute for Biology I, RWTH-Aachen, Germany) showed clear phenotypic differences as chlorosis and yellowing of the plant leaves. This chlorotic effect in transgenic tobacco plants was probably due to very high levels of *GCL* expression. Although high levels of *GCL* and *TSR* expression were detected in *Arabidopsis* plants transgenic for GT, no phenotypic effects were observed in the expressing plants. However, transformation of tobacco plants transgenic for GT that showed acceptable expression levels for *GCL* and *TSR* with a construct for cTP-*At*GDH results in the production of transgenic plants that have no chlorotic effect (information kindly provided by Krishna Thiruveedhi, Institute for Biology I, RWTH-Aachen, Germany). Thus, overexpression of a glycolate oxidizing enzyme inside the chloroplast of tobacco plants transgenic for GT impedes the negative effects of *GCL* expression in those plants. The overall effect of GTA expression in transgenic tobacco plants is currently analyzed. *A. thaliana* plants expressing *GCL, TSR* and cTP-*At*GDH (GTA plants) show enhanced growth compared to wild type plants whereas *A. thaliana* plants transgenic for A and GT plants show similar phenotypes compared to wild type plants. This leads to the conclusion that establishment of the complete GTA pathway in the plant chloroplasts is important to ensure the significance of the novel pathway.

The enzymatic activities of *GCL* and *TSR* were tested in a coupled reaction according to Gotto and Kornberg (1961). This assay was originally performed by Gotto and Kornberg, (1961) in order to test the activity of the bacterial glyoxylate carboligase from bacterial extracts in the presence of glyoxylate and an excess of tartronic semialdehyde reductase. But with chloroplast extracts, no bacterial TSR was used. The idea was to test the conversion of glyoxylate into glycerate via *GCL* and *TSR* that should be present in the chloroplast extracts isolated from plants transgenic for GT. Therefore, the assay was performed with chloroplast extracts from wild type plants and plants transgenic for GT in the presence and absence of the substrate glyoxylate (3.2.1.2). The assay with chloroplast extracts from plants transgenic for GT shows a higher oxidation of NADH compared to the chloroplast extract from wild type in the presence of glyoxylate. In the absence of glyoxylate, both extracts showed similar background (3.2.1.2). The background in this assay may be due to the presence of free glyoxylate in the chloroplast extracts. Based on this result, both enzymes are therefore seemingly active inside the chloroplast.

In order to complete the establishment of the novel pathway, another wild type *Arabidopsis* plants were transformed with a double construct for DE and a single construct for F. The aim was to target each subunit independently to the chloroplast where those were expected to assemble the active glycolate dehydrogenase enzyme. The expression of DEF transgenes in plants transgenic for DE, F and DEF was mainly checked on the RNA level by Real Time RT-PCR. Plants transgenic for DE and F showed varying expression levels of the respective genes (3.2.2.3). Moreover, *A. thaliana* plants transformed with a single construct for cTP-*At*GDH showed also varying expression levels for cTP-*At*GDH. No phenotypic effects were observed in the differentially expressing plants (plants transgenic for DE, F and A) compared to their wild type counterparts. However, plants transgenic for DEF expressing the complete *Ec*GDH show different phenotypes as the bigger and flat leaves, bigger rosette diameters, and faster growth rates compared to the other genotypes (3.6). It was observed that such phenotypes are characteristic for DEF transgenic plants. Plants transgenic for GT-DEF showed also the same phenotypes with the exception that GT-DEF plants are bigger in size (3.6). Plants transgenic for F and DE plants did not show those phenotypes. These phenotypic effects appear only when the complete *Ec*GDH is expressed in the plant chloroplast. As mentioned, DEF plants were generated by retransformation of homozygous plants transgenic for F with a double construct for DE. Thus, the integration site for *glc*F in DEF plants is the same for the plants transgenic for F. Moreover, all the generated plants transgenic for DEF

show the same phenotypes although those plants have different integration sites for DE as DEF7 and DEF4 (3.2.2.2). Therefore, the different phenotypes observed in DEF plants compared to the other genotypes cannot be due to their integration sites on the plant chromosomes.

*Ec*GDH and cTP-AtGDH enzymatic activities were tested using chloroplast extracts isolated from DEF plants and plants transgenic for A, respectively. A GDH assay (Lord, 1972) was performed using both extracts (3.2.2.4 and 3.3.2.5). Presence of peroxisomal contaminations (presence of the plant glycolate oxidase) in the chloroplast preparation can interfere with the GDH assay results. This problem was overcome by performing the assay in the presence and absence of KCN since the peroxisomal glycolate oxidase is insensitive to cyanide. The higher plant peroxisomal glycolate oxidase oxidizes L(+)-lactate preferentially over D(-)-lactate. In contrast *Ec*GDH and *At*GDH oxidize D(-)-lactate preferentially over L(+)-lactate and they are cyanide sensitive (Bari *et al.*, 2004; Nelson and Tolbert, 1970; Pellicer *et al.*, 1996). Therefore, the D-LDH assay (Gutheil, 1998) was additionally performed with the same chloroplast extracts used for the GDH assay in the presence and absence of cyanide. The background observed in the GDH assay can be related to the presence of free glyoxylate in the chloroplast extract. Moreover, the background observed in the D-LDH assay can be due to the presence of other enzymes that use NADH as a cofactor and that are insensitive to cyanide. Both assays (D-LDH and GDH) revealed that the *Ec*GDH and *At*GDH are seemingly active *in vivo*. The previously described enzymatic assays showed that the novel pathway enzymes are seemingly active in the transgenic plant chloroplasts. But the question is now: is the novel pathway functional in the transgenic plants? This will be discussed in the following chapter.

4.5 The influence of the novel pathway in the transgenic plants

I) *Influences of GTA and GT-DEF expression*

Plants transgenic for GTA and GT-DEF plants showed a better growth performance compared to wild type plants (3.6.2). Both genotypes have bigger leaf area compared to wild type plants (3.6.3). Moreover, the fresh and dry weight measurements revealed that both plant types produce more biomass compared to wild type plants (3.6.4). Although expression of the GTA pathway in the plant chloroplast enhances the plant growth under photorespiratory and non photorespiratory conditions, it is clear that the expression of GT-DEF pathway is much more efficient to the plant compared to the GTA pathway. The difference in both pathways is the

oxidation step of glycolate to glyoxylate. This could make *Ec*GDH more efficient to the plants than cTP-*At*GDH, although the physiological parameters did not reflect this difference. The latter might conversely indicate that the activities of both enzymes are similar *in vivo*. However, the growth performance measurements using GTA and GT-DEF plants lead to the conclusion that expression of the novel pathway genes in plant chloroplast enhances the plant growth and increases the total yield in the expressing plants.

In order to check the efficiency of the novel pathway in the transgenic plants, a series of biochemical and physiological analyses was performed using GTA and GT-DEF plants in addition to control plants expressing one or two genes of the novel pathway. The control plants include plants transgenic for A, GT and DEF plants.

Novitskaya *et al.* (2002) have shown a clear accumulation of the amino acid glycine in the leaves of wheat and potato plants growing under photorespiratory conditions. By measuring the Gly/Ser ratio from both plant types, they found a clear correlation between the photorespiratory rate (oxygenation reaction of Rubisco) and the measured Gly/Ser ratio. Accumulation of glycine during higher photorespiratory rates can be due to a kinetically limiting transport step that prevents glycine metabolism to match its rate of generation (Keys and Leegood, 2002). It can also be due to the requirement of a high mitochondrial glycine concentration to accelerate glycine oxidation rates, either because of a kinetic limitation at the glycine decarboxylase (GDC) or in order to push the thermodynamically unfavourable conversion of glycine to serine (Besson *et al.*, 1993). Moreover, increases in Gly/Ser ratio may reflect readjustment of the reduction state of the mitochondrial NAD^+ pool in response to the large changes in the photorespiratory flux (Douce and Neuburger, 1989). Novitskaya *et al.* (2002) suggested that the Gly/Ser ratio is considered as a marker for the rate of photorespiration. Thus, it was decided to measure Gly/Ser ratios from GTA and GT-DEF plants in addition to other control plants. By measuring the Gly/Ser ratio from both genotypes, a clear decrease in Gly/Ser ratio was observed under photorespiratory conditions compared to wild type plants (3.4.1). This decrease in Gly/Ser ratio provides a clear evidence for the partial suppression of photorespiration in GTA and GT-DEF plants.

Atkin *et al.* (1998); Bulley and Tregunna (1971) and Decker (1959) have shown that when a C_3 plant is exposed suddenly to darkness after a period of illumination, a momentary rapid outburst of CO_2 occurs before the plant achieves a steady-state dark respiration. This outburst was increased greatly at higher O_2 levels (Decker, 1959). The authors concluded that this

outburst represents the amounts of CO_2 released in the plant mitochondria during photorespiration. In order to ensure these observations, the postillumination burst (PIB) was measured from wild type maize leaves (as a C_4 plant). The PIB was absent in maize plants (data not shown). Based on these observations, it was decided to measure the PIB from transgenic as well as wild type plants as a measure for the photorespiratory flow in these plants. GTA and GT-DEF plants showed a lower CO_2 release in their mitochondria compared to wild type plants as observed from PIB measurements (3.5.1). The decrease in CO_2 released in the mitochondria of GTA and GT-DEF plants provides another evidence for the partial suppression of photorespiration in both genotypes.

In another approach for measuring the rate of photorespiration, the ammonia released in the mitochondria during the conversion of glycine to serine was measured from GTA plant leaf tissues. The accumulation of ammonia in the plant leaf tissues is due to the inhibition of GS-GOGAT cycle by the herbicide phosphinotricin present in the assay medium. Phosphinotricin is a glutamate analogue that irreversibly inhibits glutamine synthetase activity and as a result ammonia accumulates inside plant leaf tissues (Lacuesta *et al.*, 1989; Tachibana *et al.*, 1986; Wild and Ziegler, 1989). The ammonia accumulating in the leaf tissues diffuses into the surrounding medium where a colourimetric reaction indicates ammonium concentration (De Block *et al.*, 1995). GTA plants showed less ammonia release compared to wild type plants under the assay conditions (3.4.2). Such measurements could not be performed with plants transgenic for GT-DEF because these plants are resistant to phosphinotricin. This result can also be added to the positive impacts of the novel biochemical pathway on the suppression of photorespiration in GTA plants.

Measurements of the internal CO_2 compensation points (Γ_*) of *A. thaliana* plants transgenic for GTA and GT-DEF plants revealed that both genotypes have lower CO_2 compensation points compared to their wild type counterparts (3.5.3). Moreover, the chlorophyll fluorescence measurements showed that both genotypes have higher rates of photosynthesis compared to wild type plants, since GTA and GT-DEF plants have lower e/A ratios compared to wild type plants under selective conditions (3.5.4). GTA and GT-DEF plants grow also better under ambient conditions when they are compared to wild type plants. No clear differences in the e/A ratio in GTA and GT-DEF plants were observed under ambient conditions. The e/A ratio measurements were performed at a later growth phase where the plant leaves are big enough to fit into the measuring device. On the other hand, the biomass

measurements were performed at an earlier growth phase. Thus, the e/A ratio measurements could not reflect the actual performace of the tested plants.

Additionally, GTA and GT-DEF plants showed higher levels of glucose and fructose and similar levels of sucrose and starch compared to wild type plants (3.4.4). Higher levels of glucose and fructose in GTA and GT-DEF plants can be added to the positive significance of the novel pathway in the transgenic plants. Moreover, GTA and GT-DEF plants have similar levels of glyoxylate content compared to wild type plants (3.4.3). This result leads to the conclusion that the novel pathway does not interfere with the basic metabolic pathways in both genotypes. Taken together, all the measured parameters showed that the novel pathway is able to partially suppress photorespiration in the transgenic plants. Moreover, the novel pathway enhances the photosynthetic performance of the expressing plants with an increase in the total plant yield. However, the GT-DEF pathway is more efficient to plants compared to the GTA pathway. This effect was obvious from the photosynthetic and growth measurements (3.5 and 3.6, respectively). The only difference between both pathways is the glycolate oxidizing enzyme. So the question is now: is *Ec*GDH more efficient to the plant than cTP-*At*GDH? In order to answer this question, it is important to know the behaviour of the control plants in the above mentioned analyses. In the next chapter, the influence of *Ec*GDH and cTP-*At*GDH expression will be discussed.

II) *Influences of EcGDH and cTP-AtGDH expression*

Expression of *GCL* and *TSR* together with the complete *Ec*GDH in the plant chloroplasts enhances plant growth performance and shows a clear increase in the total fresh and dry weight of the expressing plants. This effect was also observed in *A. thaliana* plants transgenic for DEF. GTA plants show a little increase in their total fresh and dry weight compared to wild type plants. However, this effect is not as signifcant as in case of GT-DEF plants (3.6.4). The question is now: is the expression of a glycolate dehydrogenase in the plant chloroplast the cause for these effects? Actually, it is difficult to explain such a phenomenon because the transgenic *A. thaliana* plants expressing cTP-*At*GDH in their chloroplasts did not show any phenotypic differences compared to wild type plants, although those plants showed similar physiological benefits (3.4) compared to DEF plants. In contrast, transgenic tobacco plants expressing cTP-*At*GDH in their chloroplasts showed better growth performance (plants are bigger in size) compared to wild type plants (information kindly provided by Krishna Thiruveedhi, Institute for Biology I, RWTH-Aachen). This could indicate that the

physiological parameters determined for *A. thaliana* plants transgenic for A do not directly reflect the growth performance of those plants. However, the better growth performance of tobacco plants transgenic for A would rather indicate that the morphological effects might be species-specific.

In *A. thaliana* plants, oxidation of glycolate in the chloroplast by *Ec*GDH or cTP-*At*GDH results in a reduction in the photorespiratory flow as indicated by the reduced Gly/Ser ratios in plants transgenic for A and DEF plants (3.4.1). The decrease in Gly/Ser ratio is enhanced by the expression of the complete pathway genes in the plant chloroplast (GT-DEF and GTA plants). Similar results were obtained from the measurements of the postillumination burst (PIB) (3.5.1) and the ammonia released during photorespiration (3.4.2). During photorespiration, phosphoglycolate is produced in the chloroplast as a result of Rubisco oxygenase activity. Phosphoglycolate is dephosphorylated by phosphoglycolate phosphatase forming glycolate (1.4.1). In plants transgenic for A and DEF plants, glycolate is oxidized in the chloroplast forming glyoxylate. This will decrease the flow of glycolate into the photorespiratory pathway. Thus, the decrease in the Gly/Ser ratio in plants transgenic for A and DEF is expected. Furthermore, in both genotypes, glycolate oxidation occurs in the chloroplast and not in the mitochondria. As mentioned before, glycolate oxidation in the normal photorespiratory pathway occurs otherwise in the peroxisomes and not in the mitochondria. The only exception is that the novel *At*GDH is localized in the mitochondria (Bari *et al.*, 2004). Thus, the inhibition of glycine decarboxylase complex by high concentration of glyoxylate (Peterson, 1982) could be impeded. This could provide another explanation for the decrease in the Gly/Ser ratio in plants transgenic for A and DEF plants. This could also account for the decrease in Gly/Ser ratio in plants transgenic for GTA and GT-DEF plants. Additionally, the reduction in the photorespiratory flow in the above mentioned genotypes results in a decrease in the CO_2 release in the plant mitochondria during the conversion of glycine to serine. This effect was observed by measuring the PIB from GTA, DEF, GT-DEF plants and plants transgenic for A (3.5.1).

By measuring the total glyoxylate content, it was clear that there is no significant glyoxylate accumulation in plants transgenic for A and DEF plants under ambient conditions compared to wild type plants. So it is important to know how the produced glyoxylate is metabolized by the expressing plants. The possible pathways of glyoxylate metabolism in plants were discussed by Igamberdiev and Lea (2002) as shown in figure 4.1. In the following chapter, only the reactions with possible relevance for plastidial glycolate oxidation will be discussed in more details.

The major pathway is transamination of glyoxylate to form glycine in the peroxisome during the photorespiratory pathway (1.4.1) (reaction 4 in figure 4.1). Glyoxylate in plants transgenic for A and DEF plants is produced in the chloroplast and not in the peroxisomes. However, there is a possibility that glyoxylate could be exported to the peroxisomes. In this case, glyoxylate could be transaminated to form glycine and then further to glycerate in the normal photorespiratory pathway. However, measurements of Gly/Ser ratio and postillumination burst from both genotypes (3.4.1 and 3.5.1 above, respectively) showed a clear reduction in their photorespiratory flow. Thus, this possibility can be excluded. However, one of the alanine/glyoxylate aminotransferases was identified in *Arabidopsis* genome (AGA-2; At1g72330). *In vitro*, this enzyme acts as alanine/glyoxylate aminotransferase (data kindly provided by Markus Nießen, Institute for Biology I, RWTH-Aachen). A computer prediction program (http://www.cbs.dtu.dk/services/TargetP) has shown that the coding sequence of the first 46 amino acids of AGA-2 could target the protein into the chloroplast as well as to the mitochondria in a ratio of 1/1. However, the actual localization of this enzyme is still unknown. Concerning the presence of AGA-2 in the chloroplast of plants transgenic for A and DEF plants, Glyoxylate can be transaminated forming glycine and pyruvate. Glycine could be involved in protein synthesis and pyruvate could be involved in Calvin cycle to form carbohydrates in the chloroplast. Integration of glyoxylate in a reaction with AGA-2 in the chloroplast might account for the decrease in the photorespiratory flow in both genotypes. However, this pathway for metabolizing glyoxylate could not account for the decrease in the e/A ratio and in the CO_2 compensation point that were observed in both genotypes.

Under photorespiratory conditions, the increased amounts of glyoxylate and phosphoglycolate can inhibit photosynthesis. Thus, formate is produced (reaction 5 in figure 4.1) as a response to the higher glyoxylate concentrations in the reaction of H_2O_2 with glyoxylate in the peroxisomes (Grodzinski, 1979). Formate could be used as a source of carbon for the biosynthesis of proteins, nucleic acids and other secondary metabolites. Conversion of glyoxylate into formate can reduce the flow of carbon through the normal photorespiratory pathway (Igamberdiev, 1999; Wingler *et al.*, 1999a). This metabolic pathway of glyoxylate might be possible in plants transgenic for A and DEF plants if glyoxylate could be exported to the peroxisomes and H_2O_2 is available. However, H_2O_2 is produced during the oxidation of glycolate to glyoxylate and it is directly hydrolyzed by a catalase present in the peroxisomes (Grodzinski, 1979; Igamberdiev *et al.*, 2001; Igamberdiev and Kleczkowski, 1997; Leegood *et al.*, 1995; Tolbert *et al.*, 1968). The reduction in the photorespiratory flow in plants

transgenic for A and DEF plants is due to the oxidation of glycolate to glyoxylate in the plant chloroplast. Thus, the amount of glycolate exported to the peroxisomes should be decreased. The decrease in glycolate in the peroxisomes might be accompanied by a decrease in the peroxisomal glycolate oxidase activity. This will also reduce the amount of H_2O_2 in the peroxisomes that could be involved in the reaction with glyoxylate to form formate. Thus, metabolizing glyoxylate via this pathway in plants transgenic for A and DEF plants is not expected. However, this pathway for glyoxylate metabolism might only account for the reduction in the photorespiratory flow but not for the better photosynthetic performance of both genotypes, since the CO_2 released during this reaction occurs in the peroxisomes and not in the chloroplast.

Glyoxylate can be reduced to glycolate (reactions 2 and 3 in figure 4.1) by NADPH-dependent glyoxylate reductase, or by NADPH-dependent hydroxypyruvate reductase in the cytosol and by NADH-dependent hydroxypyruvate reductase in peroxisomes (Kleczkowski and Edwards, 1989; Zelitch and Gotto, 1962). Additionaly, glyoxylate can be also reduced to glycolate in the chloroplast by NADPH-dependent glyoxylate reductase. There is evidence of glyoxylate reductase activity in the chloroplast of higher plants (Tolbert et al., 1970). This pathway of metabolizing glyoxylate can be possible in both genotypes (plants transgenic for A and DEF plants) since glyoxylate could be reduced by glyoxylate reductase in the chloroplast forming glycolate. Reduction of glyoxylate by glyoxylate reductase in the chloroplast helps only in the consumption of the excess photosynthetic reducing power (NADPH) in a glycolate/glyoxylate shuttle as described by Tolbert et al. (1970). However, this pathway can not explain the decrease in the photorespiratory flow observed in both genotypes.

During senescence, glyoxylate can enter the malate synthase reaction resulting in the formation of malate (reaction 10 in figure 4.1). This pathway for metabolizing glyoxylate could be possible in plants transgenic for A and DEF plants if glyoxylate could be exported to the cytosol. Glyoxylate can be integrated into the malate synthase pathway to form malate which in turn can be converted to pyruvate with the release of CO_2. Metabolizing glyoxylate by this pathway could also explain the reduction in the photorespiratory flow in plants transgenic for A and DEF plants. However, this pathway could not explain the decrease in the e/A ratio and in the CO_2 compensation point observed in both genotypes.

Glyoxylate can be condensed with succinate in the cytosol in the reverse reaction of isocitrate lyase forming isocitrate that could be involved in the basic plant metabolism (Igamberdiev *et al.*, 1986) (reaction 8 in figure 4.1). Such pathway for metabolizing glyoxylate can be only possible if glyoxylate could be exported to the cytosol. However, this pathway for metabolizing glyoxylate could show similar effects that could be obtained from the integration of glyoxylate into the malate synthase pathway as mentioned above.

Condensation of two molecules of glyoxylate followed by decarboxylation can result in the formation of tartronic semialdehyde (reaction 11 in figure 4.1) which can be reduced to glycerate. This pathway for metabolizing glyoxylate is only found in bacteria (Lord, 1972; Pellicer *et al.*, 1996). *A. thaliana* genome was completetly sequenced and no homologous genes to *GCL* and *TSR* were characterized. Thus, metabolizing glyoxylate by this pathway is impossible.

Oxalate can be formed as a side product of glycolate oxidase reaction when the enzyme uses glyoxylate as a substrate (reaction 6 in figure 4.1). Differences in glycolate oxidase affinity for glyoxylate were found for C_3 and C_4 species (Devi *et al.*, 1996). Oxidation of glycolate in chloroplasts of plants transgenic for A and DEF plants results in a reduction in the photorespiratory flow. This could result in a decrease in the amount of glycolate exported into the peroxisomes. If glyoxylate is exported into the peroxisomes, it can be therefore used as a substrate for the peroxisomal glycolate oxidase instead of glycolate. This will result in the production of oxalate that can be further metabolized by other metabolic pathways in the peroxisomes. Metabolizing glyoxylate by this pathway could explain the reduction in the photorespiratory flow in plants transgenic for A and DEF plants. But this metabolic pathway could not explain the better growth performance of DEF plants compared to wild type plants. Moreover, this pathway could not account for the better photosynthetic performance (i.e. the decrease in the CO_2 compensation point and the e/A ratio) of plants transgenic for A and DEF plants.
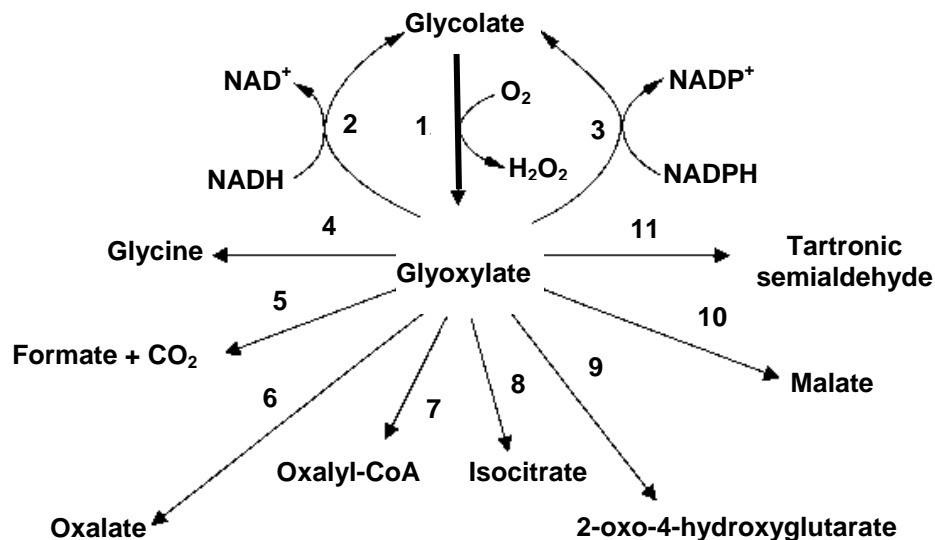
Figure 4.1: Diagramatic representation of the pathways of glyoxylate metabolism in plants.

Shown are the possible metabolic pathways of glyoxylate in plants.1= plants. Oxidation of glycolate by glycolate oxidase in peroxisomes; 2, 3 = Reduction of glyoxylate by NADPH-dependent glyoxylate reductase or by NADPH-dependent hydroxypyruvate reductase in the cytosol and by NADH-dependent hydroxypyruvate reductase in peroxisomes; 4 = Transamination of glyoxylate to glycine; 5 = Non-enzymatic conversion of glyoxylate by H_2O_2 to formate and CO_2; 6 = Oxidation of glyoxylate to oxalate in the side reaction of glycolate oxidase; 7 = Synthesis of oxalyl-CoA; 8 = Formation of isocitrate in the synthase reaction of isocitrate lyase, in green leaves, this reaction may occur in the cytosol; 9 = Non-enzymatic formation of oxalomalate, a strong inhibitor of isocitrate dehydrogenase, following decarboxylation and formation of 2-oxo-4-hydroxyglutarate; 10 = Formation of malate in malate synthase reaction and 11 = Formation of tartronic semialdehyde by condensation of two glyoxylate molecules following decarboxylation (likely absent from higher plants). This figure was taken from Igamberdiev and Lea (2002).

In many green algal species, glycolate dehydrogenase is present in mitochondria where it produces glyoxylate from glycolate. The glyoxylate is further metabolized to glycine in the mitochondrion and afterwards by different pathways to glycerate, serine or related compounds (Igamberdiev and Lea, 2002; Winkler and Stabenau, 1992). This pathway is part of the algal photorespiration. Presence of a glycolate oxidizing enzyme (*At*GDH) in the mitochondria of *A. thaliana* plants (Bari *et al.*, 2004), supports the hypothesis that a second photorespiratory pathway is present in the mitochondrion of higher plants. Liepman and Olsen (2001); Liepman and Olsen (2003) have identified several glyoxylate aminotransferases that work in the plant peroxisomes. Glyoxylate produced in the plant mitochondria can be involved in transamination reactions including alanine, serine or glutamate to form glycine. We are currently working on a project for identifying the actual localization of those aminotransferases in the plant cells. This can provide a new evidence for the presence of an alternative photorespiratory pathway in plants. Presence of an alternative photorespiratory pathway in *A. thaliana* plants can interfere with the novel pathway that was established in the

plant chloroplast if glycolate is exported from the chloroplast to the mitochondria. However, this could provide another pathway for glyoxylate produced in the chloroplast (in plants transgenic for A and DEF plants) if glyoxylate is exported to the mitochondria. However, this pathway can not account for the decrease in the CO_2 release in the mitochondria during photorespiration observed in both genotypes. There may be another glycolate/glyoxylate shuttle between chloroplast and mitochondria resembling the glycolate/glyoxylate shuttle described for the alga *Euglena gracilis* (Yokota *et al.*, 1985b; Yokota and Kitaoka, 1979b) and similar to the glycolate/glyoxylate shuttle between chloroplast and peroxisomes (Tolbert *et al.*, 1970). However, export of glyoxylate into the mitochondria or chloroplast will depend on the re-import of glycolate. Moreover, glycolate could move to the cytoplasm in an exchange for glycerate in a glycolate/glycerate shuttle (Heber and Kirk, 1975). This shuttle is normally acting in the opposite reaction. Integration of glyoxylate in these pathways could not explain the reduction in the photorespiratory flow in plants transgenic for A and DEF plants. Taken together, export of glyoxylate into the peroxisomes and/or the cytosol and its integration into all the previously described pathways (malate synthase pathway, formation of formate, condensation with succinate and formation of oxalate) might be possible to take place in plants transgenic for A and DEF plants. All these metabolic pathways of glyoxylate might only explain the reduction in the Gly/Ser ratios, ammonia release and postillumination burst. However, none of those pathways could account for the lower CO_2 compensation point in both genotypes compared to wild type plants. Furthermore, integration of glyoxylate into the alanine/glyoxylate aminotransferase in the chloroplast might be the most possible pathway for glyoxylate metabolism in both plant types.

The efficiency of *Ec*GDH and *At*GDH concerning glycolate oxidation *in vivo* is still unclear for us. Although the reduction in photorespiration is similar for both genotypes, it is clear that overexpression of *Ec*GDH in the plant chloroplast enhances the plant growth whereas this effect is absent in *A. thaliana* plants transgenic for A (3.6). To understand this phenomenon, it is important to follow the flow of the carbon from glycolate inside the different transgenic plants. This can be achieved by feeding ^{14}C-labelled glycolate to plant chloroplasts. In an approach for understanding this phenomenon, chloroplasts were isolated from leaves of the different transgenic plants. Chloroplast proteins were extracted and fed with ^{14}C- labelled glycolate. The products from the feeding process were characterized on 2D-TLC (2.2.3.13). Unfortunately, feeding of ^{14}C-glycolate to chloroplast extracts was not successful (data not shown). It was expected to find out what happens to glyoxylate produced in the chloroplasts

of the plants transgenic for A and DEF plants. Feeding the chloroplasts with ^{14}C-labelled glycolate needs several optimization steps in order to find out a standard method for this feeding process. An alternative is the feeding of ^{14}CO$_2$ to plant leaf discs under ambient conditions. This approach was performed as described (3.4.5) but no major differences in the labelled products were observed. Kumarasinghe *et al.* (1977), in an experiment involving a short time feeding of wheat leaf segments with ^{14}CO$_2$, have demonstrated that the flux of carbon through the glycolate pathway exceeds the assimilation rates under 150 ppm CO$_2$ concentration in air whereas both rates are approximately equal under 350 ppm CO$_2$ concentration. Based on these results, it might be helpful if the ^{14}CO$_2$ feeding experiment is performed under photorespiratory conditions. The aim is to produce ^{14}C-labelled products from the normal photosynthetic pathway (i.e. ribulose-1,5-bisphosphate). Under photorespiratory conditions, a ^{14}C-labelled glycolate will be produced in the chloroplast that could be in turn metabolized by the novel pathway enzymes. Chloroplast should be then isolated and the labelled products could be characterized by thin layer chromatography. This could perhaps help in identifying the actual pathways for metabolizing glyoxylate in plants transgenic for A and DEF. However, performing this experiment under photorespiratory conditions also needs several optimization and safety procedures. Although, I can't offer a concise metabolic pathway describing the benefits of glycolate oxidation in the chloroplast, the results in this study clearly showed that such a benefit is obvious at least for *A. thaliana* plants transgenic for DEF.

III) *Influences of GT expression*

Interestingly, overexpression of *GCL* and *TSR* in the chloroplast of *A. thaliana* plants results in a lower Gly/Ser ratio compared to WT plants under low CO$_2$ environment. Moreover, plants transgenic for GT showed a clear decrease in their glyoxylate content compared to the other tested genotypes (3.4.3). How can the expression of *GCL* and *TSR* genes in the plant chloroplast affect the rate of photorespiration and why their glyoxylate content is lower than the other tested genotypes? Goyal and Tolbert (1996) provided an evidence for the presence of a glycolate oxidation system inside the plant chloroplast that is associated with the photosynthetic electron transport chain, but this enzyme is still not isolated. Thus, glycolate oxidation by this unknown enzyme inside the chloroplast could result in the formation of glyoxylate. The produced glyoxylate could be consumed by the glyoxylate carboligase enzyme (*GCL*) in the chloroplast of GT transgenic plants. Aternatively, a NADPH-dependent glyoxylate reductase in spinach chloroplast was reported (Tolbert *et al.*, 1970). The

glyoxylate reductase consumes the excess photosynthetic reducing power (NADPH) in the reduction of glyoxylate to glycolate. Glycolate would move to the peroxisomes and be reoxidized to glyoxylate. Glyoxylate returns back to the chloroplast to complete a glycolate/glyoxylate shuttle (Tolbert *et al.*, 1970). Thus, part of the imported glyoxylate from the peroxisomes can also be used by *GCL* in the chloroplast of GT transgenic plants. This could account for the decrease in the glyoxylate content of *A. thaliana* plants transgenic for GT. However, glyoxylate is known to be involved in many regulatory and signal transduction mechanisms in plant cells (Igamberdiev and Lea, 2002). Glyoxylate is an inhibitor, regulating the activity of Rubisco and its activation process (Igamberdiev and Kleczkowski, 1997). Glyoxylate plays a role in regulating mitochondrial enzymes. It inhibits the glycine decarboxylase complex in a non-competitive manner (Peterson, 1982). Glyoxylate is also known to inhibit the glycolate/glycerate carrier in the inner chloroplast membrane, which mediates photorespiratory fluxes between chloroplasts and cytosol (Robinson, 1982). In peroxisomes, glyoxylate plays an active role in the regulation of the peroxisomal aminotransferases, especially in the presence of ammonium ions (Havir, 1986). Concerning all these aspects, the decrease in glyoxylate content in GT plants could not interfere with the regulatory mechanisms associated with glyoxylate. However, the decrease in Gly/Ser ratio in those plants (3.4.1) could be due to two main reasons: (1) Glyoxylate could be consumed by *GCL* in the chloroplast and therefore its flow through the photorespiratoty pathway is decreased. (2) Consumption of glyoxylate will decrease its concentration and its negative influence on the photosynthetic performance of GT plants will be therefore retarded. Although GT plants have a lower Gly/Ser ratio compared to wild type plants, the growth characteristics of GT plants are similar to wild type plants (3.6). Future investigations are planned to show the behaviour of GT plants in the other biochemical and physiological analysis.

4.6 Future work

In the progress of the current study, transgenic *A. thaliana* plants expressing a glycolate oxidizing pathway inside the chloroplast (GTA and GT-DEF pathways) were generated. The enzymatic activity analysis has revealed that all the enzymes involved in the novel pathways are active *in vitro* and thus they could be active *in vivo*. The biochemical analysis of the transgenic plants has shown that there is a clear reduction in the fluxes through photorespiration. Moreover, the photosynthetic performance of the transgenic plants is better than wild type plants under photorespiratory conditions. At the same time, the growth

performance of the transgenic plants (especially DEF, GT-DEF and GTA plants) is also better compared to their wild type counterparts. The biochemical and the physiological analysis of the transgenic plants have answered the crucial question whether this pathway improves the CO_2 fixation in transgenic plants or not. But many other questions arise that need to be answered. One of these questions is: can this novel pathway functionally work in crop plants as wheat? To answer this question, the novel pathway should be transferred to these plants; transgenic lines expressing all the necessary genes for the novel pathway in the chloroplast should be generated, finally, the productivity of the transgenic plants should be checked under photorespiratory conditions compared with control plants. Before transferring the novel pathway to crop plants, some further analyses should be performed using the transgenic *A. thaliana* plants expressing the novel pathway. Firstly, the flux of carbon in the novel pathway should be studied in more details in order to characterize the end products of this pathway in plants and its relation to the plant growth. Secondly, it is important to study the incorporation of the intermediates produced in the progress of the novel pathway (as glyoxylate) to the basal transport system in the plant chloroplast and its integration in the regulation of the various metabolic processes.

It is also important to use another promoter for controlling the transgene expression. Perhaps, the novel pathway will be more significant for the plants when the necessary enzymes are expressed at the time of need. Thus, promoter that induces expression under low CO_2 conditions, or other promoters that work only in illuminated parts of the plant, can be used instead of the p35S promoter. Additionally, it may be equally useful to transform the novel pathway genes into *A. thaliana* mutants with impaired post-transcriptional gene silencing (PTGS) (Butaye *et al.*, 2004; Elmayan *et al.*, 1998) or into lines expressing proteins that suppress PTGS (Vaucheret *et al.*, 2001). By this, a more efficient expression of the glycolate pathway genes can be achieved.

Somerville and Ogren (1982) have created mutants with deficiencies in enzymes of the photorespiratory pathway. Photosynthesis and growth are normal in these mutants under non-photorespiratory conditions (high CO_2), but plants died in ambient air. It would be very interesting to cross transgenic plants containing the novel pathway with the photorespiratory mutants and see if the plants can survive under photorespiratory conditions. Transfer of the glycoate pathway into crop plants will ultimately lead to an increase in their productivity under unfavourable growth conditions.

5 LIST OF ABBREVIATIONS

Abbreviation	Full form
2D-TLC	Two dimension- thin layer chromatography
A gene	cTP-AtGDH
Amp	Ampicillin
APS	Ammonium persulfate
A. thaliana	*Arabidopsis thaliana*
AtGDH	*Arabidopsis thaliana* glycolate dehydrogenase
ATP	Adenosine triphosphate
bla	β--lactamase gene for selection in bacteria (ampicillin/carbenicillin resistance).
bps	Base pairs
BSA	Bovine serum albumin
BSC	Bundle sheath cell
C_2-cycle	Photorespiratory cycle (2 Carbon cycle)
C_3-cycle	Benson calvin cycle (3 Carbon cycle)
C_4-cycle	C_4-like CO_2 assimilation pathway
Ca	The external CO_2 concentration outside plant leaf
CA	Carbonic anhydrase
CAT	Catalase
CAM	Crassulacean acid metabolism
CaMV	Cauliflower mosaic virus
Carb	Carbenicillin
cDNA	Complementary DNA
Ci	The internal CO_2 concentration inside plant leaf
CoA	Coenzyme A
cTP-AtGDH	*Arabidopsis thaliana* glycolate dehydrogenase w/o mTP fused to chloroplast targeting peptide
DCIP	2,6 dichlorophenolindophenol sodium salt
DE plants	*A.thaliana* plants expressing *glc*D and *glc*E subunits of EcGDH
DEF plants	*A. thaliana* plants expressing the complete EcGDH genes
D-LDH	D(+)-lactate dehydrogenase

DMSO	Dimethyl sulfoxide
DNA	Deoxyribonucleic acid
dNTP	Deoxyribonucleoside triphosphate
DsRED	Red fluorescence protein
DTT	Dithiothreitol
*Ec*GDH	*E. coli* glycolate dehydrogenase
EDTA	Ethylene diamine tetraacetic acid
F gene	The coding sequence for *glc*F subunit of the *Ec*GDH
G3P	Glyceraldehyde-3-phosphate
GCL	Glyoxylate carboxyligase
GC/MS	Gas Chromatography/Mass Spectromrtry
GDC	Glycine decarboxylase
GDC/SHMT	Glycine decarboxylase/serine hydroxymethyl transferase
GDH	Glycolate dehydrogenase
gfp	Green fluorescent protein
GGAT	Glutamate:glyoxylate aminotransferase
GK	Glycerate kinase
*Glc*D	Coding sequence for the D subunit of glycolate dehydrogenase in *E. coli*
*Glc*E	Coding sequence for the E subunit of glycolate dehydrogenase in *E. coli*
*Glc*F	Coding sequence for the F subunit of glycolate dehydrogenase in *E. coli*
Gly	Glycin
GOGAT	Glutamate:glyoxylate aminotransferase
GOX	Glycolate oxidase
GS	Glutamine synthetase
GT plants	*A.thaliana* plants expressing *GCL* and *TSR*
GTA plants	*A.thaliana* plants expressing *GCL*, *TSR* and cTP-*At*GDH
GT-DEF plants	*A.thaliana* plants expressing *GCL*, *TSR* and *Ec*GDH
h	Hour
HCO$_3^-$	Bicarbonate
Hepes	N-2-hydroxyethylpiperazine-N´-2-ethanesulfonic acid
His	The coding sequence for His-tag protein
HPR	Hydroxypyruvate reductase
Hyg	The coding sequence, which confers resistance to hygromycin

IPTG	Isopropyl-β-D-thiogalactoside
Kan	Kanamycin
kb	Kilobase pair
kDa	Kilodalton
Km	Michaelis constant
LB medium	Luria Bertani medium
LCF	Leaf chamber fluorometer
MC	Mesophyll cell
ME	Malic enzyme
min	Minute
MOPS	3-(N-morpholino) propane sulfonic acid
mRNA	Messenger RNA
MS medium	Murashige and Skoog Basal medium
mTP	Mitochondrial targeting peptide
NAD-ME	NAD-malic enzyme
NAD+/NADH	Nicotinamide adenine dinucleotide (oxidized/reduced form)
NADP+/NADPH	Nicotinamide adenine dinucleotide phosphate (oxidized/reduced form)
NPtII	Neomycin phosphotransferase type II that confers resistance to aminoglycoside antibiotics (i.e. kanamycin and neomycin) and was used for selection of transgenic plants in axenic culture.
OAA	Oxalo acetic acid
OD	Optical density
p35SS/pA35S	Promotor (duplication) and Polyadenylation-/Termination sequence from CaMV
PAnos	Polyadenylation promoter of Nopaline synthetase gene from *A.tumefaciens*
PAT	The coding sequence, which confers resistance to phosphinotricin
PCK	Phosphoenolpyruvate carboxykinase
pCO$_2$	Partial pressure of CO_2
PCR	Polymerase chain reaction
PCR-cycle	Photosynthetic carbon reduction cycle
PEPC	Phosphoenolpyruvate carboxylase
PEP-CK	Phosphoenolpyruvate carboxykinase

PFD	Photon flux density
PG	Phosphoglycolate
PGA	Phosphoglycerate
PGP	Phosphoglycolate phosphatase
PIB	Postillumination burst
PMS	Phenazine methosulfate
Pnos	Promoter of Nopaline synthase gene from *A. tumefaciens.*
PPDK	Pyruvate-orthophosphate dikinase
PTGS	Post-transcriptional gene silence
PYR	Pyruvate
rbcS1-cTP	Transit peptide of the small subunit of Rubisco from potato. The sequence was derived from gi 21562 (gene rbcs1)
rfp	Red fluorescent protein
Rif	Rifampicin
Rn	Leaf dark respiration
RNA	Ribonucleic acid
rpm	Rotation per minute
RT	Room temperature
RT	Reverse transcriptase
RT-PCR	Reverse transcriptase-polymerase chain reaction
Rubisco	Ribulose 1,5 bisphosphate carboxylase/oxygenase
RuBP	Ribulose 1, 5 bisphosphate
SAR	Scaffold Attachment Region from the tobacco RB7 gene (gi U67919).
SDS-PAGE	Sodium dodecyl sulphate-polyacrylamide gel electrophoresis
sec	Second
Ser	Serine
SGAT	Serine:glutamate aminotransferase
Sul	The coding sequence, which confers resistance to sulfadiazine
TEMED	N, N, N´, N´-tetramethyl ethylene diamine
TLC	Thin layer chromatography
TPP	Thiamine pyrophosphate
TSR	Tartronic semialdehyde reductase
U	Unit

UV	Ultraviolet
vol	Volume
v/v	Volume per volume
w/v	Weight per volume
WT	Wild type

6   LIST OF FIGURES AND TABLES

6.1   List of Figures

6.2   List of Tables

7   REFERENCES

Aebi, H. (1984). Catalase *in vitro*. Methods in Enzymology. *105*, 121-126.

Agarie, S., Miura, A., Sumikura, R., Tsukamoto, S., Nose, A., Arima, S., Matsuoka, M., and Miyao-Tokutomi, M. (2002). Overexpression of C_4 PEPC caused O_2-insensitive photosynthesis in transgenic rice plants. Plant Science *162*, 257-265.

Andrews, J. T., and Whitney, S. M. (2003). Manipulating ribulose bisphosphate carboxylase/oxygenase in the chloroplasts of higher plants. Arch Biochem Biophys *414*, 159-169.

Andrews, T. J., and Lorimer, G. H. (1987). RUBISCO: structure, mechanisms and prospects for improvement. Academic press, New York, The biochemistry of plants *10*, 131-218.

Arnon, D. I. (1949). Copper enzymes in chloroplasts. Polyphenol oxidase in *Beta vulgaris*. Plant Physiol *24*, 1-15.

Arp, W. J., Van Mierlo, J. E. M., Berendse, F., and Snijders, W. (1998). Interactions between elevated CO_2 concentration, nitrogen and water: Effects on growth and water use of six perennial plant species. Plant, Cell & Environment *21*, 1-11.

Atkin, O. K., Evans, J. R., and Siebke, K. (1998). Relationship between the inhibition of leaf respiration by light and enhancement of leaf dark respiration following light treatment. Plant Physiol *25*, 437-443.

Ausubel, F. M., Brent, R., and Kingston, R. E. (1994). Current Protocols in Molecular Biology. Wiley Interscience, New York.

Badger, M. (2003). The roles of carbonic anhydrases in photosynthetic CO_2 concentrating mechanisms. Photosynth Res. *77*, 83-94.

Badger, M. R., and Spalding, M. H. (2000). CO_2 acquisition, concentration and fixation in cyanobacteria and algae. Photosynthesis: Physiology and Metabolism (book) *9*, 369-397.

Bari, R., Kebeish, R., Kalamajka, R., Rademacher, T., and Peterhänsel, C. (2004). A glycolate dehydrogenase in the mitochondria of *Arabidopsis thaliana*. J Exp Bot *55*, 623-630.

Becker, W. M. (1986). The world of the cell. Benjamin/Cummings, Menlo Park, CA.

Beckmann, K., Dzuibany, C., Biehler, K., Fock, H., Hell, R., Migge, A., and Becker, T. W. (1997). Photosynthesis and fluorescence quenching, and the mRNA levels of plastidic glutamine synthetase or of mitochondrial serine hydroxymethyltransferase (SHMT) in the leaves of the wild-type and of the SHMT-deficient stm mutant of *Arabidopsis thaliana* in relation to the rate of photorespiration. Planta *202*, 379-386.

Besson, V., Rebeille, F., Neuburger, M., Douce, R., and Cossins, E. A. (1993). Effects of tetrahydrofolate polyglutamates on the kinetic parameters of serine hydroxymethyltransferase and glycine decarboxylase from pea leaf mitochondria. Biochemical journal *292*. 425-430.

Betsche, T., Schaller, D., and Melkonian, M. (1992). Identification and characterization of glycolate oxidase and related enzymes from the endocyanotic alga Cyanophora-Paradoxa and from leaves. Plant Physiology *98*, 887-893.

Bock, R. (2001). Transgenic plastids in basic research and plant biotechnology. J Mol Biol *312*, 425-438.

Bock, R., and Hagemann, R. (2000). Extranuclear inheritance: Plastid genetics: manipulation of plastid genomes and biotechnological applications. Progress in Botany *61*, 76-90.

Bowes, G. (1996). Photosynthetic responses to changing atmospheric carbon dioxide concentration. in advances of photosynthesis, photosynthesis and environment Baker,NR (ed) Kluwer Academic publisher, Dordrecht, the Netherlands *5*, 387-407.

Bowes, G., Ogren, W. L., and Hageman, R. H. (1971). Phosphoglycolate production catalyzed by ribulose diphosphate carboxylase. Biochem Biophys Res Commun *45*, 716-722.

Bowes, G. R. S. K., Estavillo G.M., and Reiskind J.B (2002). C_4 mechanism in aquatic angiosperms: comparisions with terresterial C_4 systems. Functional plant biology *29*, 379-392.

Bradford, M. M. (1976). A Rapid and sensitive method for the quantitation of microgram quantities of protein utilizing the principle of protein-dye binding. Anal Biochem *72*, 248-254.

Brukhin, V., Clapham, D., Elfstrand, M., and von Arnold, S. (2000). Basta tolerance as a selectable and screening marker for transgenic plants of Norway spruce. Plant Cell Reports [print] *19*, 899-903.

Bulley, N. R., and Tregunna, E. B. (1971). Photorespiration and the postillumination CO_2 burst. Canadian Journal of Botany *49*, 1277-1284.

Butaye, K. M. J., Goderis, I. J. W. M., Wouters, P. F. J., Pues, J. M.-T. G., Delaure´, S. L., Broekaert, W. F., Depicker, A., Cammue, B.P.A., and De Bolle, M. F. C. (2004). Stable high-level transgene expression in *Arabidopsis thaliana* using gene silencing mutants and matrix attachment regions. plant J *39*, 440-449.

Calvin, B. (1989). Forty years of photosynthesis and related activities. photosynth Res *21*, 3-16.

Chang, Y. Y., Wang, A. Y., and Cronan, J. E., Jr. (1993). Molecular cloning, DNA sequencing, and biochemical analyses of *Escherichia coli* glyoxylate carboligase. An enzyme of the acetohydroxy acid synthase-pyruvate oxidase family. J Biol Chem *268*, 3911-3919.

Clough, S., and Bent, A. (1998). Floral Dip: a simplified method for Agrobacterium-mediated transformation of *Arabidopsis thaliana*. Plant J *16*, 735-743.

Cocciolone, S. M., Chopra, S., Flint-Garcia, S. A., McMullen, M. D., and Peterson, T. (2001). Tissue-specific patterns of a maize Myb transcription factor are epigenetically regulated. Plant J *27*, 467-478.

Collins, N., and Merrett, M. J. (1975). The localization of glycolate pathway enzymes in Euglena. Biochem J *148*, 321-328.

Conway G. and Toennissen G. (1999). Feeding the world in the twenty - first century. nature *402*, 55-58.

Cushman, J. C. (2001). Crassulacean acid metabolism. A plastic photosynthetic adaptation to arid environments. Plant Physiol *127*, 1439-1448.

Cushman, J. C., and Bohnert, H. J. (1997). Molecular Genetics of Crassulacean Acid Metabolism. Plant Physiol *113*, 667-676.

Davis, W. L., and Goodman, D. B. (1992). Evidence for the glyoxylate cycle in human liver. Anat Rec *234*, 461-468.

Day, C. D., Lee, E., Kobayashi, J., Holappa, L. D., Albert, H., and Ow, D. W. (2000). Transgene integration into the same chromosome location can produce alleles that express at a predictable level, or alleles that are differentially silenced. Genes Dev *14*, 2869-2880.

De Block, M., De Sonville, A., and Debrouwer, D. (1995). The selection mechanism of phosphinothricin is influenced by the metabolic status of the tissue. Planta *197*, 619-626.

Decker, J. P. (1959). Comparative responses of carbon dioxide outburst and uptake in tobacco. Plant Physiol *34*, 100-102.

Devi, M. T., Rajagopalan, A., and Raghavendra, A. S. (1996). Purification and properties of glycolate oxidase from plants with different photosynthetic pathways, distinctness of C4 enzyme from that of a C_3 species and a C_3–C_4 intermediate. Photosynthesis Research *47*, 231-238.

Douce, R., and Neuburger, M. (1989). The uniqueness of plant mitochondria. Annual Review of Plant Physiology and Plant Molecular Biology *40*, 371-414.

Douce, R., and Neuburger, M. (1999). Biochemical dissection of photorespiration. Curr Opin Plant Biol *2*, 214-222.

Dougherty, W. G., and Parks, T. D. (1995). Transgenes and gene suppression: telling us something new? Curr Opin Cell Biol *7*, 399-405.

Edwards, G. E., Furbank, R. T., Hatch, M. D., and Osmond, C. B. (2001). What does it take to be C_4? Lessons from the evolution of C_4 photosynthesis. Plant Physiol *125*, 46-49.

Edwards, J. W., and Coruzzi, G. M. (1989). Photorespiration and light act in concert to regulate the expression of the nuclear gene for chloroplast glutamine synthetase. Plant Cell *1*, 241-248.

Elmayan, T., Balzergue, S., Beon, F., Bourdon, V., Daubremet, J., Guenet, Y., Mourrain, P., Palauqui, J. C., Vernhettes, S., Vialle, T. (1998). Arabidopsis mutants impaired in cosuppression. Plant Cell *10*, 1747-1758.

Evans, J. R., and Von Caemmerer, S. (1996). Carbon Dioxide Diffusion inside Leaves. Plant Physiol *110*, 339-346.

Fagard, M., and Vaucheret, H. (2000). (TRANS)GENE SILENCING IN PLANTS: How Many Mechanisms? Annu Rev Plant Physiol Plant Mol Biol *51*, 167-194.

Farineau, J., Lelandias, M., and Morot-Gaudry, J. F. (1984). Operation of the glycolate pathway in isolated bundle sheath strands of maize (*Zea mays*) cultivar Inra-258 and Panicum maximum. Physiologia Plantarum *60*, 208-214.

Flügge, U., Weber, A., Fisher, K., Häusler, R., and Kammerer, B. (1996). Molecular characterization of plastid transporters. CR Acad Sci *319*, 849-852.

Frederick, S. E., Gruber, P. J., and Tolbert, N. E. (1973). The occurence of glycolate dehydrogenase and glycolate oxidase in green plants: An evolutionary survey. Plant Physiol *52*, 318-323.

Freitag, H., and Stichler, W. (2002). Bienertia cycloptera Bunge ex Boiss, Chenopodiaceae, another C_4 plant without Kranz tissues. Plant Biology *4*, 121-132.

Fry, D. W., and Richardson, K. E. (1979). Isolation and characterization of glycolic acid dehydrogenase from human liver. Biochim Biophys Acta *567*, 482-491.

Furbank, R. T., and Taylor, W. C. (1995). Regulation of photosynthesis in C_3 and C_4 plants: A molecular approach. Plant Cell *7*, 797-807.

Gaunt, S. R., Riley, A., Lazzeri, P., and Barcelo, P. (1998). A facile method for screening for phosphinothricin (PPT)-resistant transgenic wheats. Molecular Breeding *5*, 255-262.

Genty, B., Briantais, N., and Baker, R. (1989). The relationship between the quantum yield of photosynthetic transport and quenching of chlorophyll fluorescence. Biochem Biophys *Acta 990*, 87-92.

Giafi, C. F., and Rumsby, G. (1998). Kinetic analysis and tissue distribution of human D-glycerate dehydrogenase/glyoxylate reductase and its relevance to the diagnosis of primary hyperoxaluria type 2. Ann Clin Biochem *35 (Pt 1)*, 104-109.

Giersch, C. (1982). Capacity of the malate/oxaloacetate shuttle for transfer of reducing equivalents across the envelope of leaf chloroplasts. Arch Biochem Biophys *219*, 379-387.

Gotto, A. M., and Kornberg, H. L. (1961). The metabolism of C_2 compounds in micro-organisms. Preparation and properties of crystalline tartronic semialdehyde reductase. Biochem J *81*, 273-284.

Goyal, A., and Tolbert, N. E. (1996). Association of glycolate oxidation with photosynthetic electron transport in plant and algal chloroplasts. PNAS *93*, 3319-3324.

Grodzinski, B. (1979). Study of formate production and oxidation in leaf peroxisomes during photorespiration. Plant physiology *63*, 289-293.

Gutheil, W. G. (1998). A sensitive equilibrium-based assay for D-lactate using D-lactate dehydrogenase: application to penicillin-binding protein/DD-carboxypeptidase activity assays. Anal Biochem *259*, 62-67.

Hadi, M. Z., Kemper, E., Wendeler, E., and Reiss, B. (2002). Simple and versatile selection of Arabidopsis transformants. Plant Cell Reports *21*, 130-135.

Hanahan, D. (1983). Studies on transformation of *Escherichia coli* with plasmids. J Mol Biol *166*, 557-580.

Hansen, R. W., and Hayashi, J. A. (1962). Glycolate metabolism in *Eschrichia coli*. JBacteriol *83*, 679-687.

Harley, P. C., and Sharkey, T. D. (1991). An improved model of C_3 photosynthesis at high CO_2: reversed O_2 sensitivity explained by lack of glycerate reentry into the chloroplast. photosynthesis Research *27*, 169-178.

Hatch, M. D., Osmond, C., and Slatyer, R. (1971). Photosynthesis and photorespiration. New York: Wiley-Interscience.

Hatch, M. D. (1978). A simple spectrophotometric assay for fumarate hydratase in crude tissue extracts. Anal Biochem *85*: 271-275.

Hatch, M. D. (1987). C_4 photosynthesis: a unique blend of modified biochemistry, anatomy and ultrastructure. Biochim Biophys Acta *895*, 81-106.

Hatch, M. D. (1992). C_4 Photosynthesis: an Unlikely Process Full of Surprises. Plant & Cell Physiology *33*, 333-342.

Häusler, R. E., Hirsch, H. J., Kreuzaler, F., and Peterhänsel, C. (2002). Overexpression of C_4-cycle enzymes in transgenic C_3 plants: a biotechnological approach to improve C_3-photosynthesis. J Exp Bot *53*, 591-607.

Havir, E. A. (1986). Inactivation of serine: glyoxylate and glutamate: glyoxylate aminotransferases from tobacco leaves by glyoxylate in the presence of ammonium ion. Plant Physiology *80*.

Hays, J. B. (2002). *Arabidopsis thaliana,* a versatile model system for study of eukaryotic genome-maintenance functions. DNA Repair (Amst) *1*, 579-600.

Heber, U., and Kirk, M. R. (1975). Flexibility of coupling and stoichiometry of ATP formation in intact chloroplasts. Biochim Biophys Acta *376*, 136-150.

Howitz, K. T., and McCarty, R. (1983). Evidence for a glycolate transporter in the envelope of pea chloroplasts. FEBS Lett *154*, 339-342.

Howitz, K. T., and McCarty, R. (1991). Solubilization, partial purification and reconstitution of the Glycolate/Glycerate transporter from chloroplast inner envelope membranes. Plant Physiol *96*, 1060-1069.

Igamberdiev, A. U. (1999). Foundations of metabolic organization: coherence as a basis of computational properties in metabolic networks. BioSystems *50*, 1-16.

Igamberdiev, A. U., Bykova, N. V., Lea, P. J., and Gardestrom, P. (2001). The role of photorespiration in redox and energy balance of photosynthetic plant cells: A study with a barley mutant deficient in glycine decarboxylase. Physiol Plant *111*, 427-438.

Igamberdiev, A. U., and Kleczkowski, L. A. (1997). Glyoxylate metabolism during photorespiration: a cytosol connection. In pessarakli, M(Ed), handbook of photosynthesis, Marcel Dekker, New York, 269-290.

Igamberdiev, A. U., and Lea, P. J. (2002). The role of peroxisomes in the integration of metabolism and evolutionary diversity of photosynthetic organisms. Phytochemistry *60*, 651-674.

Igamberdiev, A. U., Zemlyanukhin, A. A., and Meshcheryakova, I. V. (1986). Extraglyoxysomal form of isocitrate lyase in higher plants.Soviet Plant Physiology. Soviet Plant Physiology *33*, 852-858.

Igarashi, D., Miwa, T., Seki, M., Kobayashi, M., Kato, T., Tabata, S., Shinozaki, K., and Ohsumi, C. (2003). Identification of photorespiratory glutamate:glyoxylate aminotransferase (GGAT) gene in Arabidopsis. Plant Journal *33*, 975-987.

Ireland, R. P. (1998). The enzymes of glutamine,glutamate. asparagine and aspartate metabolism. plant amino acids Edited by Singh BK, academic press, New York, 49-109.

Jach, G., Binot, E., Frings, S., Luxa, K., and Schell, J. (2001). Use of red fluorescent protein from Discosoma sp. (dsRED) as a reporter for plant gene expression. Plant J *28*, 483-491.

Jenkins, C. L. D., Furbank, R. T., and M, D., H. (1989). Mechanism of C_4 photosynthesis, A model describing the inorganic carbon pool in bundle sheath cells. plant physiol *91*, 1372-1381.

Keys, A. J., and Leegood, R. C. (2002). Photorespiratory carbon and nitrogen cycling: evidence from studies of mutant and transgenic plants. In Advances in Photosynthesis and Respiration *12*, Photosynthetic Nitrogen Assimilation and Associated Carbon and Respiratory Metabolism (eds C.H. Foyer & G. Noctor). Kluwer, Dordrecht, The Netherlands.

Kimball, B. A. (1983). Carbon dioxide and agricultural yield: an assemblage and analysis of 430 prior observations [Effect on crop yields of the increasing global atmospheric carbon dioxide concentration, growth, production includes some woody plants]. Agronomy Journal [Madison: American Society of Agronomy] Sept/Oct, 779-788.

Kleczkowski, L. A., and Edwards, G. E. (1989). Identification of hydroxypyruvate and glyoxylate reductases in maize leaves. Plant Physiology *91*, 278-286.

Koncz, C., and Schell, J. (1986). The promoter of TL-DNA gene 5 controls the tissue-specific expression of chimaeric genes carried by a novel type of Agrobacterium binary vector. Mol Gen Genet *204*, 383-396.

Kornberg, H. L., and Sadler, J. R. (1961). The metabolism of C_2 compounds in microorganisms. A dicarboxylic acid cycle as a route for the oxidation of glycolate in *Eschrichia coli*. Biochem J *81*, 503-513.

Kozaki, A., and Takeba, G. (1996). Photorespiration protects C_3 plants from photo-oxidation. Nature *384*, 557-560.

Ku, M. S., Agarie, S., Nomura, M., Fukayama, H., Tsuchida, H., Ono, K., Hirose, S., Toki, S., Miyao, M., and Matsuoka, M. (1999). High-level expression of maize phosphoenolpyruvate carboxylase in transgenic rice plants. Nat Biotechnol *17*, 76-80.

Ku, M. S. B., Kano Murakami, Y., and Matsuoka, M. (1996). Evolution and expression of C_4 photosynthesis genes. Plant Physiology *111*, 949-957.

Kumarasinghe, k. S., Keys, A. J., and Whittingham, C. P. (1977). The flux of Carbon through the glycollate pathway during photosynthesis by wheat leaves. Journal of Experimental Botany *28*, 1247-1257.

Lacuesta, M., Gonzalez-Moro, B., Gonzalez-Murua, C., Aparicio tejo, P., and Munoz-Rueda, A. (1989). Effect of phosphinotricin (glufosinate) on activities of glutamine synthetase and glutamate dehydrogenase in Medicago sativa. Plant Physiol *134*, 304-307.

Laemmli, U. K. (1970). Cleavage of structural proteins during the assembly of the head of bacteriophage T4. Nature *227*, 680-685.

Laisk, A. K., Oja, V. M., and Kiirats, O. (1984). Assimilatory power (post-illumination CO_2 uptake) in leaves-measurement, environmental dependencies and kinetic properties. plant physiology *76*, 723-729.

Lawlor, D. W. (2001). Photosynthesis, 3rd edition, BIOS scientific publishers Ltd.

Leegood, R. C. (2002). C_4 photosynthesis: principles of CO_2 concentration and prospects for its introduction into C_3 plants. J Exp Bot *53*, 581-590.

Leegood, R. C., Lea, P. J., Adcock, M. D., and Haeusler, R. E. (1995). The regulation and control of photorespiration. Journal of Experimental Botany *46*, 1397-1414.

Lefebvre, S., Lawson, T., Zakhleniuk, O. V., Lloyd, J. C., Raines, C. A., and Fryer, M. (2005). Increased sedoheptulose-1,7-bisphosphatase activity in transgenic tobacco plants stimulates photosynthesis and growth from an early stage in development. Plant Physiol *138*, 451-460.

Lieman-Hurwitz, J., Rachmilevitch, S., Mittler, R., Marcus, Y., and Kaplan, A. (2003). Enhanced photosynthesis and growth of transgenic plants that express ictB, a gene involved in HCO_3 accumulation in cyanobacteria. Plant Biotechnology *1*, 43-50.

Liepman, A. H., and Olsen, L. J. (2001). Peroxisomal alanine: glyoxylate aminotransferase (AGT1) is a photorespiratory enzyme with multiple substrates in Arabidopsis thaliana. Plant J *25*, 487-498.

Liepman, A. H., and Olsen, L. J. (2003). Alanine Aminotransferase Homologs Catalyze the Glutamate:Glyoxylate Aminotransferase Reaction in Peroxisomes of Arabidopsis. Plant Physiol *131*, 215-227.

Lipka, V., Häusler, R. E., Rademacher, T., Li, J., Hirsch, H. J., and Kreuzaler, F. (1999). *Solanum tuberosum* double transgenic expressing phosphoenolpyruvate carboxylase and NADP-malic enzyme display reduced electron requirement for CO_2 fixation. Plant Sci *144*, 93-105.

Lord, J. M. (1972). Glycolate oxidoreductase in Escherichia coli. Biochim Biophys Acta *267*, 227-237.

Maroco, J. P., Ku, M. S. B., Lea, P. J., Dever, L. V., Leegood, R. C., Furbank, R. T., and Edwards, G. E. (1998). Oxygen Requirement and Inhibition of C_4 Photosynthesis. An analysis of C_4 plants deficient in the C_3 and C_4 cycles: An Analysis of C_4 Plants Deficient in the C_3 and C_4 Cycles. Plant Physiol *116*, 823-832.

Maxwell, K., and Johnson, G. N. (2000). Chlorophyll fluorescence--a practical guide. J Exp Bot *51*, 659-668.

Medrano, H., Keys, A. J., Lawlor, D. W., Parry, M. A. J., Azcon-Bieto, J., and Delgado, E. (1995). Improving plant production by selection for survival at low CO_2 concentrations. J Exp Bot *46*, 1389-1396.

Meinke, D. W., Cherry, J. M., Dean, C., Rounsley, S. D., and Koornneef, M. (1998). *Arabidopsis thaliana*: a model plant for genome analysis. Science *282*, 679-682.

Meuer, S., Wittwer, K., and Nakagawara, K. (2001). Rapid Cycler Real-Time PCR. Methods and applications Springer -Berlin, Heidelberg.

Migge, A., Carryol, E., Kunz, C., Hirel, B., Foch, h., and Becker, T. (1997). Expression of the tobacco genes encoding plastidic glutamine synthetase or ferredoxin- dependent glutamate synthase doesn't depend on nitrate reduction and is unaffected by suppression of photorespiration. J Exp Bot *48*, 1175-1184.

Miyagawa, Y., Tamoi, M., and Shigeoka, S. (2001). Overexpression of a cyanobacterial fructose-1,6-/sedoheptulose-1,7-bisphosphatase in tobacco enhances photosynthesis and growth. Nat Biotechnol *19*, 965-969.

Mourrain, P., Beclin, C., and Vaucheret, H. (2000). Are gene silencing mutants good tools for reliable transgene expression or reliable silencing of endogenous genes in plants? Genet Eng (N Y) *22*, 155-170.

Nelson, E. B., and Tolbert, N. E. (1970). Glycolate dehydrogenase in green algae. Arch Biochem Biophys *141*, 102-110.

Ninneman, O., Jauniaux, J., and Frommer, W. B. (1994). Identification of a high affinity NH3 transporter from plants. EMBO J *13*, 3464-3471.

Normile, D. (1999). genetic engineers aim to soup up crop photosynthesis. Science *283*, 314-316.

Novitskaya, L., Trevanion, S. J., Driscol, L. S., Foyer, C., and Noctor, G. (2002). How does photorespiration modulate leaf amino acid contents? A dual approach through modelling and metabolite analysis. Plant, Cell and Environment *25*, 821-835.

Nybom, N. (1955). The pigment characteristics of chlorophyll mutations in barley. Heriditas *41*, 510-512.

Ogren, W. L. (1984a). The CO_2/O_2 specificity of ribulose 1,5-bisphosphate carboxylase/oxygenase. Dependence on ribulose bisphosphate concentration, pH and temperature. Planta *161*, 308-313.

Ogren, W. L. (1984b). Photrespiration: Pathways, regulation and modification. Annual Review in Plant Physiology *35*, 415-442.

Ogren, W. L., and Jordan, D. B. (1983). Species variation in kinetic properties of ribulose 1,5-bisphosphate carboxylase/oxygenase. Arch Biochem Biophys *227*: 425-433.

Oliver, D., Neuburger, M., Bourguignon, J., and Douce, R. (1990). Glycine metabolism by plant mitochondria. Physiologia Plantarum *80*, 487-491.

Osmond, C. B. (1978). Crassulacean acid metabolism:a curiosity in context. annu Rev. Plant physiology *29*, 379-414.

Osmond, C. B. (1979). Integration of photosynthetic carbon metabolism during stress. Basic Life Sci *14*, 171-185.

Padidam, M., and Cao, Y. (2001). Elimination of transcriptional interference between tandem genes in plant cells. Biotechniques *31*, 328-330.

Pastore, D., Di Pede, S., and Passarella, S. (2003). Isolated durum wheat and potato cell mitochondria oxidize externally added NADH mostly via the malate/oxaloacetate shuttle with a rate that depends on the carrier-mediated transport. Plant Physiol *133*, 2029-2039.

Pellicer, M. T., Badia, J., Aguilar, J., and Baldoma, L. (1996). glc locus of *Escherichia coli*: characterization of genes encoding the subunits of glycolate oxidase and the glc regulator protein. J Bacteriol *178*, 2051-2059.

Peterson, R. B. (1982). Regulation of glycine decarboxylase and l-serine hydroxymethyltransferase activities by glyoxylate in tobacco leaf mitochondrial preparations. Plant Physiology *70*, 61-66.

Pinelli, P., and Loreto, F. (2003). $^{12}CO_2$ emission from different metabolic pathways measured in illuminated and darkened C_3 and C_4 leaves at low atmospheric and elevated CO_2 concentrations. Journal of Experimental Botany *54*, 1761-1769.

Plasterk, R. H., and Ketting, R. F. (2000). The silence of the genes. Curr Opin Genet Dev *10*, 562-567.

Rademacher, T., Häusler, R. E., Hirsch, H. J., Zhang, L., Lipka, V., Weier, D., Kreuzaler, F., and Peterhänsel, C. (2002). An engineered phosphoenolpyruvate carboxylase redirects carbon and nitrogen flow in transgenic potato plants. Plant Journal *32*, 25-39.

Raghavendra, A. S., Reumann, S., and Heldt, H. W. (1998). Participation of mitochondrial metabolism in photorespiration. Reconstituted system of peroxisomes and mitochondria from spinach leaves. Plant Physiol *116*, 1333-1337.

Ranson, S. L., and Thomas, M. (1960). Crassulacean acid metabolism. annu. Rev. plant physiology *11*, 81-110.

Rao, S. K., Magnin, N. C., Reiskind, J. B., and Bowes, G. (2002). Photosynthetic and Other Phosphoenolpyruvate Carboxylase Isoforms in the Single-Cell, Facultative C_4 System of Hydrilla verticillata. Plant Physiol *130*, 876-886.

Rau, M. H., and Senger, H. (1965). Untersuchungen zur Synchronisierbarkeit einzlner Pigmentmangel-Mutanten von Chlorella. Planta *65*, 186-194.

Reiskind, J. B., Madsen, T. V., Van Ginkel, L. C., and Bowes, G. (1997). Evidence that inducible C-4-type photosynthesis is a chloroplastic CO_2-concentrating mechanism in Hydrilla, a submersed monocot. Plant, Cell & Environment *20*, 211-220.

Robinson, S. P. (1982). Transport of glycerate across the envelope membrane of isolated spinach chloroplasts. Plant Physiology *70*, 1032-1038.

Roessner, U., Wagner, C., Kopka, J., Trethewey, R. N., and Willmitzer, L. (2000). Simultaneous analysis of metabolites in potato tuber by gas chromatography-mass spectrometry. Plant J *23*, 131-142.

Ryuzi Kanai, E. G. (1999). The biochemistry of C_4 photosynthesis. C_4 Plant Biology, Ed: Monson RK and Sage RF, Academic Press, San Diego, 49-87.

Sage, R. F. (1999). Why C_4 photosynthesis. C_4 Plant Biology, Ed: Monson RK and Sage RF, Academic Press San Diago *3*, 3-16.

Sage, R. F. (2001). Environmental and evolutionary preconditions for the origin and diversification of the C_4 photosynthetic syndrome. Plant Biology *3*, 202-213.

Sage, R. F. (2004). The evolution of C_4 photosynthesis. New phytologist *161*, 341-370.

Saiki, R. K., Gelfand, D. H., Stoffel, S., Scharf, S. J., Higuchi, R., Horn, G. T., Mullis, K. B., and Erlich, H. A. (1988). Primer-directed enzymatic amplification of DNA with a thermostable DNA polymerase. Science *239*, 487-491.

Sambrook, J., and Russel, D. W. (2002). Molecular Cloning - A Laboratory Mannual, Vol 1-3, 3 edn (Cold Spring Habour, New York: Cold Spring Habour Laboratory Press).

Sanger, F., Nicklen, S., and Coulson, A. R. (1977). DNA sequencing with chain-termination inhibitors. Proc Natl Acad Sci USA *74*, 5463-5467.

Schubert, D., Lechtenberg, B., Forsbach, A., Gils, M., Bahadur, S., and Schmidt, R. (2004). Silencing in *Arabidopsis* T-DNA transformants: the predominant role of a gene-specific RNA sensing mechanism versus position effects. Plant Cell *16*, 2561-2572.

Sharkey, T. D. (1988). Estimating the rate of photorespiration in leaves. plant physiology *73*, 147-152.

Sharkey, T. D. (2001). Photorespiration. ENCYCLOPEDIA OF LIFE SCIENCES, 1-5.

Shingles, R. W., and Grodzinski, B. (1984). Effects of glycolate pathway intermediates on glycine decarboxylation and serine synthesis in Pea (Pisum sativum). Plant Physiol *74*, 705-710.

Somerville, C. R. (1990). The biochemical basis for plant improvement. in plant physiology and plant molecular biology DennisDT, Turpin DH (eds) longman group, Essex, UK, 490-501.

Somerville, C. R., and Ogren, W. L. (1982). Genetic modification of photorespiration. Trends in Biochemical Sciences *7*, 171-174.

Spreitzer, R. J. (1999). Questions about the complexity of chloroplast ribulose-1,5-bisphosphate carboxylase/oxygenase. Photosynthesis Research *60*, 29-42.

Stabenau, H., and Beevers, H. (1974). Isolation and characterization of microbodies from the alga Chorogonium elongatum. Plant Physiol *53*, 866-869.

Stabenau, H., and Säftel, W. (1981). localization of enzymes of the glycolate metabolismin Mougeotia. Ber Dtsch Bot Ges *94*, 59-64.

Stabenau, H., Winkler, U., and Saftel, W. (1984). Mitochondrial metabolism of glycolate in the alga Eremosphaera viridis. Zeitschrift fuer Pflanzenphysiologie *114*, 413-420.

Staehelin, L. A. (1986). Chloroplast structure and supermolecularorganization of photosynthetic membranes. Encyclopedia of plant physiology New series *19*, 1-84.

Staub, J., and Maliga, P. (1995). Expression of a chimeric uidA gene indicates that polycistronic mRNAs are efficiently translated in tobacco plastids. Plant J *7*, 845-848.

Staub, J. M., and Maliga, P. (1994). Translation of psbA mRNA is regulated by light via the 5'-untranslated region in tobacco plastids. Plant J *6*, 547-553.

Stitt, M., Lilley, R., Gerhardt, R., and Heldt, H. (1989). Determination of metabolite levels in specific cells and subcellular compartments of plant leaves. Methods in Enzymology *174*, 518-552.

Stockhaus, J., Schlue, U., Koczor, M., Chitty, J. A., Taylor, W. C., and Westhoff, P. (1997). The Promoter of the Gene Encoding the C4 Form of Phosphoenolpyruvate Carboxylase Directs Mesophyll-Specific Expression in Transgenic C4 Flaveria spp. Plant Cell *9*, 479-489.

Suzuki, K., Iwamoto, K., Yokoyama, S., and Ikawa, T. (1991). GLYCOLATE-OXIDIZING ENZYMES IN ALGAE. Journal of Phycology *27*, 492-498.

Tachibana, K., Watanabe, T., Sekizawa, Y., and Takematsu, T. (1986). Accumulation of ammonia in plants treated with Bialaphos. Pesticide Sci *11*, 33–37.

Tolbert, N. E. (1997). The C_2 Oxidative Photosynthetic Carbon Cycle. Annu Rev Plant Physiol Plant Mol Biol *48*, 1-25.

Tolbert, N. E., Oeser, A., Kisaki, T., Hageman, R. H., and Yamazaki, R. K. (1968). Peroxisomes from spinach leaves containing enzymes related to glycolate metabolism. J Biol Chem *243*, 5179-5184.

Tolbert, N. E., Yamazaki, R. K., and Oeser, A. (1970). Localization and properties of hydroxypyruvate and glyoxylate reductases in spinach leaf particles. J Biol Chem *245*, 5129-5136.

Van Ginkel, L. C., Bowes, G., Reiskind, J. B., and Prins, H. B. A. (2001). A CO_2-flux mechanism operating via pH-polarity in Hydrilla verticillata leaves with C_3 and C_4 photosynthesis. Photosynthesis Research [print] *68*, 81-88.

Vaucheret, H., Be´ clin, C., and Fagard, M. (2001). Post-transcriptional gene silencing in plants. J Cell Sci *114*, 3083–3091.

Von Caemmerer, s., and Furbank, R.T. (2003). The C_4 pathway: an efficient CO_2 pump. photosynth Res *77*, 191-207.

Von Caemmerer, S. (2003). C_4 photosynthesis in a single C_3 cell is theoretically inefficient but may ameliorate internal CO_2 diffusion limitations of C_3 leaves. Plant, Cell & Environment *26*, 1191-1197.

Von Caemmerer, S., and Furbank, R. T. (1999). Modeling C_4 photosynthesis. In biology of C_4 photosynthesis (eds RF Sage and RK Monson). Academic press, New York, 173-211.

Voznesenskaya, E. V., Franceschi, V. R., Kiirats, O., Freitag, H., and Edwards, G. E. (2001). Kranz anatomy is not essential for terrestrial C_4 plant photosynthesis. Nature *414*, 543-546.

Weber, A., Menzlaff, E., Arbinger, B., Gutensohn, N., Eckerskorn, C., and Flügge, U. (1995). The 2-oxoglutarate/malate translocator of chloroplast envelope membranes: molecular cloning of a transporter containing a 12-helix motif and expression of the functional protein in yeast cells. Biochemistry *34*, 2621-2627.

Whitney, S. M., and Andrews, T. J. (2001). Plastome-encoded bacterial ribulose-1,5-bisphosphate carboxylase/oxygenase (Rubisco) supports photosynthesis and growth in tobacco. Proc Natl Acad Sci U S A *98*, 14738-14743.

Wild, A., and Ziegler, C. (1989). The effect of bialaphos on ammoniumassimilation and photosynthesis. I. Effect on the enzymes of ammonium-assimilation. Naturforsch *44*, 97-102.

Wilson, T. (1993). Strategies to protect crop plants against viruses: pathogen-derived resistance blossoms. Proc Natl Acad Sci USA *90*, 3134-3141.

Wingler, A., Lea, P. J., and Leegood, R. C. (1997). Control of photosynthesis in barley plants with reduced activities of glycine decarboxylase. Planta *202*, 171-178.

Wingler, A., Lea, P. J., and Leegood, R. C. (1999a). Photorespiratory metabolism of glyoxylate and formate in glycine-accumulating mutants of barley and Amaranthus edulis. planta *207*, 518-526.

Winkler, U., Säftel, W., and Stabenau, H. (1982). Studies on the aminotransferases participating in the glycolate metabolism of the alga mageotia. Plant Physiol *70*, 340-343.

Winkler, U., and Stabenau, H. (1992). Metabolism of glycolate in mitochondria and peroxisomes of green algae. In Phylogenetic changes in peroxisomes of algae Phylogeny of plant peroxisomes, (ed H Stabenau), pp 80-91 Oldenburg: University of Oldenburg.

Ye, F., and Signer, E. R. (1996). RIGS (repeat-induced gene silencing) in *Arabidopsis* is transcriptional and alters chromatin configuration. Proc Natl Acad SciUSA *93*, 0881–10886.

Yokota, A., Haga, S., and Kitaoka, S. (1985a). Purification and some properties of glyoxylate reductase (NADP$^+$) and its functional location in mitochondria in *Euglena gracilis* z. Biochem J *227*, 211-216.

Yokota, A., and Kitaoka, S. (1979a). Occurrence and operation of the glycollate-glyoxylate shuttle in mitochondria of *Euglena gracilis* z. Biochem J *184*, 189-192.

Young, G., Naghizadeh, F., King, J., and Morgan, H. G. (1973). Reduction of glyoxylate by human serum. Clin Chem *19*, 425-428.

Zelitch, I. (1989). Selection and characterization of tobacco plants with novel O_2 resistant photosynthesis. Plant physiology *90*, 1457-1464.

Zelitch, I., and Gotto, A. M. (1962). Properties of a new glyoxylate reductase from leaves. Biochem J *84*, 541-546.

Zhu, X.-G., Portis, A. R., and Long, S. P. (2004). Would transformation of C_3 crop plants with foreign Rubisco increase productivity? A computational analysis extrapolating from kinetic properties to canopy photosynthesis. Plant Cell Environ *27*, 155-165.

8   ACKNOWLEDGEMENTS

CURRICULUM VITAE

Personal data:

Name	: Rashad Mohamed Ahmed Kebeish
Date of birth	: 10-04-76
Place of birth	: Sharkia, Egypt
Nationality	: Egyptian
Religion	: Moslim
Marital status	: Married
Address in Egypt	: Zagazig, Sharkia, Egypt
Address in Germany	: Rütscher Str 155 App.110 , 52072 Aachen, Germany

Educational data:

1983-1988	: Abu-Hebal primary school (excellent grade) - Sharkyia/Egypt
1988-1991	: El-Fath prep school (excellent grade) - Sharkyia/Egypt
1991-1994	: Salhyia secondary school (very good grade) - Sharkyia/Egypt
1994-1998	: Bachelor science (excellent) – Faculty of science/ Zagazig university - Sharkyia/Egypt
2001-2002	: Diploma in Biology (very good grade) – Institute for Biology I/ RWTH-Aachen – Aachen/Germany

Publication:

Bari, R, <u>Kebeish, R</u>**,** Kalamajka, R, Rademacher, T, and Peterhänsel, C. (2004). A glycolate dehydrogenase in the mitochondria of *Arabidopsis thaliana*. J Exp Bot *55*, 623-630.

Declaration / Erklärung

Herewith I declare that I have written this PhD thesis myself, using only the referenced literature.

Hiermit versichere ich, dass ich die vorliegende Doktorarbeit selbstständig verfasst und keine anderen als die angebenen Hilfsmittel und Quellen verwendet habe.

Aachen, 2006